UNIVERSITÀ
DEGLI STUDI
DI PADOVA

Administrative unit: Università degli Studi di Padova

Department: Territorio e Sistemi Agro-Forestali (TESAF)

PhD Program : Land, Environment, Resources, Health (LERH)

Batch: XXIX

Thesis title: Stream Power and Geomorphic Effects of Flash Floods

PhD Program Coordinator: Prof. Davide Matteo Pettenella

Supervisors: Dr. Lorenzo Marchi

Prof. Marco Borga

Prof. Ellen E. Wohl

PhD candidate: William Amponsah

UNIVERSITÀ
DEGLI STUDI
DI PADOVA

STREAM POWER AND GEOMORPHIC EFFECTS OF FLASH FLOODS

BY

WILLIAM AMPONSAH

BSC. KWAME NKRUMAH UNIVERSITY OF SCIENCE AND TECHNOLOGY, GHANA, 2010

MSC. UNIVERSITY OF COPENHAGEN AND UNIVERSITY OF PADOVA, 2013

A THESIS
SUBMITTED IN PARTIAL FULFILMENT OF THE
REQUIREMENTS FOR THE DEGREE OF
DOCTOR OF PHILOSOPHY
AT THE
UNIVERSITY OF PADOVA
2017

RESEARCH INSTITUTE FOR GEO-HYDROLOGICAL PROTECTION,
NATIONAL RESEARCH COUNCIL OF ITALY (CNR-IRPI), PADOVA

“The man of science is of no country;
the world is his country,
all mankind his countrymen”

(James Smithson)

ABSTRACT

As one of the most devastating natural hazards, flash floods are responsible for major and abrupt geomorphic effects in the fluvial system as well as significant loss of life and socio-economic damages. Flash floods are characterized by strong spatio-temporal rainfall variability and therefore show variations in discharge and energy expenditure: associated geomorphic effects depend on geological controls on channel geometry and sediment characteristics, as well as on variations in flood intensity. Geomorphic effects usually take the form of erosional and depositional modification of the pre-flood channel. The central question of this thesis is to evaluate why flash floods of similar magnitudes and intensities sometimes produce dissimilar geomorphic results. The use of peak instantaneous hydraulic flow parameters such as discharge, velocity, shear stress, and stream power to quantify geomorphic changes has commonly been non-deterministic. This thesis aims at investigating how factors such as channel geometry, substrate, and flood magnitude and duration can interact and influence geomorphic effectiveness of high magnitude floods. A combined analysis of data from post-flood surveys and hydrological modelling permitted a comprehensive hydro-geomorphic investigation of seven major flash flood that occurred between 2007 and 2014 in different hydro-climatic regions in central and southern Europe. High peak discharge coupled with long flow duration ensured significant geomorphic impacts in Mediterranean basins. Values of stream power are generally consistent with observed geomorphic changes in the studied cross sections. However, bedrock channels show the highest values of energy expenditure but no visible erosion, whereas major erosion has been observed in alluvial channels. The trends in semi-alluvial channels urge the recognition of local or event-specific conditions that increase the resistance of channel bed and banks to erosion. Short flow duration caused major sedimentological effects but limited channel widening in most semi-alluvial channels. Eight rivers that were highly affected by three of the studied flash floods were selected for detailed analysis and modelling of the contiguous downstream variability in stream power. Power functions adequately interpreted the systematic downstream increase in peak discharge, whereas contrary to the usual exponential function, a quadratic function better interpreted the high downstream variability in channel gradient. The performance of the resulting empirical models for cross-sectional stream power and unit stream power were essentially influenced by channel gradient. The availability of high-resolution pre- and post-flood satellite images allowed assessment of channel changes along seven of these channels. Statistical analysis indicated that hydraulic forces alone are not adequate to interpret the rate of channel widening, which is primarily influenced by the degree of channel confinement. Together with lateral confinement, unit stream power better predicted channel widening in steep channels, whereas cumulative energy expenditure was relatively better for moderate channel reaches. The use of different erosion-resistance thresholds to quantify the geomorphological changes of riverbeds supports the conclusion that the determination of these changes is much more difficult than to determine the hydraulic variables involved.

SOMMARIO

Le piene improvvise (*flash flood*) sono fra i processi naturali più devastanti e sono responsabili di rilevanti e subitanei effetti morfologici, nonché della perdita di vite umane e di gravi danni economici. Le piene improvvise sono caratterizzate dalla forte variabilità spazio-temporale delle precipitazioni innescanti, cui consegue una forte variabilità delle portate e della potenza della corrente. Gli effetti geomorfologici delle piene improvvise dipendono sia dal controllo che l'assetto geologico esercita sulla geometria del canale e sulle caratteristiche del sedimento, sia dall'intensità della piena. Gli effetti geomorfologici delle piene improvvise si manifestano attraverso processi sia erosivi che deposizionali che determinano variazioni nell'assetto del canale rispetto alle condizioni antecedenti l'evento. La questione centrale di questa tesi è valutare perché piene improvvise di simile intensità producano talvolta effetti morfologici nettamente differenti. L'uso dei valori istantanei massimi di variabili di tipo idraulico, quali la portata, la velocità, lo sforzo tangenziale e la potenza della corrente, si è spesso rivelato non conclusivo nel quantificare i cambiamenti morfologici. Questa tesi mira a studiare come fattori quali la geometria del canale, il substrato, l'intensità e la durata dell'evento possano interagire e influenzare l'azione morfologia delle piene improvvise. Un'analisi combinata, basata rilievi post-evento e sulla modellazione idrologica, ha consentito di caratterizzare sette importanti eventi di piena improvvisa verificatisi fra il 2007 e il 2014 in diverse regioni dell'Europa centrale e meridionale. Nei bacini mediterranei gli elevati valori delle portate di picco, uniti alla durata relativamente lunga degli eventi, hanno determinato le condizioni favorevoli a significativi impatti geomorfologici. I valori della potenza della corrente sono generalmente coerenti con i cambiamenti morfologici osservati. Inoltre, i canali in roccia mostrano i valori di dispendio energetico più elevati ma senza erosioni apprezzabili, mente ingenti fenomeni di erosione sono stati osservati in canali alluvionali. Gli andamenti dei processi geomorfologici nei canali semi alluvionali richiedono il riconoscimento di situazioni locali che aumentano la resistenza del letto del canale e delle sponde all'erosione, o di condizioni specifiche di un particolare evento. Piene di breve durata causano talvolta abbondante trasporto solido, peraltro non associato a significativi allargamenti del canale nella maggior parte degli alvei semi-alluvionali. Otto corsi d'acqua, individuati fra quelli maggiormente interessati da tre delle piene studiate sono stati scelti per ulteriori analisi e per la modellazione della variazione longitudinale dei valori della potenza della corrente. Funzioni di potenza interpretano adeguatamente l'aumento verso valle delle portate di picco, mentre funzioni quadratiche si sono dimostrate più soddisfacenti delle relazioni esponenziali comunemente utilizzate per rappresentare la variazione longitudinale della pendenza dell'alveo. Le prestazioni dei modelli empirici per la variazione longitudinale della potenza della corrente per unità di larghezza dell'alveo (*unit stream power*) evidenziano il fondamentale controllo esercitato dalla pendenza dell'alveo. La disponibilità di immagini satellitari ad elevata risoluzione riprese prima e dopo gli eventi oggetto di studio ha permesso di valutare le modifiche del canale lungo sette di questi canali. Analisi statistiche hanno indicato che le sole variabili idrauliche non sono sufficienti per interpretare il tasso di allargamento del canale, che è principalmente influenzato dal grado di confinamento del canale stesso. Insieme al confinamento laterale, la potenza della corrente per unità di larghezza dell'alveo appare un valido predittore dell'allargamento in alvei ad elevata pendenza, mentre l'energia complessiva della corrente calcolata per l'intero evento fornisce prestazioni migliori nell'interpretare la variabilità dell'allargamento dell'alveo in canali a pendenza moderata. L'uso di differenti soglie di resistenza all'erosione per quantificare i cambiamenti geomorfologici degli alvei supporta la conclusione che la determinazione di tali cambiamenti è molto più difficile della determinazione delle variabili idrauliche coinvolte.

ACKNOWLEDGEMENT

First of all, I would like to thank my Creator, Lord and Saviour for the grace, mercies and protections throughout my life and academic career. I wish to express my profound gratitude to the Research Institute for Geo-hydrological Protection of the National Research Council of Italy (CNR-IRPI, Padova), for funding my PhD fellowship at the University of Padova (agreement no. 1681, dated 10/07/2013). This work contributed to the HyMEX programme (www.hymex.org) and was partly funded by the HYDRATE project (European Commission, Sixth Framework Programme, Contract No. 037024) and partly in the framework of NextData Project (Italian Ministry of University and Research and CNR). This gratitude also goes to the respective staffs of CNR-IRPI, Padova and the PhD School of Land, Environment, Resources and Health of the University of Padova for the administrative supports.

On a more personal level, I am particularly indebted to Dr. Lorenzo Marchi and Prof. Marco Borga for their supervision and guidance throughout this 3-year PhD period. I couldn't have wished for better advisors than these two Researchers with incredible collaborative chemistry. Special thanks to Prof. Ellen E. Wohl for hosting me at the Department of Geosciences (Colorado State University, USA) between June and November, 2015 and serving as a co-advisor for my PhD project. This PhD project has been partly carried out in collaboration with a PhD project by Margherita Righini supervised by Prof. Nicola Surian at the Department of Geosciences (University of Padova). The support of Dr. Davide Zoccatelli, Dr. Francesco Marra, Dr. Efthymios I. Nikolopolos and Dr. Stefano Crema, among others, whose participation in field surveys and contributions to data analysis and modelling did much to support the PhD project, are gratefully acknowledged. Specifically, Dr. Davide Zoccatelli and Dr. Francesco Marra are acknowledged for their collaboration in the implementation of the rainfall-runoff models and processing of radar-rainfall data, respectively. Prof. Luca Mao (Pontifical Catholic University of Chile) and Dr. Virginia Ruiz-Villanueva (University of Geneva) are acknowledged for serving as external evaluators of my PhD thesis and their positive evaluations that subsequently helped to improve the final document presentation.

My deepest gratitude goes to my family. To my parents, Mr. W. K. Amponsah and Ms. Victoria Yensu, I will forever remain thankful to you for your love and particularly your support through my basic, secondary and first-degree education. To my brothers George, Emmanuel and Louis and my sisters Gloria and Felba, thanks for your support and prayers. Last but not the least, to my nephews Kinsley, Emmanuel and Kenny, and my nieces Tracy and Jocelyne, I love you so much and am proud to be your uncle and a great role model.

To my love, Cathy.

ACRONYMS

a.s.l.	(Height) Above Sea Level
AMC	Antecedent Moisture Condition
ArcGIS	GIS software package developed by Esri
CET	Central European Time (UTC+01.00)
CN	Curve Number
DEM	Digital Elevation Model
EU	European Union
HG	Hydraulic Geometry
HWM	High Water Mark
HYDRATE	Hydrometeorological Data Resources and Technologies for Effective Flash Flood Forecasting
IPEC	Intensive Post-Event Campaign
KLEM	Kinematic Local Excess Model (Hydrological model)
MatLab	Matrix Laboratory
SCS-CN	Soil Conservation Service- Curve Number

CROSS-SECTION TYPES (XS TYPES):

AL	Alluvial
S-A	Semi-alluvial
BR	Bedrock
AT	Artificial

OBSERVED GEOMORPHIC EFFECTS (OGE):

M	Major
S-M	Small-to-Moderate
N	Negligible

TABLE OF CONTENTS

LIST OF FIGURES

LIST OF TABLES

1 INTRODUCTION AND DESCRIPTION OF THE STATE-OF-THE-ART WITH RESPECT TO FLOOD GEOMORPHIC EFFECTS

1.1 BACKGROUND AND JUSTIFICATION

Exceptional rainstorms can shed light on the geomorphic processes that shape the landscape. In the long standing debate of which event magnitudes are more significant in long term landscape evolution, i.e., frequent, moderate-size rain events (Wolman and Miller, 1960) or exceptional rain events (Hack and Goodlett, 1960), less is known about the latter (Kirchner et al., 2001). Wolman and Miller (1960) argued that events of moderate frequency and magnitude are more effective in doing geomorphic work (defined as mass transfer of sediments) than extreme rainstorm events because of the high frequency of occurrence. Baker and Pickup (1987), however, recognized that rare, large events play the most important geomorphic role in some fluvial environments, and 100-year floods may be necessary to transport the coarser sediment in some streams. As indicated by Kirchner et al. (2001), these formative events often arise from extremely episodic sediment delivery, dominated by events that are large but rare; so rare that they are unlikely to be reflected in measurements over years or decades. Typical of such rare events are floods that occur over limited spatial and temporal scales and in, an extreme case, described as '*flash floods in small basins that rise quickly and are gone in a matter of minutes*' (Costa and O'Connor, 1995, p. 55).

Flash floods are usually the consequence of short, high-intensity rainfalls mainly of spatially confined convective origin and commonly orographically enhanced (Gaume et al., 2009). Other flash flood types exist in the form of landslide-, man-made dam-, or glacial lake outbreaks, but those are typically designated by their specific name and are not considered here. Because of the limited duration of flash-flood triggering storms, the area of the impacted catchment is relatively small (generally less than 1000 km^2). The response time of flash floods therefore depends on both the catchment size and the activation surface runoff that generates the process (Marchi et al., 2010). The surface runoff generation process depends on the combination of rainfall intensity, antecedent moisture condition and soil hydraulic properties, which are influenced by land use changes, and climate change and variability. Land use changes resulting from socio-economic development and/or human influences are potential cause of the increasing frequency and severity of flash flood hazards as well as related risks (Marchi et

al., 2010; Borga et al., 2011). According to Huntington (2006), the global hydrological cycle has been intensifying due to global warming. This is supported by evidence of increasing heavy regional precipitation (Groisman et al., 2004; Beniston, 2009) and global precipitation (Groisman et al., 2005; Trenberth et al., 2007; Giorgi et al., 2011). Global climate change and variability could be responsible for the increase in the magnitude and severity of flood peaks in many regions of the world (e.g., Milley et al., 2002), through the impacts on storm–weather systems and river discharge conditions.

The co-occurrence of flash floods and major geomorphic effects is of particular concern, because it may amplify the hazard corresponding to the individual generative processes alone. Indeed, the simultaneous occurrence of intense flooding, landslides and/or debris flows may trigger cascading or progressive events (e.g., Helbing, 2013). These floods are commonly associated with widespread slope failures, and high flood power that causes significant erosion and sedimentation in alluvial channels and floodplains. Flash floods are therefore natural candidates for analysing the geomorphic effects of floods. Stream power has widely been used in literature as a measure of the geomorphic effectiveness of floods because its measures quantify river energy expenditure in fluvial systems (Rhoads, 1987). Several studies (e.g., Miller, 1990; Magilligan, 1992; Costa and O'Connor, 1995; Magilligan et al., 2015; Marchi et al., 2016) have built on the pioneering work by Baker and Costa (1987) to explore river energy expenditure associated with extreme rainstorms that are usually responsible for major and abrupt morphological changes in river channels and valley floors. Energy expenditure (or dissipation) plays a key role in fluvial and geomorphic processes (i.e., supply and transport of water and sediment loads). This is because as potential energy of runoff across the basin is converted into kinetic energy, most of the energy is dissipated by friction at the channel boundary (grain, form, system roughness), morphological adjustment (bed and bank erosion) and in sediment transport (Molnar, 2013). Stream power therefore represents the time rate of energy lost as water flows downstream in channel reaches, and provides an effective measure of energy available to drive fluvial, geomorphological and ecological changes (Barker et al., 2009).

Geomorphic modification is expected to occur in river channels when driving forces (i.e., hydraulic and abrasive forces of water and sediment acting on the channel) exceed threshold of resisting forces (i.e., the ability of channel boundaries to remain unchanged by the passage of water and sediments). However, these driving and resisting forces that determine the capacity of floods to modify

existing channel configuration are extremely difficult to quantify (Wohl et al., 2001; Kale, 2008). Stream power measures associated with geomorphic effectiveness of extreme floods are usually estimated in relation to peak instantaneous discharge, either at-a-station (e.g., Baker and Costa, 1987; Miller, 1990; Magilligan, 1992; Wohl et al., 2001), or along the longitudinal profile of channel reaches (e.g., Lawler, 1992; Lecce, 1997; Knighton, 1999; Fonstad, 2003; Reinfelds et al., 2004; Barker et al., 2009; Surian et al., 2016), or with respect to spatial variability across different climatic and topographic regions (e.g., Marchi et al., 2016). Lawler (1992) initially revealed a theoretical assumption of non-linear downstream variations in stream power, which has been confirmed through empirical studies by Lecce (1997), Knighton (1999), Fonstad (2003) and Reinfelds et al. (2004). Significant advances have also been made in the representation of the spatial distribution of stream power and other hydraulic and topographic variables, through use of high resolution *DEM,* which led to the development of useful stream assessment tools (e.g., Reinfelds et al., 2004; Barker et al., 2009; Krapesch et al., 2011; Vocal Ferencevic and Ashmore, 2012; Thompson and Croke, 2013; Parker et al., 2014). Spatial representation of stream power sheds more light on how the geographical variability of energy expenditure within a high mountain stream basin could fully capture the variability in geomorphic effects (e.g., Fonstad, 2003).

The hydrologic and geomorphic impacts of extreme floods in a valley (i.e., erosion and sedimentation) are highly contingent on time- and place-specific factors, which make it important to examine geomorphic effects of flash floods in a variety of situations (Phillips, 2002). The study of the relations between floods and geomorphic changes in channels is fully within the scope of *hydrogeomorphology*, a research approach that has been defined by Sidle and Onda (2004 p. 598) as '*an interdisciplinary science that focuses on the interaction and linkage of hydrologic processes with landforms or earth materials and the interaction of geomorphic processes with surface and subsurface water in temporal and spatial dimensions*'. Indeed, the geomorphic effectiveness of extreme floods is likely to depend on the combined influences of the geological controls on channel geometry and sediment characteristics, as well as on variations in flood intensity. The time- and place-specific hydrologic and geomorphic settings that control the spatial distribution of stream power are therefore very crucial in quantifying the geomorphic effects of flash floods for a specific catchment and/or hydro-climatic region (Costa and O'Connor, 1995). The variation of stream power and other

topographic controls (mainly channel gradient and geo-lithologic features) along the longitudinal profile of river channels could better explain the intricate downstream geomorphic processes including sediment yield, transport and deposition during rainfall-runoff events (Knighton, 1999; Reinfelds et al., 2004). Coupling reach-level channel processes with the spatial arrangement of the reach morphologies, their interaction with hillslope processes and external forcing by confinement, riparian vegetation and woody debris enhances understanding and predicting channel responses to both human and natural disturbances, because the gradient and morphology of mountain channels are highly variable and prone to forcing by external influences (Montgomery and Buffington, 1997).

On the other hand, we note that flash floods are very difficult to observe, due to the mismatch between the space-time scales of occurrence and the features of the typical hydrometeorological sampling networks (Borga et al., 2011). The recognition of the poor observability of flash floods has stimulated the development of a post-event monitoring methodology in the last decade, which involves post-flood indirect estimation of peak discharges and the use of weather radar observations for hydrological modelling. These observations provide the link between the real-world processes and the perceptual and mathematical models developed to understand flash flood responses and make predictions for unobserved variability. The observation strategy was developed under the *EC FLOODsite* project (Gaume, 2006) and refined and tested under the *EC HYDRATE* project (Borga et al., 2011). The objective is to collate flash flood data by combining hydrometeorological monitoring and the acquisition of complementary information from post-flood surveys (Gaume and Borga, 2008; Borga et al., 2008; Marchi et al., 2009a). The systematic application of this observation strategy in specific regions permitted the development of a freely accessible European Flash Flood Database including hydrometeorological data and related observations concerning a wide number of flash flood occurrences in Europe since 1998 (Borga et al., 2011). Part of this archive is used, together with data from more recent flash floods, as the reference database for the work proposed in this thesis.

It should be remembered that investigations on the geomorphic effects of flash floods have significant impacts on the management of the relevant flood and geomorphic risks (Borga et al., 2014). The occurrence of flash floods and associated hazards has been a major concern in hydrology and natural hazard sciences, in terms of the proportion of fatalities and economic losses during individual events (Marchi et al., 2010). Both event- and long-term flood risk analysis and management approaches

are gaining ground and fall within the EC '*Directive on the assessment of flood risks (2007/60/EC)*'. Significant progress has been made in the last decades in the risk management of flash floods and geomorphic hazards (mainly shallow landslides and debris flows), predominantly considered in isolation. However, effective response to the problem posed by the management of the combined occurrence of flash flood and geomorphic hazards requires more than the recognition of the two individual sources of risks. With the joint occurrence of both large specific discharges and erosion at almost the same spatial scale, channel configuration becomes unstable due to sediment input from landslides and/or debris flows. Furthermore, these are associated, under appropriate conditions, with recruitment and transport of large wood (Wohl et al., 2009; Comiti et al., 2016). The analysis of the combined effects of these multiple hazard sources requires the identification of the spatial scale where the hazard coupling occurs and the development of an adequate integrated process analysis.

1.2 The Fluvial System

1.2.1 Forms and processes

The fluvial system is a landscape unit consisting of different morphological elements that are connected by hillslope and fluvial processes and driven by water and sediment transport. Hillslopes constitute about 90% of the global ice-free landscape, whereas river bodies and their floodplains occupy the remaining 10% (Huggett, 2007). Hillslopes receive precipitation and supply runoff and sediments into river channels, which then drain and transport the runoff downstream within the channel reach. The predominant types of river channels are bedrock, alluvial, and semi-controlled or channelized channels (Huggett, 2007). *Bedrock* channels cut into bedrock in their upper reaches where steep gradients and coarser bed load materials are dominant. These channels are resistant to erosion and tend to persist for long periods without significant changes. *Alluvial* channels, on the contrary, are usually formed through the transport of sediments by the action of flowing water and are less resistant to erosion compared to bedrock channels. Their formation and development depend on the variability in the grain size of the alluvium, which ranges from clay to boulders. Changes in their forms are highly influenced by changes in discharge and sediment supply. *Channelized* streams are structurally engineered (human-influenced) to control floods, improve drainage and maintain navigation.

River channels are classified according to the morphology of their plan and bed forms. In plain view, alluvial channels exhibit five forms of graded series – straight, meandering, braided, wandering and anastomosing. These classifications are usually applicable to long channel reaches or large basins and are distinguished by entrenchment, gradient, width/depth ratio and sinuosity (e.g., Leopold et al., 1960; Rosgen, 1994). On the basis of bed forms, Montgomery and Buffington (1997) categorized seven distinct reach types in mountain streams – bedrock, colluvial and five alluvial channels (cascade, step-pool, plane bed, pool riffles and dune ripples) – based on Schumm's (1977) general delineation of erosion, transport and deposition processes. These classifications are based on channel slope, drainage area, relative bed roughness and the bed-surface grain sizes. The relative magnitudes and trends of sediment supply and transport capacity exhibit significant influence on the stability of alluvial channels (Montgomery and Buffington, 1997).

Streams are powerful geomorphic agents capable of eroding, transporting and depositing sediments by the fluvial action of flowing water. The largest size of sediment that can be moved in traction as bed load defines a stream's *competence,* while its *capacity* describes the maximum amount of debris that can be carried in traction as bed load (Huggett, 2007; Wainwright et al., 2015). The capacity of a stream to do geomorphic work is related to its *power*, i.e., the rate at which a stream works by transporting sediments, overcoming frictional resistance and generating heat (Wolman and Miller, 1960). The three main fluvial processes in alluvial channels (sediment production, transport and deposition) are presented in an idealized model of the fluvial system in Fig. 1.1 (Schumm, 1977). Upstream reaches dominate the sediment production or erosional landform (Zone 1). This is also the water and sediment source area. The main river channel is characterised by sediment transport (Zone 2) as a result of the high energy gradient of the flowing water, whereas depositional landforms (Zone 3) store sediments because of the abrupt change in topographic gradient. In reality, sediment production (erosion), transport and deposition are interconnected, complex processes that occur at almost the same spatial scale (Lee, 2005). However, these processes are dominant in the respective zones as illustrated in Fig. 1.1 (Grant et al., 2013), which are influenced by the flow and sediment characteristics together with the topographic gradient along a channel-reach.

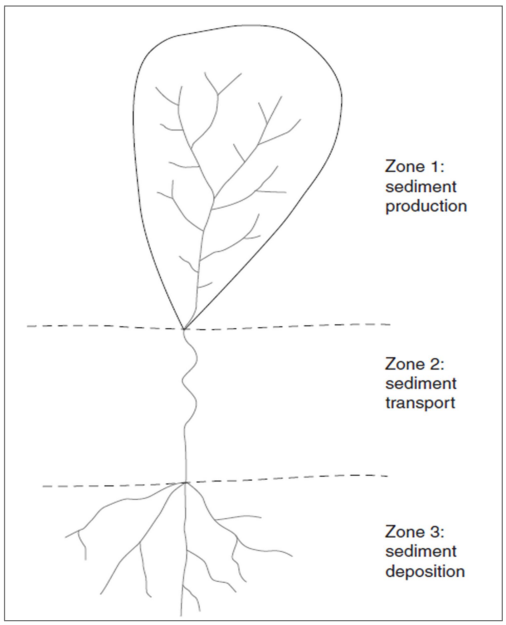

FIG.1.1. Idealized model of the fluvial system (Schumm, 1977) (*Adapted from Grant et al., 2013*).

Streamflow causes channel bed and bank erosions under suitable flow and channel conditions. Streams attack their channel beds and banks by three main erosional processes: corrosion, corrasion and cavitation (Huggett, 2007). *Corrosion* refers to the chemical weathering of beds and banks by streamflow that produces dissolved stream loads. *Corrasion* (abrasion) describes the wearing away of surfaces by the shear action of particles moving with the water body. Evorsion is a form of corrasion caused by the action of flowing water with negligible effect of stream load. This latter process is termed 'hydraulicking' in alluvial channels and describes the removal of loose materials by the action of water alone. This is also known as 'plucking' in alluvial channels and 'quarrying' in bedrock channels. *Cavitation* on the contrary, is a process whereby high flow velocity causes sufficiently large reduction in absolute pressure of the flowing water such that the water vapour pressure is reached. The water vapour occurs in small bubbles or voids, which implode and generate intense shockwaves that smash into channel walls and cause intense erosion, typical of bedrock channel erosion processes (e.g., Baker and Kale, 1998). Streams may erode their channels downwards (vertical erosion) or sideways (lateral erosion) (Huggett, 2007). *Vertical* erosion in alluvial channels is identified as a net removal of sediments, characterized by channel bed aggradation and degradation processes. *Lateral* erosion

usually occurs during flooding, when the channel banks are worn away due to bank overflow. This is also accomplished when streamflow undercuts the channel bank, which leads to slumping and bank collapse.

A river in flood demonstrates sediment transport from source to mouth under different conditions. Materials carried in streamflow (stream loads) are classified as dissolved, suspended and bed loads (Lee, 2005; Huggett, 2007). The flow conditions within a river reach determine the composition of solid-debris load (combination of suspended and bed loads). Solid-debris loads may move as singles or groups by rolling or sliding along channel beds and banks. The movement partly depends on the grain size and shape – coarse grains move more easily and faster than fine particles, while rounded particles move more readily than flat and angular ones (Huggett, 2007). Bed load moves more slowly in traction than the water flow and hence requires high flow velocity for traction. Stream power has widely been used as a basis to quantify sediment transport in fluvial systems (Bagnold, 1977).

Rivers deposit stream loads anywhere along their course but mainly at locations with low gradients (e.g., valley bottoms), with abrupt change in gradient and where channels diverge, causing a reduction in flow depth and velocity (Huggett, 2007). Stream loads may be deposited along channels, on channel margins, on valley margins, as overbank floodplain deposits or on alluvial fans. Stream erosion and deposition are dominant during flood events, characterized by high specific discharges and flow velocities. Erosion rates increase with discharge and velocity and hence streambeds are significantly scoured during floods. As a flood abates, sediments are redeposited along the channel network subject to suitable flow and channel conditions. Changes in sediment storage and overall channel form along a river reach after flood events strongly depend on the magnitude of the flow forces to erode and transport sediments on one hand, and the channel boundary forces to resist bed and bank erosion on the other hand. Therefore, for a specific channel reach, geomorphic changes are likely to depend on magnitude and history of external perturbations.

1.2.2 Channel hydraulic geometry

Hydraulic geometry (HG) describes the relationships between the mean stream channel form (width, depth, cross-section, meander length) and discharge both at-a-station and downstream along a

stream network in a hydrologically homogeneous basin (Singh, 2003). Changes in channel hydraulic properties (channel top width, flow depth, and mean flow velocity) have been shown to depend primarily on the variations in discharge (Leopold and Maddock, 1953; Wohl and Wilcox, 2005) rather than the usual 'master variable' – drainage area (e.g., Modrick and Georgakakos, 2014 and references therein). The dependency of hydraulic geometry on variations in discharge is obvious for flash floods, which are characterized by strong spatial gradients of rainfall inputs that hit different parts of a river basin with different intensity. While simple HG relates specifically to at-a-station hydraulic geometry (AHG), regime theory is more related to downstream hydraulic geometry (DHG) (Gleason, 2015). Another distinction relates to the reference discharge: mean annual and bankfull discharge are usually used to describe HG, whereas stable, regime discharge is used for regime theory (Clifford, 2004).

Regime theory describes the relations amongst governing equations used to predict the geometry of a stable channel if discharge and sediment supply and characteristics are known (Eaton et al., 2004; Kaless et al., 2014). Singh (2003) discussed a number of theories governing channel hydraulic geometry but pointed out that the classic work of Leopold and Maddock (1953) still remains the benchmark contribution. These power function relations have been validated using a set of data at mean annual discharge (Dury, 1976) and shown to be similar over varying environments (Chong, 1970), although Park (1977) argued that simple power functions may be misleading. For example, the downstream power function models may not reflect the true hydraulic nature if the rate of change in channel roughness, confinement and slope are not uniform (e.g., Richards, 1973, 1976). Nevertheless, the work of Leopold and Maddock (1953) is the basis in recent studies on regime theories of hydraulic geometry (Eaton et al., 2004; Wohl and Wilcox, 2005; Kaless et al., 2014; Gleason, 2015). Correlations between (bankfull) discharge, Q [m^3 s^{-1}], and the corresponding cross-sectional channel top width, w [m], flow depth, d [m] and mean flow velocity, V [m s^{-1}] usually take the form of power-law regressions as follows (Leopold and Maddock, 1953):

$$w = a \cdot Q^b \quad [1.1]$$

$$d = c \cdot Q^f \quad [1.2]$$

$$V = k \cdot Q^m \quad [1.3]$$

such that, $b + f + m = 1$; and $a \cdot c \cdot k = 1$, since $Q = w \cdot d \cdot V$.

Eaton et al. (2004) developed a theoretical rational regime model for predicting equilibrium alluvial channel form. The model is based on three relations that govern geometry of a canal (Henderson, 1966): (i) a bed material transport equation; (ii) a flow resistance equation; and (iii) a bank stability criterion. The model combines independent governing variables (discharge, sediment supply and characteristics, and channel gradient) to define a dimensionless alluvial state that exhibits unique values of Froude number and sediment concentration. Kaless et al. (2014) used the concept of regime theory based on models that incorporate external hypothesis (Miller, 2005) and other physically based models (Ikeda et al., 1988; Parker et al., 2007), to explain morphological changes and to predict potential recovery in Italian rivers under the classical hypothesis that, while channel width and depth adjust quickly to changes in discharge and sediment supply, reach slope persists over longer time spans.

Gleason (2015) discussed the importance of the utilities of channel hydraulic geometry of natural rivers as well as aspects that may direct future research. Hydraulic geometry is useful for the following reasons: (i) rating curves based on hydraulic geometry provide critical discharge monitoring capacity of rivers, (ii) applied to estimate flood risks and extent, (iii) investigate flow conditions in the distant past, and (iv) understand river habitat conditions. Gleason (2015, p. 19) highlighted the main issues with the use of hydraulic geometry by noting that: '*The utility of hydraulic geometry is unquestioned, but its elevation from empirically observed relationship to physical principle is not complete, despite universal acceptance of its existence. It may be that such a transition is never made, in which case future research of hydraulic geometry will focus almost exclusively on its applications.*'

1.3 Flash Floods: Observations and Characterisation

Flash floods are generated by extreme rainstorms that occur in basins that are relatively small and with short response time (Borga et al., 2007; Marchi et al., 2010). Flash flood occurrences are characterised by large spatial and temporal variability of precipitation in complex terrains that make monitoring and forecasting of rainfall very difficult (Borga et al., 2010). There exists a substantial body of work on physical flood processes in small research catchments where processes can be observed by field campaigns and detailed instrumentation (e.g., Delrieu et al., 2005; Boudevillain et al., 2011).

However, a central problem in the study of extreme floods and flash floods is that investigations are focused precisely in the realm of events that are locally rare and spatially limited and characterized by spatially highly heterogeneous precipitation forcing, and peak discharge distributions even within small catchments, with the majority of highly impacted small tributaries usually ungauged (Gaume and Borga, 2008). Dunne (1978, p. 290) characterizes this problem by noting that "*within a particular basin, the dominant runoff process may vary with the characteristics of rainstorms. Even the highest infiltration capacities of forest soils will not accommodate the highest recorded rainfall intensities.*"

The main challenges affecting flash flood predictions are tied to the relevant temporal and spatial scales of their occurrence. Fig. 1.2 presents the monitoring capabilities and the scales of convective cells, mesoscale convective systems (MCS) and fronts that usually trigger extreme floods. The flash floods in Fig. 1.2 are characterized by small spatial and temporal scales (usually less than 1000 km^2 and 36 hours, respectively). The mismatch between the spatial and temporal scales of flash flood occurrences and the associated conventional rainfall and river discharge measurement networks makes such events very difficult to observe (Creutin and Borga, 2003; Borga et al., 2010).

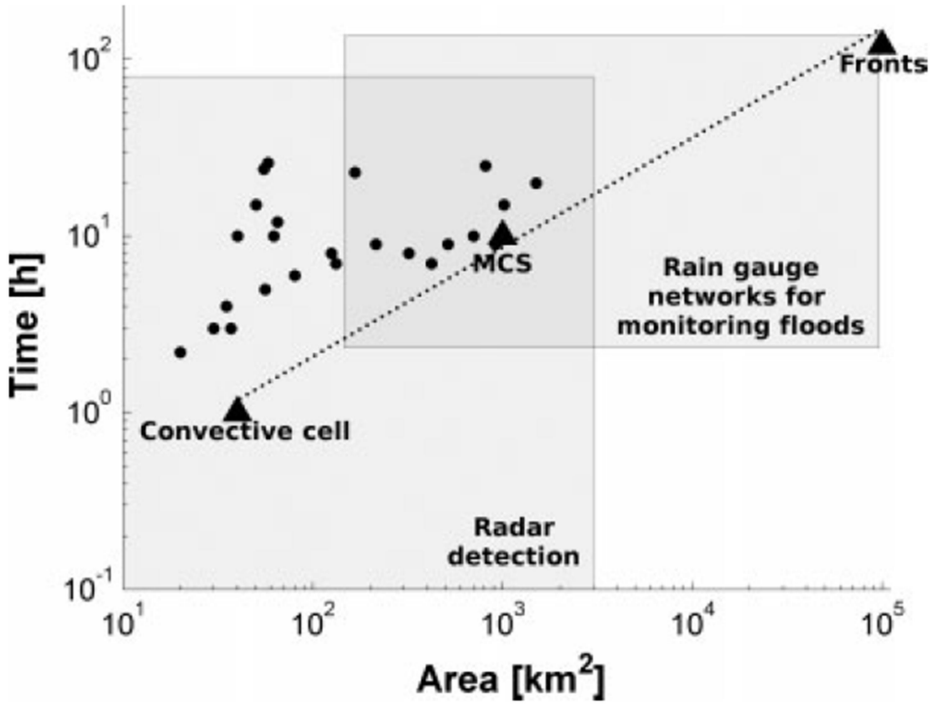

FIG.1.2. Spatio-temporal scales of flash flood-triggering storms versus monitoring capabilities of radar and raingauge networks. Dots represent a number of flash flood generating storms observed in Europe (Borga, 2007) (*Adapted from Borga et al., 2008*).

Lack of long-term hydro-meteorological data with the appropriate spatial and temporal resolutions has rendered the process understanding of these extreme events relatively poor (Borga et al., 2008). Observation of such extreme events using raingauge networks is uncertain. Although the accuracy of weather radar rainfall estimates are influenced by orography (Pellarin et al., 2002; Germann et al., 2006), they provide relatively better spatial rainfall representation compared to rain gauge networks (Fig. 1.2). However, BASC (2005) demonstrated that radar rainfall estimations become less reliable with high intensity rainfall; which characterises flash floods.

The challenges affecting flash flood investigations are highly linked to the uncertainties affecting the estimation of spatially variable precipitation forcing, the complexity of the hydrogeomorphic response of the physical processes and the potential co-occurrence of flash floods and other hazards (e.g., debris flows and/or landslides). These challenges may affect the quality of flash flood predictions (Collier, 2007) and may pose uncertainties in flash flood warning procedures in real-time, which plays a key role in the design and planning of flood risk management measures (Norbiato et al., 2008). The need for coping with these hazardous phenomena has stimulated research on meteorological, hydrological and hydraulic aspects of flash floods (Borga et al., 2010), as well as on their social impact (Ruin et al., 2014). A proposed methodology for post-flash flood survey (Gaume and Borga, 2008) plays a critical role in gathering essential observations concerning flash floods, thereby '*gauging the ungauged extremes*' (Borga et al., 2008). The key methodologies involved are: (i) use of radar rainfall estimates for water balance and hydrologic response analysis; (ii) post-event survey to document geomorphic effects and peak discharges, and (iii) eye-witness interviews to establish the chronology of the event. Standard use of post-flood surveys has been recommended to gather flood peak magnitude and timing with the objective to advance understanding of flash floods and causative processes (Lumbroso and Gaume, 2012; Le Boursicaud et al., 2016). Traces left by water and sediments during a flood provide an opportunity for assessing peak discharge by means of detailed post-flood surveys along the channel network. The spatially detailed flood peak estimates may be compared with the flood simulations from hydrological models driven by the space–time estimates of rainfall typically obtained by means of radar rainfall analysis, with the objective of evaluating the consistency between the rainfall and discharge observations. The hydrological simulations so obtained ensure closure of the water balance at the event scale and consistent dynamics of the rainfall-runoff sequence.

Characterising flash floods over various spatial and temporal scales is very important in climatic and hydrologic studies . This is typically built on investigations to examine the control of watershed physiographic and channel network geometry to flood response (Gaume et al., 2009). Climate variability influences flood-generating processes in two ways. First, directly through the variability of precipitation and flow characteristics (Lane et al., 2007) and secondly, in an indirect way associated to its effect on the seasonality of rainfall and evapotranspiration, which affect the water balance of catchments for specific storm events (Sivapalan et al., 2005). Catchments under energy-limited conditions are mostly predominant in humid climatic regions, which affect the antecedent moisture condition of soils for individual storm events. As an example, Penna et al. (2011) found that soil moisture exerts strong influence on runoff in an alpine headwater catchment. European flash floods occur both under energy-limited conditions and under water supply-limited conditions; the latter characterise Mediterranean environments (Marchi et al., 2010). Climate may also influence runoff response to extreme rainstorms through the control of soil formation and erosion processes.

Orographic effects causing rainfall and topographic relief accelerating concentration of stream flow are the main mechanisms associated with a catchment's physiographical factors that affect flash flood occurrence (O'Connor and Costa, 2004). The orography of a basin plays a major role in the type, amount, intensity and duration of precipitation events. In addition, orography is one of the important elements that causes convective systems (Davolio et al., 2006). This is why flash floods are predominant in regions of steep terrain. Heavy convective rains may fall on plains, but to promote high flow concentration along drainage paths, the topographic relief of a catchment plays a key role in ensuring a kinematic component that propagates high discharges over diverse time scales and produces the hazard potentials of flash floods. Hillslope and channel gradients and the ratio of catchment area to channel length are the basic characterization of the steepness or topographic relief of a catchment (Collier and Fox, 2003).

Rainfall amount and duration are the main characteristic variables of rainstorms that control flash flood generation and are controlled by the local climate. The relationship between total event rainfall accumulation and duration gives a clear idea about the intensity and severity of a storm event. For similar total event rainfall depths, shorter rainfall duration would produce higher peak discharges than long rainfall duration over a specific catchment and hence intense and severe floods, which is a

characteristic feature of flash flood-generating rainstorms. However, rainstorm characteristic relationship between rainstorm duration and the ratio of total event rainfall to mean annual precipitation provides a context to compare rainstorms under different climatic conditions, most importantly considering the differences in the mean annual precipitation. Flash floods are locally rare and therefore the impacts of flash flood-generating rainstorms on the local annual water balance for different climates may vary. Marchi et al. (2010) reported that the ratio of event to annual precipitation in Mediterranean climatic regions is generally higher than that of Continental, Alpine and Alpine-Mediterranean regions. In addition, major flash floods in the Mediterranean region (e.g., Italy, southern France and Spain) occur in the autumn months, whereas those in the Continental region (e.g., Germany, Austria and Romania) mostly occur in the summer months. These analyses have revealed smaller spatial extent and duration for Continental events compared to Mediterranean events. This shows the seasonality effects and associated space-time scales in the distribution of flash flood events across different climatic regions in Europe.

One of the important characteristics of flash floods is the high magnitude of unit peak discharges (i.e., peak discharges normalized by the upstream contributing area) produced. Gaume et al. (2009) developed the following envelope curve for the relationship between unit peak discharges and catchment area for multiple flash flood events in Europe:

$$Q_u = 97.0 \cdot A^{-0.4} \qquad [1.4]$$

where Q_u [m^3 s^{-1} km^{-2}] is the unit peak discharge and A [km^2] is the upstream contributing area. The exponent in the power-law relationship (Eq. 1.4) is smaller than that resulting from another study on high magnitude floods in Europe (Herschy, 2002) and that developed for the analysis of 41 maximum floods in the world (Herschy and Fairbridge, 1998). This can be ascribed to the fact that these analyses included other flood types.

The importance of analysing flash floods is the potential ability to reveal unexpected hydrological behaviour on the basis of weaker response or unobserved behaviours which might be anticipated (Delrieu et al., 2005; Archer et al., 2007; Borga et al., 2007), hence enhancing the learning process and understanding of these extreme events. Documenting runoff response to extreme storms also provides a

guidance to extend hydrological predictability with increasing storm severity (Blöschl and Zehe, 2005). Marchi et al. (2010, p. 119) expressed the importance of flash flood characterisation by noting that: '*Characterising the response of a catchment during flash flood events, thus, may provide new and valuable insights into the rate-limiting processes for extreme flood response and their dependency on catchment properties and flood severity*'. In conclusion, flash flood investigations aim at identifying the landscape and hydro-climatic variables that control hydrogeomorphic response to extreme rainfalls.

1.4 Flood Power: Shear Stress and Stream Power

An important concept in fluvial geomorphology is the '*flood power*', which is linked to the geomorphic effectiveness of floods in channels and valley floors (Baker and Costa, 1987). Fluvial adjustments only occur when the flood power exceeds the channel boundary resistance threshold, which depends on river bed and bank cohesive forces along the channel reach. The boundary shear stress and stream power are the two dominant expressions that characterize flood power (Magilligan, 1992). Channel boundary shear stress and stream power have been shown to be more useful concepts than discharge alone in assessing the potential of floods to cause geomorphic changes (Baker and Costa, 1987). Therefore, the magnitude of geomorphic adjustment for any flood event can be focused on flood power, which represents the flow energy and not just the (peak) discharge (Magilligan, 1992; Knighton, 1999).

A body of water moving downstream along a channel reach exerts an instantaneous shear force on the wetted perimeter of the channel cross section that is equal to the downslope component of its weight. Shear force per unit wetted area is given by:

$$\tau = \rho \cdot g \cdot R \cdot S \qquad [1.5]$$

where τ [N m^{-2}] is the shear stress or tractive force, ρ [1000 kg m^{-3}] is the density of water, g [9.81 m s^{-2}] is the gravitational acceleration, R [m] is the hydraulic radius and S [m m^{-1}] is the channel or energy gradient (defined as $\Delta H/X$ with reference to Fig. 1.3). The shear stress defines a stream's ability to set a sediment particle in motion; hence, it is directly related to the transport capacity of the stream flow

(Rhoads, 1987). Work is performed when the body of water moves downstream through a distance, as the gravitational potential energy of the flowing water is converted to kinetic energy (Fig. 1.3).

The concept of stream power was first introduced by Bagnold (1966) and has since been used extensively as a basis to quantify sediment transport (Bagnold, 1977), explain bedrock channel incision (Whipple et al., 2000), bank erosion (Lawler et al., 1999), channel pattern (Chang, 1979) and riparian habitat development (Bendix and Hupp, 2000). Stream power is therefore an effective measure of energy available to drive fluvial, geomorphological and ecological changes (Barker et al., 2009). The term stream power is associated with flowing water having the properties of mechanical power (Rhoads, 1987), which is defined by McEwen (1994, p. 359) as *'the rate of energy supply at the channel bed that is available for overcoming friction and transporting sediments'*. Rhoads (1987) found the literature on stream power confusing and therefore proposed a standardized nomenclature for the application of its associated measures. However, the commonly used term in literature is the stream power per unit channel length, Ω [W m^{-1}], referred to as *cross-sectional stream power* and expressed as:

$$\Omega = \rho \cdot g \cdot Q \cdot S \qquad [1.6]$$

where Q [m^3 s^{-1}] is the flood discharge. Stream power per unit-wetted area is termed *unit stream power*, ω [W m^{-2}] and expressed as:

$$\omega = \Omega / w \qquad [1.7]$$

where w [m] is the top channel width corresponding to the flood level. Substituting Eq. [1.5] and [1.6] into Eq. [1.7] and approximating channel width as the wetted-channel perimeter yields:

$$\omega = \tau \cdot V \qquad [1.8]$$

where V [m s^{-1}] is the average flow velocity. The various stream power variables presented in Fig. 1.3 are defined above, except for power per unit weight of water VS, which is often not applied as a measure of stream power (Rhoads, 1987).

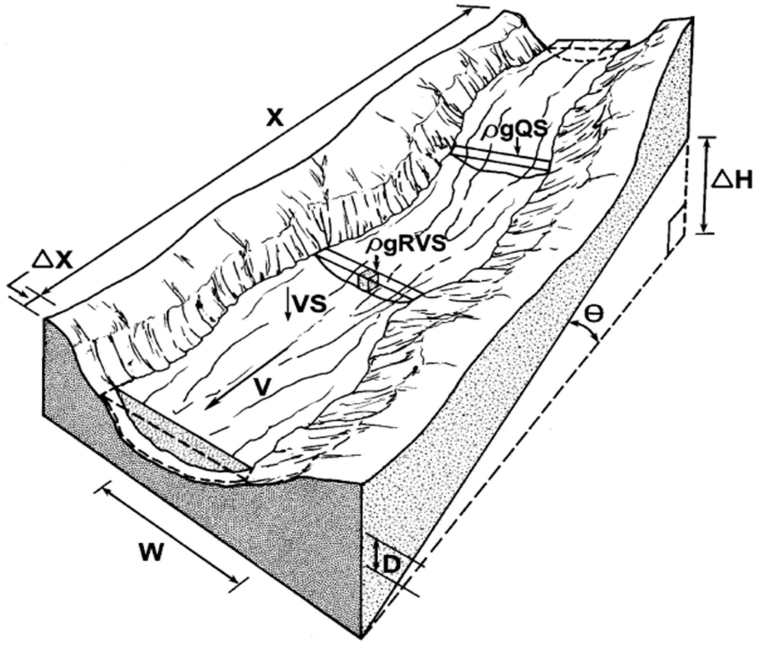

FIG.1.3. Channel dimensions describing stream power variables (*Adapted from Fonstad, 2003*).

The downstream variation in stream power is primarily influenced by the interplay of catchment hydrology, channel gradient and degree of confinement, which usually changes systematically along the longitudinal profile of river channels (Knighton, 1999; Reinfelds et al., 2004). Lawler (1992) initially developed a conceptual model for the spatial distribution of stream power by establishing empirical relationships among downstream changes in hydraulic properties of rivers. The model suggests that the downstream changes in discharge, Q [m^3 s^{-1}] and slope, S [m m^{-1}] are better represented respectively by power and exponential functions of the channel length, L [m] as follows:

$$Q = \alpha \cdot L^{\beta} \quad [1.9]$$

$$S = S_o \cdot e^{-rL} \quad [1.10]$$

where α and β are dimensionless power function constants, S_o [m m^{-1}] is the initial slope at an upstream reference section and r is the coefficient of slope reduction. Substituting Eq. [1.9] and [1.10] into [1.6] yields a generalized reach-scale downstream change model for cross-sectional stream power:

$$\Omega = [\rho \cdot g \cdot (\alpha \cdot L^{\beta}) \cdot (S_o \cdot e^{-rL})] \quad [1.11]$$

The model shows a non-linear downstream change in stream power and suggests an intermediate location of maximum total stream power along the longitudinal profile of channel reaches. This theoretical assumption has been confirmed through empirical studies by Lecce (1997), Knighton (1999) and Reinfelds et al. (2004). Lawler (1995) and Knighton (1999) further predict that unit stream power is expected to peak about half way between the source of river and the location of the maximum cross-sectional stream power. Magilligan (1992) recognized two main controlling factors on stream power in relation to differing geo-lithological features which may be responsible for the non-linear downstream pattern. At-a-station, the dominant control on stream power is attributed to the local geologic and geomorphic characteristics whereas the general downstream changes in the longitudinal profile of rivers control the downstream variations in stream power. Lithological controls on valley width and channel slopes reflect the irregular downstream pattern of stream power, especially in relation to valley width (Magilligan, 1992). Narrow (usually resistant) valleys convey large amounts of runoff during large magnitude floods as the increasing rate of flood depth increases, thus maximizing flood power, while wide valleys on the other hand minimize flood power due to limited boundary resistance.

The effect of flood power on the fluvial system includes a variety of sedimentologic and hydraulic processes such as suspension of gravels, erosion of alluvial and bedrock channels, movement of large diameter boulders and the transport of large quantities of sediment (Baker and Costa, 1987). In relation to sediment transport, Baker and Costa (1987) reported that exceptionally powerful floods with shear stresses of 1000 N m^{-2} can transport gravels of diameter between 10 and 30 cm as suspended loads. Also, Williams (1983) reported that unit stream power of about 1000 W m^{-2} can move boulders of approximately 1.5 m in diameter, whereas shear stresses of about 500 N m^{-2} will move boulders of approximately 3 m in diameter. In relation to erosion intensity, Miller (1990) and Magilligan (1992) identified a unit stream power value (300 W m^{-2}) as the potential threshold above which significant geomorphic adjustment is likely to occur in unconfined channel reaches. This threshold, usually referred to as the Miller-Magilligan critical threshold (e.g., Kale, 2008), although perhaps questionable for universal acceptance, has been used and supported in several studies (e.g., Hauer and Habersack, 2009; Ortega and Heydt, 2009; Thompson and Croke, 2013; Buraas et al., 2014). However, Magilligan (1992) highlighted that this value is not rigidly an absolute threshold, but represents a close

approximation of the minimum threshold. Miller (1990, p 128) expressed the relations among flood power, erosion intensity and channel-reach morphology types by noting that: *'The largest values of unit stream power and boundary shear stress are developed in bedrock canyons, where the boundaries are resistant to erosion and the flow cross-section cannot adjust its width to accommodate extreme discharges'.*

In relation to comparing the geomorphic effectiveness of different flood events at the channel-reach scale, Costa and O'Connor (1995) considered the importance of flood-flow duration and cumulative energy expenditure by developing a conceptual model that combines flow duration, stream power per unit area and threshold for alluvial and bedrock channel erosion. However, it should be noted that quantifying landscape-scale erosional thresholds is much more difficult than quantifying the hydraulic forces. Three distinct flood types are identified in the conceptual model with respect to the combined influence of flood-flow duration and cumulative energy expenditure on quantifying the geomorphic effectiveness of extreme floods (Fig. 1.4).

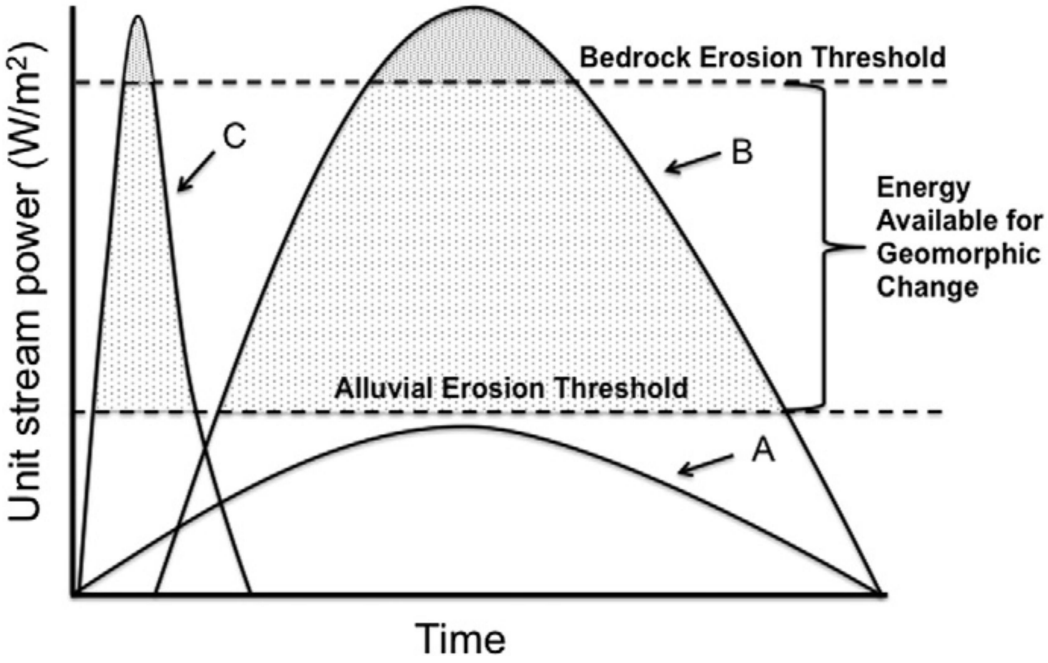

FIG.1.4. Conceptual model of Costa and O'Connor (1995) describing the relative role of flow duration and unit stream power in generating an effective flood (*Adapted from Magilligan et al., 2015*).

Curve A represents floods with long duration and large cumulative energy expenditure but low peak instantaneous stream power that may not be effective channel- and floodplain-disrupting events. Curve B corresponds to floods with a combination of high peak instantaneous stream power, sufficient flow duration and large cumulative energy expenditure, which may significantly alter landforms. Curve C represents floods with very large peak instantaneous stream power per unit area but low cumulative energy expenditure (as a results of short flow duration), which may also not be effective events. The shortfall of the model is to evaluate a feasible critical landscape-scale erosion-resistant threshold to estimate the proportion of cumulative energy available for significant geomorphic changes. In a nut shell, while peak instantaneous stream power values are necessary to cross landscape-scale erosional resistant thresholds to significantly disrupt channels and floodplains, flow-duration and cumulative energy expenditure may also play important roles in assessing the geomorphic work of the flow.

1.5 Geomorphic Effects of Flash Floods on the Fluvial System

1.5.1 Concept

Flash floods usually occur in small-sized, rugged-relief catchments in mountain areas. The combined effect of very intense rainstorms and high specific discharges is such that the occurrence of flash floods in complex terrain represents an important geomorphic agent in the fluvial system. Given the association of large runoff generation and steep topography, it is not surprising that where abundant sediment is available for entrainment, flash floods are associated with debris flows, erosion and sediment transport (Borga et al., 2014; Bodoque et al., 2015). However, the large spatial variability of precipitation forcing and geomorphological settings associated with the occurrence of flash flood in complex terrains implies that the corresponding geomorphic response would vary even within small catchments. A basin's response to extreme floods depends on an intricate set of variables associated with the spatio-temporal characteristics of the precipitation forcing, spatial distribution of channel-reach morphology types and hillslope hydrology. It is therefore important to focus on time- and place-specific hydrologic and geomorphic settings in assessing a basin's response to flash floods (Phillips, 2002).

The concept of magnitude and frequency of floods as a surrogate of effectiveness of their geomorphic forces has often been inconclusive through field investigations (e.g., Andrews, 1980). Wolman and Gerson (1978) reported that the magnitude and frequency approach, which is usually invoked in terms of the geomorphic work performed by floods, does not satisfactorily explain the effectiveness of an individual event to shape or form the landscape. The authors defined effective events as those responsible for creating or modifying landscape forms that persist over time while geomorphic work is basically the sediment transport rate, which often adjusts fluvial systems in equilibrium to external perturbations and internal feedbacks. Therefore geomorphic effects of extreme floods should be focused on disequilibrium rather than on equilibrium conditions (Magilligan, 1992).

A central problem in associating energy expenditure with the resulting geomorphic impacts of extreme floods hinges on initial channel conditions, particularly the recovery processes between two high magnitude events (Wolman and Gerson, 1978; Newson, 1980). For instance, Wohl et al. (2001) extrapolated the relations between hydraulic variables and mapped patterns of erosion and deposition landforms, which then permitted prediction of probable future geomorphic patterns along neighbouring channels in Nepal. Furthermore, quantitative data on channel erodibility, sediment volume and transport rates to corroborate stream power measures are rarely available at the space and time scale of flash flood occurrences. In effect, geomorphic impacts or hazards usually take the form of erosional and depositional modification of the pre-flood channel and valley geometry (Wohl et al., 2001). Post-flood field surveys and observations provide important context to assess the magnitude of channel modification caused by extreme floods at cross-sectional or channel-reach scales. Remote sensing may also be used to estimate channel widening from high resolution digital images, usually expressed as width ratio (i.e., ratio of channel width after flood to channel width before flood), which also provides an important quantitative measure of geomorphic response to floods (Krapesh et al., 2011; Magilligan et al., 2015; Surian et al., 2016).

Rinaldi et al. (2016) proposed an integrated methodological framework for assessment of geomorphic responses to extreme floods according to the schematic diagram in Fig. 1.5. The methodology uses a range of approaches at different spatial scales with interlinked hydrometeorological and geomorphological observations and analyses to investigate the geomorphic impacts of extreme rainstorm events on the fluvial system.

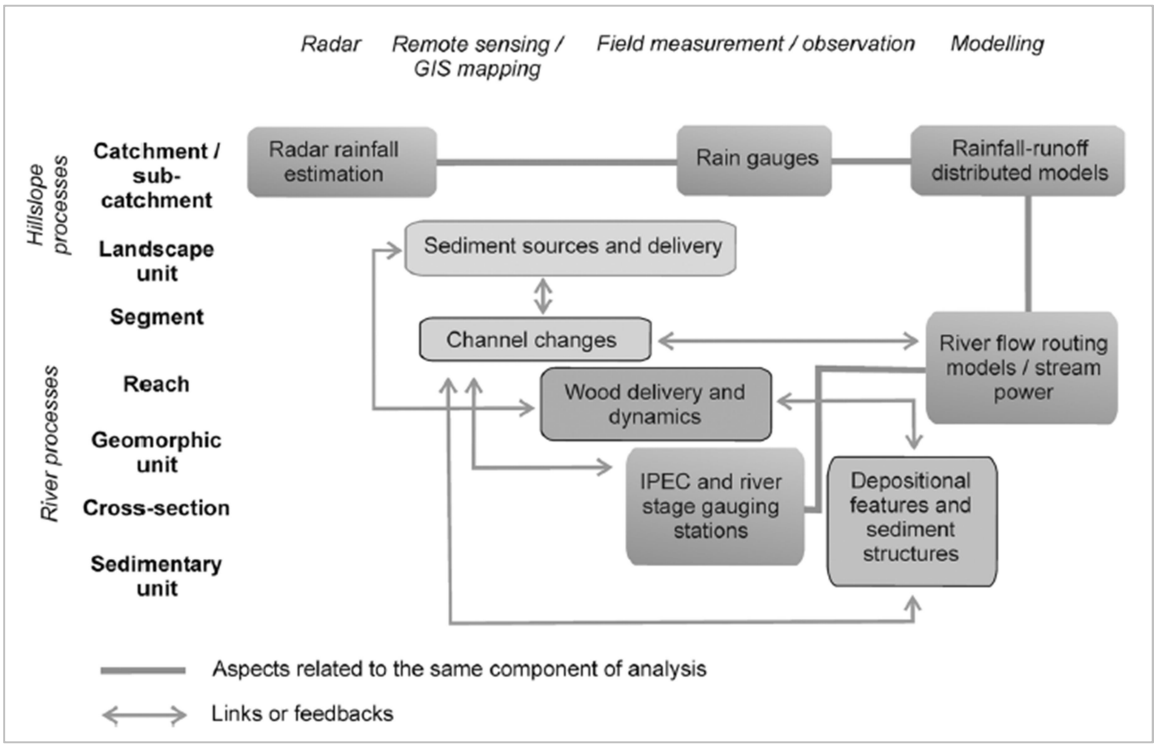

FIG.1.5. Schematic diagram of spatial scales, approaches, and coupling of process controls on the flood timescale (*Adapted from Rinaldi et al., 2016*).

1.5.2 GEOMORPHIC EFFECTS AT THE CHANNEL-REACH SCALE

The geomorphic impacts of flash floods at the channel-reach scale are predominantly channel bed and bank erosion, and transport and deposition of sediment and woody debris, which cause abrupt and significant channel changes. Flash floods produce the most effective discharge, which leaves geomorphological traces such as boulder berms (Foulds et al., 2014) in some fluvial environments where more common bank-full discharges have no significant impact in terms of coarser sediment transport and channel modification (Baker and Costa, 1987). The dominant determinants of geomorphic effects are flow magnitude (e.g., peak instantaneous discharge, stream power and shear stress) and hydrogeomorphic resisting factors (e.g., valley width, flood duration, sequence and initial conditions of floods), which are place- and time-specific factors (Phillips, 2002). However, channel-reach morphology types exhibit different response potentials to extreme rainfall events due to the coupled influence of reach-level channel processes with spatial arrangement of the reach morphologies,

their interaction with hillslope processes and external forcing by confinement, riparian vegetation and woody debris (Montgomery and Buffington, 1997).

Stream power has widely been used in literature as a predictor of geomorphic changes at the channel-reach scale because its measures quantify energy expenditure in fluvial systems (Rhoads, 1987). The use of stream power and its associated measures have been advocated to '*be used in a conceptual context only*' (Rhoads, 1989, p 189). This is because it is extremely difficult to quantify geomorphic effects of floods at the channel-reach scale based on computed stream power values because quantitative data on channel erodibility, sediment volume and transport rates to corroborate stream power measures are rarely available at the space and time scales of flash-flood occurrence. Fonstad (2003) described stream power as a principal indicator of river energy expenditure that has significant influence on many form and process attributes of the fluvial system. Stream power has also been used as a 'screening tool' (e.g., Brookes and Wishart, 2006) – an indicator of how a river channel might be potentially affected by processes of erosion and sedimentation. Vocal Ferencevic and Ashmore (2012) used the concept of stream power as an initial stream assessment method to develop a DEM-based stream power map. This is particularly useful to compare with other geographical data as a tool to assess the main controls on stream power distribution, and from the point of view of public safety, to assess infrastructure vulnerability, particularly to extreme floods.

The application of stream power to quantify the geomorphic effectiveness of extreme floods has shown that this variable is 'just a conceptual' representation of the time rate of energy expenditure as water travels down a channel reach (e.g., Miller, 1990; Magilligan, 1992; Costa and O'Connor, 1995; Magilligan et al., 2015; Marchi et al., 2016), because the actual energy expended in causing geomorphic adjustments in the fluvial system is extremely difficult to measure (Fonstad, 2003). Furthermore, Miller (1990) highlights the unreliability of this variable as a predictor of geomorphic change for individual sites, suggesting that a detailed investigation of interactions between local site characteristics and the flood flow patterns would provide a better understanding of flood impacts on valley floors. Fonstad (2003) posed the following two principal questions on associating stream power to the spatial distribution of river forms: (i) how does stream power vary geographically within a high mountain stream basin? and (ii) if traditional hydraulic geometry variables describing the stream power distribution do not fully capture the geographic variability, are there other variables and methods that

can be used instead? These questions throw light on how the present measures of stream power usually misrepresent the geomorphic impacts of high magnitude floods in most fluvial environments.

The concept of flood-flow duration and cumulative energy expenditure (Costa and O'Connor, 1995) is very important with respect to geomorphic effectiveness of floods because the use of peak instantaneous hydraulic variables such as discharge, velocity, shear stress, and stream power to quantify channel response to extreme floods has often been inconclusive and/or non-deterministic (e.g., Miller, 1990; Magilligan, 1992; Marchi et al., 2016; Surian et al., 2016). Magilligan et al. (2015) investigated the combined role of flow duration and cumulative energy expenditure on hydraulic and geomorphic impacts produced by the tropical storm Irene in two gravel-bed rivers of the north-eastern United States. Their study reveals that floods with high instantaneous peak stream power but short duration may show limited erosion and produce minimal channel widening, but may be formative events, in that they are associated with widespread long-lasting impacts (e.g., Wolman and Gerson, 1978; Hicks et al., 2005). These floods are usually responsible for major sedimentological effects, including entrainment and transport of coarse sediment and its deposition across floodplains (Magilligan et al., 2015). Kale (2008) attributed the main geomorphic role of high cumulative energy expenditure of maximum annual floods in the monsoon-fed Narmada River (central India) to the transport of sediment supplied from upstream areas. These studies reveal that flow duration and cumulative energy expenditure may play complex roles in the capability of floods to produce significant geomorphic impacts, which is less studied at the regional scale. Specifically, investigations are needed on how factors such as channel geometry, substrate, riparian vegetation, sediment supply, and flood magnitude and duration can interact and influence geomorphic effectiveness of high magnitude floods.

1.5.3 Geomorphic effects at the basin-scale

Geomorphic systems are viewed as the operation of a large physical system with a series of interlinked complex systems operating at different scales (Fookes and Lee, 2005) rather than the isolated physical systems depicted by Schumm's model of the fluvial system (Fig. 1.1). This implies that any process at any location within a basin would affect the form and process at another location.

Most studies of high magnitude flood events have focused on the geomorphic impact at the channel scale with little or no attention to the tremendous impacts of hillslope processes on channel form and stability. Channel and hillslope processes are intricate processes that occur at almost the same spatial scale within a river basin and are responsible for landscape forms. The nine-unit hillslope surface profile (Dalrymple et al., 1968) (which includes from the summit, interfluve, seepage slope, convex creep slope, fall face, transportational midslope, colluvial footslope, alluvial toeslope, channel wall and channel bed) clearly depicts the interconnection between hillslope and fluvial processes. Hillslopes mainly supply water and sediment (and large wood) to river channels within a river basin, but their forms may be influenced by fluvial activities at the valley floor. On one hand, hillslope failures, thus mass movement of sediment (e.g., debris flows and/or landslides) can cause large-scale deposition (alluviation) and dams, which affect the form and stability of river channels and fluvial processes. On the other hand, active fluvial processes on the valley floor may cause significant scouring or undercutting of channel banks which eventually leads to slope instability and collapse. It is therefore necessary to take the broad perspective of erosion and deposition associated with fluvial and hillslope processes to better understand the geomorphic impacts of high magnitude floods at the basin scale.

The concept of sediment connectivity (Hooke, 2003; Cavalli et al., 2013; Fryirs, 2013; Bracken et al., 2015), which quantifies coupling and decoupling of hillslope and channel processes (Harvey, 2001) and longitudinal stream connectivity (Wohl et al., 2016), may be very important in assessing the geomorphic effectiveness of floods at the basin scale. The spatial characterization of connectivity patterns can help in estimating the transfer paths of the sediment detached from source areas within a catchment. Sediment connectivity can also be linked to hydrological connectivity in runoff-dominated catchments (Bracken and Croke, 2007) to address the concept of transport capacity and sediment supply in fluvial systems (Montgomery and Buffington, 1997). Effective coupling between hillslope and channel processes, which is controlled by morphological conditions of catchments, is expected to provide efficient downstream transfer of sediments and vice versa. However, the peculiar characteristics of flash floods may render the concept of sediment connectivity non-deterministic in assessing catchment-scale geomorphic effectiveness of such extreme floods. On one hand, the devastating nature of flash floods may create effective coupling between hillslopes and channels in the realm of the event to ensure efficient sediment delivery. On the other hand, the short duration of flash

flood-triggering rainstorms as well as the corresponding flood response may delay the delivery of sediment supply from hillslope processes (landslide) relative to the time of adequate transport capacity to ensure effective channel processes (debris flows and sediment transport). The latter phenomenon may cause channel obstructions (i.e., barriers sensu Fryirs, 2013), which may require floods of similar magnitude to achieve equilibrium conditions.

The comparison of the geomorphic effectiveness of two successive high magnitude flood events studied by Newson (1980) in a basin in mid-Wales in August 1973 and 1977, respectively clearly shown the effects of hillslope processes on the flood response of river basins. These two rare floods had similar return periods and identical rate of work. As indicated by Newson (1980), the August 1973 flood was more effective on slopes whereas the August 1977 flood had severe impact on the channel forms. These distinct phenomena may imply that most of the hillslope stability thresholds were crossed by the first event and hence the second flood had no significant impact on the already adjusted slopes. However, the second flood was very effective in adjusting channel geometry through erosion and transport of deposited sediments from the slope failures mostly caused by the first flood. Wolman and Gerson (1978) recognized that the biggest information gap in assessing the geomorphic effectiveness of flood events at the basin scale is that concerning the recovery time between high magnitude events, which suggests that a better quantification of the geomorphic effectiveness at the basin scale can be achieved and predictions made of the influence of the next rare event by considering the impacts of the previous rare event and the recovery processes between the two events.

Borga et al. (2014) reviewed early warning systems for flash floods, shallow rainfall-induced landslides, and debris-flows. Most of the efforts in this area focus on evaluating the likelihood of triggering flash flood or debris flow activity in terms of alert levels by comparing quantitative precipitation forecasts against rainfall intensity–duration thresholds and antecedent precipitation conditions (soil wetness). The challenges in these early warning systems are the relationships among hydrological, hydro-geological and slope stability during individual events, the uncertainty in the characterization of geotechnical conditions, including land use, and lead time of the precipitation forecasts. Due to the small areas and steep slopes of headwater catchments in mountainous regions, large rainfall events tend to produce flash flood response and multiple debris flows within the same watershed. From the point of view of public safety and warning systems, predicting the flash flood

peaks and the location of debris flow occurrence is essential, although ultimately the utility of the forecast strongly hinges on the lead time (Tao and Barros, 2014).

The need for coupling spatially explicit, dynamic hydrologic models with debris flow susceptibility models has been articulated earlier (Simoni et al., 2008; Tao and Barros, 2014; and references therein). Most of the available literature is focused on the coupling of dynamically distributed hydrologic models with slope stability models for the prediction of shallow landslides, which are triggered by increases in pore water pressure at a slip surface (e.g., Iverson, 2000; Baum et al., 2010). Distributed models have been developed to analyse the control of topography and the hydraulic and mechanical characteristics of soils on shallow landslides (Montgomery and Dietrich, 1994; Pack et al., 1998). These models couple a saturated subsurface flow model with the infinite slope stability approach; the topography is represented through digital terrain models. The model SHALSTAB (Montgomery and Dietrich, 1994) includes a module that simulates landslide routing, which can assess the possibility that material mobilised by landslides reaches the channel network. Steady-state stability models (Montgomery and Dietrich, 1994; Pack et al., 1998) assess slope stability/instability for constant rainfall rates, representing the control of topography on shallow landslides. Quasi-dynamic models (Iida 1999, 2004; Borga et al., 2002; Lanni et al., 2012) take into account the intensity and duration of rainfall, thus representing a closer link between the topographic, hydrologic and mechanical characteristics of landslide-prone hillslopes and landslide-triggering rainfall.

However, in several areas debris flow initiation is typically due to runoff from low-permeability surfaces during rainstorms, which at a critical discharge threshold mobilizes loose sediment downslope (Coe et al., 2008a). In these cases, debris flows initiate through channel bed mobilization mechanisms when a critical surface discharge, rather than a critical groundwater level, is reached (Berti and Simoni, 2005; Larsen et al., 2006; Godt and Coe, 2007). Slope stability analyses used to assess slide prone areas are therefore inappropriate for areas that are susceptible to debris flows generated through runoff and erosion. At closely monitored sites, calibrated rainfall-runoff models have been successfully used to investigate the hydrological conditions for channelized debris flows, by providing estimates of the rainfall needed to produce the critical level of discharge for debris flow initiation (Berti and Simoni, 2005; Coe et al., 2008a,b; Gregoretti and Dalla Fontana, 2008).

1.6 Research Questions and Objectives

Two main research questions are examined in this study. The first is a general question in fluvial geomorphology, an observation Costa and O'Connor (1995, p 45) describe as '*a dilemma for geomorphologists*': *why do flash floods of similar magnitudes and intensities sometimes produce dissimilar geomorphic results?* An overarching phenomenon is that large magnitude floods do not always produce major geomorphic changes in channels and valley floors. In fact, some lower magnitude floods in terms of discharge per unit of drainage area have been found to produce more major geomorphic damage than some high magnitude events (e.g., Miller, 1990). This phenomenon presupposes that the magnitude (discharge) and frequency (recurrence interval) of flash floods do not adequately quantify the geomorphic modifications caused by such extreme events in channels and slopes (Baker and Costa, 1987; Miller, 1990; Magilligan, 1992; Marchi et al., 2016). Integrated analysis of the relevant topographic, climatic and vegetation controls may provide an essential insight to understanding the hydrologic and geomorphic responses to extreme floods.

The second question is directly linked to the overall research objective of this study, thus, *can the analysis of the distribution and variation of stream power contribute to explain the variability of the geomorphic effects a flash flood?* As indicated by Miller (1990), the highest values of stream power are usually developed in bedrock channels which are resistant to erosion and hence the use of computed stream power values to quantify the geomorphic effects or as an indicator of channel adjustment at such cross-sections becomes questionable. Several questions have been raised about the association of peak instantaneous unit stream power with the corresponding geomorphic effects (e.g., Fonstad, 2003; Kale, 2008; Magilligan et al., 2015). The influence of flood flow-duration expenditure will be examined together with peak instantaneous stream power and the relevant topographic variables (mainly, variations in channel slopes, lithology and reach level morphologies) at cross-sections and downstream variation along the longitudinal profile of river channels. The latter may provide an explanation of the complex processes of sediment production, transport and deposition that occur during extreme flash floods.

The general objective of this thesis is to explore and analyse the spatial distribution of the various measures of stream power for a number of flash flood events in Europe and the relevant topographic,

hydro-climatic and hydraulic controls to better quantify and discuss the geomorphic effectiveness of such events at the channel-reach scale. In collaboration with a Ph.D project at the Department of Geosciences (University of Padova), this thesis focussed on estimating, modelling and evaluating the hydro-climatic and hydraulic variables, whereas the other thesis focussed on the geomorphic responses.

The specific objectives are:

1. To establish a common archive of flash floods, through combined analysis of data from post-flood surveys and hydrological modelling, for selected flash floods across different hydro-climatic and geomorphic settings in central and southern Europe,
2. To analyse the spatial variation and distribution of stream power and other hydraulic and topographic variables for the studied flash floods to quantify the main controls on geomorphic responses at the cross-sectional scale,
3. To evaluate the combined influences of flood-flow duration and cumulative energy expenditure on geomorphic effectiveness of extreme floods, relative to peak instantaneous stream power.
4. To model the downstream variations in stream power and other relevant controls along longitudinal profiles of selected rivers,
5. To quantify channel widening associated with flash flood responses and the corresponding controlling factors at the channel-reach scale.

These questions will be examined through field observations and model-based analyses of seven major flash flood events that occurred across different hydro-climatic and geomorphic settings between 2007 and 2014 in central and southern Europe. This project is expected to develop better understanding of the regional behaviour of stream power and the corresponding geomorphic impacts for extreme flash floods in Europe, thus contributing to bridging the scientific gap between hydrologic and geomorphic processes in flash flood studies. Research results are expected to be suitable for managers of flood-prone catchments and regulatory agencies in land use planning, hillslope management and flash flood hazard and risk management.

2 STUDY AREAS AND FLOODS

This section gives an overview of seven selected flash flood events that occurred in different hydro-climatic and geomorphic settings in central and southern Europe between 2007 and 2014. These floods have been documented through post-event surveys and analysis of comprehensive hydrometeorological and geomorphological data. Selected channels in three highly impacted catchments of the studied floods (Magra, Posada and Lierza rivers) are also used to explore the downstream trends in stream power and the corresponding channel changes at the reach-scale.

2.1 STUDIED FLASH FLOODS

Table 2.1 presents summary information of the seven selected flash floods for this study, with their spatial locations mapped over the Köppen-Geiger climate classification system (Peel et al., 2007) in Fig. 2.1. The impacted catchments are characterised by temperate climate, with four of them without a dry season throughout the year (Selška Sora, Starzel, Vizze, and Lierza) and the remaining three under dry-summer Mediterranean climate. The Vizze basin, located in the inner core of the Alps is also characterized by cold winter and mild summer. The Selška Sora catchment features mild to warm summer without a dry season. The Lierza catchment (Fig. 2.1) is located in a hilly area of northern Italy. Although Lierza lies close to the Adriatic Sea, the local climate lacks typical features of Mediterranean areas and is classified as humid subtropical (*Cfa*) according to the Köppen–Geiger classification. The Argens, Magra and Cedrino-Posada catchments, on the contrary, are located in the Mediterranean region, featuring warm to hot and a dry summer. These flash flood events were selected based on the following criteria (i) coverage of different hydro-climatic regions, (ii) rainfall of high return period (> 100 years, at least for some rainfall duration in some sectors of the studied catchments), (iii) availability of data collected and validated by means of homogeneous procedures, and (iv) rainfall-caused floods only (with durations up to 24 hours).

Data were collected for 119 cross sections; the number of cross sections per event ranges between 2 (Vizze) and 33 (Magra), mostly depending on the overall area impacted by the flood. Only two cross sections were surveyed in Vizze, which were considered sufficient to document the flood in the main

river, whereas the tributaries were affected by debris flow. The catchments corresponding to the surveyed cross sections range in area between 0.5 and 1981 km^2; however, only two catchments are larger than 1000 km^2 in size, which fits the space scale definition of flash flood adopted in this study (see also Gaume et al., 2009; Marchi et al., 2010). The duration of the events is linked to the maximal drainage areas, with the rainstorms lasting 20 hours or more in the case of those impacting areas larger than 500 km^2 (Argens, Magra, and Cedrino–Posada). Interestingly, these three events occurred in the Mediterranean region. This is consistent with observations by Gaume et al. (2009) and Marchi et al. (2010), who noted that the spatial extent and duration of the flash flood events is generally smaller for continental floods relative to those occurring in the Mediterranean area. Actually, shorter duration and smaller affected areas characterize the floods in continental and alpine areas (Starzel, Selška Sora, and Vizze), as well as the Lierza.

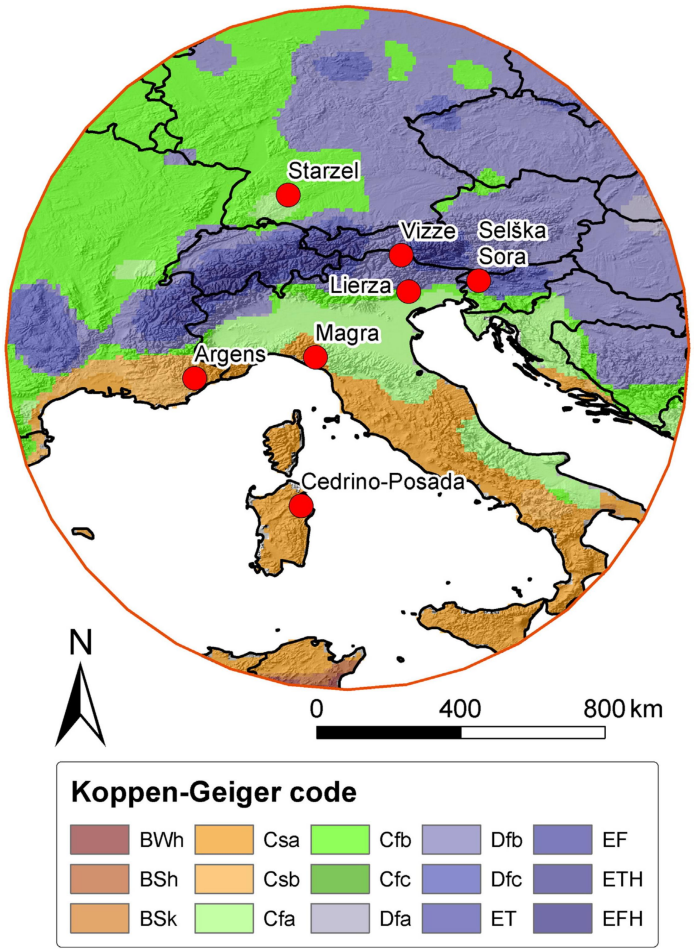

FIG.2.1. Location and climatic context of the studied flash flood events; Köppen-Geiger climate classification from Peel et al. (2007). (*Adapted from Marchi et al., 2016*).

TABLE 2.1. Summary data of the seven studied flash floods

River basin (Country)	*Date of occurrence*	*Climatic region (Köppen-Geiger)*	*Watershed area [km^2]*	*No. of studied basins*	*Storm duration [h]*	*Maximum rainfall [mm]*	*Previous studies*
Selška Sora (Slovenia)	September 18, 2007	Alpine-Mediterranean (*Cfb - Cfc*)	150	19	16.5	400	Marchi et al., 2009a; Zanon et al., 2010
Starzel (Germany)	June 2, 2008	Continental (*Cfb*)	120	17	8	130	Ruiz-Villanueva et al., 2012
Argens (France)	June 15, 2010	Mediterranean (*Csa - Csb*)	2700	24	20	400	Payrastre et al., 2012; Ruin et al., 2014
Magra (Italy)	October 25 - 26, 2011	Mediterranean (*Csa - Csb*)	1717	33	24	540	Surian et al., 2016; Amponsah et al, 2016
Vizze (Italy)	August 4 - 5, 2012	Alpine-Mediterranean (*Cfb - ET*)	140	2	8	130	
Cedrino-Posada (Italy)	November 18 - 19, 2013	Mediterranean (*Csa*)	1500	17	24	450	Niedda et al., 2015; Amponsah et al, 2017; Righini et al., 2017
Lierza (Italy)	August 2, 2014	Alpine-Mediterranean (*Cfa*)	10	7	1.5	200	Destro et al., 2016

2.1.1 SELŠKA SORA, SLOVENIA (SEPTEMBER, 2007)

The Selška Sora watershed is located in north-western Slovenia. The upper part of the watershed (closed at Železniki - 150 km^2), which was most severely affected by the flood of 18 September 2007, has been considered in this study. The topography of the watershed consists of steep slopes and a high gradient river network. The watershed is dominated by narrow valleys and ranges from 450 to 1680 m a.s.l. in elevation. The meteorology of the catchment is monitored by the *Lisca* weather radar, and several rain gauges (Fig. 2.2-A). The mean annual precipitation over the basin ranges between 1700 and 2300 mm, which is highly influenced by the orography (Zanon et al., 2010). Forests, with grassland and grazing fields in the flood plain, dominate the land use types of the basin. The geology consists of various highly fractured and fissured rock types, including limestone, schist and shale. The northern portion of the basin consists of karst geology, which influences the runoff production (Zanon

et al., 2010). On 18 September 2007, a mesoscale convective system hit north-western Slovenia, starting from 5.00 CET and lasted for over 16 hours. The flood-generating rainstorm produced an event accumulation up to 400 mm (Fig. 2.2-B). This caused severe flash floods with six casualties. Out of 210 local communities in Slovenia, 60 reported flood damages, with the total flood-related damage estimated at 210 million Euro (Rusjan et al., 2009). The Selška Sora watershed was one of the severely affected catchments, with basin averaged rainfall up to 240 mm (Fig. 2.2-B). Point hourly rainfall estimates were up to 150 mm, with a recurrence interval exceeding 200 years (Rusjan et al., 2009). Among 12 extreme floods documented in this catchment for the last century, this event recorded the highest magnitude (Komac et al., 2008; Marchi et al., 2009a). The flash flood caused widespread geomorphic impacts in the Selška Sora watershed, including shallow soil failures and several debris flows, and trees recruited into channels because of widespread bank erosion and channel avulsion in the forested valley floors (Marchi et al., 2009a). The rainfall intensity and duration were adequate to produce positive pore-water pressure necessary to reduce shear strength and initiate slope failures. Sediment supply from hillslopes and small tributaries, combined with extreme flows in river channels led to channel widening, local avulsion and overbank deposition in most of the impacted tributaries.

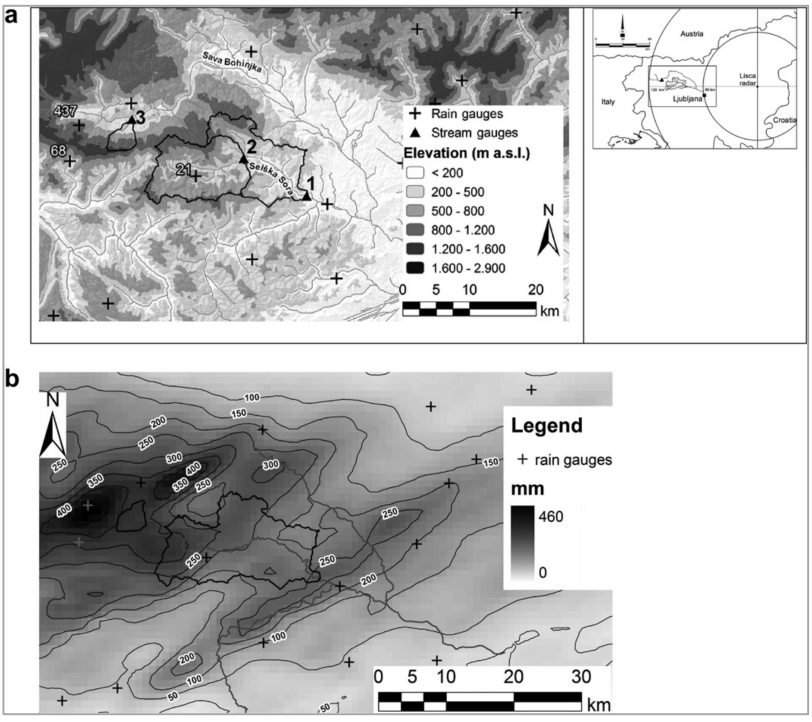

FIG.2.2. (A) Location of the Selška Sora watershed and the *Lisca* radar, with the topography of the study basins, and (B) event cumulative rainfall of the September 18, 2007 storm (*Adapted from Zanon et al., 2010*).

2.1.2 STARZEL, GERMANY (JUNE, 2008)

The Starzel River basin closing at Rangendingen (120 km^2) is located in south-western Germany, within the Neckar River system. The elevation of the catchment ranges between 419 and 954 m a.s.l. The meteorology of the catchment is monitored by the Türkheim and Feldberg weather radars (Fig. 2.3-A). The mean annual precipitation over the Starzel catchment is 836 mm, with maxima in the summer months (Ruiz-Villanueva et al., 2012). The main land use types are forests, agriculture and urban areas. The catchment is dominated by coniferous, mixed and deciduous forests on the slopes. Agricultural areas are mostly arable lands, orchards and meadows. Three urban areas are located within the catchment: Jungingen, Hechingen and Rangendingen (Fig. 2.3-B). The geological features of the catchment consist of Jurassic sedimentary rocks, predominantly limestone, marls and clay stone. Karst topography in the eastern part of the catchment, where limestone outcrops with fissures, sinkholes and caverns, influences runoff production in this part of the catchment (Ruiz-Villanueva et al., 2012).

The flash flood producing rainstorm on the Starzel catchment was part of a sequence of mesoscale precipitation systems (called *Hilal* - Ruiz-Villanueva et al., 2012), which occurred from 28 May to 2 June 2008 covering most of western Germany. The thunderstorms formed along a stationary air mass boundary separating warm, moist Mediterranean air in the southwest from dry air in the northeast. The first system occurred on 28 May in mid-west Germany (Dortmund) and the second on 29-30 May, causing flooding in Luxembourg, Rhineland-Palatinate and North Rhine-Westphalia (Ruiz-Villanueva et al., 2012). On the evening of 2 June, the Neckar River system was hit by extremely high intensity torrential storms that led to flash flooding and inundation. The Starzel catchment was severely affected by this flash flooding. The most intense phase of the rainstorm over the catchment, which lasted for 90 minutes, produced intensities up to 55.5 mm h^{-1} with mean areal rainfall depth of 85.6 mm in 10 hours for the entire storm event. This rainstorm was exceptional in the Starzel catchment because a 100-year rainfall of 10 hours duration amounts to 67.6 mm (DWD, 2006). The flash flood triggered only few shallow landslides on the catchment area most impacted by the storm close to the town of Jungingen (Ruiz-Villanueva et al., 2012). This can be ascribed to the morphological characteristics of the catchment (relatively short hillslopes) and, more importantly, the short duration of the most intense phase of the rainstorm.

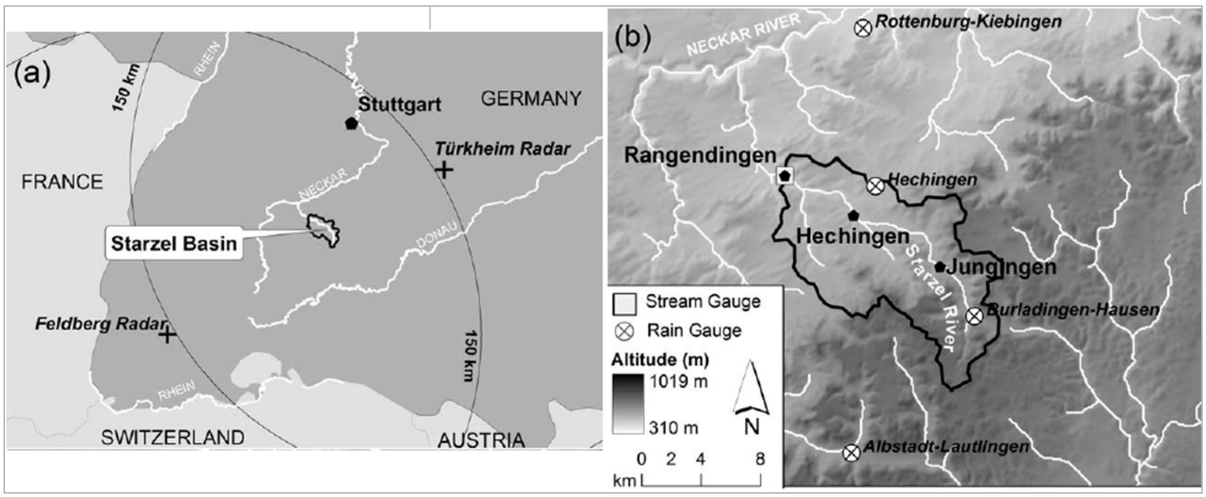

FIG.2.3. (A) Location of the Starzel basin with the two weather radars, Türkheim and Feldberg (crosses) and corresponding 150 km range circles; and (B) the basin with orography and the location of the four raingauge stations within the catchment and of the streamgauge (*Adapted from Ruiz-Villanueva et al., 2012*).

2.1.3 ARGENS, FRANCE (JUNE, 2010)

The Argens River is located within the Var department (southern France) and drains a total area of approximately 2700 km^2. The basin drains several tributaries and then flows into the Mediterranean Sea. The catchment is characterized by differing geo-lithological features; the geology of the basin is dominated by limestones and granite. On 15-16 June 2010, the Var department was hit by a violent storm. The daily accumulated rainfall which caused flash flooding reached 200 and 300 mm over 2000 and 250 km^2, respectively (Rouzeau et al., 2010). The maximum rain amount recorded at the Meteo-France station (Fig. 2.4) reached over 400 mm in 20 hours (including 330 mm in less than 10 hours), corresponding to a return period of the order of 100-years (Martin, 2010; Payrastre et al., 2012). The rainstorm was characterized by two phases (Ruin et al., 2014): first, the atmospheric flux came from S-SW and led to intense precipitation up to 16:00 local time but it quickly swept nearly the entire Var department. During the second phase, the flow was oriented SE and precipitation stayed quasi-stationary after 16:00 local time over the Nartuby watershed (184 km^2) upstream from Draguignan. The event caused 27 casualties and economic damages were evaluated at 1 billion Euros (Ruin et al., 2014). Large karst formations in the limestone area attenuated runoff formation in one of the sectors of the basin in which very high rainfall accumulation occurred (Payrastre et al. 2012).

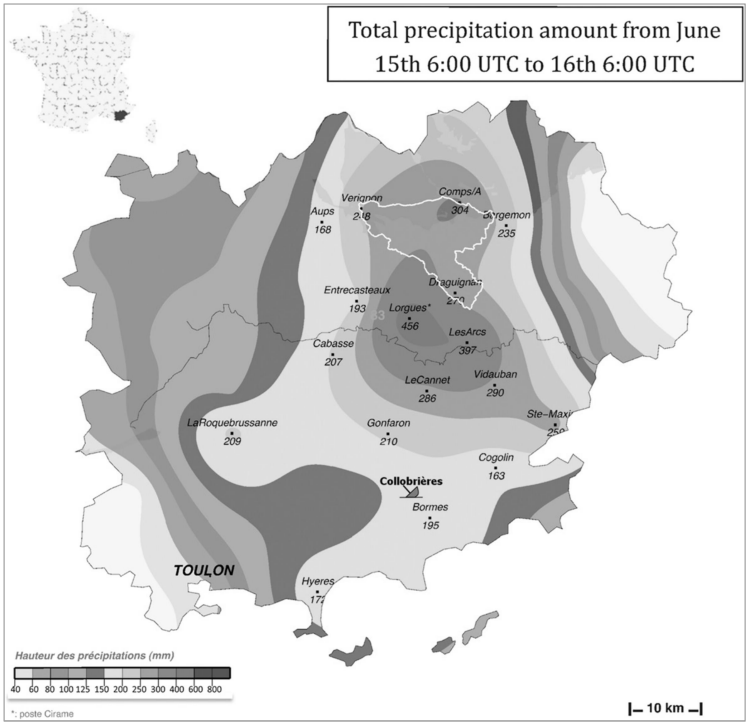

FIG.2.4. Total precipitation amount from 0600 UTC 15 Jun 2010 to 0600 UTC 16 Jun 2010 from Meteo-France (*Adapted from Ruin et al., 2014*).

2.1.4 MAGRA, ITALY (OCTOBER, 2011)

The Magra River basin is located in central-northern Italy within the Tuscany and Liguria regions with highest elevation of 1900 m a.s.l. and ends at the Tyrrhenian/Ligurian Sea (Fig. 2.5-A). The total drainage area of the affected basin is 1717 km^2, of which the Vara River (the major tributary to the Magra River) drains an area of 605 km^2. The climate is Mediterranean, with a dry summer and high precipitation, especially in the autumn months. The mean annual precipitation of the river system accumulates up to 1770 mm, and reaches 3000 mm in the upper parts of the basins due to orographic effects. The Magra basin is monitored by the *Monte Sette Pani* weather radar (station located at 100 km west of the basin), and about 40 rain gauges. The geology of the basin mostly consists of arenaceous and muddy bedrock, featuring low permeability and high erodibility. Three main land use classes can be identified within the study basin: forest (> 80% of the total area), agricultural lands (predominant in the valley floor) and urbanized areas and infrastructure.

On October 25, 2011, the Magra River basin was hit by a mesoscale convective system from 01:00 CET that lasted for 24 hours. The rainstorm produced rainfall intensities up to 150 mmh^{-1} and accumulations up to 540 mm (Fig. 2.5-B). Large rainfall accumulations in this region typically result from the coupled influences of orographic effect and low-level mesoscale flow over the Ligurian Sea that develop pronounced convergence bands (Buzzi et al., 2014). This phenomenon usually produces intense and quasi-stationary mesoscale convective structures near the coast, as observed over the Magra basin on October 25, 2011. The rainstorm of October 25, 2011 produced flash flooding in the main river channels and in several tributaries, with severe damage to roads, building and infrastructure in downstream settlements; nine people died as a consequence of the flash flood. The extreme rainstorm also triggered widespread landslides (mostly earthflows, soil slips and translational slides), especially in the sectors of the basin that were affected by the highest rainfall rates (Mondini et al., 2014). The flood caused major morphological changes in the channel of the studied basin and in some tributaries (Nardi and Rinaldi, 2015; Rinaldi et al., 2016; Surian et al., 2016) and recruited large amounts of large wood from the floodplain (Lucía et al., 2015). Several bridges were partly or fully clogged by large wood jams.

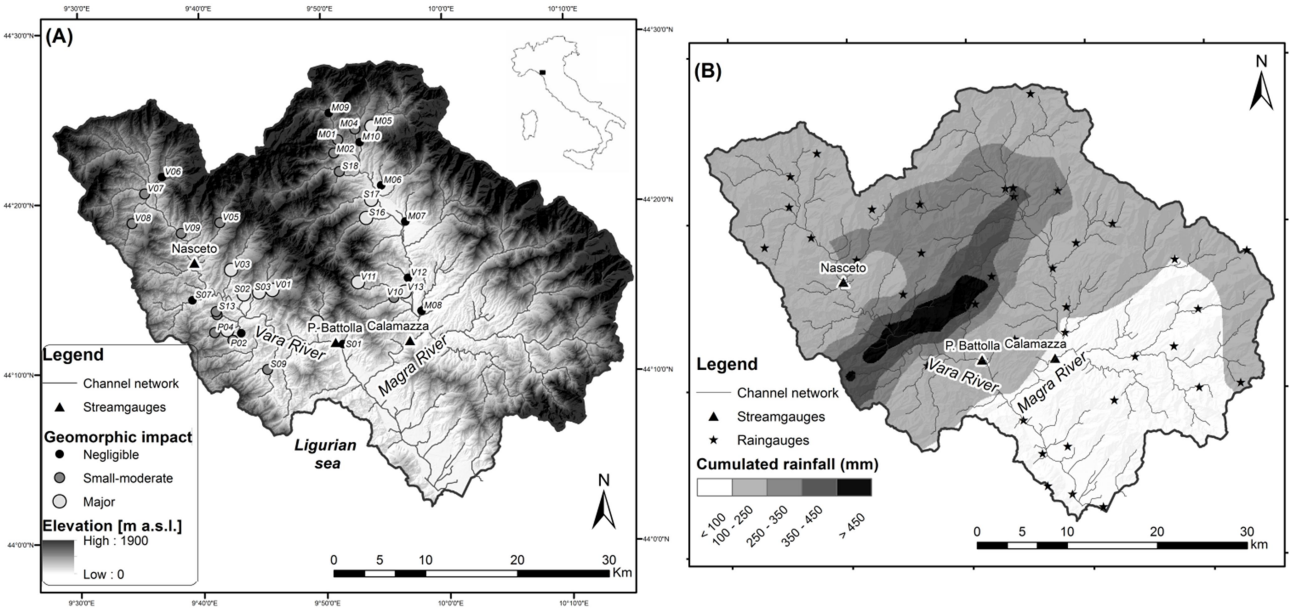

FIG.2.5. (A) The Magra basin with topography and the three stream gauge stations. Locations of surveyed cross sections are also reported, with the corresponding intensities of observed geomorphic impacts, and (B) total rainfall accumulation with raingauge network (*Adapted from Amponsah et al., 2016*).

2.1.5 VIZZE, ITALY (AUGUST, 2012)

The Vizze basin (140 km^2) is located in the Autonomous Province of Südtirol - Bolzano (Italy). The basin is located about 45 km north of the city of Bolzano, on the border with Austria and within the Upper Adige basin on the Eastern Italian Alps. The region is characterised by a cold, Alpine-continental climate and records mean annual precipitation up to 800 mm, with maximum occurring in the month of July. The Vizze basin is monitored by the *Monte Macaion* weather radar (station located at 60 km south of the basin) and surrounded by few rain gauges. The land use is dominated by forest, with agricultural activities in the low altitudinal plains. The geology of the valley consists of metamorphic rocks (gneiss, micaschist, calcschist, amphibolite); Quaternary deposits (moraine and scree) are widespread. The Vizze basin is an alpine watershed, and the morphology shows several interferences developed among alluvial, glacial and fluvio-glacial depositions and widespread erosional surfaces (Astori and Venturini, 2011).

The August 4-5, 2012 extreme rainstorm that affected the Vizze basin, started around 16:00 CET and lasted for 8 hours. The event-rainfall accumulation (Fig. 2.6-B) shows that the area close to the basin outlet received the highest event-rainfall accumulation, with up to 120 mm. The storm total precipitation decreases moving towards the upper part of the basin, and from the left side to the right side of the valley. The storm total rainfall distribution reflects southwest–northeast motion of the storm elements and west–east shift of the tracks of the storms. The storm accumulation can be distinguished in two phases. In the initial period (16:00–18:00 CET) the rainfall maxima (30-50 mm) concentrated over the area close to the basin outlet. In the second period (18:30-22:00 CET) the entire left side of the basin was impacted by heavy rainfall, ranging from 40 to 80 mm. While these cumulative values are relatively moderate when compared to those reported for Mediterranean flash flood events (Marchi et al., 2010), the severity of the storm event is significant when considered in the frame of the local climatology. The return period for the largest rainfall depths, considered over the basin for different duration, increases from 30 years at one hour duration to 300 years for six hours duration, which approximately corresponds to rainstorm duration, to decrease again to 30 years for 24 hours duration. The causative rainfall event triggered a large number of debris flows in the tributaries of the Vizze valley, causing two casualties and an estimated 18 million Euros in economic damages (Dinale et al., 2014).

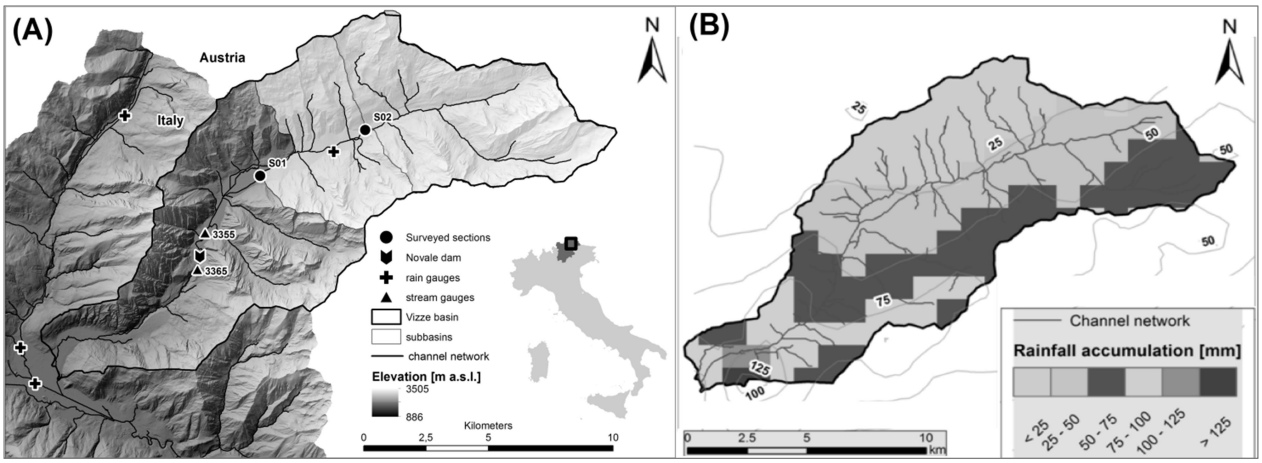

FIG.2.6. (A) The Vizze basin with topography and two stream gauge stations; locations of two surveyed cross sections are also reported, and (B) total rainfall accumulation.

2.1.6 CEDRINO - POSADA, ITALY (NOVEMBER, 2013)

Cedrino and Posada are two rivers of eastern Sardinia (Italy). The main impacted area (Fig. 2.7) is up to 1500 km^2 (central-north-eastern Sardinia), which includes the catchments of Cedrino, ending at the Prede Othoni dam (627 km^2), and Posada, ending at Maccheronis dam (611 km^2) and the intermediate Sologo basin (300 km^2). The Sologo River is a tributary of the Cedrino basin downstream of the dam. The study basin is monitored by the *Monte Rasu* weather radar and a dense rain gauge network (Fig. 2.7-B). Two dominant geological landscapes can be distinguished in the region: (i) metamorphic and granitic rocks, and (ii) sedimentary rocks (dolostones and limestones). Sedimentary rocks outcrop especially in the Rio Flumineddu catchment area, within the catchment closing at the Cedrino dam. The Rio Flumineddu catchment is characterised by karst landscape, with sub dendritic drainage pattern. The metamorphic and granitic rocks mostly occupy the northern part of the catchment closing at the Posada dam with dendritic drainage pattern. Main river channels are aligned according to faults in the phyllites and their steep slopes testify to their rapid evolution. Land cover is characterized by Mediterranean *maquis* on the Palaeozoic rocks (with a more or less thin soil cover) and degraded *Quercus Ilex* forests on the carbonate rocks (De Waele et al., 2010). The largest urban area is the town of Nuoro (approximately 37,000 inhabitants) in the upper part of the Cedrino catchment; a number of smaller settlements are present in the studied catchments.

On November 18, 2013, the central-north-eastern part of Sardinia was impacted by extreme flash flooding associated with an extra tropical cyclone in the western Mediterranean basin, which developed slow-moving embedded thunderstorm complexes, as cold air flowing from the north entered the Mediterranean and interacted with warm moist air to the east. The cyclone brought extremely heavy rain to the area, with up to 450 mm of rain in 24 hours, starting from 07:00 CET, resulting in flooding over a large area and swollen rivers bursting their banks. Two convective bands impacted the region with a SSE to NNW direction (Fig. 2.7-B) and both developed during two storm bursts at: 06:00-13:00 and 13:00-20:00 CET (Amponsah et al., 2017). Despite the strong observed winds, convection continued to be triggered over the same locations, accumulating rainfall over a relatively small area. The strong spatial gradients of the precipitation and geo-lithological features had a major influence on flood responses, with large differences in peak discharges among neighbouring catchments. The flash flooding caused up to 1 billion Euro in economic damages and 19 casualties (Niedda et al., 2015), but most of them were outside the Cedrino and Posada basins.

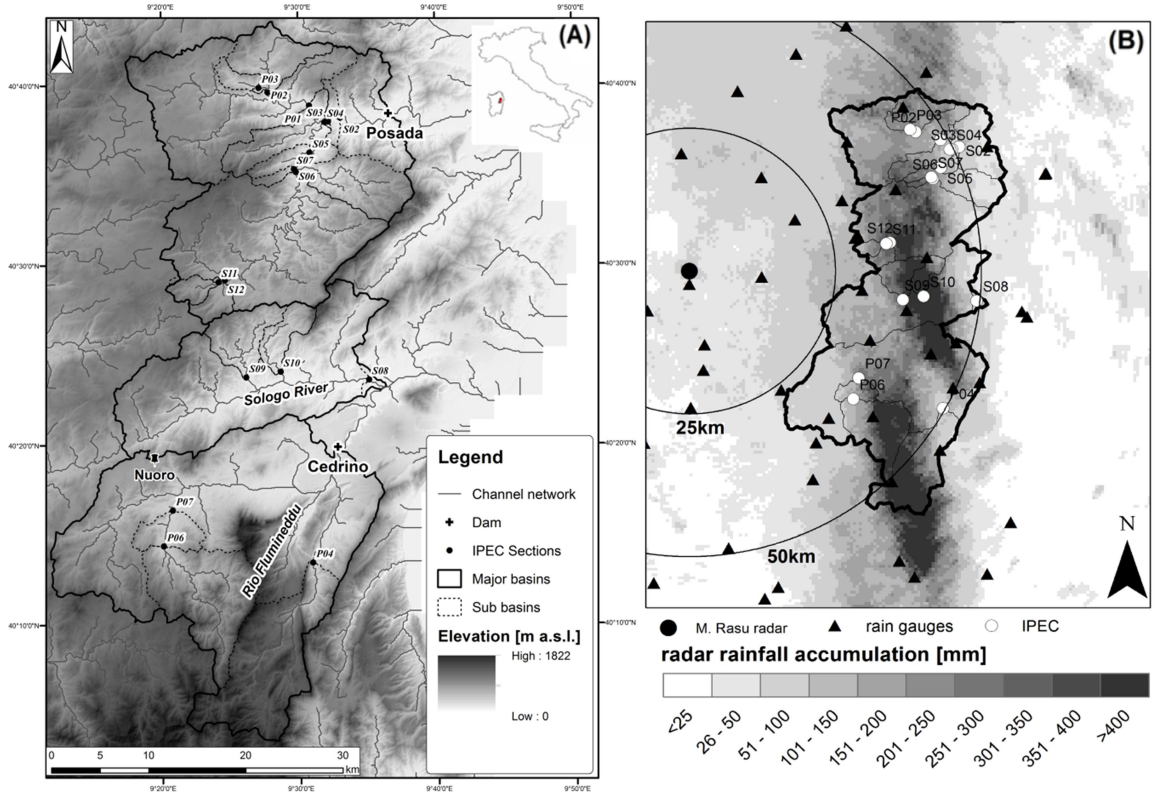

FIG.2.7. (A) The Cedrino-Posada basins with topography and Sologo River; locations of surveyed cross sections are also reported, and (B) total rainfall accumulation, with the *M. Rasu* weather radar (*Adapted from Amponsah et al., 2017*).

2.1.7 LIERZA, ITALY (AUGUST, 2014)

The Rio Lierza creek (Fig. 2.8-A) is located in the north-eastern Italian Pre-alps (Veneto region) and belongs to the Piave River system. The basin is characterized by hilly topography and maximum elevations are up to 470 m a.s.l. The study area is located in the monoclinal relief of hogback type called *Vette Feltrine*, typical of the Southern Alps. The geology consists of Miocene conglomerates and mudstone affected by tectonic deformation. The soils are mostly silt loams, with low permeability underlying clayey bedrocks. The upper Lierza basin features both forests and vineyards as the dominant land use. The basin is ungauged: the closest rain gauge station is located approximately 5 km NW of the basin, where data are available since 1994. Examination of rainfall data from this rain gauge station shows that average annual precipitation amounts to 1630 mm, with the highest monthly average precipitation in May and November. On August 2, 2014, the Lierza Creek was hit by an extreme rainstorm that triggered severe flash flooding and shallow landslides (Destro et al., 2016). The flood-generating rainstorm produced maximum accumulations exceeding 200 mm (Fig. 2.8-B) within 1.5 hours. Post-flood observations have shown a complex spatial pattern and large variability in the intensity of sediment transport. In some channel reaches there are no evidences of sediment transport, whereas in others intense sediment transport is demonstrated by overbank deposits up to the size of large cobbles. Also, channel erosion was characterized by major spatial variability: in spite of extreme flood flows, significant channel widening was observed only at some sites. The flood response also involved interaction with infrastructure; four people died as a result of the flash flood.

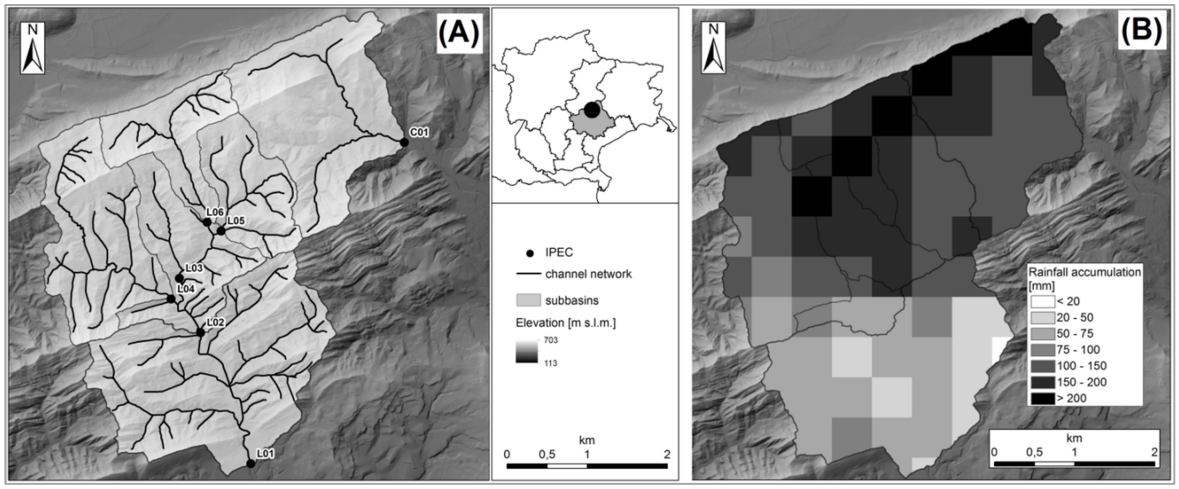

FIG.2.8. (A) The Lierza basin with topography and locations of surveyed cross sections, and (B) total rainfall accumulation (*Adapted from Destro et al., 2016*).

2.2 SELECTED CHANNELS

Eight river channels that were affected by three of the studied flash floods (Magra, Cedrino-Posada, and Lierza – Fig. 2.1) were selected for a more detailed analysis of the downstream trends in stream power and the corresponding channel responses. Table 2.2 reports summary data of the selected river profiles: five within the Magra basin, two within the Posada basin and the main Lierza Creek. The selected channels are located in the sector of the corresponding major basins that received maximum rainfall, which could shed more light on the main controlling factors on the downstream changes in channels affected by extreme floods. The study reaches correspond to the middle and lower portions of these creeks, which are characterized by partly confined or unconfined channel conditions. The number of sub reaches of the selected catchments vary from 12 (Geriola) to 28 (Posada), depending on the stream length, and, more importantly, the spatial unit of the sub reach length. Sub reaches are defined as spatial units with approximately constant channel slope, confinement, morphology and hydrology (Rinaldi et al., 2013; Surian et al., 2016). The catchment areas are generally larger for the two Posada channels compared to the channels of the Magra River and the Lierza Creek. This also reflects the length of the studied reaches and the corresponding peak discharges at the outlets. Catchment sizes may also affect the basin-averaged rainfall accumulation, although the maximum event rainfall (Table 2.1) reflects total rainfall accumulations reported in Table 2.2. The Lierza Creek is located in a hilly area of northern Italy and is characterised by relatively lower basin relief compared to the other catchments. The channels of the Posada River have much lower channel gradients.

TABLE 2.2. Summary data of the selected channels of the Magra, Posada and Lierza rivers

Major Basins	*Selected Channels*	*Watershed area [km^2]*	*Basin relief [m]*	*Stream length [km]*	*Mean gradient [%]*	*No. of studied reaches*	*Total rainfall [mm]*	*Unit peak discharge [m^3 s^{-1} km^{-2}]*
Magra	Pogliaschina	25.1	95 – 706	4.6	5.6	13	387	23.7
	Gravegniola	34.6	95 – 1177	5.5	7.0	14	387	15.1
	Mangiola	26.2	144 – 1155	8.9	6.6	27	376	15.5
	Osca	21.8	68 – 1159	8.0	4.1	22	243	12.8
	Geriola	8.5	120 – 1010	5.5	8.8	12	267	14.2
Posada	Posada	562	70 – 1116	22.4	1.1	28	215	6.6
	Mannu di Bitti	305	42 – 1116	18.2	0.7	20	250	7.3
Lierza	Lierza Creek	7.5	169 – 470	1.8	2.5	23	147	17.6

2.2.1 TRIBUTARIES OF THE MAGRA RIVER

Five catchments in the Magra River basin (Pogliaschina, Gravegnola, Mangiola Osca, and Geriola – Fig. 2.9) that were highly impacted by the October 25, 2011 flash flood have been selected to explore the downstream variations of stream power and channel response. The Mangiola, Geriola, and Osca Rivers are tributaries of the main Magra River, while Pogliaschina and Gravegnola Rivers are tributaries of the Vara River (Fig. 2.9). The length of the studied sub reaches are in the order of 300–500 m. All five Magra tributaries exhibit typical characteristics of mountain rivers with average channel slope (Table 2.2) ranging from 4.1 % (Osca) to 8.8 % (Geriola), coarse sediments (mainly gravels and cobbles), and a wide range of conditions in terms of lateral confinement. The tributaries of the Magra River show similar flood responses with unit peak discharges of 15.5 (Mangiola), 12.8 (Osca) and 14.2 m^3 s^{-1} km^{-2} (Geriola), consistent with basin-averaged rainfall and catchment area (Table 2). An interesting observation is the flood responses at the outlets of the two tributaries of the Vara River; unit peak discharges of 15.1 (Gravegnola) and 23.7 m^3 s^{-1} km^{-2} (Pogliaschina) for equal rainfall accumulation. This phenomenon can be ascribed to the space and time organisation of the convective rainstorm over these catchments, relative to the channel network orientation (cf. Fig. 2.5).

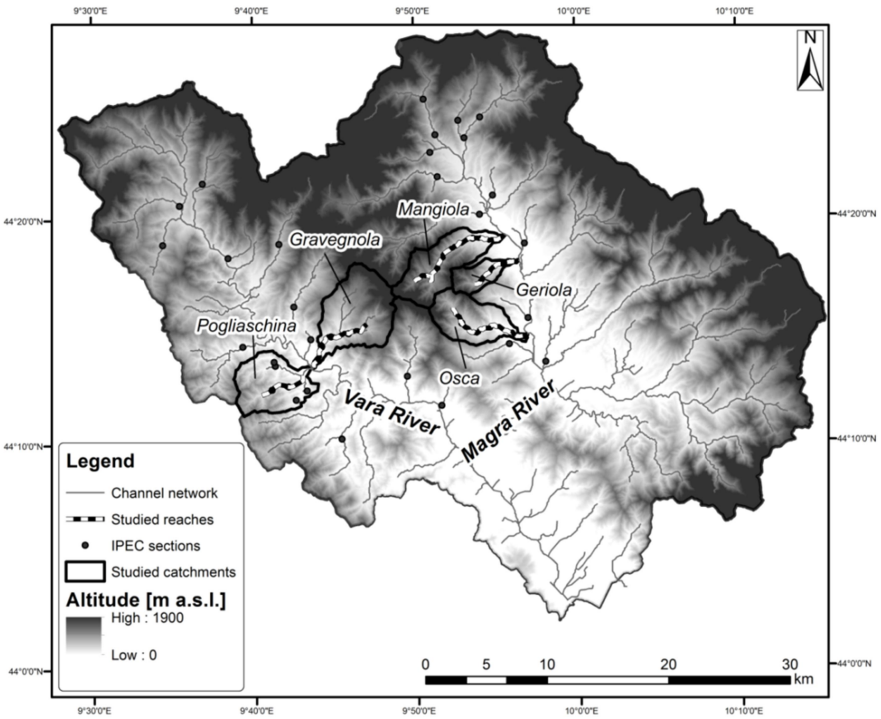

FIG.2.9. Locations and topographic features of the five selected channels of the Magra River.

2.2.2 THE POSADA AND MANNU DI BITTI RIVERS

The Posada River closing at Maccheronis dam (611 km^2), which was highly impacted by the November 18, 2013 flash flood in the Sardinia region of Italy has also been selected to explore the downstream variations of stream power and channel response. Studied channel reaches were selected on the main Posada stream and the Mannu di Bitti channel (the major tributary of the Posada River – Fig. 2.10). The length of the sub reaches are on the order of 700–1100 m. The Mannu di Bitti River contributes approximately 50% drainage area to the main Posada channel. The two channels are characterised by relatively low average reach gradients (Table 2.2). The morphology of the channels is partly influenced by lithology, with rugged and steep mountain and hilly areas, predominantly characterised by metamorphic and granite rocks. Unit peak discharges of 6.6 (Posada) and 7.3 $m^3\ s^{-1}\ km^{-2}$ (Mannu di Bitti) for drainage areas in the range of 300 – 600 indicate relatively high flood responses.

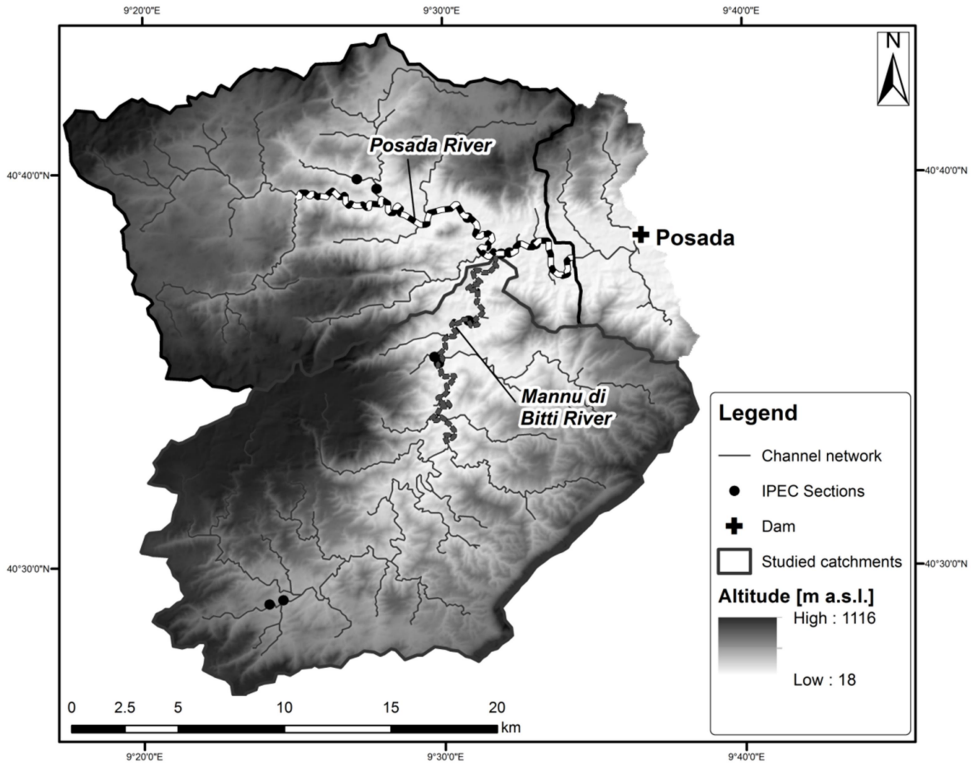

FIG.2.10. Locations and topographic features of the Posada and Mannu di Bitti Rivers.

2.2.3 THE LIERZA CREEK

The Lierza Creek, identified by the outlet at *Molinetto della Croda* (Mill of the rock fall) covers about 7.5 km^2 (Fig. 2.11). The creek is about 1800 m long, characterized by hilly topography and elevations range between 170 and 470 m a.s.l. (the mean elevation is 295 m a.s.l.), with average channel gradient of 2.5% for the surveyed sub reaches. The lengths of the sub reaches are on the order of 15–200 m. The studied channel reaches consist of cohesive bed and bank materials, mostly clayey rocks, with riparian vegetation, which makes the river network highly resistant to erosion. Unit peak discharge of 17.6 m^3 s^{-1} km^{-2} generated by basin-average rainfall accumulation of about 150 mm for a duration of 1.5 h indicates intense flood response at the outlet of this small basin. This caused intense sediment transport in some channel reaches, but limited widening.

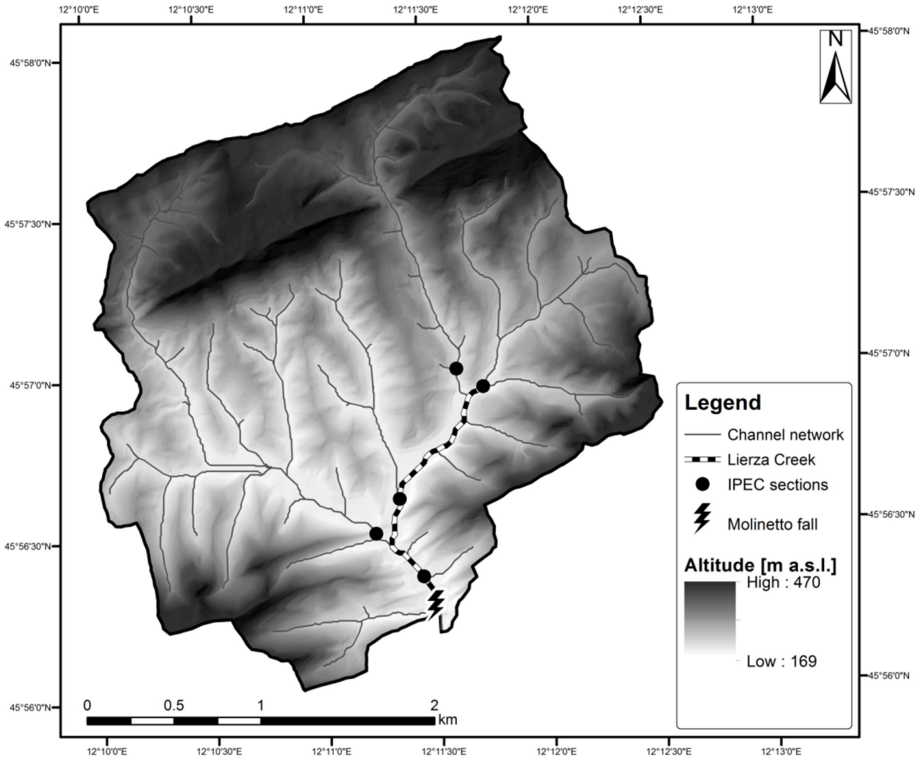

FIG.2.11. Location and topographic features of the Lierza Creek.

3 RESEARCH METHODOLOGY

Observational difficulties of hydrometeorological synopsis of flash floods (Borga et al., 2011) and lack of a comprehensive archive of flood events across Europe (Marchi et al., 2010) hinder the development of a coherent framework for the analysis of regional flood climatology, hazard and vulnerability at the pan-European scale (Barredo, 2007). The main methodological framework for the research is based on an integrated interdisciplinary approach for the collation of data and analyses of flood responses, and subsequent estimations and analysis of the various measures of stream power to quantify the geomorphic effectiveness of extreme flash flood that occurred in different hydro-climatic and geomorphic settings in Europe between 2007 and 2014. An integrated methodological framework that integrates hydrometeorological and geomorphological observations and analyses at different spatial scales (Rinaldi et al., 2016) is adopted to investigate the geomorphic impacts of the studied flash floods.

3.1 INTENSIVE POST-EVENT CAMPAIGN (IPEC)

Intensive Post-Event Campaign (hereinafter referred to as IPEC) have been carried out to document the flood response and geomorphic effectiveness of the studied flash floods. IPEC include collation of data from river authorities, post-flood field observations and surveys, and interviews with eyewitnesses to events through an. Table 3.1 presents detailed guidelines of a methodology on how to identify, collect and analyse data available after extreme flash flood events (Gaume and Borga, 2008). The methodological framework for data collection and elaboration includes (i) assessment of event rainfall from weather radar observations and rain gauge networks, (ii) post-flood surveys to document flood peaks in ungauged rivers and, (iii) geomorphic reconnaissance to assess the magnitude of geomorphic impacts in different channel reach types. The principles of methodology outlined in Table 3.1 have been employed to document and analyse the studied flash floods.

TABLE 3.1. Principles of methodology for post-flash flood data collection and analysis (*Adapted from Gaume and Borga (2008), p 177*)

Data collation process	*Data analysis process*
Phase 1: Just after the flood • Collect the data on the rainfall event (rain gauge measurements, radar images) to locate the affected areas. • If possible, the first reconnaissance visit of the affected areas, pictures (flood marks, large debris, river bed state) can be taken, but no survey work can generally be conducted during the crisis time *Phase 2*: A few weeks after the flood The cross-section surveys can begin as well as some interviews of witnesses depending on the local atmosphere. *Phase 3*: A few months after the flood • It is certainly the best period for the survey work especially for the interviews. The area is fully accessible and the stress has fallen again. The river beds and marks may have been cleaned out; this is why the pictures taken in phase 1or 2 are important. • Collect additional data useful for the analysis (river gauge measurements, digital terrain model, soil, land-use, geological map, soil moisture measurements, satellite or pictures taken by plane, flood mark inventories, etc.) Preparation of the rainfall-runoff stimulations to support the interpretations. *Phase 4*: The year after the flood Owing to the inaccuracy of the available data, a post flood investigation has some similarities with police inquiries. It is a long-lasting work, requiring cross-checking and possible returns to the phase 3.	*Step 1*: peak discharges estimation and mapping • Based on the cross sections surveyed, peak discharges and specific discharges can be estimated at various locations of the considered river and of its tributes and reported on a map. • Test of the spatial constituency of the estimates and comparison with rainfall data to get a first idea of possible runoff rates. • A comparison with rainfall, geological, land use maps gives some first idea of the possible factors affecting the flood magnitude. *Step 2*: Rainfall-runoff dynamics • Where radar quantitative representation precipitation estimates appear reliable and where complete or spatial flood hydrographs can be retrieved from measured data or accounts or documents (dated pictures) from the witnesses, they can be compared with simple rainfall-runoff (RR) simulations to get better idea about the RR dynamics, especially about the revolutions of runoff rates during the flood. *Step 3*: Comparison with previous floods • If step 2 could be performed, the same RR simulations can be conducted for previous large floods that occur on the same catchment if it is gauged or on nearby similar gauged catchments. *Step 4:* Accompanying process • When the runoff is described, accompanying processes such as erosion intensity on hill slopes, sediments transport or local flow characteristics can be studied.

3.1.1 RADAR-RAINFALL ESTIMATION

Rainfall estimates for each event were obtained by combining available weather radar observations and rain gauge data. The small scales as well as the localized nature of flash-flood triggered rainstorms is a crucial problem in the estimation of rainfall fields (Krajewski and Smith, 2002; Bouilloud et al., 2010). Reflectivity data from the original radar volume scans were elaborated using a set of algorithms and procedures described by Marra et al. (2014) in order to correct radar-related errors associated with heavy rain. The correction methods include, (i) analysis of the detection domain and correction for ground/anthropic clutters (Pellarin et al., 2002), (ii) implementation of corrections for range-dependent errors (e.g. screening, attenuation, vertical profiles of reflectivity), and (iii) optimization of the rainfall estimation procedure by comparison between radar and rain gauges at the event scale (Bouilloud et al., 2010). Detailed algorithms for the correction of radar reflectivity due to heavy rains can be found in Bouilloud et al. (2009). Rain rate estimates are produced using a reflectivity-to-rain rate (Z-R) relationship derived from measurement of convective events in the study regions (e.g., Anagnostou et al., 2010), and adjusting the residual bias with respect to ground data (Berne and Krajewski, 2013).

Radar and rain gauge measurements were merged using the technique based on adaptive multi-quadric surface fitting algorithm described by Martens et al. (2013) to produce a spatial representation of the flash flood-generated rainfall fields. The assessments of radar rainfall estimation accuracy were performed by comparison with ground based observations, on the event-cumulative values in order to minimize the sampling uncertainties due to the different scales of gauges and radar at short time intervals (Gires et al., 2014). The assessment of the quality of the final rainfall estimates were carried out by using a leave-one-out cross-validation (Efron, 1983). Three statistical parameters (fractional standard error, biases and correlation coefficient), largely used for this kind of assessment (Marra et al., 2014), were calculated for the quantitative assessment of the total water volume of radar estimates over raingauges. The spatial distribution of event-rainfall accumulations over the studied river basins are presented in section 2.1, whereas the maximum values are reported in Table 2.1 for the studied flash floods. Re-analysis of the radar rainfall fields helps to identify sections within the impacted areas that received significant amounts of rainfall for flood investigation through field surveys and observations, as well as being used to force a spatially distributed hydrological model for water balance analysis.

3.1.2 POST-FLOOD SURVEYS AND INDIRECT PEAK DISCHARGE ESTIMATES

Flood documentation by means of post-flood survey is an opportunistic, event-based approach that focuses on specific extreme events rather than on specific watersheds. In basins where runoff data are unavailable or scanty, post-flood surveys provide relevant information and observations in developing and consolidating a flash flood database and hence play a very important role in '*gauging the ungauged extremes*' (Borga et al., 2008). Post-flood surveys aim at understanding the hydro-meteorological, hydraulic and geomorphological processes that operate during extreme floods. The main types of data collated in the survey include; (i) discharge data at stream gauge stations and reservoir operations, (ii) peak discharge estimates at ungauged cross sections, and (ii) reconstructing the time sequence of the flood. This is valuable to document the spatially variable flood responses associated with flash floods, particularly in ungauged basins. Selected pictures during post-flood field surveys of the studied flash floods are presented in Appendix A1.

The aim of the cross-sectional surveys (*Phase 2 and 3*, Table 3.1) is to collate data on channel geometry and flood marks to reconstruct the peak discharges in the river sections of the studied flash floods. Surveyed cross sections were selected based on the following criteria: (i) preference to natural channels, (ii) spatial distribution to enable detection of flood response in different sectors of the basin and (iii) sections with different geomorphic impacts. The slope conveyance method (Gaume and Borga, 2008) was used for the indirect estimation of the flood peaks. This method requires topographical survey of cross-sectional geometry, high water marks (corresponding to flood levels), channel bed slope and the estimation of flow roughness to compute peak discharge at a single river section by means of the one-dimensional Manning-Strickler hydraulic equation, which assumes a uniform flow along a channel reach according to the following equation:

$$Q = V \cdot A_c \cong \frac{1}{n} \cdot A_c \cdot R^{2/3} \cdot S^{1/2} \qquad [3.1]$$

where Q_p [m^3 s^{-1}] is the peak discharge, V [m s^{-1}] is the average flow velocity, A_c [m^2] is the wetted cross-sectional area, R [m] is the hydraulic radius, S [m m^{-1}] is the energy line slope (usually estimated by the water surface and channel bed slope) and n is the roughness coefficient. The roughness coefficient is estimated based on complex parameters and processes such as channel bed forms,

sediment characteristics, riparian vegetation, flow type and regimes, and geomorphological processes (Lumbroso and Gaume, 2012).

Fig. 3.1 presents cross-sectional longitudinal and transversal profiles based on data obtained through post-flood field surveys for illustration purpose. The longitudinal profile (Fig. 3.1-A) provides the values of the water surface and channel bed slopes from the surveyed flood marks and longitudinal profile, respectively. These two slopes are usually parallel and a surrogate for the energy line slope, S_e. The transversal profile (Fig. 3.1-B) provides the detailed parameters of the cross-sectional hydraulic geometry required for the estimation of the flood peak. The area bounded by the channel cross section and the water surface is the wetted cross-sectional area, A_c [m^2]. The wetted perimeter, P [m] is the wetted length of the channel cross section below the water surface and hence the hydraulic radius can be estimated as $R = A_c/P$. With these parameters, peak discharges at surveyed cross sections were estimated based on Eq. [3.1]. The length of the water surface (Fig. 3.1-B) represents post-flood channel width w [m], which was used to compute unit stream power at the various cross sections.

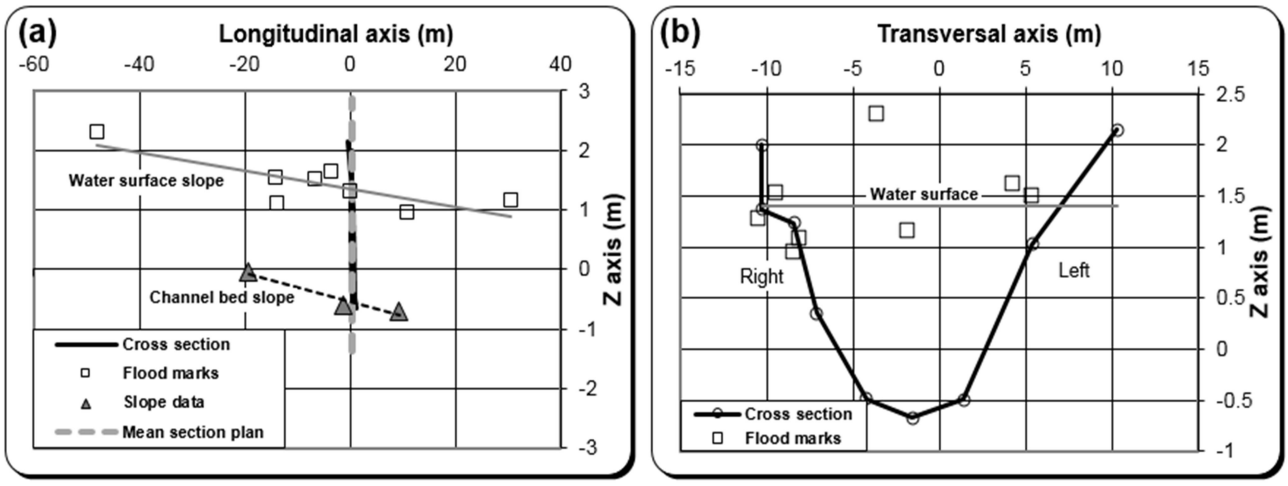

FIG.3.1. (A) Longitudinal and (B) transversal profiles of a surveyed cross section

3.1.3 GEOMORPHOLOGICAL RECONNAISSANCE: CHANNEL TYPES AND OBSERVED GEOMORPHIC EFFECTS

Geomorphological reconnaissance is usually carried out before conducting indirect peak discharge estimates to recognize and distinguish the types of flow processes: water floods and/or debris flows (Marchi et al., 2009b). This is because the non-Newtonian nature of debris flows may result in gross overestimation of discharges with the use of Newton-based relations (Jarrett, 1994). The geomorphological settings of 59 surveyed cross sections were investigated for the four recent flash floods in Italy (Magra, Vizze, Cedrino-Posada and Lierza) through field observations and aerial photo interpretation; aerial photos have also enabled recognition of pre-flood channel conditions for these floods. Such a detailed analysis of flood impacts was not possible for previous floods (Selška Sora, Starzel, and Argens).

The surveyed channel cross sections were categorized into four distinct channel reach types according to bed and bank materials (Marchi et al., 2016): Alluvial, Semi-alluvial, Bedrock and Artificial. Alluvial cross sections consist entirely of alluvial material; Semi-alluvial cross sections partly consist of alluvial materials and other parts could have been artificially modified or consist of bedrock outcrops. Bedrock cross sections are entirely on bedrock (thin sediment cover can be present); and artificial cross sections are lined channels, channel banks protected with riprap.

Observed geomorphic effects were categorized into negligible, small-moderate and major through field observations and digital image analysis of the cross sections (Marchi et al., 2016). Negligible geomorphic impacts are usually without significant modification to channel form. Small to moderate geomorphic effects are characterized by localized erosion and small widening of the cross sections mainly due to fluvial entrainment, whereas major impacts are classified as relevant channel widening, with major erosion of banks and floodplains. Fig. 3.2 presents examples of cross-section types and observed geomorphic effects in the studied channel reaches, whereas the corresponding cross-tabulation is reported in Table 3.2. These classifications served to qualitatively associate stream power values with observed geomorphic effects in different channel cross sections, which may shed more light on how the geographical variability of stream power within mountain stream basins could fully capture the variability in geomorphic effects (e.g., Fonstad, 2003).

TABLE 3.2. Cross-tabulation of channel types and observed geomorphic effects for the 59 surveyed sections in the Magra, Vizze, Cedrino-Posada and Lierza Rivers

Channel types	*Observed geomorphic effects*		
	Major (M)	Small-to-moderate (S-M)	Negligible (N)
Alluvial (AL)	10	11	-
Semi-alluvial (S-A)	5	16	5
Bedrock (BR)	-	-	4
Artificial (AT)	-	-	8

FIG.3.2. Examples of channel types and different intensities of observed geomorphic impacts of floods in the studied river channels: (A) major geomorphic impacts in alluvial channels, (B) major geomorphic impacts in semi-alluvial channels, (C) negligible geomorphic impacts in bedrock channels, and (D) negligible geomorphic impact in artificial channels.

3.2 Basin Analysis and Channel Characterisation

MATLAB (Matrix Laboratory) numerical programming language functions in TopoToolbox (Schwanghart and Kuhn, 2010) and *ArcGIS* were combined and used to extract important data and information from high resolution *DEM* and aerial photos. For all river sections of interest (both cross sectional and sub reaches of the selected channels), the master variable 'drainage area' and channel networks were extracted from *DEM* for hydrological modelling and analysis of the scale-dependent flood responses. For sub reach units along longitudinal profiles of the selected channels of the Magra, Cedrino, and Lierza, channel gradients were extracted from *DEM*, whereas morphological changes represented by channel widening, as well as channel confinement, were estimated from high-resolution aerial photos were estimated for the Magra and Cedrino channels only.

3.2.1 Delineation of basin area and channel network

The corresponding MATLAB functions in TopoToolbox (Schwanghart and Kuhn, 2010) were used to calculate flow direction and flow accumulation from high-resolution *DEM* of the studied catchments. The *ArcGIS* algorithm '*fill*' was used to eliminate '*pits*' or small imperfections in the surface raster that could destruct the theoretical down-slope flow of the hydrological process. The '*flow direction*' function uses the *D8* algorithm to create a raster flow direction from the adjusted surface raster by assigning direction codes to each cell such that each cell flows into the steepest of the eight adjacent cells. The '*flow accumulation*' function then creates a raster of accumulated number of cells flowing into each cell using the flow direction raster. The upslope area draining to each cell was calculated as the product of the flow accumulation value and the unit area of the resolution of the grid cells. The channel network of the basin is delineated from the last raster by applying a constant flow accumulation threshold to distinguish between hillslope and channel paths.

3.2.2 ESTIMATION OF CHANNEL GRADIENT, WIDENING, AND CONFINEMENT

In collaboration with a Ph.D project at the Department of Geosciences of the University of Padova (PhD candidate Margherita Righini, supervisor Prof. Nicola Surian), remote sensing was used to estimate important channel properties for sub reaches of the selected channels. Sub reaches were in the range of 300–500, 700–1100, and 15–200 m in length on the Magra, Posada, and Lierza respectively, partly depending on the total length of the selected channels. Channel gradients were estimated for the Magra, Posada, and Lierza sub reaches from the *DEM* using the corresponding MATLAB function in TopoToolbox (Schwanghart and Kuhn, 2010). The algorithm is similar to the '*horizontal slice*' method suggested by Vocal Ferencevic and Ashmore (2012). Unlike the *GIS* slope-based algorithm, which calculates slope as an average over the entire landscape or the maximum slope between any cells surrounding a target cell, the horizontal slice method calculates slopes in a specific direction along the channel in order to estimate channel slope and/or an approximation of water-surface slope.

The availability of pre-flood and post-flood aerial satellite imagery with high spatial resolution permitted estimation of channel widening and confinement index for the Magra (Surian et al., 2016) and Posada (Righini et al., 2017) Rivers. Morphological response to the studied flash flood was defined in terms of channel widening – the main geomorphic effects that occurred along the studied channels of the Magra and Posada Rivers. Analysis and interpretation of pre-flood and post-flood aerial satellite imagery enabled quantification of the geomorphic changes at the channel-reach scale that prevailed during the extreme flood. Active channel areas before and after the flood, and alluvial plain widths were digitized from the respective aerial photos using *ArcGIS*. Average channel widths, were then estimated as the ratio of the channel areas to the corresponding length of the sub-reach units. The width ratio, defined as the ratio of the channel width after the flood to the channel width before the flood (Krapesch et al., 2011) was used as representative of channel widening. Fig. 3.3 shows an example of remotely sensed channel changes and lateral confinement from pre- and post-flood aerial photos for one of the studied rivers. Confinement index was defined as the ratio of the alluvial plain width to the channel width before the flood (Rinaldi et al., 2013).

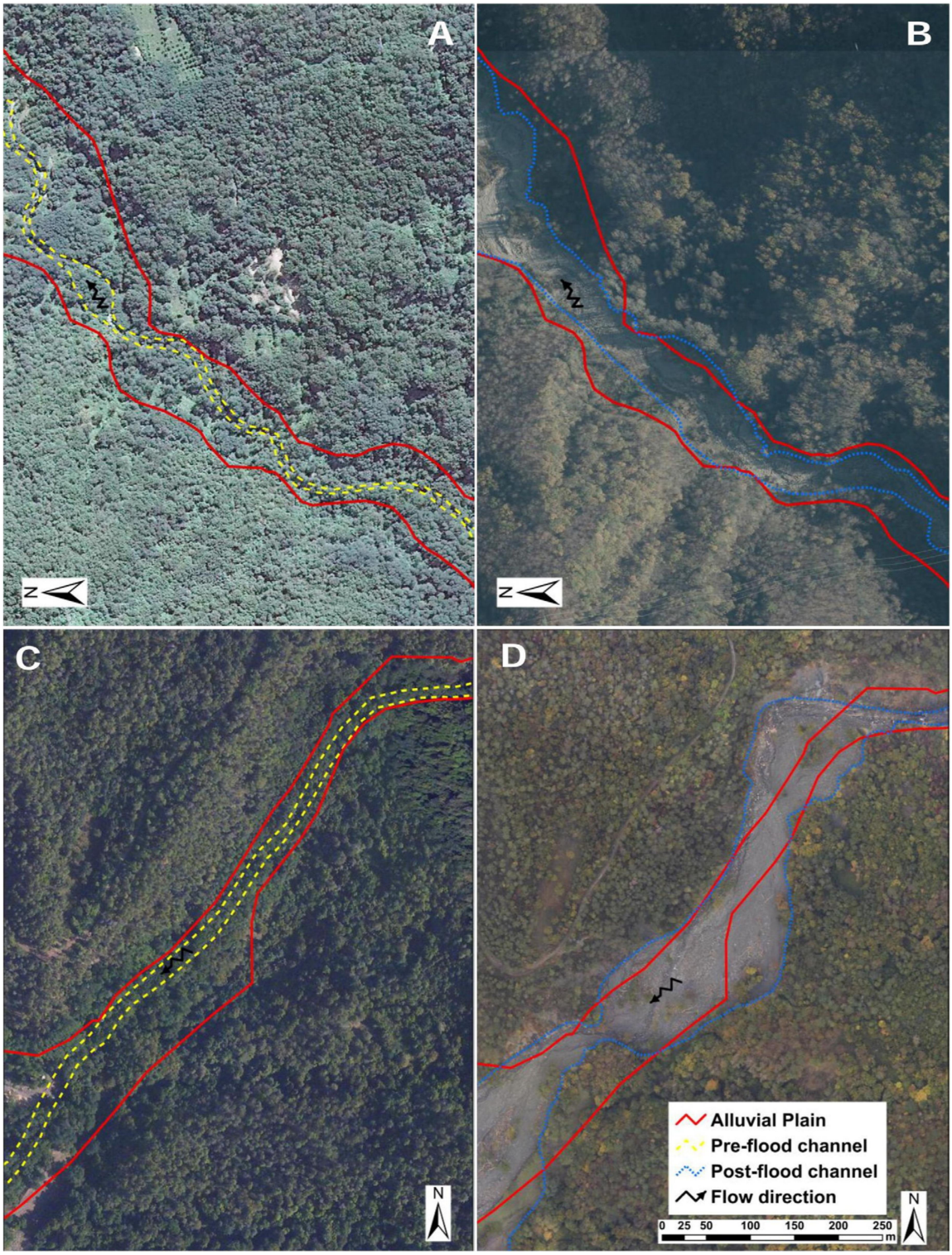

FIG.3.3. Examples of remotely sensed channel changes observed along the longitudinal profiles of one of the studied rivers (*Adapted from Surian et. al., 2016*).

3.3 Flood Modelling and Uncertainty Analysis

3.3.1 Spatially distributed flood response model

The Kinematic Local Excess Model (*KLEM*), which integrates spatially distributed radar rainfall estimates and basin properties (i.e., *DEM,* soil hydraulic properties, land use, antecedent moisture conditions), has been implemented to check the consistency of the rainfall-runoff dynamics for the studied flash floods and to simulate peak discharge for the computation of stream power in ungauged cross sections. The model uses a mixed Curve Number – Green-Ampt method for rainfall excess modelling (Grimaldi et al., 2013). The procedure consists of applying the *SCS-CN* approach (Ponce and Hawkins, 1996) to quantify the storm net rainfall total amount and using this value to estimate the effective saturated hydraulic conductivity of the Green-Ampt method. Using the Green-Ampt infiltration model with moisture redistribution (Ogden and Saghafian, 1997), rainfall in each point of the catchment is divided into surface and subsurface runoff components. In the method, the relationship between the effective rainfall (or direct runoff) accumulated up to time *t,* P_e (*t*) and the cumulative precipitation at the same time *P* (*t*) is given by:

$$P_e(t) = \begin{cases} \frac{(P(t)-I_a)^2}{(P(t)-I_a+S)}, & P(t) > I_a \\ 0, & P(t) < I_a \end{cases} \quad [3.2]$$

where *S* [mm] is a conceptual subsurface reservoir volume, defined by the maximum soil-water retention and I_a [mm] represents the initial abstraction before direct runoff begins, given as a function of *S*. Following Ponce and Hawkins (1996), the value of the *S* parameter in the *SCS-CN* method for a given soil is related to the curve number *CN* parameter through a calibration parameter *X*, called infiltration storativity. The potential value of the volume infiltrated *S,* is represented by:

$$S = 254.0\left(\frac{100}{CN} - 1\right) \cdot X \quad [3.3]$$

CN is a spatially distributed absorption parameter, which is a function of the hydrologic soil-cover complex. Unlike *CN,* which is spatially distributed, the *X* parameter is assigned to the basin or sub basin scale. The parameter *X* is a function of the absorption capacity of the superficial layers of the soil over the duration of the event. The use of this parameter ensures the calibration of a spatial distribution

of *CN* values in order to correctly simulate the observed flood water balance. In the conceptualization of the model, the initial wetting states of the basin are represented in three classes of AMC (Antecedent Moisture Condition, AMC-I, AMC-II and AMC-III), representing, respectively, initially dry, normal, and wet soil conditions. The index parameter AMC adjusts the *CN* originally assigned to generate a correct distributions of CN_{adj}, according to the formula:

$$CN_{adj} = \frac{CN \cdot A}{(CN \cdot B)+10} \quad [3.4]$$

where, $A = 2.08454\, exp(AMC\ 0.80709) - 0.0.47225$ and $B = \frac{A-4.2}{100} - 0.058$

The distributed runoff propagation is based on the identification of drainage paths and requires the characterization of hillslope and channel paths. A simple model (Da Ros and Borga, 1997; Giannoni et al., 2003) is used to represent the runoff propagation for the response of the drainage system. This requires the separation of hillslope and channel elements based on a channelization support area, A_s, which is considered constant at the sub basin scale and two invariant hillslope and channel flow velocities. The model computes discharge Q (t) at any location (x, y) along the river network as follows:

$$Q(t) = \int_A q[t - \tau(x,y), (x,y)]\, dA \quad [3.5]$$

where A is the area draining to the specific outlet location (x, y), q (t, x, y) is the total runoff at time t; and τ (x, y) is the routing time from a generic point (x, y) to the outlet of the basin specified by the region A. The routing time is defined as:

$$\tau(x,y) = \frac{L_h(x,y)}{v_h} + \frac{L_c(x,y)}{v_c} \quad [3.6]$$

where L_h (x, y) is the distance from point (x, y) to the channel network following the steepest descent path; L_c (x, y) is the length of the subsequent channel drainage path to the watershed outlet and v_h and v_c are the two invariant hillslope and channel flow velocities, respectively. The use of invariant channel and hillslope velocities for flash-flood simulation has been discussed by Ruiz-Villanueva et al. (2012). Rodriguez-Iturbe and Rinaldo (1997) support the assumption that models of the hydrologic response employing basin-constant channel celerity explain observed travel time distributions, at least for high flow conditions (e.g., Giannoni et al., 2003; Nicótina et al., 2008; Marchi et al., 2010). The invariant

hillslope celerity assumption is more conceptual in nature (Botter and Rinaldo, 2003). In fact, great variability in hillslope transport properties is expected, particularly when it is driven by local topographic gradients as subsurface runoff through partially saturated areas and in the presence of preferential flow paths (Dunne 1978; Beven and Wood, 1983).

The model framework is based on six calibration parameters: the channelization support area (A_s), two kinematic parameters (v_h and v_c), the infiltration storativity parameter, X required for the calibration of the *SCS-CN* procedure and the parameters I_a and AMC required for the specification of the initial abstraction and antecedent moisture conditions, respectively. The model also includes a linear relation for base flow modelling, whose input is computed using the *SCS-CN* method (Borga et al., 2007). The application and verification procedure of the flood response model is based on the concept of 'hydrological similarity' (Parajka et al., 2013), which involves (i) calibration on runoff data at a gauged station, (ii) verification of the constructed model through cross-validation by comparing simulated peak discharges with field-estimated values from post flood surveys at the ungauged sections and (iii) transposition of model parameters to simulate runoff responses any location of interest within the region defined by the gauged station

3.3.2 Uncertainty framework for the integration of field-estimated and model-based peak discharges

Post-flood indirect peak discharge estimates can be undermined by theoretical errors and are affected by significant observational uncertainties, which should be considered together with the important uncertainties in the rainfall-runoff modelling of flash floods response (Amponsah et al., 2017). Theoretical error, which can be avoided by means of proper recognition of the flow process, involves assumptions and application of hydraulic models suitable for water flows to non-Newtonian flows (e.g., debris flows and hyper-concentrated flows – Costa and Jarrett, 1981, 2008; Hungr et al., 1984; Jarrett, 1994; Prochaska et al., 2008), as well as the causative processes leading to the flood peaks is very important in documenting and understanding flood response. Some flood peaks are caused by failure of landslide dams or other types of channel obstructions. Landslides and large wood jams may block the river and, when these burst, it may generate a flood peak which is not related to

rainfall-runoff generation processes, but rather to the volume of water stored and the velocity of dam breaching. Hence, estimates of these flood peaks should not be used for comparison with rainfall-runoff models. Even when a post-flood estimate passes the theoretical consistency checks in relation to flow process type and channel obstruction, it is important to carry out an uncertainty estimate which accounts for observational errors that may affect the accuracy of the estimated peak discharge. Fig. 3.4 presents a flowchart for a sound estimate of peak discharge using the slope conveyance method and a subsequent comparison with model-based peak discharges.

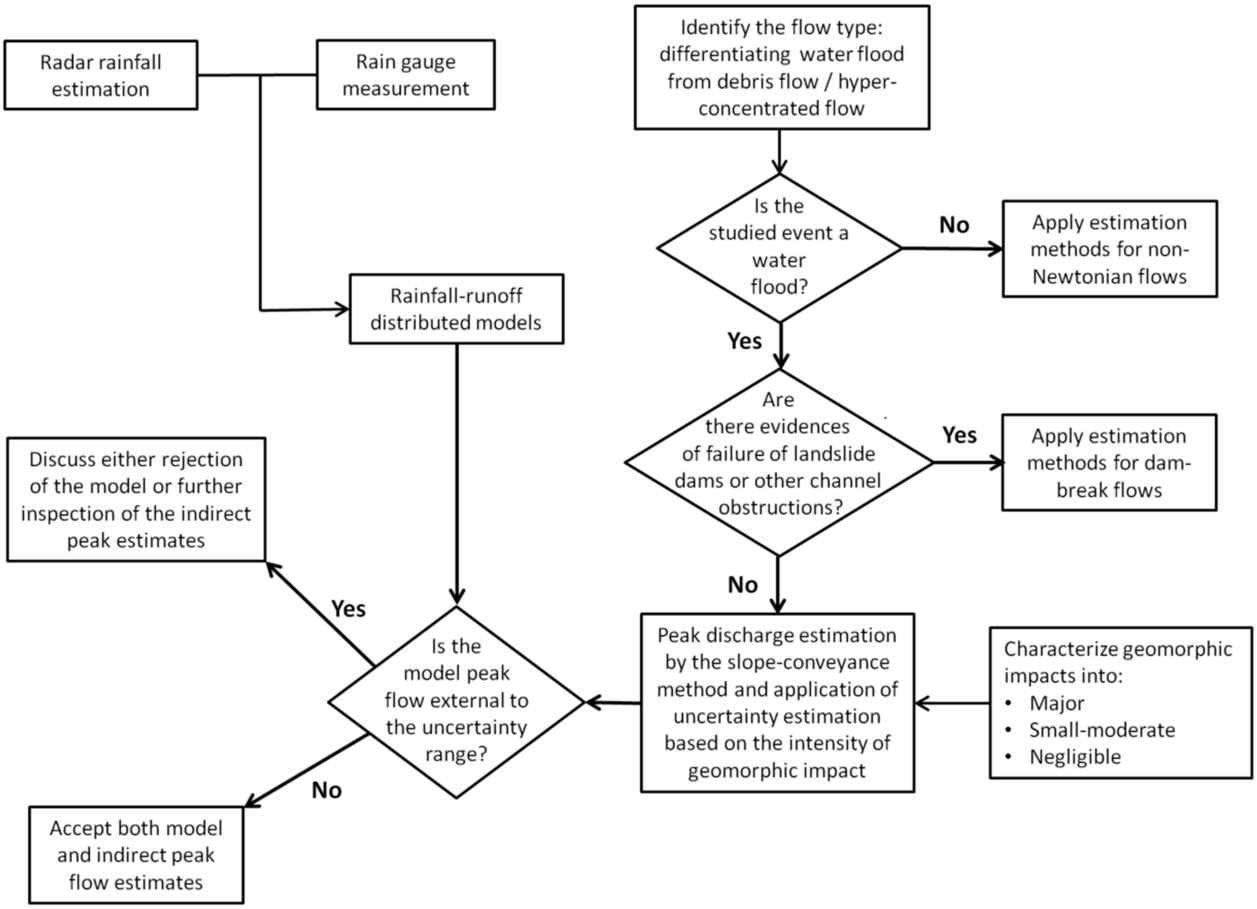

FIG.3.4. Flowchart for integrated hydrologic flash flood analysis: indirect estimate of peak discharge, uncertainty assessment and comparison with rainfall-runoff model results (*Adapted from Amponsah et al., 2016*).

Observational errors involve the discrepancies between true values of all variables and the corresponding surveyed, estimated and assumed values actually used in the estimation of the flood peak. These may include measurement errors in high water mark and channel geometry, choice of roughness coefficient, and channel erosion and/or aggradation that might potentially modify surveyed channel geometry with respect to peak flow hydraulic conditions. Geomorphic processes and impacts may place considerable limitations on the reliability of indirect methods for flood peak estimation (Gaume and Borga, 2008). For instance, scour and/or fill may occur after the high water marks are left by the current. The effect is that the cross-section geometry surveyed after the flood is different from the one existing at the time of the peak flow. The uncertainties in indirect estimation of peak flows during post-event surveys are evaluated by error analysis of the slope-conveyance peak discharge determination (Amponsah et al., 2016; 2017).

The linear error analysis permits explicit consideration of the effects of discrepancies between the true values of a number of variables and the corresponding measured or estimated values (Kirby, 1987). The effect of these error sources on the accuracy of the computed peak discharge is estimated by statistical error analysis using a Taylor-series approximation of the discharge equation and the equation for the variance of a sum of correlated random variates as follows (Amponsah et al., 2016):

$$var\ \Delta Q_p = \left(\frac{\partial Q_p}{\partial h_w}\right)^2 var\Delta h_w + \left(\frac{\partial Q_p}{\partial L}\right)^2 var\Delta L + \left(\frac{\partial Q_p}{\partial n}\right)^2 var\Delta n + \left(\frac{\partial Q_p}{\partial A}\right)^2 var\Delta A + \left(\frac{\partial Q_p}{\partial P}\right)^2 var\Delta P + 2\left(\frac{\partial Q_p}{\partial P}\right)\left(\frac{\partial Q_p}{\partial A}\right) var\Delta P var\Delta A \quad [3.7]$$

where the terms $var\ \Delta A$ and $var\ \Delta P$, which represent the variances in the change in measured cross-sectional area and wetted-perimeter, respectively, incorporate the errors in the measurements of the section width (b), section mean depths (d) and scour/fill (s). The scour (if any) is assumed to be of constant depth across the section. Fill is treated as negative scour. The development of the Eq. [3.7] through partial derivatives with respect to the variables in the Manning-Strickler discharge equation (Eq. [3.1]) and assuming the algebraic sum of the covariance terms to be either zero or else negligible as compared to the squared terms yields the following the approximation of the error variance in the estimated peak discharge:

$$\frac{var\ \Delta Q_p}{{Q_p}^2} = \varepsilon_{Q_p}^2 = \frac{1}{4}\varepsilon_{h_w}^2 + \frac{1}{4}\varepsilon_L^2 + \frac{25}{9}\left(\frac{\varepsilon_b^2}{N-1} + \varepsilon_d^2 + \varepsilon_s^2\right) + \frac{4}{9}\frac{\varepsilon_b^2}{N-1} + \varepsilon_n^2 \quad [3.8]$$

where N is the number of ground points and the term ε_z^2 indicates the relative error variance in the measurement or estimation of the variable z and the corresponding influence coefficients of error variance obtained through the partial derivative of the discharge equation. Eq. [3.8] reveals that the various error variances are observable although errors themselves are not observable (Kirby, 1987). In Eq. [3.8], measurement errors in d and s are expressed in terms of relative error variances ε_d^2 and ε_s^2, respectively, referenced to mean depth A/b, whereas the error in w are expressed in terms of relative error variance ε_b^2 referenced to $b/(N\text{-}1)$, i.e. the average spacing between ground points. Eq. [3.8] shows that the observational error variance depends on the measurement uncertainties ($\varepsilon_{S_e}^2$; ε_b^2; ε_d^2), on the uncertainties in the evaluation of the roughness parameter (ε_n^2), and on the impact of the geomorphic effects (ε_s^2). It should be noted that geomorphological changes are likely to affect both terms ε_s^2 and ε_n^2, given the influence that changes in bed geometry and morphology may have on flow resistance (Ferguson, 2007; Church and Ferguson, 2015). The standard deviation obtained from Eq. [3.8] is used to derive confidence intervals for the field-based estimates of the peak flows. Flood peak simulations obtained from hydrological models may then be compared with these uncertainty ranges according to the flowchart presented in Fig. 3.4.

The observational variances were categorised and stratified according to the three impacts of geomorphic effects – negligible, small-to-moderate and major, – as reported in Table 3.3. The table shows that the error terms ε_s and ε_n are variable with the geomorphic changes, whereas the other terms are kept constant, since they depend only on the topographical and HWM surveying uncertainties. Errors in the surveying of HWM and of the cross sections are distinguished because the measurements of ground points and of high water marks are characterised by different accuracies. The evaluation of errors in section width and section mean depth that define channel cross-sectional area and wetted-perimeter, was based on sensitivity analysis of the surveyed cross-sectional geometry because of the non-uniformity of the channel morphology.

TABLE 3.3. Summary values of the error variances of peak discharge uncertainty for the three categories of geomorphic effects

Relative error terms	*Geomorphic impacts*		
	Negligible	*Small to moderate*	*Major*
ε_s	0.04	0.12	0.20
ε_{h_w}	0.10	0.10	0.10
ε_b	0.01	0.01	0.01
ε_d	0.02	0.02	0.02
ε_n	0.10	0.10	0.15
ε_L	0.01	0.01	0.01
$var\,\Delta Q_p/Q_p{}^2\,(10^{-4})$	182	537	1373
$std.dev\Delta Q_p/Q_p(\%)$	±13.5	±23.2	±37.1

Observational error variance in the energy line gradient (ε_{Se}^2), was evaluated as the sum of squared errors of surveyed HWM with respect to the regression that defines the energy line gradient in both axes, respectively, defined in Table 3.3 as error terms in HWM assessment (ε_{h_w}) and location along the channel reach (ε_L). It should be noted that in the slope-conveyance peak discharge determination method, multiple flood mark points are identified everywhere they are visible on channel banks for estimating the energy line gradient, and hence surveys in both HWM and the corresponding location along reach length are subject to random measurement errors. The Orthogonal Distance Regression (ODR) is therefore appropriate as the errors-in-variables regression method to account for errors in both variables, rather than the classical Ordinary Least Squares (OLS) analysis, in which best fit is chosen to minimize the residual errors in the *y* direction only. The values of the error standard deviation are computed by using *N=11* for the ground points, which represent a mean value across the IPEC sections. The confidence interval which extends one standard deviation on both sides of the central estimate, may thus be expressed based on Eq. [3.8] with percentage uncertainty bounds of ±13.5%, ±23.2% and ±37.1% for cross sections that showed negligible, small to moderate and major geomorphic impacts, respectively (Table 3.3).

A statistical analysis of the accuracy of the model was performed using the Nash Sutcliffe Statistics Efficiency score (NSE) (Nash and Sutcliffe, 1970). NSE permits reliable comparison between the estimated and simulated peak discharges since it is dimensionless and easy to interpret. This efficiency score is given as:

$$NSE = 1 - \frac{\sum_{i=1}^{n}(Q_i^r - Q_i^s)^2}{\sum_{i=1}^{n}(Q_i^r - Q_{ave}^r)^2} \quad [3.9]$$

where Q_i^r is the estimated peak discharge value for the i^{th}-basin; Q_i^s is the simulated peak discharge value for the i^{th}-basin, and Q_{ave}^r is the mean value of the estimated peak discharges.

According to Eq. [3.9], if NSE = 1, then the model is perfect (zero errors) and if NSE = 0, the model is considered as good as the average of the observed values. Negative NSE implies that the residual variance is larger than the data variance and therefore the mean of the estimated peak discharge values could be a better predictor than the model.

3.4 Stream Power Analysis

3.4.1 Peak stream power and uncertainty assessment

This section presents standardized measures of stream power associated with flash floods based on a combined analysis of field data from post-flood surveys and hydrological modelling to better quantify their geomorphic effects and the corresponding hydrologic and hydraulic controls. Two sets of stream power measures related to field-based peak instantaneous discharges were computed for the 119 surveyed cross sections of the seven studied flash floods: *cross-sectional stream power* and *unit stream power*. Cross-sectional stream power Ω [W m^{-1}], which expresses the rate of energy expenditure per unit channel length, is calculated as follows:

$$\Omega = \gamma \cdot Q_p \cdot S \quad [3.10]$$

where γ [9810 N m^{-3}] is the specific weight of water, Q_p [m^3 s^{-1}] is peak discharge and S [m m^{-1}] is the channel bed slope. Unit stream power ω [W m^{-2}] is calculated as cross-sectional stream power per unit channel width w [m] and represents the rate of energy expenditure per unit area of the channel bed.

$$\omega = \Omega / w \quad [3.11]$$

For purposes of error analysis, we express the estimated cross-sectional stream power as a function of the following variables $\Omega = f(Q_p, S)$ according to Eq. [3.10]. The error in Ω due to errors ΔQ_p and ΔS, in Q_p and S respectively, may then be treated in first-order Taylor series as follows:

$$\Delta\Omega = \frac{\partial\Omega}{\partial Q_p}\Delta Q_p + \frac{\partial\Omega}{\partial S}\Delta S + 2\left(\frac{\partial\Omega}{\partial Q_p}\right)\left(\frac{\partial\Omega}{\partial S}\right)\Delta Q_p \Delta S \quad [3.12]$$

where $\frac{\partial\Omega}{\partial z}\Delta z$ is the error in Ω due to an error Δz in variable z only.

Squaring Eq. [3.12] and conveniently taken the algebraic sum of the covariance term as either zero or else negligible as compared to the squared terms yields:

$$\Delta\Omega^2 = \left(\frac{\partial\Omega}{\partial Q_p}\Delta Q_p\right)^2 + \left(\frac{\partial\Omega}{\partial S}\Delta S\right)^2 \quad [3.13]$$

The error variance in estimated cross-sectional stream power may then be treated in first-order Taylor series as follows:

$$var\ \Delta\Omega = \left(\frac{\partial\Omega}{\partial Q_p}\right)^2 var\Delta Q_p + \left(\frac{\partial\Omega}{\partial S}\right)^2 var\Delta S \quad [3.14]$$

$$\frac{var\ \Delta\Omega}{\Omega^2} = \varepsilon_\Omega^2 = \varepsilon_{Q_p}^2 + \varepsilon_S^2 \quad [3.15]$$

The errors in the energy line gradient is expressed as a function of errors affecting the measurements of HWMs (h_w) and channel length (L): $S = f(h_w, L)$. Relative standard deviation in estimated cross-sectional stream power may then be expressed as:

$$\varepsilon_\Omega = \pm\left(\varepsilon_{Q_p}^2 + \varepsilon_{h_w}^2 + \varepsilon_L^2\right)^{1/2} \quad [3.16]$$

Errors in peak instantaneous unit stream power is affected by errors in the estimation of cross-sectional stream power as well as the intensity of geomorphic impacts that may cause discrepancy between channel width at the time of flood peak and the measured post-flood channel width actually used in the computation of unit stream power. This effect may be represented by the scour/fill parameter. From Eq. [3.11], the errors in estimated unit stream power can be expressed as a function of the following variables $\omega = f(\Omega, s)$. Relative standard deviation in unit stream power may then be expressed as:

$$\varepsilon_\omega = \pm(\varepsilon_\Omega^2 + \varepsilon_s^2)^{1/2} \quad [3.17]$$

TABLE 3.4. Summary values of the observational error variances of cross-sectional stream power and unit stream power for the three categories of geomorphic effects

Relative error terms	*Geomorphic impacts*		
	Negligible	*Small to moderate*	*Major*
ε_{Q_p}	0.135	0.232	0.371
ε_{h_w}	0.10	0.10	0.10
ε_L	0.01	0.01	0.01
ε_s	0.04	0.12	0.20
$var\,\Delta\Omega/\Omega^2\ (10^{-4})$	283	639	1477
$std.dev\Delta\Omega/\Omega(\%)$	±16.8	±25.3	±38.4
$var\,\Delta\omega/\omega^2\ (10^{-4})$	299	783	1877
$std.dev\Delta\omega/\omega(\%)$	±17.3	±28.0	±43.3

From Table 3.3, the relative errors in estimated peak discharge amounted to percentage uncertainty bounds of ±13.5%, ±23.2% and ±37.1% for cross sections that underwent negligible, small to moderate and major geomorphic impacts, respectively. Table 3.4 reports the observational error variances for the estimation of cross-sectional stream power and unit stream power categorized according to the three classes of geomorphic impacts. Relative errors in measurements of HWMs and channel length as well as the scour/fill parameter are from Table 3.3. Relative errors in estimated cross-sectional stream power (unit stream power) amounted to percentage uncertainty bounds of ±16.8%, ±25.3% and ±38.4% (±17.3%, ±28.0% and ±43.3%) for cross sections that underwent negligible, small to moderate and major geomorphic impacts, respectively. Table 3.4 shows that observational errors variances increases for peak discharges, cross-sectional stream power and unit stream power in that order. This is because of the increase in the number of parameters used in the estimation of the corresponding variables that increases the sum of correlated random variates.

3.4.2 STREAM POWER HYDROGRAPH AND CUMULATIVE ENERGY EXPENDITURE

The distributed flood response model was implemented to compute flood hydrograph characteristics for 59 basins of the four recent floods in this study (Magra, Vizze, Cedrino-Posada and Lierza floods) and the 159 sub reaches of the selected channels. The flood hydrograph was combined with channel slope and cross-sectional channel width to produce the stream power hydrograph (Fig. 3.5). This provided a context to evaluate the combined influence of flood-flow duration and cumulative

energy expenditure (Costa and O'Connor, 1995; Kale, 2008; Magilligan, et al., 2015) on the potential geomorphic effectiveness of different flood events relative to peak instantaneous stream power measures. Cumulative energy expenditure, $\mathcal{E}$ [J m^{-2}] represents the distribution of stream power per unit cross-sectional area throughout the flood hydrograph, computed by integrating unit stream power ω [W m^{-2}] over the duration of the flood event, $t = t_o \rightarrow T$ [s] as follows:

$$\mathcal{E} = \int_{t_o}^{T} [\gamma \cdot Q(t) \cdot S/\mathrm{w}]dt \qquad [3.18]$$

Two main parameters were derived from the stream power hydrograph (Fig. 3.5). First, the event energy expenditure ($\mathcal{E}_e$ [J m^{-2}], hereinafter), computed as the area under the hydrograph between the inflection points. The inflection points on the stream power hydrograph, as shown in Fig. 3.5 (joined by the dot-dash line), correspond to the duration of the flood response, i.e., from the start to the end of the runoff event. The value of the starting point of $\mathcal{E}_e$ on the rising limb corresponds to unit stream power value at the first rise of event hydrograph. The end of $\mathcal{E}_e$, on the other hand, was identified graphically on the recession limb plotted on a logarithmic chart, corresponding to the end of event direct runoff. Second, a proportion of $\mathcal{E}_e$ associated with energy above the threshold for major geomorphic change, referred to as above-threshold energy expenditure ($\mathcal{E}_{th}$ [J m^{-2}], hereinafter). In Fig. 3.5, $\mathcal{E}_{th}$ is defined as the energy above the Miller-Magilligan critical stream power threshold of 300 W m^{-2}. A dimensionless parameter, referred to as energy ratio ($\mathcal{E}_r$, hereinafter) is proposed as a predictor of possible occurrence of geomorphic changes and defined as the ratio of the energy above the threshold for major geomorphic change to the overall energy expended as follows:

$$\mathcal{E}_r = \mathcal{E}_{th}/\mathcal{E}_e \qquad [3.19]$$

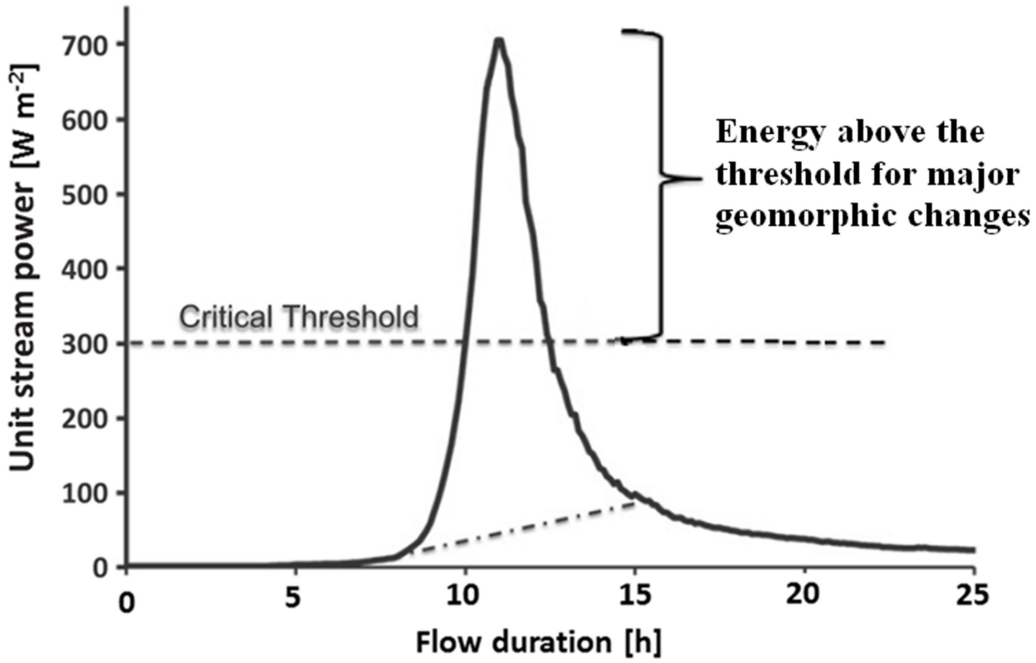

FIG.3.5. Stream power hydrograph of a typical flash flood. Discharge data from model simulations, together with channel cross-sectional geometry and slope data, were used to generate unit stream power. Dashed line indicates the Miller-Magilligan critical threshold (300 W m^{-2}), and the dot-dash line joins the inflection points on the rising and recession limbs of the hydrograph. (*Modified from Magilligan et al., 2015*).

4 RESULTS

4.1 FLASH FLOOD RESPONSE

The reference database for this study consists of 119 catchments that were affected by seven major flash floods in Europe. Table 4.1 presents a summary of basin, flood response and channel hydraulic properties of the studied flash floods, with cross sections ranging per event between 2 (Vizze) and 33 (Magra), mostly depending on the spatial extent of affected watershed and on the topology of the channel network. The database for the 119 catchments of the seven studied flash floods is reported in Appendix A2.

TABLE 4.1. Summary parameters of the flood database for the seven studied flash floods: average and (*standard deviation*)

Parameters, *Symbol* [*unit*]	Selška Sora	Starzel	Argens	Magra	Vizze	Cedrino-Posada	Lierza
No. of sections	19	17	24	33	2	17	7
Catchment size, A [km^2]	24.6 (*26.9*)	29.3 (*33.2*)	219.1 (*498.2*)	20.0 (*17.5*)	59.1 (*19.6*)	184.6 (*196.8*)	4.7 (*3.9*)
Peak discharge, Q_p [m^3/s]	100.2 (*107.5*)	52.1 (*50.2*)	339.9 (*462.6*)	154.9 (*136.0*)	74.2 (*6.0*)	1644.6 (*1409.5*)	74.8 (*47.0*)
Energy line gradient, S [m/m]	0.023 (*0.014*)	0.019 (*0.009*)	0.019 (*0.016*)	0.027 (*0.025*)	0.015 (*0.001*)	0.014 (*0.008*)	0.025 (*0.010*)
Cross-sectional area, A_c [m^2]	33.9 (*35.8*)	19.5 (*20.1*)	111.1 (*138.1*)	46.2 (*38.2*)	23.1 (*1.8*)	316.3 (*270.0*)	21.9 (*11.3*)
Top channel width, w [m]	25.2 (*26.1*)	11.9 (*10.5*)	30.2 (*26.1*)	27.7 (*22.7*)	13.5 (*0.7*)	71.5 (*44.3*)	12.8 (*2.6*)
Wetted perimeter, P [m]	27.4 (*25.4*)	13.2 (*11.1*)	33.6 (*27.1*)	30.8 (*24.4*)	14.9 (*0.5*)	74.2 (*44.7*)	14.4 (*2.9*)
Hydraulic radius, R [m]	1.11 (*0.48*)	1.34 (*0.74*)	2.59 (*1.44*)	1.45 (*0.43*)	1.54 (*0.07*)	3.69 (*1.75*)	1.45 (*0.48*)
Mean flow depth, d [m]:	1.28 (*0.36*)	1.43 (*0.74*)	3.03 (*1.58*)	1.66 (*0.50*)	1.71 (*0.05*)	3.88 (*1.84*)	1.64 (*0.57*)
Mean flow velocity, V [m/s]:	3.12 (*1.01*)	2.87 (*0.66*)	3.52 (*0.95*)	3.00 (*0.63*)	3.22 (*0.01*)	5.00 (*1.10*)	3.24 (*0.67*)
Froude number, Fr [-]	0.81 (*0.24*)	0.76 (*0.21*)	0.67 (*0.22*)	0.75 (*0.12*)	0.78 (*0.01*)	0.85 (*0.14*)	0.82 (*0.13*)
Manning's roughness coefficient, n [-]	0.054 (*0.014*)	0.056 (*0.027*)	0.063 (*0.012*)	0.067 (*0.021*)	0.050 (*0.000*)	0.050 (*0.010*)	0.060 (*0.013*)
Cross-sectional stream power, Ω [W/m]	16494 (*13623*)	8658 (*13132*)	33706 (*30976*)	33390 (*27296*)	7053 (*3186*)	132569 (*147621*)	8856 (*5130*)
Unit stream power, ω [W/m^2]	866 (*602*)	666 (*509*)	1651 (*1845*)	1409 (*1124*)	517 (*209*)	1850 (*1371*)	661 (*311*)

4.1.1 CHANNEL HYDRAULIC GEOMETRY

The relationships between peak discharges and channel hydraulic properties, including channel width, flow depth, and mean flow velocity, are reported in Fig. 4.1 for the studied cross sections. The regressions clearly show a linear dependence of the hydraulic properties on peak discharge, with differing orders of magnitude. Channel geometry, i.e., width and depth that define the cross-sectional area and are directly used to compute peak discharge, exerts much influence on the pattern of estimated peak discharge compared to the estimated flow velocity. The relatively lower explained variance for the relationship between peak discharge and flow velocity (Fig. 4.1C) can be attributed to the high uncertainties in the evaluation of the roughness parameter and assumptions concerning the estimation of energy line gradient compared to errors in the measurement of channel width (Fig. 4.1A) and flow depth (Fig. 4.1B), which depend only on the surveying accuracy.

Table 4.2 reports a summary of the power-law regressions (and explained variances, R^2) developed for the relationship between peak discharges, and the corresponding channel width, flow depth and flow velocity for the studied cross sections. The sum of the exponents, and product of the multipliers for the power-law regressions (Table 4.2), approaches unity for each event, which is comparable to the average regressions reported in Fig. 4.1. This result supports the usually described downstream correlations in power-law regressions between bankfull discharge and channel hydraulic geometry reported in literature based on the classic work on regimes theories of channel hydraulic geometry (Leopold and Maddock, 1953).

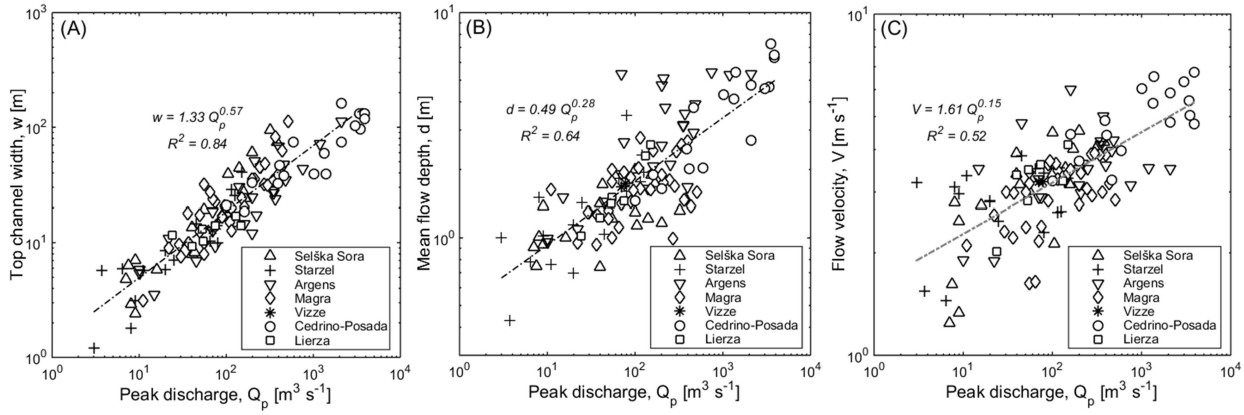

FIG. 4.1. Relationship between peak discharge and (A) top channel width, (B) mean flow depth, and (C) flow velocity.

TABLE 4.2. At-a-station channel hydraulic geometry for the studied flash floods

Study basins	*Width-discharge relationship*		*Depth-discharge relationship*		*Velocity-discharge relationship*	
	Regression	R^2	*Regression*	R^2	*Regression*	R^2
Selška Sora	$w = 0.81 \cdot Q_p^{0.75}$	*0.88*	$d = 0.76 \cdot Q_p^{0.12}$	*0.34*	$V = 1.23 \cdot Q_p^{0.22}$	*0.59*
Starzel	$w = 1.05 \cdot Q_p^{0.62}$	*0.77*	$d = 0.48 \cdot Q_p^{0.30}$	*0.57*	$V = 2.12 \cdot Q_p^{0.08}$	*0.16*
Argens	$w = 1.20 \cdot Q_p^{0.57}$	*0.81*	$d = 0.55 \cdot Q_p^{0.31}$	*0.60*	$V = 1.92 \cdot Q_p^{0.11}$	*0.32*
Magra	$w = 0.92 \cdot Q_p^{0.68}$	*0.77*	$d = 0.84 \cdot Q_p^{0.14}$	*0.20*	$V = 1.60 \cdot Q_p^{0.13}$	*0.29*
*Vizze**	$w = 0.84 \cdot Q_p^{0.65}$	*1*	$d = 0.40 \cdot Q_p^{0.34}$	*1*	$V = 2.86 \cdot Q_p^{0.03}$	*1*
Cedrino-Posada	$w = 1.94 \cdot Q_p^{0.50}$	*0.80*	$d = 0.25 \cdot Q_p^{0.38}$	*0.79*	$V = 1.86 \cdot Q_p^{0.14}$	*0.54*
Lierza	$w = 4.92 \cdot Q_p^{0.23}$	*0.49*	$d = 0.20 \cdot Q_p^{0.50}$	*0.95*	$V = 1.03 \cdot Q_p^{0.27}$	*0.59*

*regressions for only two data points of the Vizze River

4.1.2 HYDROLOGICAL MODELLING

The availability of high-resolution radar rainfall estimates, digital elevation models and soil-cover hydrologic complex for specific flash floods and affected catchments permitted an integrated analysis for the reconstruction of 6 out of 7 of the studied flash floods (Selška Sora, Starzel, Magra, Vizze, Cedrino-Posada and Lierza) using the spatially distributed rainfall-runoff model described in section 3.3.1. Model results for Selška Sora and Starzel were obtained from Zanon et al. (2010) and Ruiz-Villanueva et al. (2012), respectively. A similar modelling approach had been applied (Payrastre et al., 2012) for the analysis of the Argens flood. Reference is made to the previous studies reported in Table 2.1 for a more complete description of the application of the spatially explicit hydrologic model for the specific events. Fig. 4.2 presents a comparison between field-estimated and model-simulated flood peaks for the 6 flash floods. The Nash-Sutcliffe efficiency score (NSE) reported for the regressions indicates a high correspondence between simulated and observed peak and unit peak discharges. The relatively lower efficiency score reported in Fig. 4.2-B can be attributed to bias corresponding to the comparison when peak discharges are normalized by upstream drainage area. Model simulations have served to check the consistency between rainfall and discharge data collated after such extreme events.

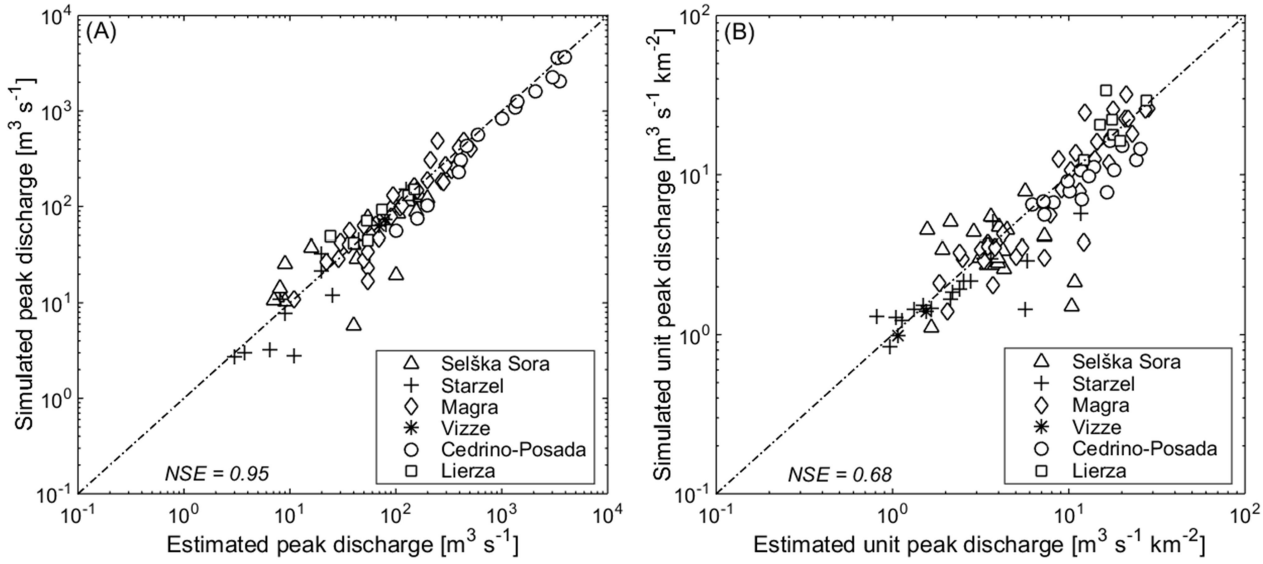

FIG. 4.2. Regression between field-estimated and model-simulated (A) peak discharges, and (B) unit peak discharges for 6 of the studied flash floods. NSE: Nash-Sutcliffe model efficiency score.

The accuracy of the simulations for the four recent flash floods in Italy (Magra, Vizze, Cedrino-Posada and Lierza), where comprehensive geomorphic reconnaissance was carried out together with indirect peak flow estimates, included the observational error analysis of the slope-conveyance method (cf. section 3.3.2). Fig. 4.3A-B reports the relationship between simulated peak discharges and the corresponding relative uncertainty deviations for the four flood events and observed geomorphic effects, respectively for the 59 studied basins. The relative uncertainty deviation was estimated as the ratio of the relative errors in simulated peak discharges (with respect to the field-estimated central values) to the geomorphic effects-based standard errors of the field values. A threshold of relative uncertainty deviation of 1 indicates that the simulated peak discharge is within the uncertainty range provided by the error analysis. From Fig. 4.3, thresholds of 1, 1.5 and 2 indicate that for 61%, 73% and 85% of the studied cross sections, respectively, the simulated peak discharges are within the observational uncertainty bound. As expected, in most cases, cross sections that underwent major geomorphic changes, which are responsible for larger uncertainty in estimated peak discharges, provided simulations within the uncertainty bounds compared to sections that underwent negligible and moderate changes.

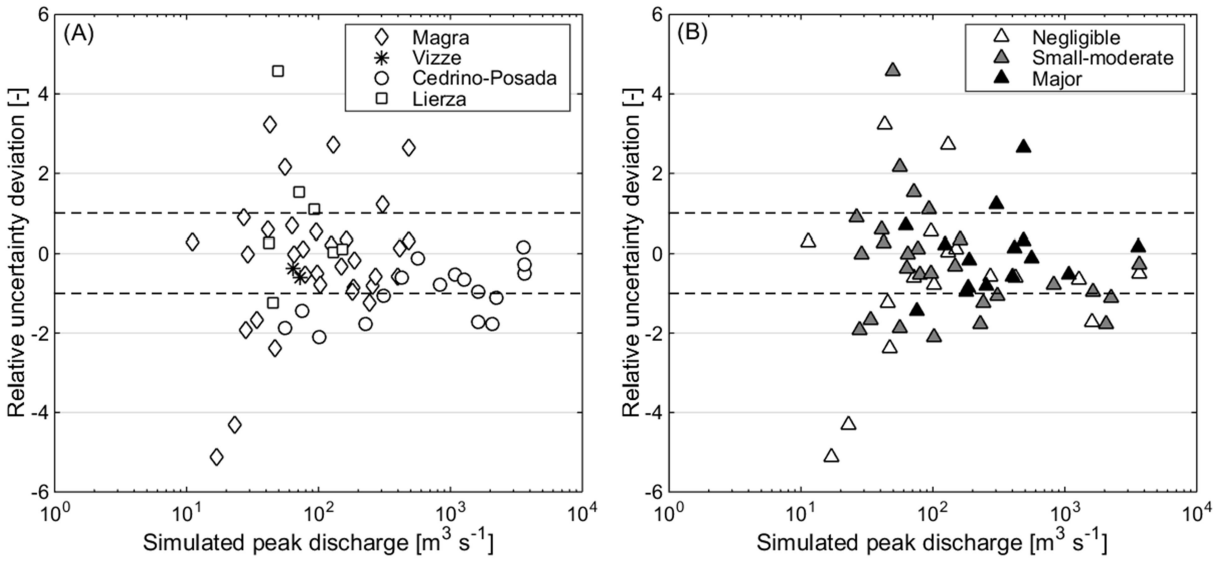

FIG. 4.3. Relationship between simulated peak discharges and relative uncertainty deviations based on (A) flood event, and (B) observed geomorphic effects, for the four recent floods in Italy.

4.1.3 Analysis of the flood response properties

The dependency of discharge on watershed area gives a fundamental idea about the spatial extent and severity of the flood responses to rainstorm events. The relationship between unit peak discharge and upstream drainage area was investigated for the studied flash floods in a log-log plot (Fig. 4.4). The resulting envelope curve is analysed. Fig. 4.4 shows two upper limit envelope curves: the grey-dashed line represents the envelope curved developed by Gaume et al. (2009) and confirmed by Marchi et al. (2010) for multiple flash flood events in Europe between 1994 and 2008. The database for this study, which includes some recent and severe flash floods, provides an envelope curve as follows:

$$Q_u = 45.0 \cdot A^{-0.2} \qquad [4.1]$$

where, Q_u [m^3 s^{-1} km^{-2}] is the unit peak discharge and A [km^2] is the upstream drainage area. The exponent of the envelope curve for this study indicates slow decrease of unit peak discharge and shows that high unit peak discharges are also observed for larger drainage areas. This can be observed for the flood responses in basins of the Cedrino-Posada Rivers, which cross the upper envelope of European flash floods and passed the rainfall-runoff consistency checks through hydrological modelling.

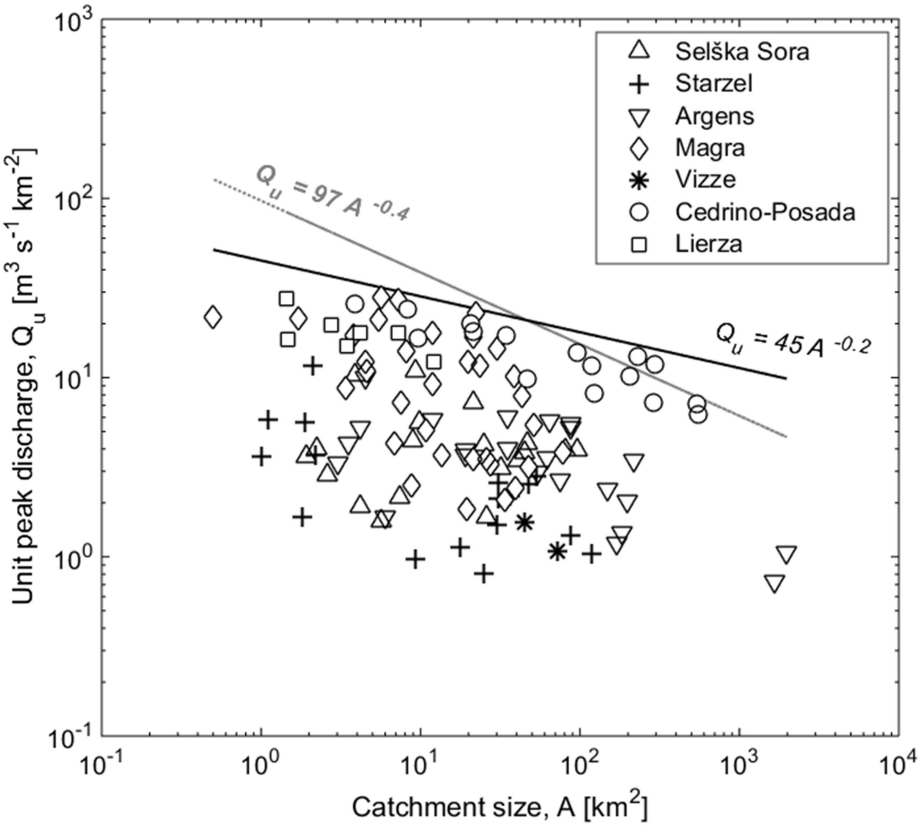

FIG. 4.4. Unit peak discharge against upslope drainage area for the studied flash floods. Envelope curves: Grey line from Gaume et al.(2009) for European flash floods between 1994 and 2008; Black line from the dataset of this study.

Similar to the findings by Gaume et al. (2009) and Marchi et al. (2010), the highest unit peak discharges are observed for events from the Mediterranean regions (Magra, and Cedrino-Posada) due to the larger peak discharges that characterize flash floods in this region. The Lierza flood approaches the envelope curve for drainage areas less than 10 km^2 (Fig. 4.4). The upper limit envelope is defined by unit peak discharges up to 20-30 $m^3\ s^{-1}$ for basin areas less than 10 km^2 in the Magra, Cedrino-Posada, and Lierza Rivers whereas unit peak discharges reached up to 10-20 $m^3\ s^{-1}$ for basin areas larger than 100 km^2 in the Cedrino-Posada Rivers.

The relationships between basin-averaged rainfall accumulation and flood response features (unit peak discharge and runoff coefficient) are reported for the floods of Magra, Vizze, Cedrino-Posada and Lierza in Fig. 4.5. Runoff coefficient is computed as the ratio of the direct runoff to the event rainfall depth. The direct runoff was obtained by separating the baseflow component from the simulated flood hydrographs. Baseflow was assumed to remain constant up to the time of flood peak, and then to increase linearly until the end of direct runoff (Marchi et al., 2010). The end of direct runoff was identified graphically on the recession limb plotted on a logarithmic chart (Tallaksen, 1995). From Fig. 4.5, there is a general pattern of increasing rainfall intensities with both unit peak discharges and runoff coefficients. Runoff coefficient for the Lierza, Vizze and moderate rainfall basins of the Magra flood are generally below 0.3, whereas that for Cedrino-Posada and high rainfall basins of the Magra flood are above, although with a wide scatter between different floods. This suggests that a threshold of 0.3 runoff coefficient could discriminate flood response intensities for rainfall accumulation around 200-250 mm.

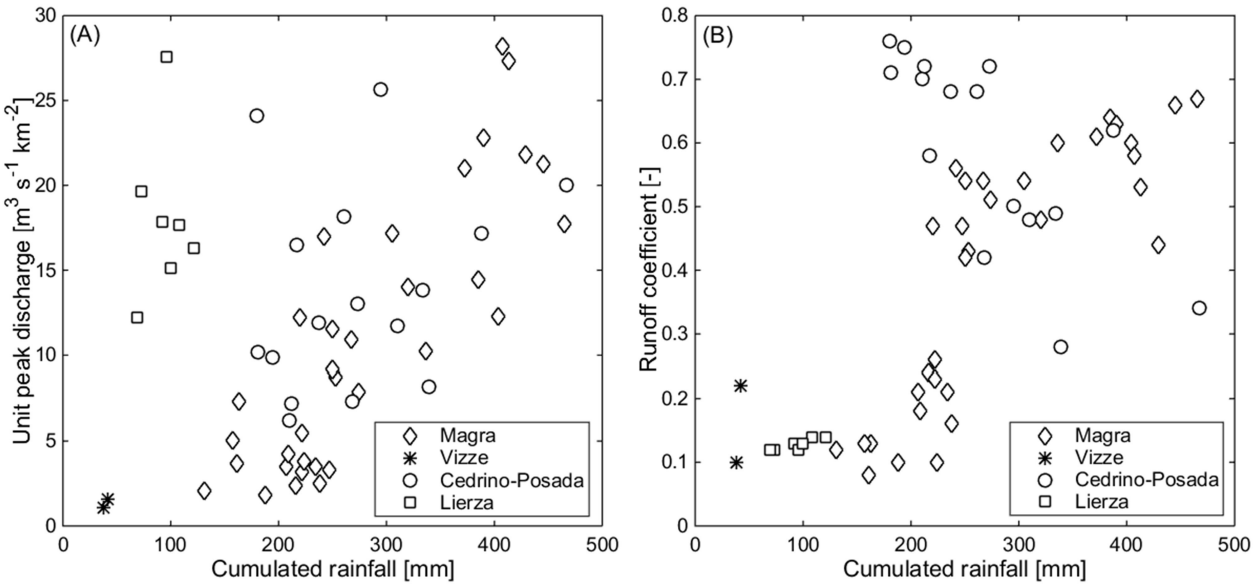

FIG. 4.5. Relationship between event rainfall accumulation and (A) unit peak discharge and, (B) runoff coefficient for the four recent floods in Italy.

4.2 At-a-Station Stream Power

4.2.1 Peak stream power and controlling factors

Stream power incorporates river discharge and channel gradient to express river energy expenditure, which has been considered as an index of the hydraulic energy required for geomorphic work associated with major floods (e.g., Baker and Costa, 1987; Magilligan, 1992; Thompson and Croke, 2013), as well as near-bankfull flows (e.g., Knighton, 1999; Fonstad, 2003). The analyses of the main hydrologic and topographic controlling factors (i.e., peak discharge and channel gradient) and their relationship with the master variable 'drainage area' permitted exploration of the variability of stream power for specific flood events and among the different flood events for this study. Figs. 4.6A-B present the relationship between upslope drainage area and the corresponding peak discharge and channel gradient at the surveyed cross sections, i.e., the two variables used for computing cross-sectional stream power (Eq. 3.10), respectively. The relationship between peak discharge and drainage area is highly linear on the logarithmic scale for most of the studied flash floods. The upper limit reported in Fig. 4.6A is characterized by a slope of 0.8 and features flash flood events in the Magra, Cedrino-Posada, and Lierza Rivers. This implies that the slope of the upper envelope between peak discharges and drainage area for the studied flash floods has increased to a more linear value of 0.8, which translates to a gradient of -0.2 for the upper envelope of the relationship between drainage area and unit peak discharge (Fig. 4.4). Peak discharges exceeded 1000 m^3 s^{-1} for catchments draining greater than 100 km^2 in Mediterranean basins (Argens, and Cedrino-Posada).

The relationship between energy slope and drainage area (Fig. 4.6B), on the contrary, is characterized by two upper envelopes at a break point of about 100 km^2, where the slope of the power-law regression increases from -0.193 to -0.981. This represents a sharp decrease in channel slope for upslope drainage areas greater than 100 km^2, which feature basins affected by the flash floods in the Mediterranean climates (Cedrino-Posada, and Argens rivers). Contrary to the systematic increase in peak discharge with drainage area (Fig. 4.6A), there is not an unique upper envelope over the whole range of basin area for the relationship with energy gradient (Fig. 4.6B). The wide scatter in Fig. 4.6B can be attributed to the geological controls on channel morphology that are highly variable and independent of the contributing drainage area.

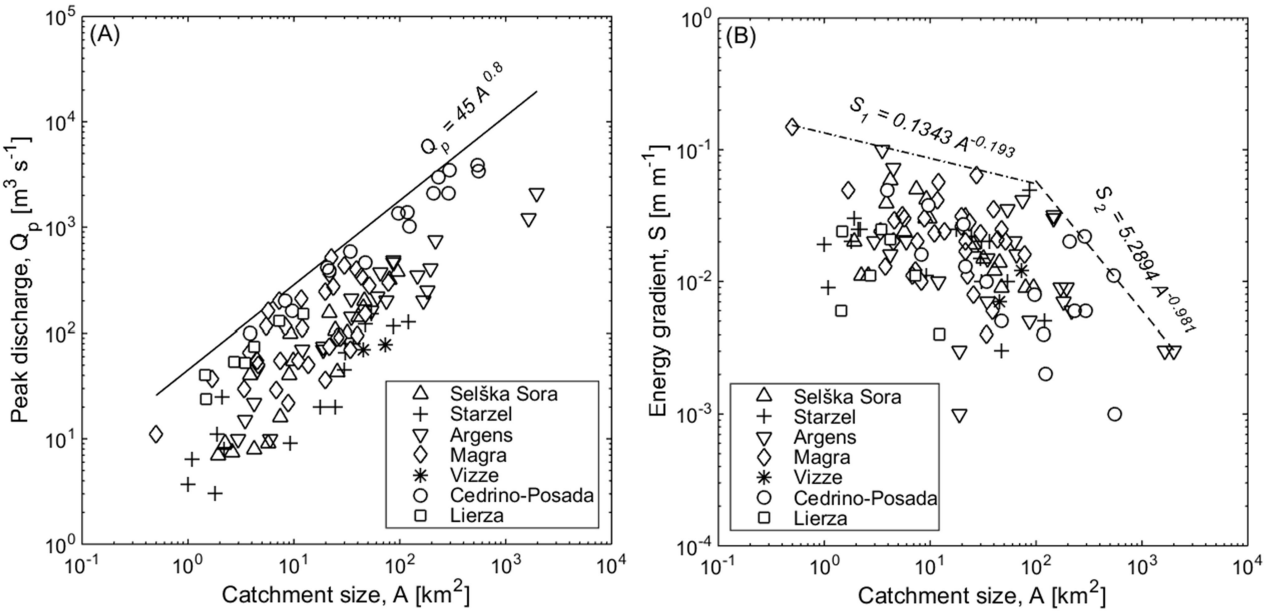

FIG. 4.6. Relationship between upslope drainage area and stream power variables (A) peak discharge and (B) channel gradient for the seven studied flash floods.

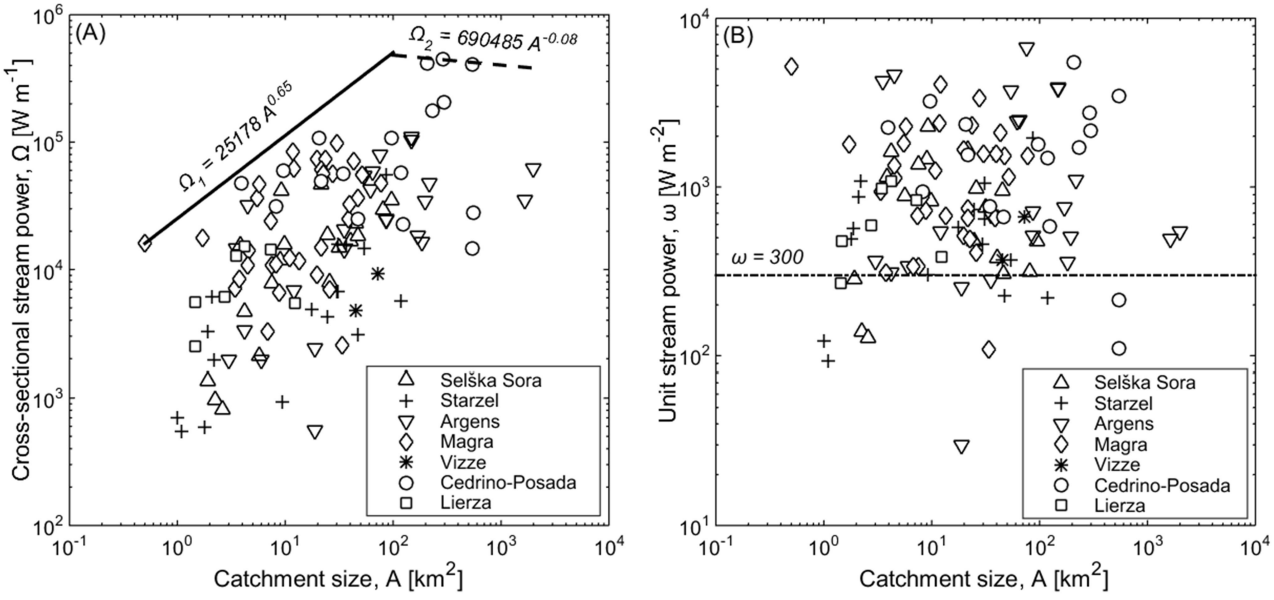

FIG. 4.7. Relationship between upslope drainage area and (A) cross-sectional stream power, and (B) unit stream power.

The relationship between cross-sectional stream power and drainage area (Fig. 4.7A) reflects the flood intensities and spatial extent of the flood responses as reported in Fig. 4.6A. Maximum cross-sectional stream power values were up to 400,000 W m^{-1} for the Cedrino-Posada flood in catchments draining 100-1000 km^2. The upper limit envelope is defined by the Mediterranean events (Magra, and Cedrino-Posada), although the other Mediterranean event in the Argens River features lower values even for similar drainage areas. The relationship is non-linear, with an increase of cross-sectional stream power with upslope drainage area and a subsequent decrease at a break point of 100 km^2. The reported upper envelope curves in Fig. 4.7A reflect the upper envelopes provided in Fig. 4.6A-B, which indicate that the rate of decrease and the non-linear trend of channel gradient with drainage area may influence the available energy expenditure for geomorphic work at the channel-reach scale, particularly for larger basins.

The scatter plot between unit stream power and upslope drainage area (Fig. 4.7B) shows higher values of unit stream power for Mediterranean events (Cedrino-Posada, Magra, and Argens). The highly non-linear trend in Fig. 4.7B is influenced by the variability in the degree of confinement at the individual cross sections, expressed as post-flood channel width. Post-flood channel width corresponding to high water marks was used to estimate unit stream power because it was possible to carefully measure it in the field and it is consistent with topographic and hydraulic variables related to peak discharge computation. It should, however, be noted that the use of post-flood channel width for the computation of unit stream power at a cross section may underestimate the potential maximum energy expenditure if post-flood channel width occurred in whole or in part during flood recession. The smallest catchment in our database draining an area of 0.5 km^2 recorded unit stream power of 5000 W m^{-2}. This bedrock channel with no significant channel changes typically exemplifies the effects of the use of post-flood channel width for different cross-section types affected by different intensities of geomorphic effects. Peak instantaneous unit stream power values for about 88% of the 119 studied cross-sections were greater than the Miller-Magilligan critical threshold of 300 W m^{-2}. This implies that the studied flash floods were geomorphically significant events.

The nonlinear variation of unit stream power with drainage area has been interpolated by Lecce (1997) using power functions or log quadratic functions. The application of log-quadratic regression to six of the studied flash floods (Vizze basin was excluded because data are available for two cross

sections only) is shown in Fig. 4.8 (Marchi et al., 2016). In four of the six cases, the log-quadratic fitting permits a satisfactory interpretation of the dependence of unit stream power on basin area, although the explained variance is rather low. Because of small sample sizes and uneven distribution of drainage areas within some samples, single cases may have a major impact on the representation of the relationship between unit stream power and drainage area. This is clearly visible in the Magra: one small catchment (0.5 km^2, indicated by an arrow in Fig. 4.8D), which lies in the sector of the basin that received the most intense rainfall, is drained by a steep bedrock channel and is not balanced by other catchments of similar size with different morphological characteristics. This catchment biases the value of maximum unit stream power toward small-sized basins (dashed line in Fig. 4.8D). This catchment was retained in the database and used in all other analyses as it can be deemed representative of high values of stream power attained in small, steep bedrock channels. However, it was not considered for fitting the regression of unit stream power with basin area (continuous line in Fig. 4.8D). A decrease of unit stream power with increasing basin area is not clearly visible for the Cedrino-Posada flood (Fig. 4.8E).

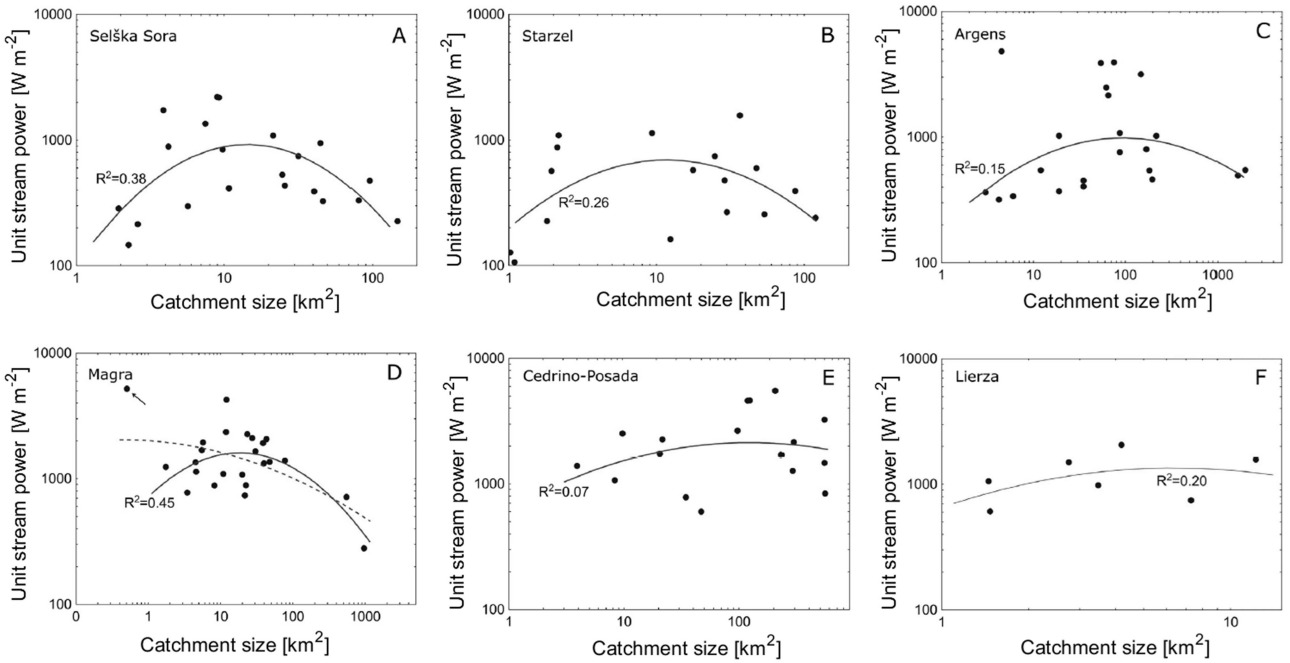

FIG. 4.8. Log-quadratic interpolation between unit stream power and drainage area for six of the studied flash floods.

The variance explained by a log quadratic regression for the Cedrino–Posada flood is very low and only marginally higher than that of a power relationship that would indicate a slight increase of unit stream power with increasing basin area. This can be partly ascribed to the large extent of flood-generating convective bands, which produced very high values of peak discharge even for large drainage areas. Moreover, the lowermost, low-slope channel reaches, which could have shown a decrease of unit stream power because of the low slope near the river outlet to the sea, have not been surveyed because the flood discharge was altered by the presence of reservoirs. A similar pattern (i.e., the absence of a clearly defined decrease of unit stream power with increasing drainage area) was observed in the Lierza (Fig. 4.8F), where it can be attributed to the structural controls on local channel slope, which frequently cause very gentle slopes even for small drainage areas.

The drainage area at which the log-quadratic regression identifies maximum values of unit stream power shows relevant differences between the six studied floods and ranges from 6.4 km^2 for the Lierza to 94 and 123 km^2 for the Argens and the Cedrino–Posada, respectively. The areas corresponding to the highest values of unit stream power depend on the extent of the rainstorm that triggered the flood and on the spatial organization of the drainage network affected. Significantly, in the Magra flood, notwithstanding the large total area of the drainage basin considered (more than 900 km^2 in the main stream and 500 km^2 in its main tributary), the log-quadratic interpolation indicates the maximum value of unit stream power for a drainage area of 18 km^2, closer to the floods of the Selška Sora and Starzel (14 and 12 km^2, respectively) than to the other large-extent Mediterranean floods. This can be attributed to the spatial distribution of the rainfall that caused the flood of 25 October 2011 in the Magra River, which occurred with the highest intensity in a narrow belt that covered the right tributaries of the main river and the central sector of its most important tributary, the Vara River (Rinaldi et al., 2016; Surian et al., 2016). As a consequence, very intense flash floods occurred in several catchments that drain areas up to approximately 40 km^2 (Mondini et al., 2014; Rinaldi et al., 2016) and are characterized by relatively steep and narrow channels, thus resulting in high values of unit stream power. The peak discharge in the main channels, although relevant, was attenuated by the limited contribution from the sectors of their drainage basins that had received significantly lower rainfall amounts. Accordingly, unit stream power peaked at small drainage areas and substantially decreased in the largest basins.

4.2.2 INFLUENCE OF FLOOD-FLOW DURATION

The influences of flow duration and cumulative energy expenditure in relation to geomorphic effectiveness were evaluated for the 59 cross sections of the four recent flash floods in Italy (Magra, Vizze, Cedrino-Posada and Lierza). This was based on an integrated analysis of flood hydrographs from hydrological simulations and field data to compute unit stream power for the whole flood hydrograph (cf. section 3.4.2). Figs. 4.9A-B report regressions between simulated and field-estimated cross-sectional and unit stream power, respectively. The Nash-Sutcliffe efficiency scores reported in both regressions indicate a high correspondence between field-estimated and model simulated peak instantaneous stream power, which permits use of the simulated flood hydrographs for this analysis. However, to ensure consistency in the evaluation of the combined influence of flow duration and total energy expenditure on geomorphic responses, five basins (two each for Magra and Cedrino-Posada and one for Lierza) were eliminated from the analysis because the maximum unit stream power values were below the Miller-Magilligan critical threshold (300 W m^{-2}), hence no energy was available for major geomorphic change according to Fig. 3.5. Detailed datasets for the 59 catchments of the four recent flash floods in Italy are reported in Appendix A3.

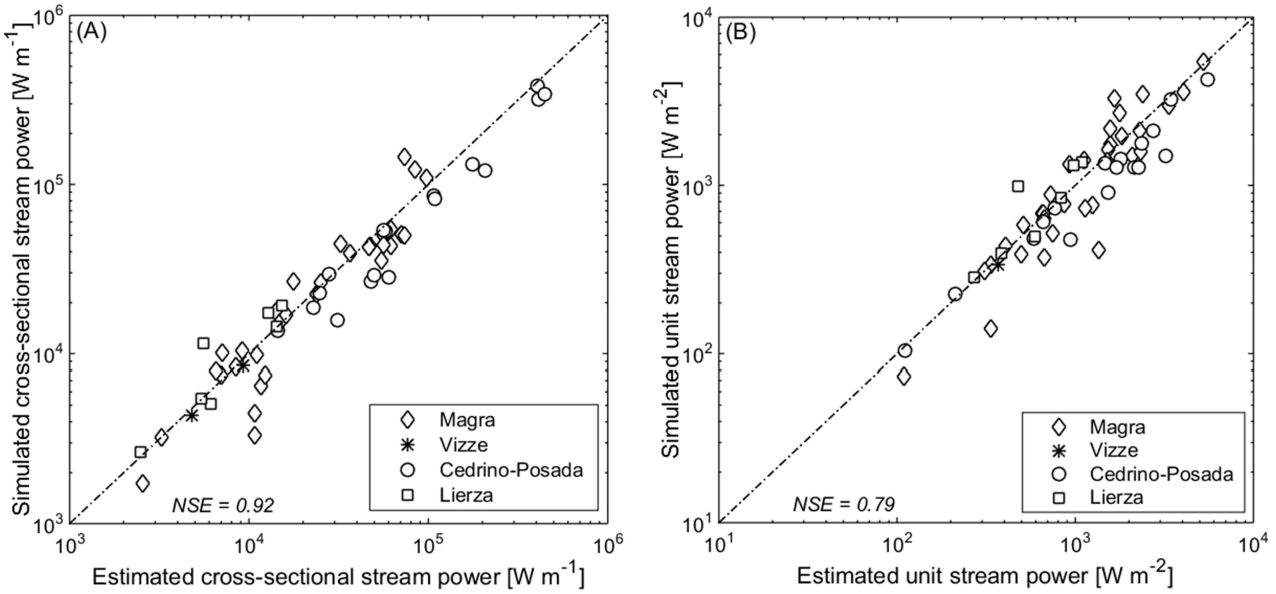

FIG. 4.9. Regression between estimated and simulated (A) cross-sectional stream power, and (B) unit stream power. NSE: Nash-Sutcliffe model efficiency score.

The accuracy of the simulated cross-sectional stream power and unit stream power for the cross-sections reported in Fig. 4.9 was carried out using the observational error analysis of field-estimated peak instantaneous stream power (cf. section 3.4.1). Fig. 4.10A-B reports the relationship between relative uncertainty deviations, and simulated cross-sectional stream power and unit stream power, respectively for the 59 studied basins. The relative uncertainty deviation was estimated as the ratio of the relative errors in simulated stream power (with respect to the field-estimated values) to the geomorphic effects-based standard errors of the field values. A threshold of relative uncertainty deviation of 1 indicates that the simulated cross-sectional (or unit) stream power is within the uncertainty range provided by the error analysis. From Fig. 4.10A, thresholds of 1, 1.5 and 2 indicate that for 64%, 76% and 90% of the studied cross sections, respectively, the simulated cross-sectional stream power are within the observational uncertainty bound. Similarly, from Fig. 4.10B, thresholds of 1, 1.5 and 2 indicate that for 68%, 81% and 90% of the studied cross sections, respectively, the simulated unit stream power are within the observational uncertainty bound. As expected, in most cases, cross sections that underwent major geomorphic changes, which are responsible for larger uncertainty in estimated stream, provided simulations within the uncertainty bounds compared to sections that underwent negligible and moderate changes.

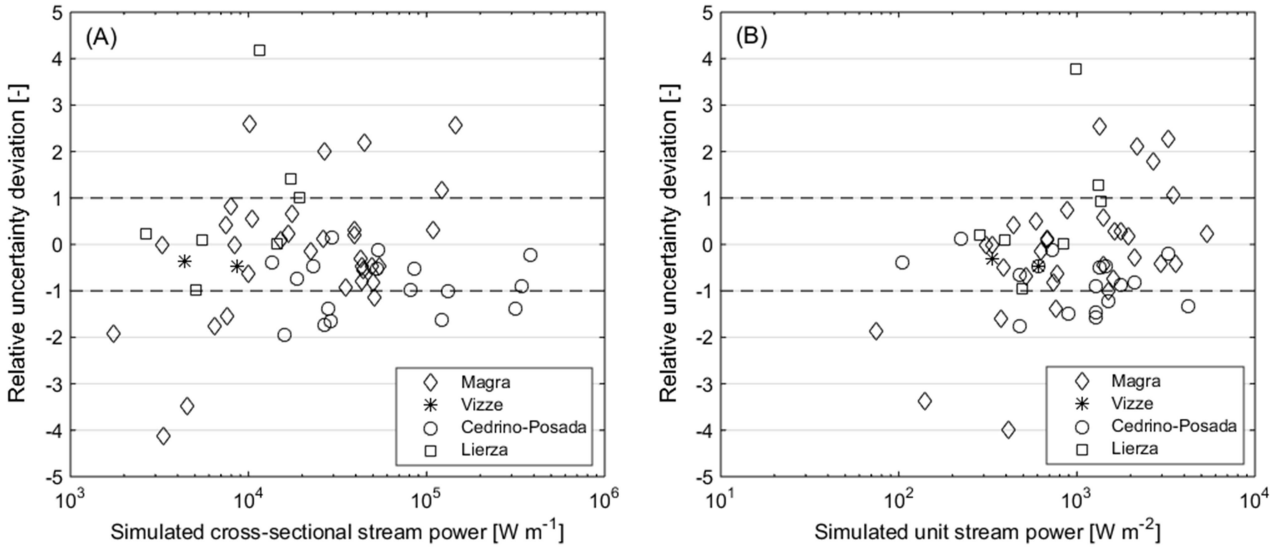

FIG. 4.10. Relationship between estimated relative uncertainty deviation and simulated (A) cross-sectional stream power, and (B) unit stream power for the four recent floods in Italy.

Figs. 4.11A-D report the spatial extent of peak instantaneous unit stream power, event energy expenditure, above-threshold energy expenditure, and above-threshold flow duration (defined as the flow duration above the Miller-Magilligan critical threshold) for the 54 considered cross sections in a log-log plot with upstream drainage area. The plots show similar large scatter and suggest that cumulative energy expenditure and flow duration are likely to depend on the area hit by the flood rather than peak stream power for the individual flood events. As to the climatic context, the highest values of the considered energy expenditure usually occur in Mediterranean regions (Magra, and Cedrino-Posada), which can be attributed to the combined influences of larger discharges and long duration rainstorms that characterize these flash floods. The short flood duration (1.5 hours) associated with the Lierza flood produced relatively lower cumulative energy expenditure compared to the Mediterranean events, although the peak instantaneous unit stream power values are comparable.

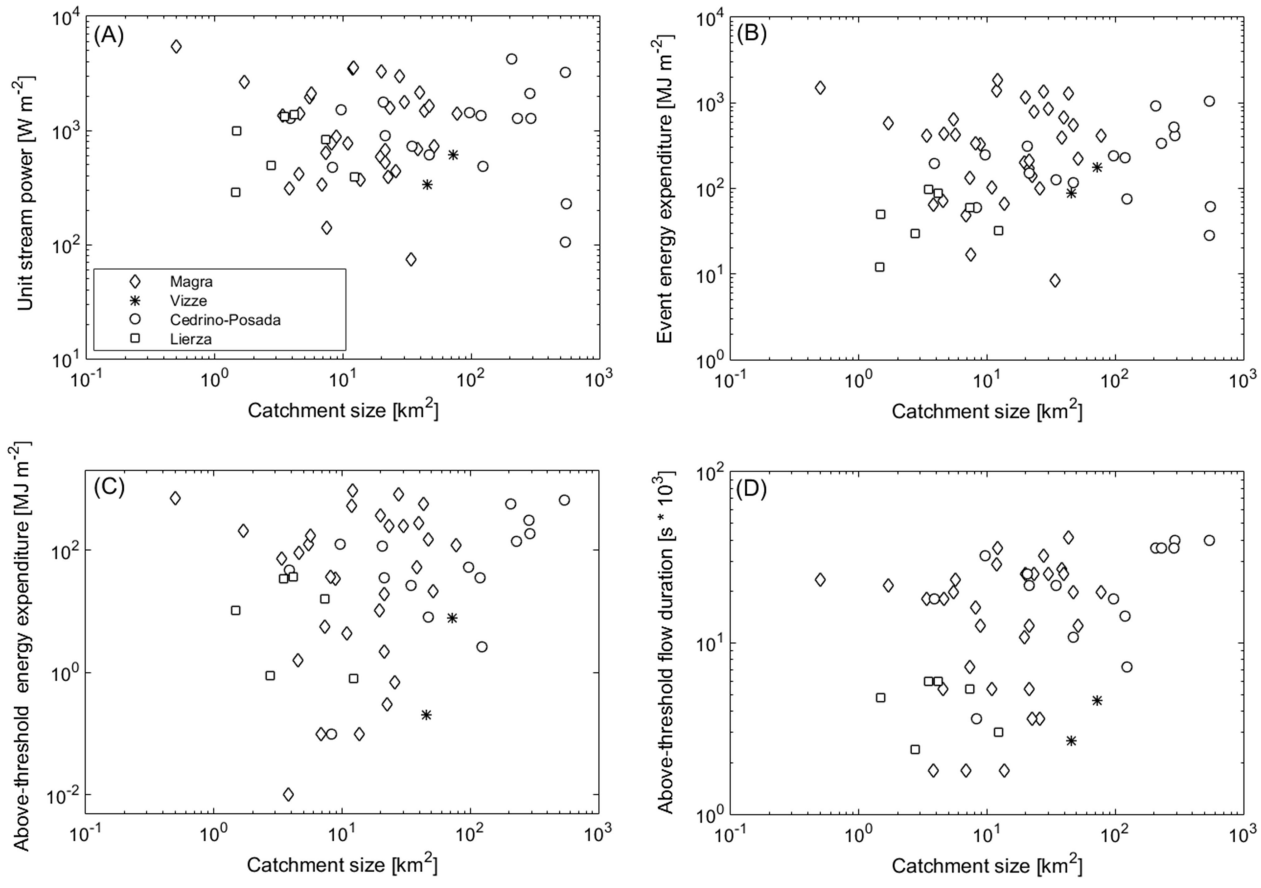

FIG. 4.11. Relationship between upslope drainage area and (A) unit stream power, (B) event energy expenditure, (C) above-threshold energy expenditure, and (D) above-threshold flow duration.

Another important analysis is to assess the relationship between peak unit stream power and the variables related to the combined influences of flow duration and cumulative energy expenditure. Figs. 4.12A-D report regressions between unit stream power and event energy expenditure, above-threshold energy expenditure, above-threshold flow duration and energy ratio, respectively. It should be recalled that energy ratio is defined as the ratio of above-threshold energy expenditure to event energy expenditure. The relationships are characterized by differing regressions, better represented by log-quadratic (Fig. 4.12-A and D) and log-linear (Fig. 4.12-B and C) functions. The scatter and higher explained variances imply that above-threshold energy expenditure and flow duration (Fig. 4.12-B and C) potentially increase linearly with peak instantaneous unit stream power. This suggests that peak instantaneous unit stream power, which is usually used as a surrogate for the most effective energy expenditure in literature, has similar trends as the combined influences of flow duration and cumulative energy expenditure for short duration, high magnitude floods such as flash floods.

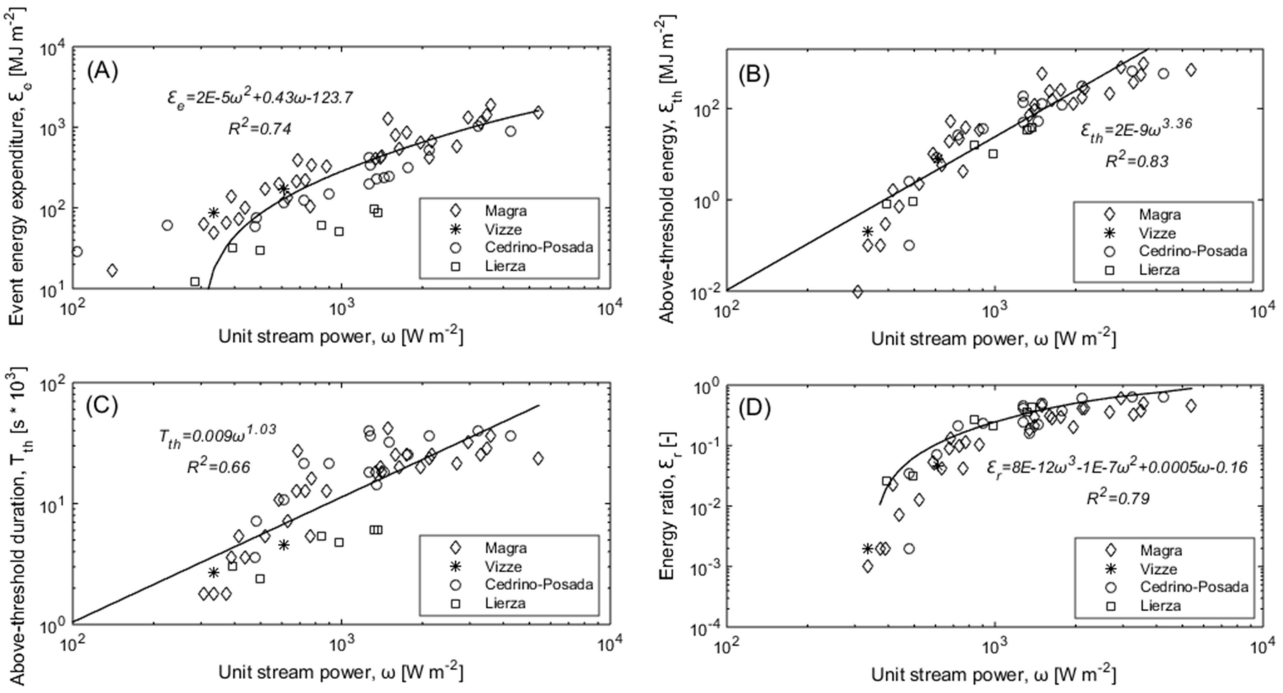

FIG. 4.12. Regressions between unit stream power and (A) event energy expenditure, (B) above-threshold energy expenditure, (C) above-threshold flow duration, and (D) energy ratio.

Table 4.3 reports a compilation of the various measures of the flash flood-related energy expenditure for the four studied events excluding the five basins with peak instantaneous unit stream power less than 300 W m^{-2}. Generally, higher energy expenditures were estimated for the affected basins in the Magra and Cedrino-Posada rivers compared to the Lierza and Vizze Rivers. This can be ascribed to the combined influences of large spatial extent of the flood responses and the high duration of flash flood-triggered rainstorms in Mediterranean regions compared to other European climatic regions (Marchi et al., 2010). The Magra event recorded higher cumulative energy expenditure than the Cedrino-Posada event, although the latter had relatively higher peak instantaneous stream power and flow duration above the Miller-Magilligan critical threshold. An interesting observation in Table 4.3 relates to the mean values of energy ratio for the Magra and Lierza events, with similar mean and standard deviation values. The fact that the Magra event was associated to significant geomorphic effects compared to the Lierza event suggests that the non-dimensional parameter is event specific and should therefore be compared between different sectors of the same impacted river basin.

TABLE 4.3. Compilation of energy expenditure for the 54 basins affected by the four recent flash floods in Italy: mean and *standard deviation* values. Ω: cross-sectional stream power; ω: unit stream power; $\mathcal{E}_e$: event energy expenditure; $\mathcal{E}_{th}$: above-threshold energy expenditure; T_{th}: above-threshold flow duration; $\mathcal{E}_r$: energy ratio

Event	*No. of cross sections*	*Catchment size [km^2]*	Ω *[W m^{-1}]*	ω *[W m^{-2}]*	$\mathcal{E}_e$ *[MJ m^{-2}]*	$\mathcal{E}_{th}$ *[MJ m^{-2}]*	T_{th} *[$s*10^3$]*	$\mathcal{E}_r$ *[-]*
Magra	31 (2*)	19.9 (*17.8*)	33930 (*34558*)	1509 (*1224*)	546 (*499*)	189 (*261*)	17.1 (*10.8*)	0.21 (*0.18*)
Vizze	2	59.1 (*19.6*)	6468 (*2965*)	474 (*195*)	131 (*61*)	4 (*5.5*)	3.7 (*1.4*)	0.02 (*0.03*)
Cedrino-Posada	15 (2*)	136.4 (*152.0*)	114121 (*126748*)	1511 (*1035*)	331 (*290*)	155 (*207*)	24.0 (*12.1*)	0.32 (*0.22*)
Lierza	6 (1*)	5.2 (*3.9*)	12174 (*5959*)	900 (*407*)	60 (*28*)	17 (*16*)	4.6 (*1.5*)	0.22 (*0.17*)

*number of cross sections with peak instantaneous unit stream power less than 300 W m^{-2}

4.2.3 RELATIONS WITH CHANNEL TYPES AND OBSERVED GEOMORPHIC EFFECTS

Post-flood field observations provide important context to assess and document the magnitude of channel modification caused by extreme floods at cross-sectional or channel-reach scales. Geomorphic observations and reconnaissance were carried out for 59 cross sections impacted by the four recent flash floods in Italy (Magra, Vizze, Cedrino-Posada and Lierza). To recall from section 3.1.3, cross-sectional types were classified into alluvial, semi-alluvial, bedrock and artificial, whereas observed geomorphic effects were also categorized as negligible, small to moderate, and major impacts. Figs. 4.13A-B report the spatial extent of peak instantaneous energy expenditure for the cross-sectional channel types and observed geomorphic effects, respectively, in a log-log plot of unit stream power against upstream drainage area. The scatter shows no particular trend to discriminate the influence of unit stream power on the cross-sectional types and the observed geomorphic effects, with five sections of different channel materials and geomorphic impacts recording unit stream power values below the Miller-Magilligan critical threshold for major channel adjustment. Negligible geomorphic effects in bedrock channels, represented by the least catchment size in the database (Fig. 4.13), recorded the maximum unit stream power because relatively immovable channel boundaries cause rapidly increasing discharge with flow depth. Major geomorphic modifications generally occurred in alluvial channels with approximately 10-100 km^2 catchment sizes and unit stream power above the Miller-Magilligan critical threshold.

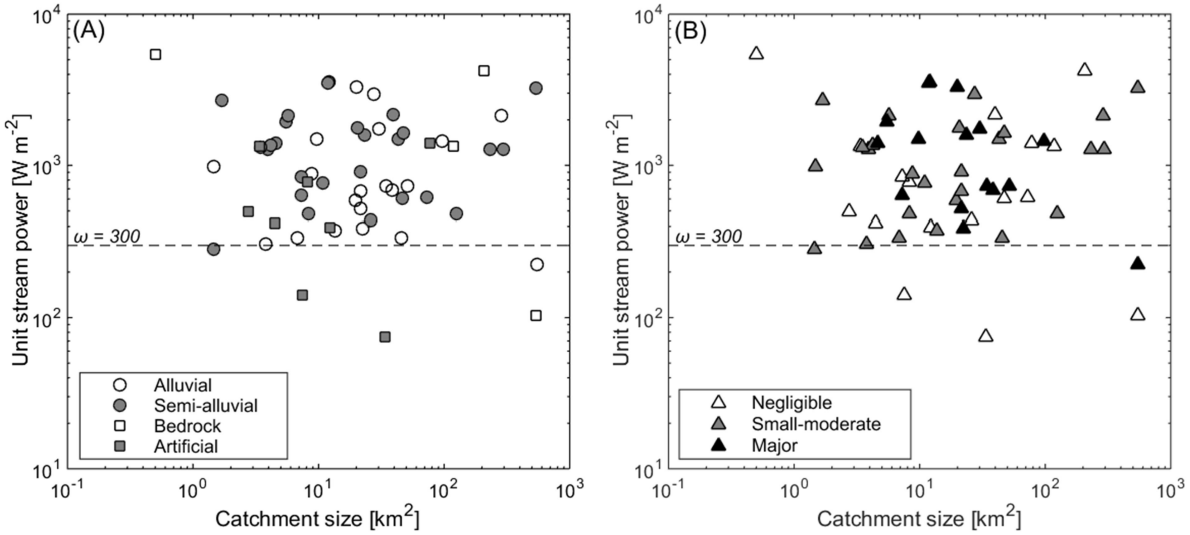

FIG. 4.13. Relationship between upslope drainage area and unit stream power based on (A) cross-section types, and (B) observed geomorphic effects.

TABLE 4.4. Compilation of energy expenditure based on channel types and observed geomorphic effects: mean and *standard deviation* values. Ω: cross-sectional stream power; ω: unit stream power; $\mathcal{E}_e$: event energy expenditure; $\mathcal{E}_{th}$: above-threshold energy expenditure; T_{th}: above-threshold flow duration; $\mathcal{E}_r$: energy ratio

Channel type/ *Geomorphic Effects*	*No. of cross sections*	*Catchment size* $[km^2]$	Ω $[W\ m^{-1}]$	ω $[W\ m^{-2}]$	$\mathcal{E}_e$ $[MJ\ m^{-2}]$	$\mathcal{E}_{th}$ $[MJ\ m^{-2}]$	T_{th} $[s*10^3]$	$\mathcal{E}_r$ [-]
Alluvial								
Major	9 (1*)	36.1 (*25.8*)	63495 (*41438*)	1226 (*909*)	393 (*361*)	100 (*128*)	19 (*9.9*)	0.20 (*0.16*)
Small-moderate	11	40.7 (*82.9*)	46891 (*100195*)	1194 (*1157*)	437 (*606*)	194 (*350*)	13.9 (*14.1*)	0.20 (*0.25*)
Negligible	0							
Semi-alluvial								
Major	5	10.5 (*7.7*)	50296 (*42221*)	1815 (*1054*)	682 (*475*)	203 (*209*)	19.8 (*8.2*)	0.23 (*0.13*)
Small-moderate	15 (1*)	90.8 (*153.7*)	67422 (*94971*)	1472 (*760*)	380 (*362*)	159 (*202*)	21 (*13.5*)	0.32 (*0.18*)
Negligible	5	38.5 (*24.4*)	19551 (*15204*)	931 (*702*)	225 (*254*)	62 (*121*)	9.9 (*9.0*)	0.16 (*0.17*)
Bedrock								
Major	0							
Small-moderate	0							
Negligible	3 (1*)	108.4 (*103*)	128761 (*163853*)	3665 (*2093*)	885 (*647*)	440 (*356*)	24.6 (*10.8*)	0.42 (*0.24*)
Artificial								
Major	0							
Small-moderate	0							
Negligible	6 (2*)	18.1 (*29.3*)	12923 (*15272*)	803 (*460*)	216 (*190*)	39 (*49*)	10.8 (*8.0*)	0.11 (*0.11*)

*number of cross sections with peak instantaneous unit stream power less than 300 W m^{-2}

Table 4.4 reports a compilation of summary data of energy expenditure and observed geomorphic effects for the 54 studied cross sections. Bedrock channels show the highest values of the various measures of stream power but with no visible erosion, whereas artificial channels showed relatively moderate values. This is ascribed to lower energy gradients associated with artificially modified channels (mean slope of 0.047 for bedrock and 0.017 for artificial cross sections). For alluvial cross sections, peak stream power and cumulative energy expenditure values are not significantly different for relatively equal numbers of cross sections with observed major and moderate geomorphic effects. The trend of the mean values reported in Table 4.4 could imply that, for alluvial channels, peak

instantaneous stream power values may be necessary to cross landscape-scale thresholds of erosional resistance and to significantly disrupt channel configurations whereas the coupled influences of flow duration and cumulative energy expenditure may play important roles in doing geomorphic work (i.e., sediment transport). The trend observed for the various measures of energy expenditure in semi-alluvial channels can be attributed to the degree of channel resistance to erosion, which suggests the need to focus on local or event-specific conditions that increase the resistance of channel bed and banks to erosion and/or reduce the geomorphic effectiveness of the flood. An interesting observation relates to the five basins excluded from the analysis because the maximum unit stream power estimated at these cross sections was less than the Miller-Magilligan threshold. From Table 4.4, these correspond to one section each of alluvial and semi-alluvial with respectively, major and moderate geomorphic impacts, and one bedrock and two artificial cross sections with negligible geomorphic impacts. This highlights the fact that 300 W m^{-2} is not rigidly an absolute erosional threshold and suggests the feasibility to consider other erosion-resistant thresholds in relation to specific events and/or catchments.

4.3 Downstream Variations in Stream Power

4.3.1 Downstream trends of peak discharge and channel gradient

The downstream trends of peak discharges and channel gradient were modelled for five tributaries of the Magra River (Pogliaschina, Gravegnola, Mangiola, Osca, and Geriola), two tributaries of the Posada River (Posada, and Mannu di Bitti) and the Lierza Creek. Detailed datasets for 159 sub reaches on these channels are reported in Appendix A4. Peak discharges were obtained through model simulations for the reconstruction of the respective flood events, whereas channel gradients were obtained from the *DEM* of the respective catchments. Fig. 4.14 and 4.15 present the empirical relationships for the downstream variations in peak discharges Q_p [m^3 s^{-1}] and channel gradient, S [m m^{-1}], respectively, represented by power and exponential functions of the channel length, L [m] as follows:

$$Q_p = \alpha \cdot L^{\beta} \quad [4.2]$$

$$S = S_o \cdot e^{-rL} \quad [4.3]$$

where k and m are dimensionless constants, S_o [m m^{-1}] is the initial slope at an upstream reference section and r is the coefficient of slope reduction. The regressions in Fig. 4.13 (4.15) show generally increasing (decreasing) peak discharges (channel gradient) downstream along the channel reaches. The cumulative downstream lengths of the channel reaches were set to start at an arbitrary point of 100 m for each tributary to avoid dealing with zeros (0) in the power and exponential functions. The reported power-law regressions between peak discharge and channel length (Fig. 4.14) generally show high explained variances for the studied tributaries. Major tributaries contribute to the Gravegnola and Posada Rivers, with the Mannu di Bitti River channel the major tributary of the latter, which made it imperative to estimate the regressions for the upstream and downstream reaches, as shown in Fig. 4.14. The discontinuity of the general exponential trend between slope and downstream length observed in some of the studied rivers in Fig. 4.15 can be attributed to geo-lithological controls that produce the striking downstream differences in morphology in mountain river systems (Knighton, 1999).

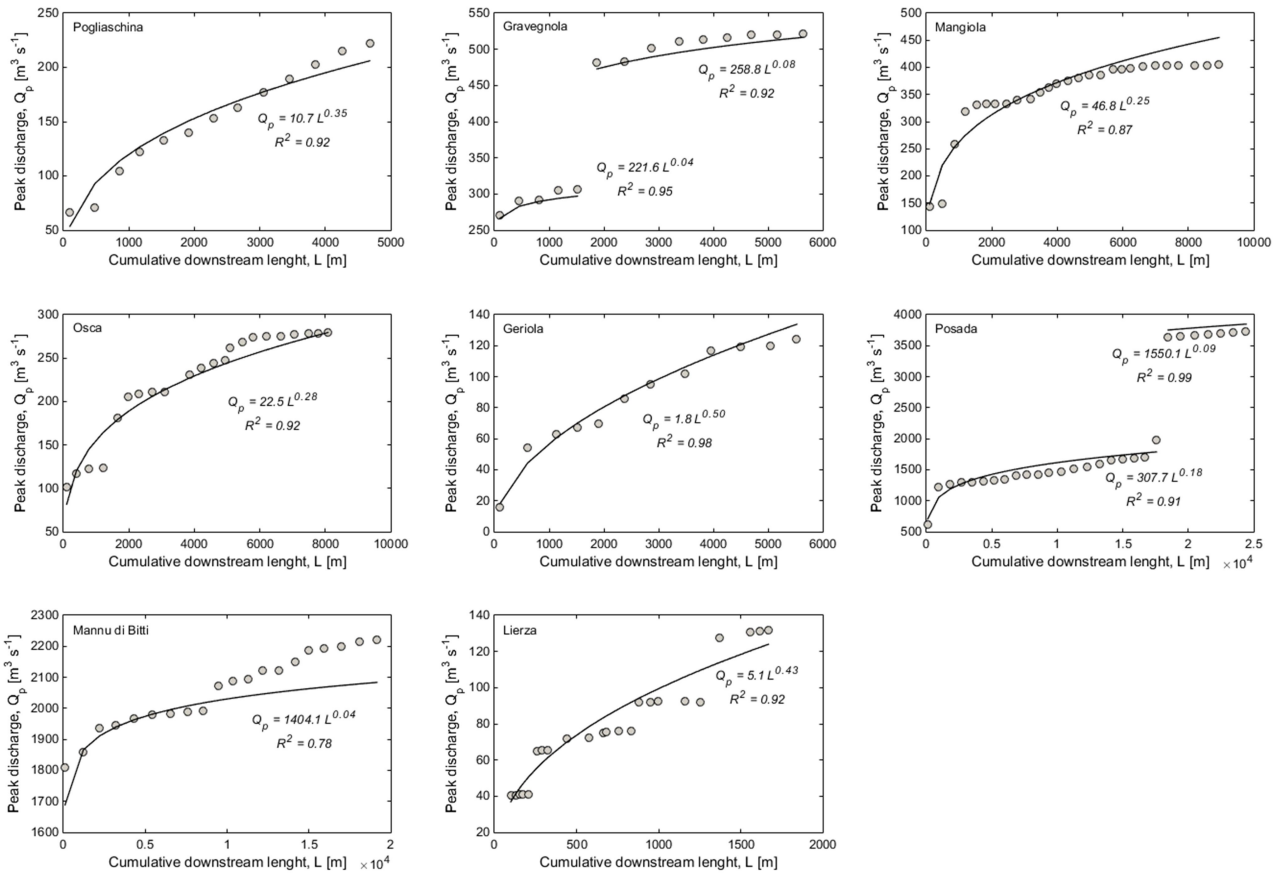

FIG. 4.14. Downstream trends of peak discharge as power function of channel length along the channels.

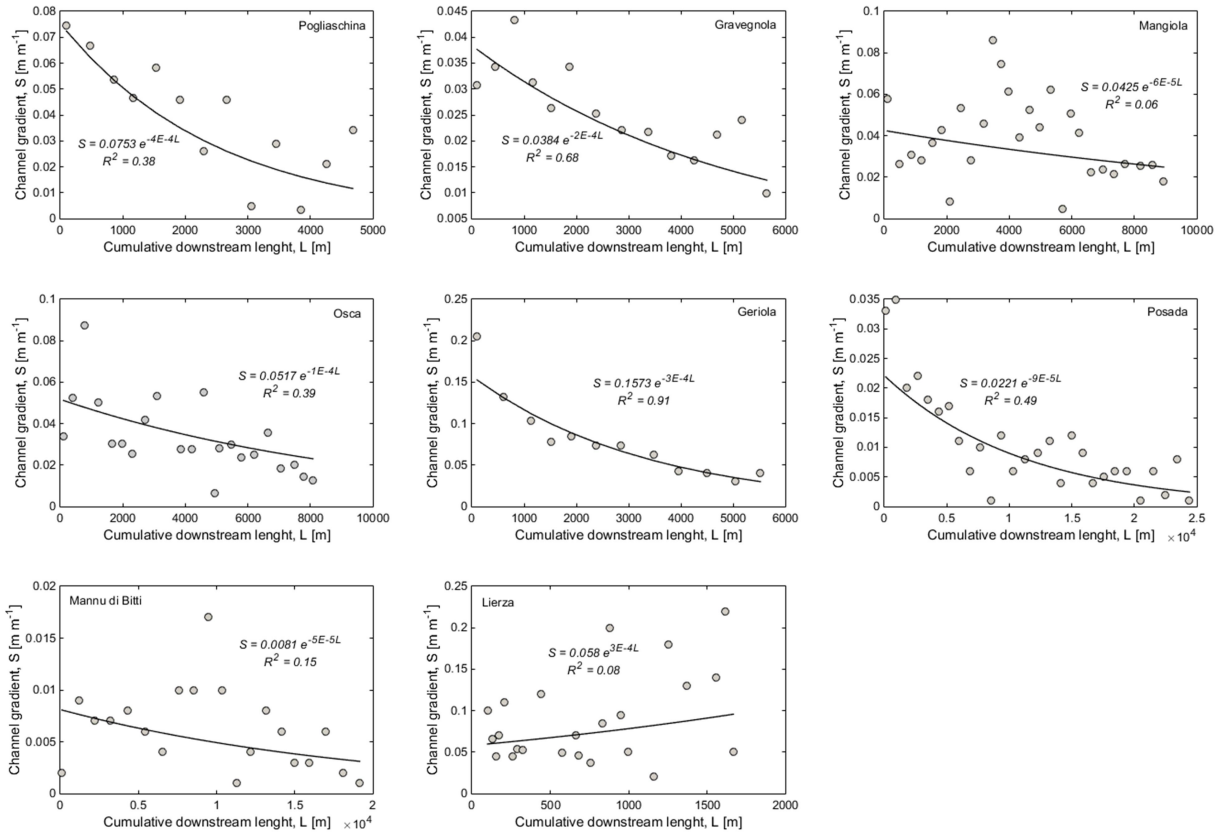

FIG. 4.15. Downstream trends of channel gradient as exponential function of channel length along the channels.

Contrary to the empirical regression proposed in literature for the downstream variation in channel gradient as an exponential function of channel length (Eq. [4.3]) (Lawler, 1992; Lecce, 1997; Knighton, 1999; Reinfelds et al., 2004), the studied tributaries generally showed relatively higher explained variance using quadratic function (Fig. 4.16), represented as:

$$S = C_1 L^2 + C_2 L + S_o \qquad [4.4]$$

where C_1 and C_2 are exponents of the quadratic function and S_o [m m^{-1}] is the initial slope at an upstream reference section. It can be noted that two out of 8 rivers (Mangiola and Mannu di Bitti) feature the highest gradient in the middle/intermediate sector along the longitudinal profile, and one (Lierza) shows a tendency (although weak) to downstream increase of slope. Generally, the quadratic function also shows a high tendency to model the striking high downstream variability in energy gradient compared to the exponential function.

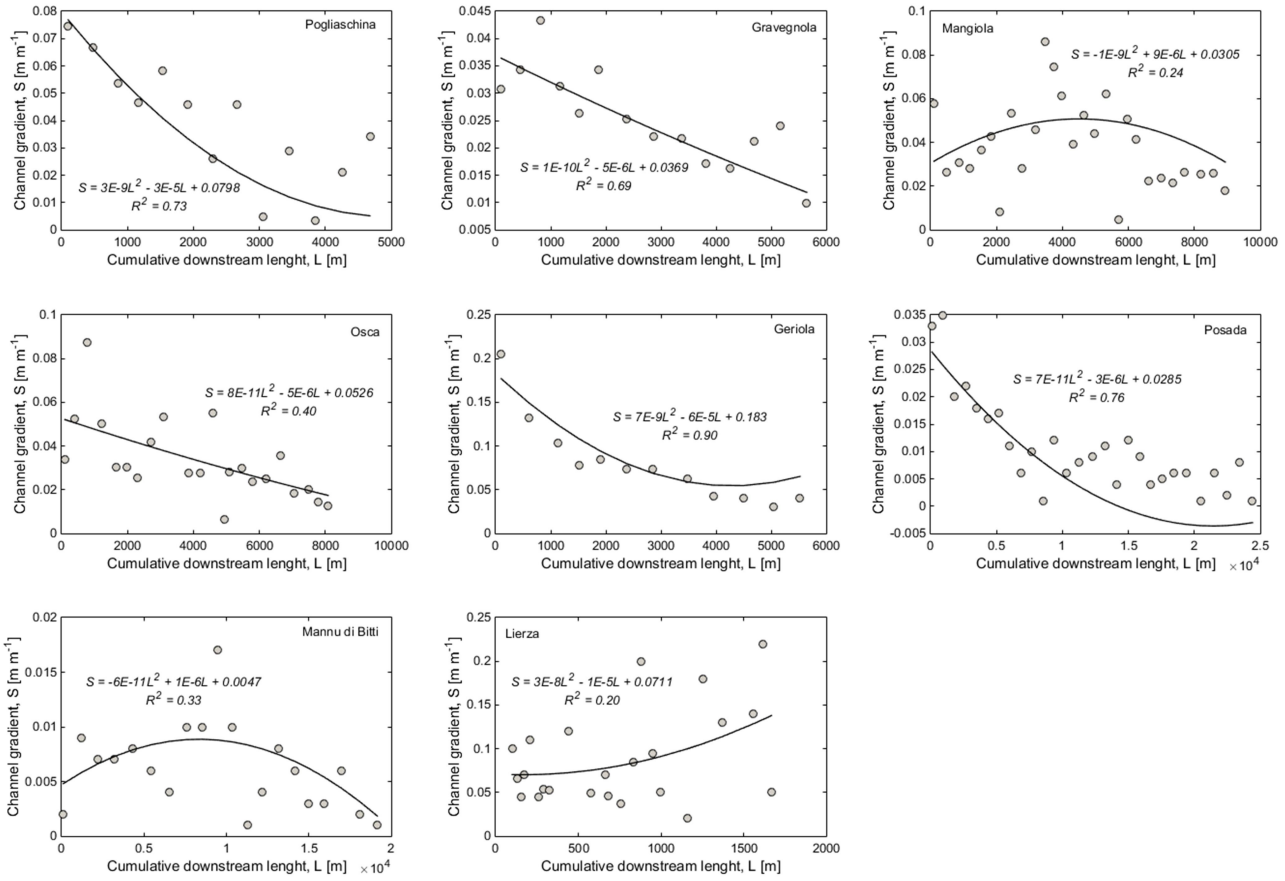

FIG. 4.16. Downstream trends of channel gradient as quadratic function of channel length along the studied tributaries.

4.3.2 MODELLING THE DOWNSTREAM TRENDS OF PEAK STREAM POWER

Fig. 4.17 presents the downstream variations in cross-sectional stream power for the studied tributaries. Cross-sectional stream power for each channel reach was estimated based on Eq. [3.10], using simulated peak discharges and DEM-derived channel gradient along the tributaries of the Magra, Posada and Lierza Rivers. The estimated stream power trend reported in Fig. 4.17 shows tremendous downstream variability, which may be attributed primarily to the high downstream variability in channel gradient (Figs. 4.15 and 4.16). Downstream trends in cross-sectional stream power were represented by the trends of peak discharge and channel gradient, which yield two generalized modelled downstream variations in cross-sectional stream power (Fig. 4.17) as follows:

$$\Omega_{mod1} = [\gamma \cdot (\alpha \cdot L^{\beta}) \cdot (S_o \cdot e^{-rL})] \quad [4.5]$$

$$\Omega_{mod2} = [\gamma \cdot (\alpha \cdot L^{\beta}) \cdot (C_1 L^2 + C_2 L + S_o)] \quad [4.6]$$

where Ω_{mod1} represents the modelled downstream trend using exponential function of the channel gradient, and Ω_{mod2} represents the modelled downstream trend using quadratic function of the channel gradient. Channel gradients usually decrease but some channels show a different trend (Figs. 4.15 and 4.16); discharges increase (Fig. 4.14) and channels generally become less confined as they enter their distal coastal or alluvial plains. These patterns usually ensure an intermediate location between the headwaters and the basin outlet where appropriate discharge and channel gradient combine to maximize stream power. The trends in Fig. 4.17 support this theoretical assumption, which has also been confirmed through empirical studies by Lecce (1997), Knighton (1999) and Reinfelds et al. (2004).

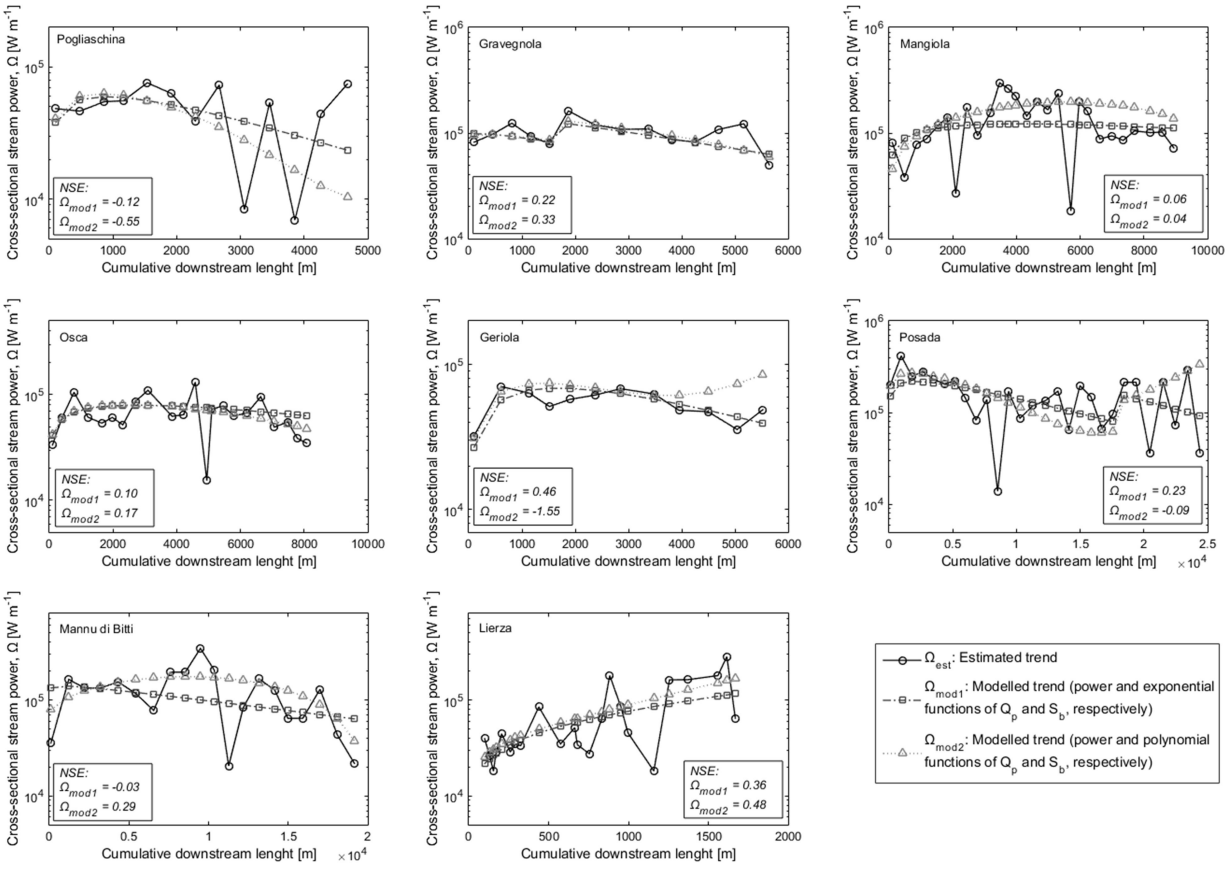

FIG. 4.17. Downstream variations in cross-sectional stream power for the studied tributaries; reporting variations in both estimated and modelled trends. NSE: Nash-Sutcliffe model efficiency score.

Estimated cross-sectional stream power shows high variability along the studied tributaries whereas the modelled trends shows consistent smoothness, depending on the nature of the downstream empirical regressions of peak discharge and channel gradient. The Nash-Sutcliffe efficiency scores (NSE) reported for the comparison between the downstream trend of the estimated and two modelled trends for the studied tributaries (Fig. 17) can be attributed primarily to the corresponding downstream regressions of exponential and/or quadratic functions of channel gradient (Figs. 4.15 and 4.16), since the power functions of the downstream trends of peak discharge (Fig. 4.17) generally show close correlations. Quadratic regressions of the downstream trend in channel gradient resulted in higher NSE for Gravegnola, Osca, Mannu di Bitti, and Lierza, whereas exponential regressions produced relatively higher NSE for Pogliaschina, Mangiola, Geriola, and Posada. The negative NSE for both modelled trends of the Pogliaschina, the quadratic model for Gravegnola and Posada, as well as the exponential model of the Mannu di Bitti imply that the average estimated values could be better predictors of the downstream variations in cross-sectional stream power. For the Mangiola tributary, the two models are as good as the average of the estimated values.

A similar analysis was carried out for the downstream trends in unit stream power, which were calculated based on Eq. [3.11]. Pre-flood channel width was used to calculate peak instantaneous unit stream power because it has been shown to perform better in terms of predicting channel adjustment compared to the use of post-flood channel width (e.g., Krapesch et al., 2011; Surian et al., 2015). The distinction between estimated and modelled unit stream power (Fig. 4.18) follows that of cross-sectional stream power. Unit stream power has also been predicted to peak at about half way between the source of river and the location of the maximum cross-sectional stream power (Lawler, 1995; Knighton, 1999). However, in most cases, unit stream power peaked at almost the same location where cross-sectional stream power peaked along the studied tributaries. The Nash-Sutcliffe efficiency scores (NSE) reported for the comparison between the estimated and modelled unit stream power for the studied tributaries (Fig. 4.18) generally show better model performance than for the modelled downstream trends of cross-sectional stream power (Fig. 4.17). Similar to the modelled trends of cross-sectional stream power, the two modelled trends of unit stream power for the Pogliaschina tributary did not perform significantly better than the use of the average value of the estimated trends.

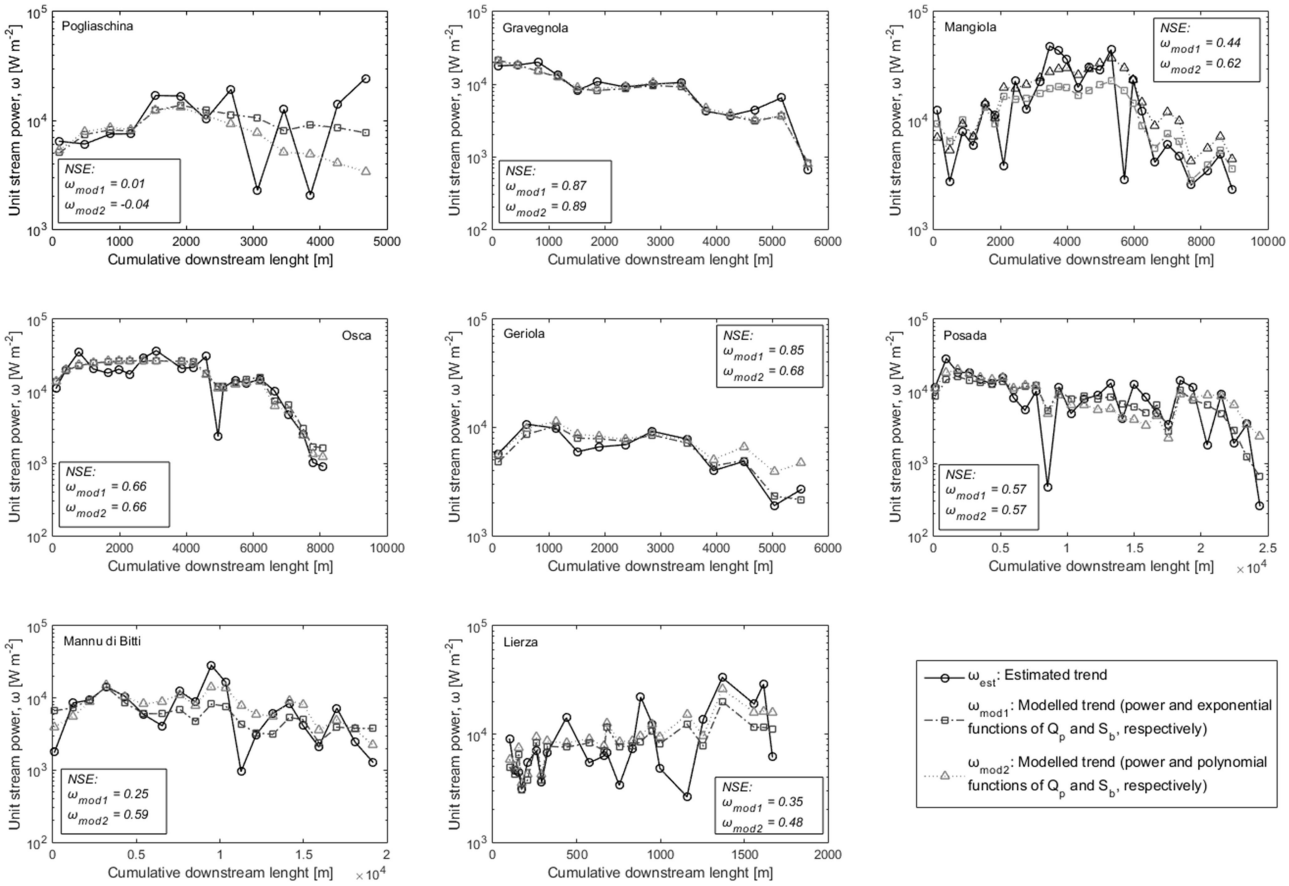

FIG. 4.18. Downstream variations in unit stream power for the studied tributaries; reporting variations in both estimated and modelled trends. Unit stream power is calculated as cross-sectional stream power per unit pre-flood channel width. NSE: Nash-Sutcliffe model efficiency score.

4.3.3 CHANNEL WIDENING AND CONTROLLING FACTORS

Channel widening, represented by width ratio (i.e., the ratio of channel width after flood to the corresponding pre-flood channel width) was estimated through remote sensing for the tributaries of the Magra and Posada Rivers, where pre- and post-flood high resolution aerial satellite imagery are available (section 3.2.2). Figs. 4.19A-B report scatter plots between width ratio, and channel width before and after the floods, respectively. The reported explained variances suggest that the channel modifications to the extreme floods primarily depend on the pre-flood channel conditions (e.g., Wohl et al., 2001).

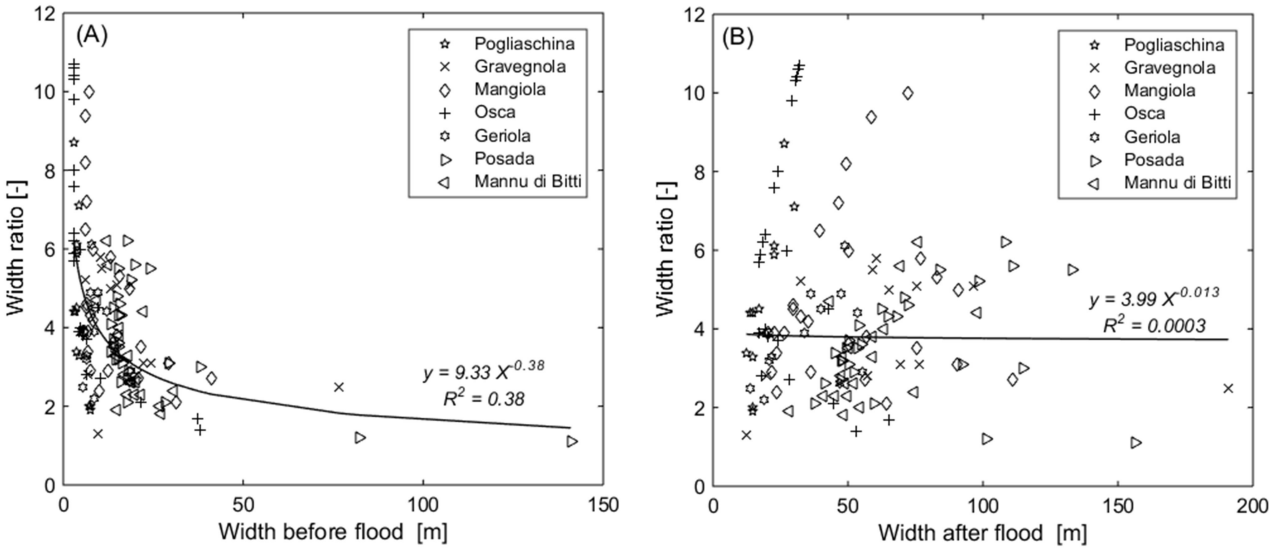

FIG. 4.19. Relationship between channel width ratio and (A) channel width before the floods and (B) channel width after the floods for the tributaries of the Magra and Posada Rivers.

Generally, maximum channel widening (> 6 times the initial channel width) was observed in the Magra tributaries, with pre-flood channel with less than 10 m (Fig. 4.19A). On the contrary, most of the studied reaches of the Posada tributaries were characterized by width ratios less than 6. Channel response to extreme floods is likely to depend on the combined influences of the geological controls on channel geometry and sediment characteristics, as well as on variations in flood intensity. The efficacy of the hydraulic forces of the flood responses were quantitatively assessed by comparing the various measures of stream power with potential channel modification in the form of channel widening (represented by width ratio) for the eight studied tributaries of the Magra and Posada Rivers.

Figs. 4.20 and 4.21 present the downstream variations in peak instantaneous unit stream power and cumulative energy expenditure, respectively, together with variations in width ratio. The patterns show similar trends for both stream power measures in most of the tributaries, with somewhat striking similar trends with the corresponding observed channel response. The plots indicate that the studied tributaries are characterized by extreme downstream variability of driving forces, with observed peaks mostly occurring at intermediate locations between the headwaters and basin outlet. This supports the non-linear downstream change in stream power findings by Lawler (1992), Lecce (1997), Knighton (1999), Fonstad (2003), Reinfelds et al. (2004) and Barker et al., 2009. The trend of decreasing energy

expenditure at the outlet is not clearly observed along the main Pogliaschina reach (Fig. 4.20 and 4.21), because the studied channel reach of Pogliaschina Creek does not end at the outlet. The downstream reach of Pogliaschina was excluded from the analysis because post-flood conditions had been altered by restoration works implemented immediately after the flood. The observed non-linear pattern between the hydraulic forces and width ratio can be attributed to the combined influences of catchment hydrology, channel gradient and degree of confinement, especially the geo-lithological controls that produce the striking downstream differences in morphology along the longitudinal profile of river channels. Although the downstream variability in stream power is non-linear and could not adequately explain channel widening, this pattern is usually responsible for the complex geomorphic hazards in the form of erosional and depositional modification of channel boundaries during a flood (Wohl et al., 2001).

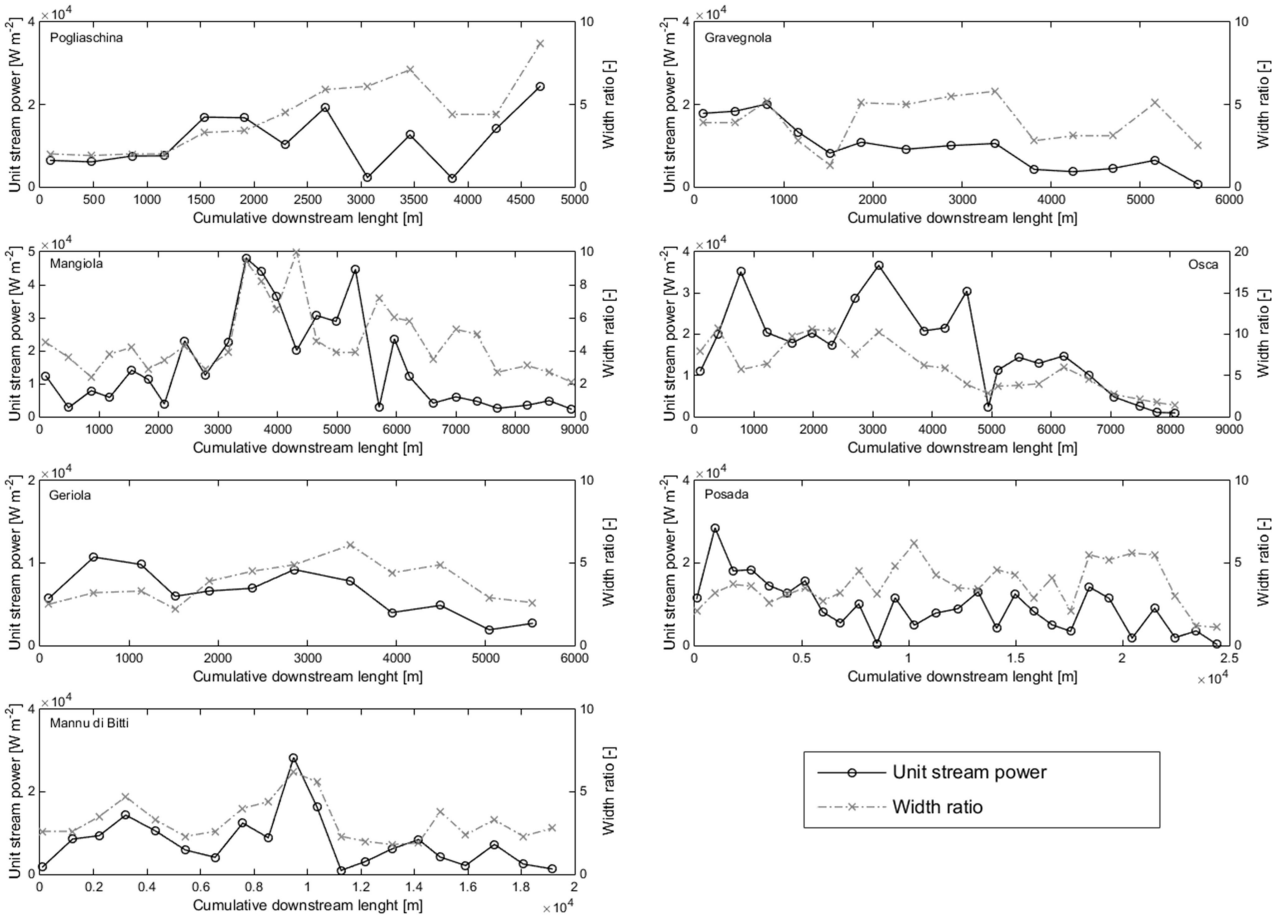

FIG. 4.20. Downstream variations in peak unit stream power and channel width ratio for the tributaries of the Magra and Posada Rivers.

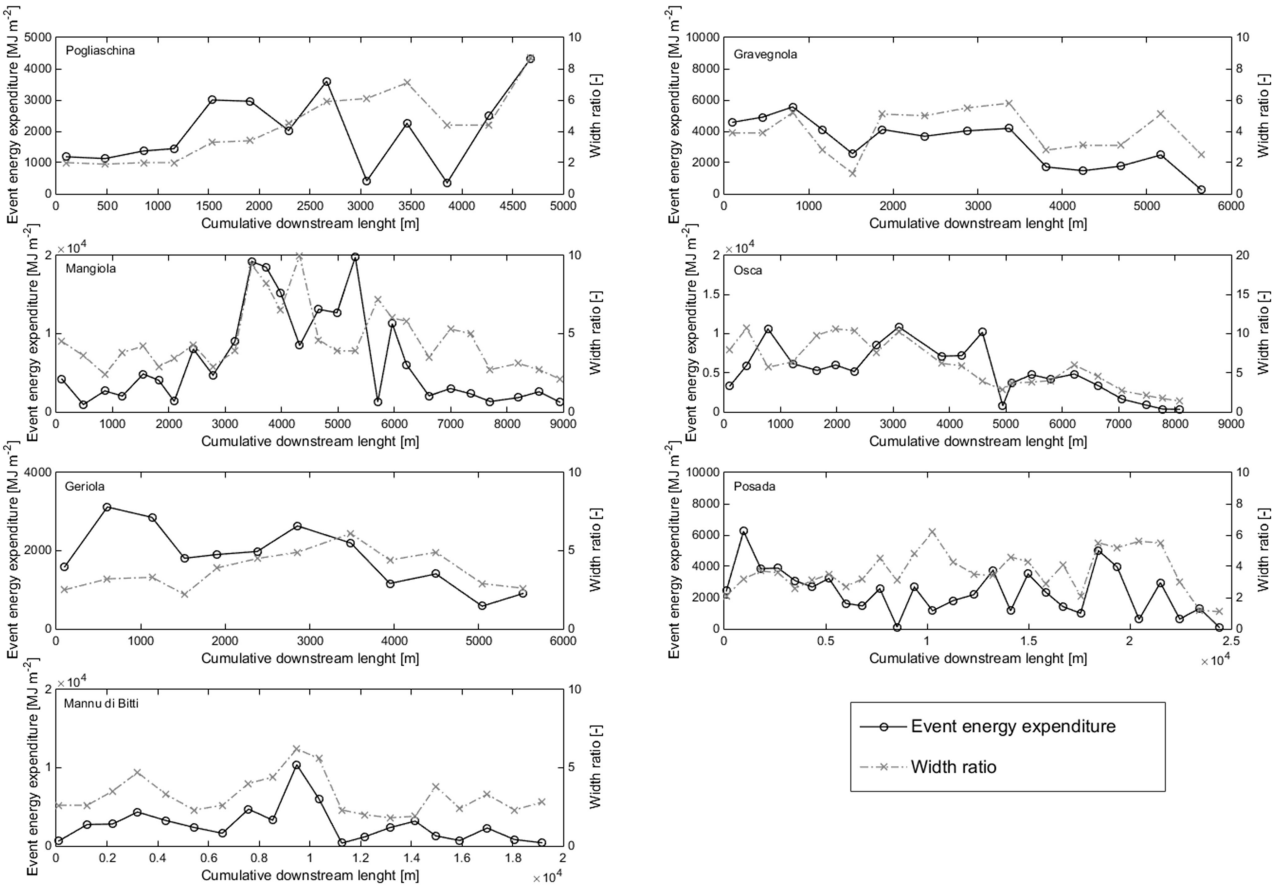

FIG. 4.21. Downstream variations in cumulative energy expenditure and channel width ratio for the tributaries of the Magra and Posada Rivers.

The efficacy of peak instantaneous stream power and the combined influences of flow duration and cumulative energy expenditure were quantitatively assessed by comparing with potential channel modification in the form of channel widening for the seven studied tributaries of the Magra and Posada Rivers. Figs. 4.22A-D show regressions for the relationship between width ratio and unit stream power, event energy expenditure, above-threshold energy expenditure and energy ratio respectively, for the studied tributaries. The regressions are interpreted by power-law functions. The regressions in Fig. 4.22 show that the peak unit stream power and event energy expenditure are not significantly different in explaining the observed variations in channel widening, whereas above-threshold energy expenditure and energy ratio performed less well. The slope of the power-law regressions and explained variances

in Figs. 4.22A and B indicate that peak instantaneous unit stream power and cumulative event energy expenditure are equal predictors of the rate of channel widening in the studied rivers.

A lack of or more specifically, the uncertainties surrounding the quantification of resisting forces, in particular, renders the association between the magnitude of energy expenditure (or driving forces) and the resulting geomorphic effectiveness of floods non-deterministic (Wohl et al., 2011; Magilligan et al., 2015). The relatively low performance of the above-threshold energy expenditure and energy ratio in quantifying channel widening (Fig. 4.22) indicates that the Miller-Magilligan critical threshold (300 W m^{-2}) is not a representative of unit stream power above which major geomorphic adjustment occurred in the studied channels. This suggests the usefulness of considering other critical erosional thresholds for these specific events and/or channels.

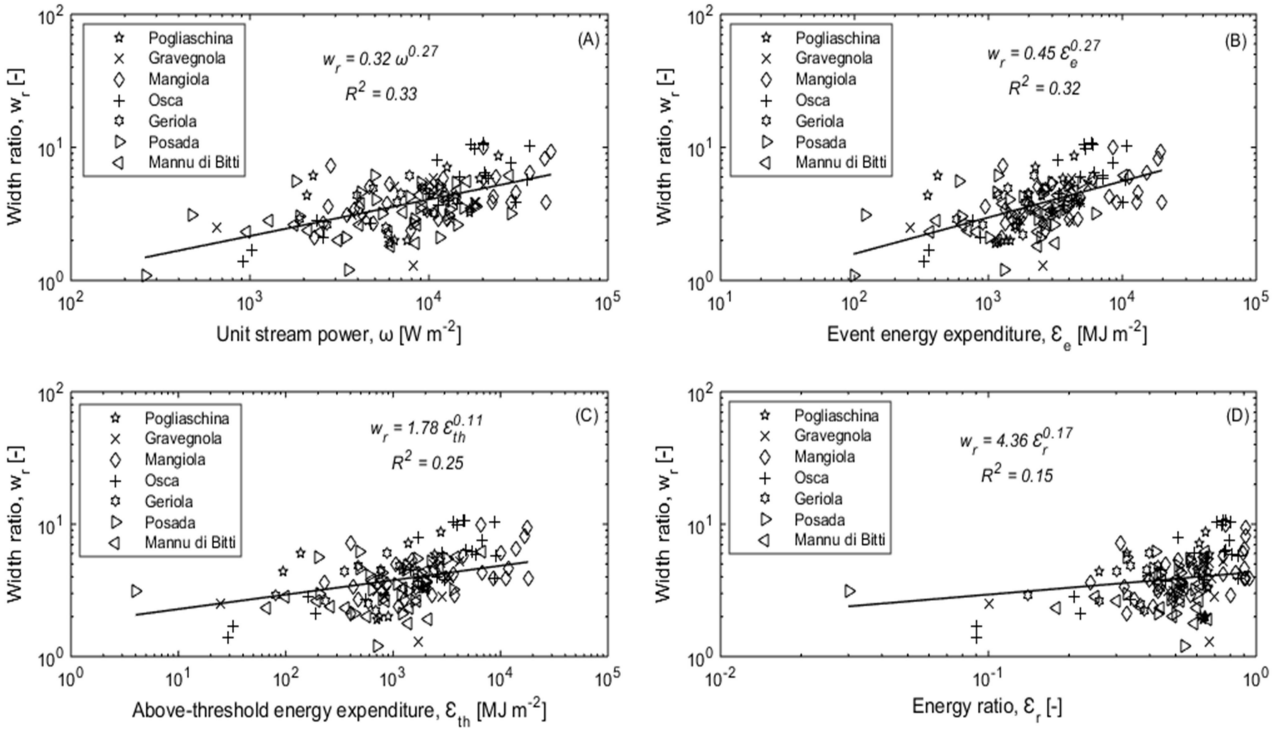

FIG. 4.22. Regressions between channel width ratio, and (A) unit stream power, (B) event energy expenditure, (C) above-threshold energy expenditure, and (D) energy ratio for the Magra and Posada tributaries.

A sensitivity analysis of the critical stream power threshold for significant channel modification was carried out to evaluate the influence on channel widening for the studied channels. In addition to the Miller-Magilligan critical threshold of 300 W m^{-2}, thresholds of 200, 400, and 500 W m^{-2} were considered in computing the above-threshold energy expenditure. The Pearson correlation coefficient statistic was used to assess the linear dependence between the response variable (channel width ratio) and the explanatory stream power hydraulic variables under the assumption that channel widening rate increases with the magnitude of the hydraulic force.

Table 4.5 reports the Pearson correlation coefficient for the linear dependence of width ratio, and the stream power measures for the studied channels. The statistics generally show positive correlation between the response and explanatory variables, which indicate increasing rate of channel widening with increasing energy expenditure. The correlations reveal that unit stream power and total energy expenditure can better explain the channel responses associated with the Magra and Posada channels than the arbitrary thresholds for major channel erosion. An interesting observation is that the performance of the above-threshold and energy ratio decreases, but not drastically, when the erosion-resistant threshold is increased. This points out that whereas peak instantaneous stream power was necessary to cross reach-scale erosional thresholds, the overall energy expenditure was also important for the overall channel modification. The results point out that hydraulic variables alone are not adequate to explain the rate of channel widening along complex morphologic settings in mountain river systems, which suggests the usefulness of considering other location specific factors, particularly the degree of channel confinement (e.g., Surian et al., 2016).

TABLE 4.5. Pearson correlation coefficient (r) between channel width ratio (response variable) and the stream power measures (explanatory variables) for the studied channels. ω: unit stream power; $\mathcal{E}_e$: event energy expenditure; $\mathcal{E}_{th,Z}$: above-threshold energy expenditure using unit stream power threshold of Z Wm^{-2}; $\mathcal{E}_{r,Z}$: corresponding energy ratio

	ω	$\mathcal{E}_e$	$\mathcal{E}_{th,200}$	$\mathcal{E}_{th,300}$	$\mathcal{E}_{th,400}$	$\mathcal{E}_{th,500}$	$\mathcal{E}_{r,200}$	$\mathcal{E}_{r,300}$	$\mathcal{E}_{r,400}$	$\mathcal{E}_{r,500}$
r	0.55	0.51	0.49	0.47	0.45	0.43	0.47	0.47	0.42	0.43

4.3.4 INFLUENCE OF CHANNEL CONFINEMENT ON CHANNEL WIDENING

The degree of channel confinement and its variability along the studied reaches provides an idea of the topographic constraints, whose interaction with hydraulic forces may be necessary to explain the rate of channel widening. It should be remembered that geomorphic adjustment is likely to depend on the complex interactions between driving and resisting forces. Fig. 4.23 reports a linear regression between channel confinement index and width ratio. It should be recalled from section 3.2.2 that channel width ratio is defined as the ratio of the channel width after the flood to the channel width before the flood, whereas channel confinement index is defined as the ratio of the alluvial plain width to the channel width before the flood. Fig. 4.23A shows the regression for the whole 136 dataset for the Magra and Posada channels, where confinement index explains 34% of the rate of channel widening. Fig. 4.23B shows the regression when the outliers in Fig. 4.23A are eliminated, which resulted in high explained variance (0.62) between the degree of channel confinement and channel widening. These outliers correspond to five sub reaches along the Osca channel and two sub reaches, where high confinement index resulted in relatively lower channel widening. This can be attributed to the striking downstream differences in morphology as well as the high variability in precipitation forcing and the corresponding flood responses along the longitudinal profile of river channels.

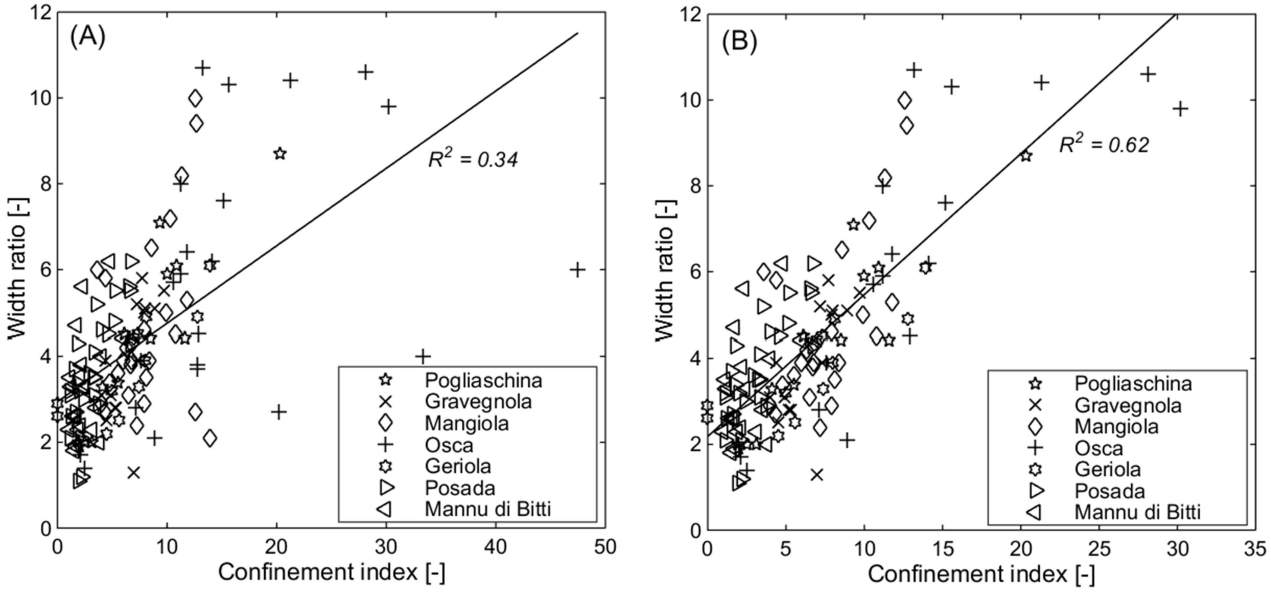

FIG. 4.23. Regressions between channel width ratio and confinement index for sub reaches of the Magra and Posada Rivers: (A) the whole 136 dataset, and (B) 126 dataset excluding the outliers.

To elucidate the combined influences of hydraulic forces and the degree of channel confinement on the flood-triggered channel widening, least square multiple regressions were carried out with the *R*-statistical software. Four different multiple regression models were carried out on the dataset, including 136 sub reaches of the studied channels of the Magra and Posada Rivers, corresponding to the four separate independent variables in order to avoid the multicollinearity issue. The models included the geomorphic variable (confinement index) and each of the considered stream power measures (unit stream power (ω), event energy expenditure ($\mathcal{E}_e$), above-threshold energy expenditure ($\mathcal{E}_{th}$), and energy ratio ($\mathcal{E}_r$)). The above-threshold energy expenditure and the corresponding energy ratio were computed based on the Miller-Magilligan critical value (300 W m^{-2}), since other thresholds did not produce significantly different and improved results. The *p-values*, the R^2 and the adjusted R^2 were compared to select the model with the best fit. The *p-values* and R^2 of the individual variables within each model were also compared to assess which variables were the most influential for the response variable (i.e., width ratio) in the models. This analysis could give more robustness on models carried out by Surian et al. (2016) and Righini et. al. (2017) for the Magra and Posada Rivers respectively, adding an important dimension in terms of flood-flow duration and cumulative energy expenditure.

All the four multiple regression models turned out to be significant (*p-value* < 0.05) operating at the 95% significance level, which indicates that significant relationships exist between width ratio and the four models (Table 4.6). The best model was the model that include confinement index and peak unit stream power (model 1), which explains 53% of variation in channel widening, followed by model 4 (50%) whereas models 2 and 3 preformed relatively the same. Indeed in all four models, the most influential explanatory variable for channel widening was the confinement index (R^2 = 0.34). Though all four stream power measures were individually significant in explaining channel widening (*p-value* < 0.05), peak unit stream power performed relatively better than the overall event energy expenditure, whereas the above-threshold energy expenditure performs equally as the proportion of the energy expenditure above the Miller-Magilligan unit stream power threshold proposed for significant channel modification.

TABLE 4.6. Summary results of multiple regression models for predicting channel widening (i.e., width ratio) for all sub reaches of the studied channels (136 sub reaches). *CI:* confinement index, ω: unit stream power, $\mathcal{E}_e$: event energy expenditure; $\mathcal{E}_{th}$: above-threshold energy expenditure; $\mathcal{E}_r$: energy ratio

	Model 1		Model 2		Model 3		Model 4	
R^2	0.53		0.49		0.49		0.50	
R^2 *adj.*	0.52		0.48		0.48		0.49	
p-value	<0.0001		<0.0001		<0.0001		<0.0001	
	R^2	*p-value*	R^2	*p-value*	R^2	*p-value*	R^2	*p-value*
CI	0.34	<0.0001	0.34	<0.0001	0.34	<0.0001	0.34	<0.0001
ω	0.31	<0.0001	–	–	–	–	–	–
$\mathcal{E}_e$	–	–	0.26	<0.0001	–	–	–	–
$\mathcal{E}_{th}$	–	–	–	–	0.23	<0.0001	–	–
$\mathcal{E}_r$	–	–	–	–	–	–	0.22	<0.0001

In order to achieve a better understanding about the combined influences of hydraulic forces and the degree of channel confinement, as in Surian et al. (2016), the dataset was split in two subsets based on channel gradient: one set with channel slope below the threshold of 4% (subset 1) and another equal or greater than 4% in channel gradient (subset 2). Multiple regression analyses were carried out on a subset of 100 sub reaches (subset 1), comprising 52 sub reaches of the Magra River and all 48 sub reaches of the Posada River, as well as a subset of 36 sub reaches of the Magra River (subset 2). The four models follow similar combinations as in Table 4.6. Table 4.7 reports the statistics of the four models for subset 1. The analysis showed that all the four models were statistically significant (*p-value* < 0.05), which indicate that a relation exit between width ratio and the four models. Models 1 and 3 performed relatively equal and better in explaining 49% of variations in channel widening for sub reaches with channel gradients less than 4%, compared to 47% for model 2 and 46% for model 4 (Table 4.7). As in the previous models (Table 3), confinement index was also an influential explanatory variable for these sub reaches (R^2 = 0.34). Interestingly, above-threshold energy expenditure performs better in model 3 (R^2 = 0.32), compared to peak unit stream power in model 1 (R^2 = 0.28), event energy expenditure in model 2 (R^2 = 0.30), and energy ratio in model 4 (R^2 = 0.21). This implies that reach-scale erosion-resistant threshold could be a better predictor of channel modification for channel reaches in the dataset with moderate channel gradient (< 4%).

TABLE 4.7. Summary results of multiple regression models for predicting channel response (i.e., width ratio) for 100 sub-reaches characterized by channel gradient < 4% (subset 1). *CI:* confinement index, ω: unit stream power, $\mathcal{E}_e$: event energy expenditure; $\mathcal{E}_{th}$: above-threshold energy expenditure; $\mathcal{E}_r$: energy ratio

	Model 1		Model 2		Model 3		Model 4	
R^2	0.49		0.47		0.49		0.46	
R^2 *adj.*	0.47		0.46		0.48		0.44	
p-value	<0.0001		<0.0001		<0.0001		<0.0001	
	R^2	*p-value*	R^2	*p-value*	R^2	*p-value*	R^2	*p-value*
CI	0.32	<0.0001	0.32	<0.0001	0.32	<0.0001	0.32	<0.0001
ω	0.28	<0.0001	–	–	–	–	–	–
$\mathcal{E}_e$	–	–	0.30	<0.0001	–	–	–	–
$\mathcal{E}_{th}$	–	–	–	–	0.32	<0.0001	–	–
$\mathcal{E}_r$	–	–	–	–	–	–	0.21	<0.0001

The analysis of subset 2 also showed four statistically significant models (*p-value* < 0.05) and a significant increase in R^2 and adjusted R^2 in all the four models (Table 4.8) compared to the respectively models run on the whole dataset (Table 4.6). Models 1 and 4 performed relatively better in explaining 75% each of variations in channel widening for sub reaches with channel gradients (Table 4.8). Similar to the models for the whole dataset (Table 4.6), peak unit stream power performed better in model 1 (R^2 = 0.36), compared to flow duration measures (Table 4.8) This implies that the magnitude of peak instantaneous stream power is necessary for channel modification for channel reaches in the dataset with steep gradients (≥ 4%).

TABLE 4.8. Summary results of multiple regression models for predicting channel response (i.e., width ratio) for 36 sub-reaches characterized by channel gradient ≥ 4% (subset 2). *CI:* confinement index, ω: unit stream power, $\mathcal{E}_e$: event energy expenditure; $\mathcal{E}_{th}$: above-threshold energy expenditure; $\mathcal{E}_r$: energy ratio

	Model 1		Model 2		Model 3		Model 4	
R^2	0.75		0.74		0.73		0.75	
R^2 *adj.*	0.73		0.71		0.71		0.73	
p-value	<0.0001		<0.0001		<0.0001		<0.0001	
	R^2	*p-value*	R^2	*p-value*	R^2	*p-value*	R^2	*p-value*
CI	0.65	<0.0001	0.65	<0.0001	0.65	<0.0001	0.65	<0.0001
ω	0.36	0.0001	–	–	–	–	–	–
$\mathcal{E}_e$	–	–	0.29	0.0008	–	–	–	–
$\mathcal{E}_{th}$	–	–	–	–	0.25	0.0017	–	–
$\mathcal{E}_r$	–	–	–	–	–	–	0.18	0.01

5 DISCUSSION

5.1 FLASH FLOOD DOCUMENTATION AND ANALYSIS

A fundamental issue in hydrology is to identify the landscape and climate variables that control the runoff response to heavy rainfall. This question has important practical implications concerning the accuracy of flood predictions for ungauged basins, which are commonly driven by observation of specific and measurable catchment attributes as indicators of hydrological similarity (Blöschl, 2005; Parajka et al., 2013). The international PUB (Prediction in Ungauged Basins) initiative is already leading to significant advances in flow estimation methods in many parts of the world. The documentation and analysis of flash floods is important because these events often reveal aspects of hydrological behaviour that either were unexpected on the basis of weaker responses or highlight anticipated but previously unobserved behaviour (Delrieu et al., 2005; Archer et al., 2007). The mismatch between space-time scales of flash flood occurrence and typical hydrometeorological monitoring networks has stimulated the development of post-event integrated hydrologic strategy, which involves post-flood indirect estimation of peak discharges, use of weather radar observation for rainfall rate estimation, and hydrological modelling for water budget analysis (Borga et al., 2008; Amponsah et al., 2016). These observations were used in the analysis of the studied flash floods, which provided the link between the real-world processes and the rainfall-runoff model implemented to understand the physical flood response processes.

Post-flood surveys and observations played an important role in the collection of rainfall maxima that produce the storm event and in the indirect estimation of peak discharges along ungauged channel networks. Flash flood peak observations and model analyses of hydrologic response also permitted to illustration of how storm structure and evolution translate into scale-dependent flood response. The spatial extent of unit peak discharge for the studied floods supports the behaviour of the different space and time scales of the generating storm events (Gaume et al., 2009; Marchi et al., 2010). The upper limit envelope for unit peak discharges against catchment sizes shows a decreasing gradient of -0.2 compared to -0.4 reported for the larger HYDRATE dataset of European flash floods (Gaume et al., 2009). Differences are attributed to observed higher peak discharges for larger drainage areas in our dataset, more specifically in the Cedrino-Posada catchments, which were not included in the

HYDRATE dataset. Also, the HYDRATE dataset (Gaume et al., 2009) consists of extreme unit peak discharges for smaller drainage areas compared to our dataset. This occurred in spite of our effort to document flash floods for small catchments, especially in the Magra catchment, which are underrepresented in other Mediterranean databases (Marchi et al., 2010). The coefficient of the envelope for the relationship between drainage area and unit peak discharges of the studied flash floods (45) shows lower magnitude flood responses compared to 97 reported for other European flash floods in the HYDRATE project (Gaume et al., 2009) as well as 350 for the world envelope (Costa, 1987). The patterns reported for the relationship between drainage area and unit peak discharges point out the larger space and time scales of flash-flood generating rainstorms for Mediterranean climates compared to Continental regions (Marchi et al., 2010).

The integrated hydrologic flash flood analysis presented in Fig. 3.4 (Amponsah et al., 2016) is affected by significant uncertainties, which affects the accuracy of event reconstruction as well as our understanding of the physical processes. The main sources of uncertainties associated with the slope-conveyance peak discharge determination adopted in this study were attributed to i) dispersion and/or vague evaluation of high water marks, which affects both the assessment of cross-sectional geometry and energy line slope (Amponsah et al., 2017), ii) evaluation of the roughness parameter for the estimation of flow velocity (Lumbroso and Gaume, 2012), and iii) effect of scour or fill after flood peak on post-flood cross-sectional geometry (Kirby, 1987; Amponsah et al., 2016; 2017). Uncertainties related to rainfall predictions, stage-discharge transformation, indirect peak flow estimates and model parameterization may underpin flash flood warning procedures in real-time, which plays a key role in the design and planning of flood risk management measures. The results from the geomorphic impact-related uncertainty assessment of the indirect peak discharge estimates of the studied flash floods, with percentage standard errors of ±13.5%, ±23.2% and 37.1% for cross sections that showed negligible, moderate and major geomorphic effects, respectively, are comparable to values reported by Kirby (1987) in the range of ±16% to ±24%. Di Baldassarre and Montanari (2009) also reported ±21% uncertainty-related deviation for the highest discharge value at the Po River outlet. The geomorphically-influenced uncertainty assessment agrees with conclusions from Kirby (1987 p. 138), who stated that "…*the most significant improvements in discharge accuracy can be obtained by reducing the uncertainty in the scour term*". The integration provided a context to advance

understanding of flash floods and causative processes. It also allowed us to extend at-a-station stream gauge measurements and indirect peak discharge estimates to simulating flood hydrographs along the channel networks, which provided detailed spatial assessment of the flow characteristics (magnitude and duration) of the flood responses.

Post-flood reconstruction of peak discharge could benefit from current progress in observation techniques, such as Structure from Motion (SfM), whose suitability for (flash) floods has been demonstrated by Smith et al. (2014). SfM does not overcome the problems mentioned in the introduction regarding the recognition of clear and reliable HWMs, but enables fast survey of a whole channel reach, thus permitting fast application of slope conveyance. Pre-flood high-resolution digital terrain models from LiDAR surveys were not available for the studied floods, but are increasingly accessible in a number of geographical areas. When pre-floods HR-DTMs are available, their comparison with post-flood surveys by SfM (or terrestrial laser scanning) permits to quantitatively assess the severity of geomorphic changes, thus enabling more precise choice of the error parameters associated to geomorphic adjustment. This thesis used a qualitative categorisation of geomorphic impact into three classes: this approach has permitted to rate of the influence of cross-section changes on the accuracy of flow peak assessment, but leaves room to some subjectivity. Quantitative data on channel scour / fill or widening could permit a more objective assessment of the parameters required for uncertainty computation or could even lead to discard some cross sections, if topographic evidences indicate that major cross section changes would undermine the reliability of discharge estimates.

5.2 At-a-Station Stream Power and Relations with Geomorphic Effects

A fundamental issue in fluvial geomorphology relates to the association between energy expenditure of flood events and the resulting geomorphic impacts. Several studies (e.g., Baker and Costa, 1987; Miller, 1990; Magilligan, 1992; Costa and O'Connor, 1995; Wohl et al., 2001; Kales, 2008; Magilligan et al., 2015; Marchi et al., 2016) have related stream power as a surrogate of the actual energy expenditure to quantify geomorphic effects of high magnitude floods at the channel-reach scale. However, key questions still remain unanswered. Can stream power explain the intensity of

flood-related geomorphic impacts along a specific channel reach? How can we quantify geomorphic effects of high magnitude floods? From the classic delineation of the concepts of 'geomorphic effectiveness' and 'geomorphic work' (Wolman and Gerson, 1978), effective events are attributed to those responsible for creating or modifying landscape forms that persist over time whereas geomorphic work may relate to the sediment transport rate, which often adjust fluvial systems in equilibrium to external perturbations and internal feedbacks. Geomorphic modification is expected to occur in the fluvial system when driving forces exceed the threshold of resisting forces. Furthermore, geomorphic effectiveness of extreme floods is likely to depend on the combined influences of the geological controls on channel geometry and sediment characteristics, as well as on variations in flood intensity. In some fluvial environments, 100-year floods may be necessary to transport the coarser sediment in streams and/or create significant geomorphic modifications, which draws in the concept of frequency and magnitude. High magnitude events such as flash flood events with recurrence intervals more than 50-100 years represent one of, if not the most, geomorphically effective events in some river basins.

This study focused on quantifying the hydraulic forces in 119 cross sections and the corresponding geomorphic responses. The concept of stream power, which represents river energy expenditure was used as the basis for quantifying the driving forces in these channels. The combined analysis of results from post-flood surveys and hydrological modelling adopted for the analysis of the studied flash floods enabled computation and assessment of the efficacy of peak instantaneous stream power and cumulative energy expenditure. The relationship between the two variables used for computing cross-sectional stream power, i.e., peak discharge and energy line gradient and basin were analysed. The upper limit for the relationship between peak discharge and drainage area for the seven studied flash floods was represented by a continuous power-law function with an exponent of 0.8 (Fig. 4.6A), contrary to the value of 0.6 generally reported for this regression (e.g., Castellarin, 2007; Gaume at al., 2009). The results were essentially influenced by the high peak discharges in large basins of the Cedrino-Posada River. On the contrary, the exponent of the power function of the upper limit for the relationship between energy gradient and drainage area decreased at a slow rate for drainage areas less than 100 km^2 and a sharp decrease for larger drainage areas (Fig. 4.6B) defined by Mediterranean catchments (Cedrino-Posada, and Argens). This break point (100 km^2) also defines the two contrasting

upper limits for the envelope curve for the relationship between cross-sectional stream power and drainage area (Fig. 4.7A).

The studied flash floods are usually characterized by very high values of unit stream power, which in 88% of the considered cross sections exceeds the Miller-Magilligan value of 300 W m^{-2} indicated by Miller (1990) and referred to in other studies (Magilligan, 1992; Nanson and Croke, 1992) as the minimum threshold for major erosion. This could indicate severe flood and geomorphic responses, as observed for most the studied channels. Surveyed post-flood channel width was used for unit stream power assessment because it was possible to carefully measure it in the field and it is consistent with topographic and hydraulic variables related to peak discharge computation, whereas pre-flood channel width was not known in several of the studied cross sections for the floods. Possible problems in the use of post-flood width for channel cross sections where significant widening has occurred during the flood must be mentioned. Since channel widening may occur, entirely or in part, during the recession phase of the flood, post-flood channel width may underestimate the maximum value of unit stream power. Moreover, in cross sections affected by relevant widening, the estimation of peak discharge is affected by major uncertainties. These phenomena are reflected in the results of this study. High values of unit stream power were observed in bedrock and artificially-reinforced channels, where erosion-resistant channel boundaries maximize stream power with no channel adjustment to accommodate increasing rate of discharge. Also, cross sections that underwent significant geomorphic changes were associated with high observational uncertainty in indirect peak discharge estimation (Amponsah et al., 2016).

Within each flood, the variability of stream power is controlled by hydrologic and topographic factors. The catchments in the sectors most severely hit by the flood obviously feature high peak discharge and high stream power, whereas the nonlinear change in channel slope with increasing drainage area contributes to attenuating the increase of cross-sectional stream power. Local topographic conditions may alter these general patterns. Log-quadratic interpolation (Lecce, 1997) has proved capable of interpreting the curvilinear variation of unit stream power with catchment area, but the variance explained by the regression equation is generally low (Fig. 4.8). Differently from the data analysed by Lecce (1997), which derived from bankfull discharge at different cross sections along the same channels, the database for this study mainly consists of data collected in different catchments for

each flash flood. The variability in geo-lithological conditions among different catchments, which is usually higher than between different parts of the same catchment, also increases the variability of stream power, causing its weaker correlation with drainage area. Moreover, data analysed in this study relate to flash floods, which are characterized by strong spatial variation in rainfall rate and hence in the intensity of flood response, even between adjacent catchments. This factor also causes the variability of stream power to be higher than the one resulting for downstream variation at bankfull discharge. A further factor that may influence the relationships between unit stream power and catchment area is the cross-sectional widening caused by the flood. As discussed above, the use of post-flood channel width may have caused underestimation of maximum value of unit stream power in the cross sections where channel widening occurred. In the plot of unit stream power against drainage area, this leads to values of stream power lower than those observed in catchments of similar size for cross sections that did not feature relevant morphological changes. The drainage basin area at which unit stream power shows the highest values varies between the studied floods and is apparently controlled by the area hit by the flood, with Mediterranean flash floods featuring the largest drainage areas. This result could partly be influenced by the choice of the sample of studied catchments, especially regarding the selection of the river sections that drain the largest areas.

Costa and O'Connor (1995) and Magilligan et al. (2015) have stressed the importance of flow duration as a measure of the distribution of stream power throughout a flood hydrograph, in combination with maximum flow rate, for determining the geomorphic effectiveness of floods. In this study, the integrated hydrologic flash flood analysis has permitted us to extend the assessment of peak stream power to modelling the characteristic stream power hydrograph at the 59 surveyed cross sections of the four recent flash floods in Italy (Magra, Vizze, Cedrino-Posada, and Lierza). Uncertainty assessment for the field estimation of cross-sectional stream power yielded percentage standard errors of ±16.8%, ±25.3% and ±38.4% for cross sections that showed negligible, moderate and major geomorphic effects, respectively, essentially influenced by the uncertainties in the estimation of peak discharge through post-flood surveys. Also, percentage standard errors for the estimations of unit stream power were ±17.3%, ±28.0% and ±43.3% for cross sections that showed negligible, moderate and major geomorphic effects, respectively. The increase in percentage standard errors between cross-sectional stream power and unit stream power can be attributed to the potential

discrepancy between the measured channel width used in the estimation of peak unit stream power and the actual channel width at the time of flood peak. The uncertainty assessment provided a framework to extend field-estimated stream power values to modelling the flow magnitude and duration for the cross sections.

Cumulative energy expenditure above the Miller-Magilligan threshold and the corresponding flow duration relate in a log-linear regression to unit stream power, whereas the overall energy expenditure accumulation and the corresponding proportion above the threshold relate in a log-quadratic function to unit stream power. Comprehensive geomorphic reconnaissance in these channels also permitted adequate qualitative evaluation of the channel materials and the intensity of the geomorphic impacts. Mediterranean flash floods (Argens, Magra, and Cedrino–Posada), in addition to high peak discharge, also feature longer duration than flash floods studied in the other considered regions, so they meet both favourable conditions to cause significant landform changes (Costa and O'Connor, 1995). The coupled influences of low peak discharges and flow duration in the main Vizze channel resulted in the lowest values of the various measures of stream power and energy expenditure in the studied database and corresponding minimal geomorphic effects. However, the steep-gradient small tributaries of the Vizze River were associated with intense channelized debris flows essentially influenced by the availability of mobilisable bed materials.

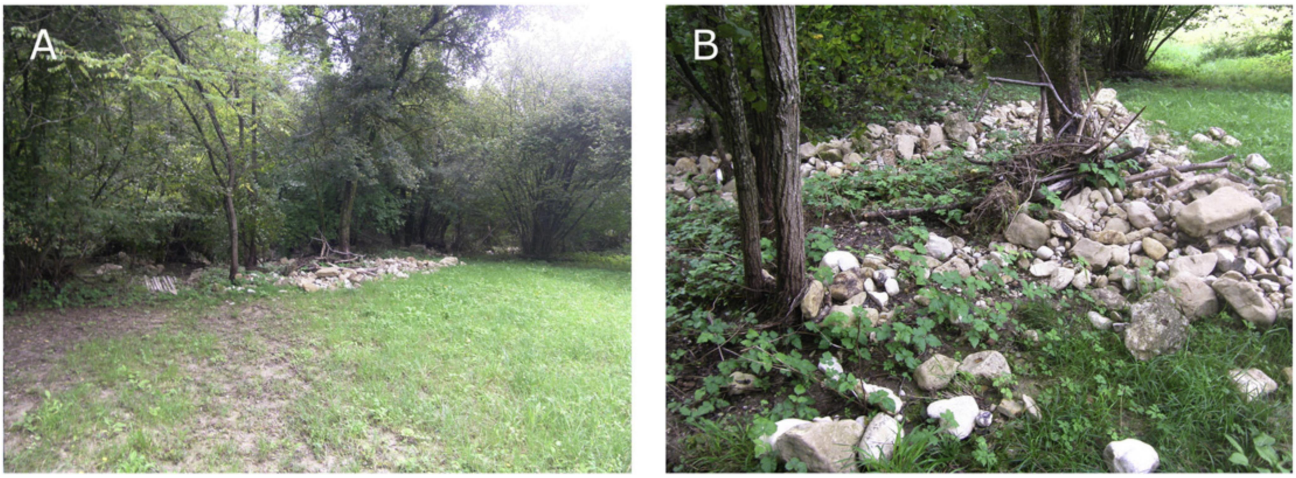

FIG.5.1. Overbank gravel and cobble deposits along the Lierza Creek. (A) Travelled path (muddy marks on the grass and elongated deposit), and (B) detail of the deposit (*Adapted from Marchi et al., 2016*).

The flash flood in the small catchment of the Lierza, caused by a rainstorm that lasted only 1.5 h, lies at the opposite end of the flood duration range. The limited channel erosion observed in semi-alluvial cross sections of the Lierza, in spite of high values of cross-sectional and unit stream power, is in agreement with the reduced capability of short-duration floods to produce significant channel changes. Field observations in the Lierza, however, showed overbank pebble deposits in channel reaches where undisturbed riparian vegetation reflected the absence of channel widening (Fig. 5.1). Such evidence of intense sediment transport supports the study of Magilligan et al. (2015), which distinguishes sedimentological effects from erosive impacts: in the Lierza, short flood duration (and erosion-resistant cohesive channel banks) prevented significant channel and bank erosion, but readily mobilisable channel bed sediment was entrained and transported.

Evaluation of the various measures of stream power and the corresponding geomorphic impacts provided a context to understand the geomorphic effectiveness of extreme flash floods in different channel reaches. High values of stream power measures agree with the occurrence of relevant erosion in most alluvial cross sections. However, other alluvial and semi-alluvial cross sections show minor erosion, or even lack evidence of erosion in some semi-alluvial cross sections (Table 4.4). This can be mainly attributed to local conditions (e.g., bank cohesion) that increased the resistance of channel banks to erosion or to effects of flood duration that reduced the geomorphic effectiveness of streamflow, particularly in the case of the Lierza flood. The rather loose correspondence between the stream power measures and channel erosion for the studied cross sections confirms its limited suitability as an index of geomorphic action of floods at specific locations (e.g., Miller, 1990). Buraas et al. (2014) demonstrated the effectiveness of parameters related to the stress in bends in assessing channel reaches susceptible to widening. The cross sections analysed in this study, however, are mostly located in straight channel reaches, which provide the best conditions for indirect peak discharge estimation by means of the slope-conveyance method (Gaume and Borga, 2008): this limits the suitability of the stress on bend metric developed by Buraas et al. (2014) in this study, which better applies to more complex reach geometries.

Closer relationships between the stream power measures and geomorphic changes in channels were identified at the channel reach scale. For instance, Krapesch et al. (2011) found that unit stream power computed on pre-flood channel width satisfactorily predicted channel widening caused by

catastrophic floods in gravel bed rivers of Austria. Working at the reach scale permits avoiding, or at least averaging, the effects of local conditions that may affect stream power values and the geomorphic effects of the flood (Krapesch et al., 2011; Parker et al., 2014; Nardi and Rinaldi, 2015). In turn, analysis at the cross-sectional scale for which discharge data are available, although potentially prone to bias in stream power computation because of local conditions, has the advantage of relying on detailed observations of water level and cross-sectional geometry, derived from either streamflow gauging or, as in the case of this study, a combined analysis of post-flood observations and hydrological modelling. Cross-sectional scale enables an overview of stream power variability between different catchments in which field analysis at the channel reach scale could be difficult because of logistic and economic constraints. Moreover, the assessment of discharge and stream power at selected channel cross sections may serve to 'anchor' the analysis of stream power and geomorphic response at the channel reach scale to specific sites where detailed measurements and hydraulic estimates have been conducted.

The differences in the stream power measures observed between the studied flash floods can be mainly ascribed to different flood intensity, which is higher in Mediterranean regions as noted in previous studies (Gaume et al., 2009; Marchi et al., 2010), whereas geomorphic responses are partly attributed to the geomorphic controls on channel geometry and sediment characteristics. Unit stream power values in several cross sections of the studied channels exceed the values of 212–2134 W m^{-2}, reported by Grodek et al. (2012) for an extreme flash flood that caused intense channel erosion in small streams of the Mediterranean climatic region of Israel. Also, cumulative energy expenditure in several of the studied channels exceed the values 13.5–16 MJ m^{-2} reported by Magilligan et al. (2015) for extreme geomorphic response associated with the tropical storm Irene in the Saxton and Williams Rivers in the north-eastern United States. Costa and O'Connor (1995) reported a range of unit stream power (4,000–90,000 W m^{-2}) and cumulative energy expenditure (4–220,000 MJ m^{-2}) for extreme geomorphic impacts in selected river basins in the United States. The extreme geomorphic impacts were influenced by the combined influences of adequate flow duration and high magnitude peak unit stream power (flood type B in Fig. 1.4) compared to river basins with small geomorphic impacts (flood types A and C). The energy expenditure values reported for the Magra and Cedrino-Posada, which were associated with significant geomorphic impacts, are higher than that reported for major

geomorphic effects produced by the tropical storm Irene in the Saxtons and Williams Rivers in the north-eastern United States (Magilligan et al., 2015) and that reported for maximum annual floods in the monsoon-fed Narmada River in central India, which have been observed to be significant hydrologic and geomorphic events in the basin (Kale, 2008). The Magra and Cedrino-Posada floods exhibited similar patterns with high peak unit stream power, long duration and cumulative energy expenditure (Table 4.3), producing high-impact geomorphic effects compared to the Lierza and Vizze floods. This points out that the geomorphic effectiveness of floods should exclusively focus on place- and time -specific hydrologic and geomorphic settings (Phillips, 2002). In this study, the observational and modelling capabilities to extend the magnitude of peak instantaneous flow parameters (discharge, velocity, shear stress and stream power) to include flow duration and cumulative energy expenditure have provided a comprehensive assessment of dominant energy expenditure measures. However, the association between these driving forces and the resulting geomorphic effectiveness still remains somewhat vague and non-deterministic. This can partly be attributed to the qualitative assessment and evaluation of geomorphic effects, which were potentially affected by subjectivity, particularly the distinctions between major and moderate geomorphic impacts.

5.3 Downstream Variation in Stream Power

The downstream variation in stream power has been modelled to explore the pattern of energy expenditure along the longitudinal profile of rivers (e.g., Lawler, 1992: 1995; Lecce, 1997; Knighton, 1999; Reinfelds et al., 2004; Barker et al., 2009). Such studies depend on the ability to determine the downstream trends of peak discharge and channel gradient, the two main variables required for the computation of cross-sectional stream power. Most of these studies have focused on the estimation of bankfull or near-bankfull discharges and channel gradient based on field measurements at selected cross-sections, as well as the use of area-discharge relations (e.g., Fonstad, 2003). These provide a framework to investigate a detailed spatial behaviour of stream power and the form and dynamics of river systems. Peak discharges generally have power functions whereas channel gradients have exponential form along river channels. Reinfelds et al. (2004) demonstrated how coupled DEM-based channel gradient through GIS analyses and catchment area based discharge estimation techniques

provide a relatively simple means of modelling the contiguous downstream variations in stream power. Barker et al. (2009) also used the combined automated flood, elevation and stream power (CAFES) novel methodology to quantify downstream change in stream power for two-year flood discharges. Barker et al. (2009) advocated extending the CAFES approach to higher magnitude floods. However, the high space-time variability of extreme flash flood-triggered rainstorms implies that flood intensities and responses may vary even along the same river channel. Stream power values may thus show similar high variations that depend on geological controls on channel geometry and sediment characteristics, as well as on the variations of flood intensity, which require more sophisticated integrated hydrologic and geomorphic approaches.

The integrated hydrologic flash flood analysis implemented for the study of the Magra flood (Amponsah et al., 2016), Cedrino-Posada flood (Amponsah et al., 2017) and Lierza flood (Destro et al., 2016) permitted comprehensive modelling and assessment of the flow magnitude and duration along the eight selected rivers (Pogliaschina, Gravegnola, Mangiola, Osca, Geriola, Posada, Mannu di Bitti, and Lierza). Empirical modelling of the downstream trends of peak discharges were better represented by power-law functions of the cumulative downstream length (Fig. 4.14). Peak discharges along the studied tributaries showed a systemic downstream increase. An interesting observation along the Gravegnola and Posada channels was the contributions of large tributaries, which led to two separate empirical models each. The Mannu di Bitti channel, in particular, contributes about of the 50% drainage area to the main Posada channel. The relatively low explained variances ($R^2 < 0.9$) for the empirical interpretation of peak discharges along the Mangiola and Mannu di Bitti compared to the other studied channels, were due to a series of closely spaced tributaries that were not large enough to cause a significant jump in peak discharge as observed for the Gravegnola and Posada channels (Fig. 4.14). The contributions of series of tributaries along the channel networks could mean that downstream changes in peak discharges more likely correlate strongly with the upstream drainage area scaling variable than the cumulative distance downstream (Barker et al., 2009).

DEM-derived channel gradient showed high downstream variability for the longitudinal profile of the studied channels. The regressions were represented by exponential (Fig. 4.15) and quadratic (Fig. 4.16) functions, with the latter generally performing better in most cases. Contrary to the usual exponential function used in literature (Knighton, 1999; Reinfelds et al., 2004; Barker et al., 2009),

which shows systematic downstream decay in channel gradient, the quadratic function shows more flexibility to capture the striking downstream variability in channel gradient as a result of geological controls in some sections along the river channel. For instance, the high variability in the downstream trend of channel gradient along the Mangiola and Mannu di Bitti channels was better interpreted with curvilinear quadratic functions compared to exponential functions, with explained variances increasing from 0.06 and 0.15 to 0.24 and 0.33, respectively. This high downstream variability is primarily attributed to geo-lithological controls on channel geometry that produce the striking downstream differences in morphology in mountain river systems (Knighton, 1999). The alternating morphology of the sub reaches along the studied river channels (Surian et al., 2016; Righini et al., 2017) particularly contributes to high downstream variability of channel gradient. The use of DEMs for the estimation of channel gradient may partly be responsible for errors in the estimation, but this should be minimised considering the high resolution of the DEM used (5–10 m) relative to the length of the channel reaches (100–1000 m). Also, the 'horizontal slice' method used to extract the DEM-based channel gradient has been extensively used in literature (e.g., Knighton, 1999; Jain et al., 2006), as well as verified using field-measured slopes (Vocal Ferencevic and Ashmore, 2012).

The downstream variations in cross-sectional stream power and unit stream power were estimated using simulated peak discharges and DEM-derived channel gradient. The empirical power-law function for the downstream trend of peak discharges and exponential/quadratic functions for channel gradient resulted in two modelled downstream variations in stream power. The performance of the empirical models for the downstream variations in stream power was assessed using the Nash-Sutcliffe model efficiency scores (Figs. 4.17 and 4.18). Generally, empirical model 2, which was derived from a downstream power-law function of peak discharge and a quadratic function of the downstream trend of channel gradient, showed closer agreement with the estimated downstream variations in stream power than model 1 (with exponential function of channel gradient). For the downstream variations in cross-sectional stream power (Fig. 4.17), model 2 showed significant improvement for the empirical interpretation for the Gravegnola, Osca, Mannu di Bitti, and Lierza channels, whereas model 1 was better for the Geriola and Posada channels. Both models were not significant to interpret the observed downstream variations of cross-sectional stream power for Pogliaschina and Mangiola. For unit stream power (Fig. 4.18), model 2 was significant to interpret the downstream variations for the Gravegnola,

Mangiola, Mannu di Bitti, and Lierza channels, whereas model 1 was better for only the Geriola channel. Both models were significant to interpret the observed downstream variations of unit stream power for Osca and Posada, whereas they were both not significant for Pogliaschina. This indicates that quadratic functions better interpreted the high downstream variability in channel gradient of the studied channels compared to the exponential functions usually implemented for interpreting this kind of regression (Lawler, 1992: 1995; Lecce, 1997; Knighton, 1999; Reinfelds et al., 2004; Barker et al., 2009).

The estimated trends for both cross-sectional and unit stream power (Figs. 4.17 and 4.18) vary nonlinearly downstream, with peaks at mid or lower basins. These results are in line with other results reported in literature (Lawler, 1992, 1995; Lecce, 1997; Barker et a., 2009), whereas the modelled trends generally follow a simple monotonic downstream increase or decrease in stream power (Graf, 1983; Knighton, 1984). The estimated trends for both cross-sectional and unit stream power peaked at about 5-50% of the total stream length within the headwaters for the studied channels. This can be compared to similar trends reported by Lecce (1995) and Knighton (1999), who both reported locations for maximum cross-sectional stream power within 50% of the total stream length. Maximum values for unit stream power occurred at the same location as the peak cross-sectional stream power for Mangiola, Geriola, Posada, and Mannu di Bitti, whereas for Pogliaschina and Lierza, maximum values of unit stream power occurred at the most downstream locations. Similar to results from Lecce (1995), unit stream power for the Osca channel peaked at about halfway between the headwaters and the location of maximum cross-sectional stream power, whereas the opposite was observed for Gravegnola channel. Knighton (1999) proposed an estimate of the location of maximum stream power as the ratio between the downstream rates of change of discharge and slope from the power-law and exponential functions, respectively (Figs. 4.14 and 4.15). These locations for maximum stream power were not absolute for the studied channels but a close estimate. It should be noted that the trends reported in Figs. 4.17 and 4.18 show no specific location of distinct high spikes in stream power. These results supports the assertion by Lecce (1997) that downstream changes in stream power are likely to vary considerably even between streams within a single watershed, partly because of different patterns of flow addition but largely because of variations in channel gradient at the profile and local scales. The high

downstream variability in stream power is responsible for the intricate erosional and depositional landforms usually observed after extreme floods (Wohl et al., 2001).

5.4 Channel Widening and Controlling Factors

The analysis of channel widening caused by bank erosion predominantly focus on hydraulic controls, especially the excess bank shear relative to bank cohesiveness (Hooke, 1979; Lawler, 1993; Julian and Torres, 2006), but Surian et al. (2016) demonstrated that hydraulic controls alone are not adequate to explain channel widening. The disparity between the hydraulic forces and the resulting geomorphic effects also suggests that floods of similar magnitude can result in diverse impacts at a site over time as well as between sites (Hooke, 2015), highlighting the fact that not all extreme floods generate major geomorphic effects (Wolman and Gerson, 1978; Costa and O'Connor, 1995). This presupposes that other factors such as lateral confinement, channel slope, hillslope sediment supply, and percentage of reach length with artificial structures (Surian et al., 2016) as well as the role of flow duration (Costa and O'Connor, 1995; Magilligan et al., 2015) are required to quantify bank erosion and channel widening. Flow duration, in particular, adds an important dimension (i.e., the combined influences of flood-flow duration and cumulative energy expenditure) to stream power measures, which may be important to explain why floods with lower values of peak instantaneous discharges, shear stress and/or stream power can have significant geomorphic impact in some alluvial channels than floods with larger instantaneous peak values (e.g., Miller, 1990), though ultimately the magnitude of geomorphic impacts of extreme floods hinges on the initial channel conditions (Wohl et al., 2001). Flow duration have significant effects on bank saturation, which fundamentally increases pore water pressure and subsequently reduces bank shear strength. Soil saturation further plays a key role in channel bank failure and erosion by increasing the unit weight of the channel bank material (e.g., Thorne, 1982; Springer et al., 1985; Rinaldi and Darby, 2007; Marchi et al., 2009a).

The availability of high-resolution pre- and post-flood satellite images enabled a comprehensive assessment of potential channel widening for seven channels of the Magra and Posada Rivers. This was represented by width ratio (the ratio of channel width after the flood to channel width before the flood). The combined influences of high peak discharges and relatively long flood flow duration (10 – 16

hours) ensured significant widespread channel bank failure and erosion along the selected channels of tributaries of the Magra river and Posada Rivers. Such spatial data were not available for Lierza Creek, where aerial views of the narrow channel reaches were partially, and in some cases completely, covered by vegetation along the banks. It should be recalled that the rate of channel changes along Lierza Creek were mostly insignificant for the August 2, 2014 flash flood. As discussed in the previous sections, the Lierza flood was associated with limited channel erosion in mostly semi-alluvial reaches but intense sediment transport (Fig. 5.1). This was mainly attributed erosion-resistant cohesive channel banks coupled with short flood duration. Also, the short duration of the Lierza flood supports the findings by Magilligan et al. (2015), in that short duration floods cause intense sediment transport rather than erosive impacts. The downstream trends of channel widening follows almost similar variations in unit stream power and cumulative energy expenditure as observed for the Pogliaschina, Gravegnola, Mangiola, Osca, Geriola, Mannu di Bitti and Lierza Rivers (Fig. 4.20 and 4.21). An interesting observation is the generally lower unit stream power and cumulative energy expenditure measures and the resulting relatively lower width ratio in the most downstream sections of the studied channels. This was attributed to initially wider downstream reaches, which implies relatively minimum unit stream power and limited widening. However, this is not observed for the most downstream point of the Pogliaschina channel, where both stream power and width ratio are higher. This is because the most downstream section of the Pogliaschina River was not included in this study due to the complexity of the channel network with a series of significant tributaries joining and channel lining in an urban area close to the catchment outlet. It should be remembered that pre-flood channel width was used to calculate unit stream power, following the finding that unit stream power computed with channel width before a flood generally better predicts channel widening compared to the use of post-flood channel width (Krapesch et al., 2011; Surian et al., 2016). These studies also contributed to the main assumption for the estimation of the cumulative energy expenditure, where pre-flood channel width was used to calculate unit stream power for the rising limb of the flood hydrograph through the peak instantaneous value and post-flood channel width was used to calculate unit stream power for the recession limb. The underlying assumption is that, channel widening occurs in part or in whole during flood recession.

Both unit stream power and cumulative event energy expenditure relates log-linearly to channel width ratio, explaining respectively, 33 and 32% of the variability in channel widening (Fig. 4.22A-B). The inclusion of cumulative above-threshold energy expenditure based on the Miller-Magilligan erosional threshold of 300 W m^{-2} and the corresponding energy ratio (i.e., the ratio between above-threshold energy expenditure and energy expenditure) in the analysis has been attempted to improve the quantification of geomorphic effects. The two regressions with width ratio (Fig. 4.22C-D), also interpreted by log-linear functions, with the magnitude performing better than the ratio. Explained variances of 0.25 and 0.15 for above-threshold energy expenditure and energy ratio, respectively, clearly lag the performance of unit stream power and event energy expenditure. This can simply imply that the Miller-Magilligan critical erosional threshold is not an absolute threshold (Magilligan, 1992). The use of erosional thresholds of 200, 400 and 500 W m^{-2} did not prove any more significant than the Miller-Magilligan threshold. The Pearson linear correlation coefficient (Table 4.5) still showed higher performance of the unit stream power and event energy expenditure in explaining the rate of channel widening compared to the use of above-threshold cumulative energy expenditure. Generally, the Pearson efficiency decreased as we moved from thresholds of 200 to 500 W m^{-2}, for the linear relationship between channel width ratio and both above-threshold energy expenditure and energy ratio. This indicates that the total energy expended is equally significant to quantify channel adjustment. These results support conclusions made by Costa and O'Connor (1995, p. 55) that, "*…..quantifying landscape resistance and erosion thresholds will prove to be much more difficult than quantifying the hydraulic forces.*"

Channel adjustment and changes are essentially influenced by the interplay of catchment hydrology, channel gradient and degree of confinement, especially the geo-lithological controls that produce the striking downstream differences in morphology along the longitudinal profile of river channels (Knighton, 1999). Surian et al. (2016) integrated geomorphic and hydraulic factors and demonstrated the weakness of hydraulic variables alone to explain the rate of channel widening associated with the October 25, 2011 Magra flood. Channel confinement index (i.e., ratio between the alluvial plain width and the channel width before the flood) was be the most variable geomorphic parameters to interpret channel widening, among other variables such as channel slope, hillslope sediment supply, and percentage of reach length with artificial structures. For the hydraulic variables,

unit stream power computed with pre-flood channel width was better than cross-sectional stream power and unit stream power computed with post-flood channel width. These results motivated the multiple regression models develop for this study (Table 4.6). The explained variances for the four models range between 0.49 and 0.53, which indicates that a combination of lateral confinement and any of the four stream power variables (unit stream power, event energy expenditure, above-threshold energy expenditure and energy ratio) are significant and can better predict channel widening. It should be noted that confinement index performs better compared to any of the hydraulic variables.

The partition of the dataset into two subsets based on the steepness of the reaches partially includes the influence of channel gradient in the individual models. The models obtained for the moderate sub reaches (< 4%), showed relatively better performance of cumulative energy expenditure in explaining the rate of channel widening compared to peak instantaneous unit stream power (Table 4.7). Interestingly the above-threshold energy expenditure was the best for these sub reaches. In the steep sub reaches (≥ 4%), channel widening occurred mainly through lateral erosion and, as confirmed by field observations, depositional processes were less significant (Surian et al., 2016). In these sub reaches, unit stream power and lateral confinement showed good relationships with the degree of channel widening (i.e., width ratio) compared to the influences of flood flow duration, although significant statistical models were obtained (Table 4.8). This suggests that the magnitude of peak unit stream power can represent the rate of geomorphic response in steep channel reaches. These results suggest that widening at the lower slopes and with less confined channels is a more complex process and that additional factors should be considered to better understand geomorphic response in these reaches. Likely, widening in these cases results from a combination of bar formation and lateral. erosion, with sediment (volumes and size) supplied from landslides and upstream reaches becoming significant. Notable bar formation and channel aggradation were observed in several of these reaches (Rinaldi et al., 2016), and repeated avulsion processes might have occurred during the event in these aggrading sub reaches. As to additional factors, large riparian trees coupled with wood jams could have played a role by occasionally reinforcing banks and, therefore, hampering channel widening. These results suggest that the widening process is essentially controlled by two main factors: flood power and valley confinement.

The severe effects of the flood in the tributaries of Magra and in some reaches of Posada mainly reflected channel dynamics (i.e., bank erosion, bed aggradation, channel avulsion, intense transport of large wood) or inundation processes caused or enhanced by bridge clogging due to large wood. Therefore, in terms of hazard, documenting the type and magnitude of channel response is crucial in identifying controlling factors of such responses and in developing tools to enable channel dynamic predictions (Surian et al., 2016). The weak correlations between the hydraulic forces and the rate of channel widening can partly be attributed to the methodology employed to estimate channel changes. The use of satellite images to estimate the rate of channel widening is potentially subject to biases and uncertainties, particularly since no field data were available for validation. A peculiar uncertainty could relate to digitizing overbank flows as channel bank failure and erosion. This analysis generally supports the conclusions of Buraas et al. (2014), who stated that there is still a general lack in the capability to predict where major geomorphic changes take place during an extreme flood event. Our analysis also supports conclusions by Newson (1980) that geomorphological effectiveness of extreme floods is easier to quantify than to justify.

5.5 General Discussion and Perspectives for Future Research

The effects that flash floods can exert on channel geometry are a central point in this PhD thesis. This issue is of high relevance as flash floods are difficult to predict, monitor, and model, and yet they are sources of major risks on the built environment, especially in mountain areas. The thesis takes advantage of literature data and hard-gained data collected in the field over the past few years in Europe. This thesis focuses specifically on the geomorphic effectiveness of flash floods, and the use of unit stream power and cumulative energy expenditure as empirical predictor of channel changes, especially channel widening. To better understand the geomorphic response of a fluvial system to floods the approach needs to be multidisciplinary (joining hydrology, hydraulics and geomorphology) and also multi-scaled (river reach, network and watershed scales), in order to analyse properly the different factors and processes involved. The work conducted in this thesis combined fieldwork, geomorphological mapping, statistical analysis, hydraulic calculations and hydrological modelling.

Thus, the PhD brings together more traditional methods with very advanced techniques and data is analysed with appropriate statistical tools, in particular, uncertainty is treated appropriately.

Post-flood surveys and analyses at 119 river cross sections affected by seven major flash floods in Europe were used to establish a common archive of flash flood database (Specific Objective 1) and analyse at-a-station stream power and controlling factors (Specific Objective 2). Hydrological modelling and geomorphic impacts assessment at 59 river cross sections affected by four major flash floods in Italy were also used to assess the combined influences of flow duration and cumulative energy expenditure on channel changes (Specific Objective 3). Furthermore, the evaluation of the contiguous downstream trends in the two main variables of stream power (peak discharge and energy gradient) for 8 selected channels affected by three flash floods in the Magra, Posada and Lierza basins were used to provide empirical models of the downstream variations in stream power (Specific Objective 4). Finally, assessment of channel widening through remote sensing for 7 channels affected by two flash floods in the Magra and Posada basins were used to quantify and associate channel changes and the relevant hydraulic and geomorphic controlling factors (Specific Objective 5). In a nut shell, the thesis uses a remarkable dataset, with appropriate statistical tools to analyse and address the research objectives of this intensive work.

The work presented in this thesis has contributed to the flood geomorphology research, with the doctoral candidate authoring and co-authoring several scientific articles in international journals. For instance, post-flood surveys and analysis of these extreme flash floods permitted to evaluate the upper limit of flash flood stream power in Europe (Marchi et al., 2016). The integration of post-flood field surveys, hydraulic analysis and hydrological modelling, taking into accounts the relevant uncertainties permitted a comprehensive reconstruction of the flood event to better understand the hydrometeorological synopsis (Amponsah et al., 2016; 2017). Such event reconstruction provided estimates of the hydraulic forces (peak discharge and stream power), which formed the basis for a proposed integrated approach that uses different methods and types of evidence to provide fundamental information for characterizing and understanding the geomorphic effects of intense flood events (Rinaldi et al., 2016) as well as evaluating the main controlling factors for channel responses to extreme floods (Surian et al., 2016; Righini et al., 2017). Finally, the quantitative assessment of geomorphic effects of extreme floods was integrated with the Event Dynamics Classification (EDC) of

the IDRAIM framework (Rinaldi et al., 2015) to propose practical procedure for predicting the expected channel widening, a guide to river corridor planning and management (Comiti et al., 2016). Thus, the assessment of the hydraulic forces and association with the corresponding geomorphic effectiveness provide fundamental knowledge of flash flood physical processes that could be helpful for practitioners of river management and flood mitigation agencies.

Some insight into the flood energy expenditure and the associated geomorphic impacts can be gained from the results provided above. In general, enormous amount of energy was expended by the studied flash floods and the Miller-Magilligan minimum threshold of critical unit stream power (300 Wm^{-1}) associated with major morphological changes was exceeded in over 88% of the studied cross-sections and in almost all the studied channel reaches along the longitudinal profiles of the selected rivers. Under such hydraulic conditions, it is expected that the flash floods perform a variety of geomorphic impacts including erosion of bed and bank material and transportation of coarse sediments during the extreme events. However, geomorphic effectiveness was limited to qualitative assessment of the intensity of geomorphic impacts at the cross-sectional scale and channel widening at the channel-reach scale. Though peak stream power and cumulative energy expenditure showed some capability (although weak) to explaining the rate of channel modification, several factors could contribute to the scatter of the collected data, especially for channel widening. Results are not always straight forward to interpret, as correlations are rarely very high, the discussion points out some of the intricate factors and physical processes that are responsible for the relatively weak correlation between energy expenditure and the corresponding geomorphic effects associated to extreme floods.

Several questions that were not addressed in this thesis but could be responsible for explaining the large scatter between energy expenditure and the associated geomorphic impacts produced by the studied flash floods need to be discussed. For example, what roles do the type of soil and vegetation growing on the floodplain play on lateral adjustments? Righini et al (2017) demonstrated that lateral erosion and incision are more dominant in alluvial channels compared to boundary resistant channels. Bedrocks cannot substantially widen, incise or shift bed and banks without eroding bedrock (Meshkova et al, 2012). This suggests that the type of soil and bed material can influence the geomorphic effectiveness of even high magnitude floods. Vegetation on the other hand, has several effects on lateral adjustment and the corresponding quantification of channel widening through remote sensing.

The geomorphic effectiveness of extreme floods can be progressive and cascading if impact is focussed on in-channel vegetation and on the channel walls eroding the topsoil and riparian riverside vegetation. Vegetation in forested areas can also make the quantification of channel widening from aerial photos much more difficult compared to urban areas. Secondly, what is the potential influence that the magnitude of previous floods can have on channel adjustment? Ideally, more lateral changes are expected in river basins where no major events occurred over a certain period before the flood under examination. Newson (1980) investigated the geomorphic effectiveness of two successive major floods in mid-Wales within four years, demonstrating the influence of previous flood on the geomorphic impacts of the latter flood. Could this factor play a role in trends of the studied floods and the scatter of the collected data? How to consider this factor in the analysis? Should one consider the time passed from the previous event and the magnitude of that event? How to parameterize this in a synthetic index?

Another question worth discussing relates to vertical changes in channel geometry caused by erosion and deposition during floods. This thesis focussed on lateral changes in cross-sectional geometry but extreme floods are responsible for overall abrupt and major changes in both lateral and vertical directions. Vertical changes are much more difficult to quantify because topographic surveys are required as aerial photos cannot provide straightforwardly this information. Structure for motion (SfM) techniques (Smith et al., 2014) may allow quantification of these changes. Also, DEM of Difference (DoD) techniques (Wheaton et al., 2010; Picco et al., 2013) can be useful provided high-quality pre- and post-flood DEMs are available. Is stream power likely to be a good predictor for vertical changes too? Is armouring a factor that could play a similar role on vertical adjustment that confinement plays with lateral changes? How should human infrastructure be considered in the framework analysis? These open questions are necessary for future research to advance our understanding of floods and their geomorphic effectiveness.

6 CONCLUSIONS

The main findings from this thesis are summarized as follows:

1. A comprehensive flash flood database has been established for seven major flash floods in different hydro-climatic regions of central and southern Europe by means of post-flood surveys and analysis of hydrometeorological data; data collection has involved 119 cross sections draining catchments from 0.5 to 1981 km^2. The database includes a variety of hydraulic and hydro-meteorological variables that describe flood responses and enable computation of stream power. Spatial distribution of the channel hydraulic geometry for the established database is in agreement with the relationships commonly reported in literature. The spatial extent of unit peak discharges shows higher values for recent Mediterranean events, with two basins of the Cedrino-Posada River crossing the upper limit envelope curve developed for flash floods in Europe.
2. The highest values of cross-sectional stream power and unit stream power occur in Mediterranean regions and are mainly ascribed to the large peak discharges that characterize flash floods in these regions. Mediterranean flash floods are also of longer duration than flash floods in alpine and continental regions. Channel slope, which has great importance for local variability of stream power, is not responsible for systematic differences between the study areas. The variability of unit stream power with catchment area has been represented by log-quadratic relations. The values of catchment area corresponding to the maximum values of unit stream power show relevant differences between the studied floods and are linked to the spatial extent of the events. If compared to threshold values reported in the literature, unit stream power in most cross sections is high and able to induce major channel changes.
3. A combined analysis of data from post-flood surveys and hydrological modelling permitted estimation of the cumulative energy expenditure for 59 basins of the four most recent floods in our database. Comprehensive geomorphic reconnaissance at the outlets of these basins also permitted us to qualitatively classify the impacts of geomorphic effects into three classes (major, small-to-moderate, and negligible) and compared with cross-section characteristics (alluvial, semi-alluvial, bedrock, and artificially reinforced cross sections). The results confirm the findings of previous studies regarding the dominant control of cross-section characteristics

on morphological changes, with bedrock and artificially reinforced channel banks undergoing negligible erosion despite high energy expenditure values, and regarding alluvial channels prone to significant widening. The analysis, however, does not display a clear association between stream power measures and the geomorphic effects. This was attributed to the complex controls on channel changes, that cannot be adequately explained only by unit stream power or related indices of energy expenditure. Also the use of post-flood channel width, which may influence unit stream power and cumulative energy expenditure values in channel sections with different geomorphic impacts, may weaken the correspondence between unit stream power and channel changes.

4. Downstream variations in stream power have been modelled for eight selected river channels that were affected by three of the studied flash floods. Hydrological modelling permitted simulation of the contiguous downstream trends of peak discharges, whereas remote sensing was used to extract the corresponding channel gradient from high-resolution DEMs. Downstream variations in peak discharge were better interpreted by power functions, whereas the corresponding channel gradients were interpreted by exponential and quadratic functions, with the latter generally performing better for this study. Exponential downstream variations in channel gradient better explained channels with systematic downstream decays, while quadratic functions better captured the high downstream variability in channel gradients. The performance of the two resulting empirical models for cross-sectional stream power and unit stream power were essentially influenced by channel gradient, with similar high downstream variability.
5. Hydraulic variables alone were not adequate to predict the downstream rates of channel widening, which were digitized from high resolution satellite images, whereas a major role is played by topographic settings, namely the confinement index (the ratio of the alluvial plain width to the channel width before the flood). Integration of lateral channel confinement and stream power variables provided improved predictions of channel widening. Results show that the rate of channel adjustment is primarily influenced by the rate of channel confinement. Regression models indicate that together with lateral confinement, peak instantaneous unit stream power can better predict the degree of channel widening in steep channels, whereas cumulative energy expenditure is a better hydraulic variables for changes in moderate channel

reaches. This study revealed that the hydraulic forces are much easier to quantify than erosional thresholds, whereas geomorphic effectiveness of floods are also easier to quantify than to justify with empirical predictors.

6. The results from this research highlight the geomorphic effectiveness of flash floods, and the use of unit stream power and cumulative energy expenditure as empirical predictor of the type, location and magnitude of geomorphic change. In particular, the questions why similar floods produce significantly different geomorphic results and whether the variation of stream power explains these geomorphic effects have been addressed. A multidisciplinary approach implemented at multi-scales of the river basins highlighted the complex processes that determine the association between energy expenditure and the associated geomorphic effectiveness of flash floods. This study has focussed on the physical factors that cause disruption of river channels during floods. Given the broad ecological and social vulnerability to extreme events, and the considerable loss to infrastructure and other domestic and economic damages, the analysis of hydraulic and geomorphological factors, together with the recognition of social impacts and preparedness at all scales, represents a fundamental step to better cope with extreme flash floods

REFERENCES

Amponsah, W., L. Marchi, D. Zoccatelli, G. Boni, M. Cavalli, F. Comiti, S. Crema, A. Lucía, F. Marra, and M. Borga, 2016: Hydrometeorological characterisation of a flash flood associated with major geomorphic effects: Assessment of peak discharge uncertainties and analysis of the runoff response. *J. Hydrometeor.*, **17** (12), 3063-3077.

Amponsah, D. Zoccatelli, W, F. Marra, L. Marchi, S. Crema, M. Niedda, and M. Borga, 2017: Coupling observational and modelling uncertainty in flash flood analysis. *J. Hydrol*. (submitted).

Anagnostou, M.N., J. Kalogiros, E.N. Anagnostou, M. Tarolli, A. Papadopoulos, and M. Borga, 2010: Performance evaluation of high-resolution rainfall estimation by X-band dual polarization radar for flash flood applications in mountainous basins. *J. Hydrol.*, **394** (1–2), 4–16.

Andrews, E.D., 1980: Effective and bankfull discharges of streams in the Yampa River Basin, Colorado and Wyoming. *J. Hydrol.*, **46**, 311-330.

Archer, D.R., F. Leesch, and K. Harwood, 2007: Learning from the extreme River Tyne flood in January 2005. *Water and Environment Journal*, **21** (2), 133–141.

Astori, A., and C. Venturini, 2011: Quarternary evolution of the middle Val di Vizze-Pfitschtal (Vipiteno, BZ, NE Italy–Aurine Alps). *GORTANIA, Geologia, Paloentologia, Palenologia*, **33**, 63-92 (in Italian, abstract in English).

Bagnold, R.A., 1966: An approach to the sediment transport problem from general physics. *USGS Professional Paper*, **422-I**, Washington, DC.

Bagnold, R.A., 1977: Bed load transport by natural rivers. *Water Resource Research*, **13**: 303-312.

Baker, V.R., and G. Pickup, 1987: Flood geomorphology of the Katherine Gorge, Northern Territory, Australia. *Geological Society of America Bulletin*, **98**, 635-646.

Baker, V.R., and J. E. Costa, 1987: Flood power. In: Mayer, L., Nash, D. (Eds.), Catastrophic Flooding. *Allen and Unwin, London*, pp. 1–24.

Baker, V.R., and V.S. Kale, 1998: The role of extreme floods in shaping bedrock channels. Rivers Over Rock: Fluvial Processes in Bedrock Channels. *Geophysics Monograph,* **107**, pp. 153-165.

Barker, D.M, D.M. Lawler, D.W. Knight, D.G. Morris, H.N. Davies, and E.J. Stewart, 2009: Longitudinal distributions of river flood power: the combined automated flood, elevation and stream power (CAFES) methodology. *Earth Surf. Process. Land*, **34**, 280–290.

Barredo, J.I., 2007: Major flood disasters in Europe: 1950–2005. *Natural Hazards*, **42**(1), 125–148.

Baum, R.L., J.W. Godt, and W.Z. Savage, 2010: Estimating the timing and location of shallow rainfall-induced landslides using a model for transient, unsaturated infiltration. *J. Geophys. Res*., **115**, F03013.

Board on Atmospheric Sciences and Climate (BASC), 2005: Flash Flood forecasting over complex terrain, the National Academies Press, http://www.nap.edu/catalog.php?record_id=11128.

Bendix, J., and C.P. Hupp, 2000: Hydrological and geomorphological impacts on riparian plant communities. *Hydro. Process*, **14**: 2977–2990.

Beniston, M., 2009: Trends in joint quantiles of temperature and precipitation in Europe since 1901 and projected for 2100. *Geophysical Research Letters*, **36**, p. L07707.

Berne, A., and W.F. Krajewski, 2013: Radar for hydrology: unfulfilled promise or unrecognized potential? *Advances in Water Resources*, **51**, 357–366.

Berti, M., and A. Simoni, 2005: Experimental evidences and numerical modelling of debris flow initiated by channel runoff. *Landslides*, **2**, 171–182, doi:10.1007/s10346-005-0062-4.

Beven, G., and E.F. Wood, 1983: Catchment geomorphology and the dynamics of runoff contributing areas. Scale Problems in Hydrology. *J. Hydrol.*, **65** (1-3), 139-158.

Blöschl, G., and E. Zehe, 2005: On hydrological predictability. Special Issue: Korea Water resource Association and Japan Society of Hydrology and Water Resources. *Hydrol. Process*. **19** (19), 3923-3929.

Bodoque, J.M., A. Díez-Herrero, M.A. Eguibar, G. Benito, V. Ruiz-Villanueva, and J.A. Ballesteros-Cánovas, 2015: Challenges in paleoflood hydrology applied to risk analysis in mountainous watersheds - A review. *J. Hydrol.*, **529** (P2), 449-467.

Borga, M., 2007: Hydrometeorological data resources and technologies for effective flash flood forecasting. Research plan. *University of Padova*, 130.

Borga, M., E. Gaume, J.D. Creutin, and L. Marchi, 2008: Surveying flash flood response: gauging the ungauged extremes., *Hydrol. Processes*, **22**, 3883–3885.

Borga, M., E.N. Anagnostou, G. Blöschl, and J.D. Creutin, 2010: Flash floods: observations and analysis of hydrometeorological controls, *J. Hydrol*., **394** (1–2) (2010), pp. 1–3.

Borga, M., E.N. Anagnostou, G. Blöschl, and J.D. Creutin, 2011: Flash flood forecasting, warning and risk management: the HYDRATE project. *Environ. Sci. Policy*, **14**, 834–844.

Borga, M., G. Dalla Fontana, and F. Cazorzi, 2002: Analysis of topographic and climatic control on rainfall-triggered shallow landsliding using a quasi-dynamic wetness index. *J. Hydrol.,* **268**, 56-71.

Borga, M., P. Boscolo, F. Zanon, and M. Sangati, 2007: Hydrometeorological Analysis of the 29 August 2003 Flash Flood in the Eastern Italian Alps. *J. Hydrometeor*., **8**, 1049–1067.

Borga, M., M. Stoffel, L. Marchi, F. Marra, and M. Jakob, 2014: Hydrogeomorphic response to extreme rainfall in headwater systems: Flash floods and debris-flows. *J. Hydrol*., **518**, 194-205.

Botter, G., and A. Rinaldo, 2003: Scale effect on geomorphologic and Kinematic dispersion. *Water Resour. Res.* **39** (10), 1286.

Boudevillain, B., G. Delrieu, B. Galabertier, L. Bonnifait, L. Bouilloud, P.E. Kirstetter, and M.L. Mosini, 2011: The Cévennes-Vivarais Mediterranean Hydrometeorological Observatory database. *Water Resources Research*, **47** (7), 2011, W07701.

Bouilloud, L., G. Delrieu, B. Boudevillain, and P.E. Kirstetter, 2010: Radar rainfall estimation in the context of post-event analysis of flash-flood events. *J. Hydrol*. **394** (1): 17-27.

Bouilloud, L., G. Delrieu, B. Boudevillain, M. Borga, and F. Zanon, 2009: Radar rainfall estimation for the post-event analysis of a Slovenian flash-flood case: application of the Mountain Reference Technique at C-band frequency. *Hydrol. Earth Syst. Sci*., **13**, 1349–1360.

Bracken, L.J., and J. Croke, 2007: The concept of hydrological connectivity and its contribution to understanding runoff-dominated geomorphic systems. *Hydrol. Process,* **21**, 1749–1763.

Bracken, L.J., L. Turnbull, J. Wainwright, and P. Bogaart, 2015: Sediment connectivity: a framework for understanding sediment transfer at multiple scales. *Earth Surf. Process. Land,* 40, 177–188.

Brookes, A., and D. Wishart, 2006: Application of a Stream Power Screening Tool: In Wallerstein, N. (lead author) Accounting for Sediment in Rivers: A toolbox of sediment transport and transfer analysis methods and models to support hydromorphologically-sustainable flood risk management in the UK. *FRMRC Research Report.* UR9, 13-24.

Buraas, E.M., C.E. Renshaw, F.J. Magilligan, and W.B. Dade, 2014: Impact of reach geometry on stream channel sensitivity to extreme floods. *Earth Surf. Process. Land,* **39**, 1778–1789.

Buzzi, A.A., S. Davolio, P. Malguzzi, O. Drofa, and D. Mastrangelo, 2014: Heavy rainfall episodes over Liguria in autumn 2011: numerical forecasting experiments. *Nat. Hazards Earth Syst. Sci.,* **14**, 1325–1340.

Castellarin, A., 2007: Probabilistic envelope curves for design flood estimation atungauged sites. Water Resour. Res. **43**, W04406.

Cavalli, M., S. Trevisani, F. Comiti, and L. Marchi, 2013: Geomorphometric assessment of spatial sediment connectivity in small Alpine catchments. Geomorphology, **188**, p. 31–41.

Chang, H.H., 1979: Minimum stream power and river channel patterns. *J. Hydrol*., **41**: 303–327.

Chong, S.E., 1970: The width, depth and velocity of Sungei Kimla, Perak. *Geographica*, **6**, 72-63.

Church, M., and R.I. Ferguson, 2015: Morphodynamics: Rivers beyond steady state. *Water Resour. Res.*, **51**,1883–1897.

Clifford, N.J., 2004: Channel processes and forms. In: Burt TP, Chorley RJ, Cox NJ and Goudie AS (eds) History of the Study of Landforms vol 4. London: the Geological Society of London., Chapter 7.

Coe, J. A., D. A. Kinner, and J. W. Godt, 2008 (a): Initiation conditions for debris flows generated by runoff at Chalk Cliffs, central Colorado. *Geomorphology.* **96** (3–4), 270–297.

Coe, J. A., S. H. Cannon, and P. M. Santi, 2008 (b): Introduction to the special issue on debris flows initiated by runoff, erosion, and sediment entrainment in western North America. *Geomorphology*, **96** (3–4), 247–249.

Collier, C., and N. J. Fox, 2003: Assessing the flooding susceptibility of river catchments to extreme rainfall in the United Kingdom. *International Journal of River Basin Management*. **1** (3), 1–11.

Collier, C., 2007: Flash flood forecasting: What are the limits of predictability? *Quarterly Journal of the Royal Meteorological Society*, **133** (622A), 3–23.

Comiti, F., M. Righini, L. Nardi, A. Lucìa, W. Amponsah, M. Borga, M. Cavalli, L. Marchi, M. Rinaldi, and N. Surian, 2016: Channel widening during extreme floods: how to integrate it within river corridor planning. Hazard and Risk Assessment (Analysis, Evaluation). *Conference Proceedings, 13th Congress INTERPRAEVENT 2016, Lucerne, Switzerland*, p. 477–486.

Costa, J.E., 1987: A comparison of the largest rainfall–runoff floods in the United States with those of the People's Republic of China and the World. *J. Hydrol.*, **69**, 101–115.

Costa, J.E., and R.D. Jarrett, 1981: Debris flows in small mountain stream channels of Colorado and their hydrologic implications. *Association of Engineering Geologists Bulletin*, **14**, 309-322.

Costa, J.E., and R.D. Jarrett, 2008: An evaluation of selected extraordinary floods in the United States reported by the U.S. Geological Survey and implications for future advancement of flood science: *U.S. Geological Survey Scientific Investigations Report* 2008-5164, 232 p.

Costa, J.E., and J.E. O'Connor, 1995: Geomorphically effective floods. Natural and Anthropogenic Influences in Fluvial Geomorphology. *Geophysical Monograph*, **89**, 45-56.

Creutin, J.D., and M. Borga, 2003: Radar hydrology modifies the monitoring of flash flood hazard. *Hydrol. Process* **17** (7): 1453–1456.

Da Ros, D. and M. Borga, 1997: Use of digital elevation model data for the derivation of the geomorphologic instantaneous unit hydrograph. *Hydrol. Process*, **11**, 13–33.

Dalrymple, J.B., R.J. Blong, and A.J. Conacher, 1968: A hypothetical nine-unit landsurface model. *Zeitschriftfür Geomorphologie NF* **12**, 60–76.

Davolio, S., A. Buzzi, and P. Malguzzi, 2006: Orographic influence on deep convention: case study and sensitivity experiments. *Meteorologische Zeitschrift* **15** (2), 215–223.

De Waele, J., M.L.V. Martina, L. Sanna, S. Cabras, and Q.A. Cossu, 2010: Flash flood hydrology in karstic terrain: Flumineddu Canyon, central-east Sardinia. *Geomorphology*, **120**, 162–173.

Delrieu, G., V. Ducrocq, E. Gaume, J. Nicol, O. Payrastre, E. Yates, P.E. Kirstetter, H. Andrieu, P.A. Ayral, C. Bouvier, J.D. Creutin, M. Livet, A. Anquetin, M. Lang, L. Neppel, C. Obled, J. Parent-du-Chatelet, G.M. Saulnier, A. Walpersdorf, and W. Wobrock, 2005: The catastrophic flash-flood event of 8–9 September 2002 in the Gard region, France: a first case study for the Ce'vennes–Vivarais Mediterranean Hydrometeorological Observatory. *J. Hydrometeor*., **6**, 34–52.

Destro, E., L. Marchi, W. Amponsah, P. Tarolli, S. Crema, D. Zoccatelli, F. Marra, and, M. Borga, 2016: Hydrological analysis of the flash flood event of August 2, 2014 in a small basin of the Venetian Prealps. *Quaderni di Idronomia Montana*, in press (in Italian, abstract in English).

Dinale, R., V.W. Verant, M. Borga, and M. Tollardo, 2014: Colate detritiche e piena improvvisa (flash flood) del 4 agosto 2012 in provincia di Bolzano. *Eventi Meteo*, NIMBUS 71-72, in press (in Italian).

Dunne, T., 1978: Field studies of hillslope flow processes. In Hillslope Hydrology, Kirkby M.J. (Ed.), Wiley: Chichester, pp. 227–293.

Dury, G.H., 1976: Discharge prediction, present and former, from channel dimensions. *J. Hydrol*., **30**, 219-245.

DWD, 2006: Deutscher Wetterdienst: KOSTRA-DWD-2000. Starkniederschlagsh¨ohen f¨ur die Bundesrepublik Deutsch- land (1951–2000) – Fortschreibungsbericht, Offenbach am Main, Eigenverlag des Deutschen Wetterdienstes (in German).

Eaton, B.C., M. Church, and R.G. Millar, 2004: Rational regime model of alluvial channel morphology and response. *Earth Surf. Process. Land,* **29**, 511–529.

Efron, B., 1983: Estimating the error rate of a prediction rule: Some improvements on cross-validation. *J. Am. Stat. Assoc.*, **78**, 316 - 331.

European Commission, 2007: Directive 2007/60/EC of the European Parliament and of the Council of 23 October 2007 on the assessment and management of flood risks.

Ferguson, R, 2007: Flow resistance equations for gravel- and boulder-bed streams, *Water Resour. Res*., **43**, W05427.

Fonstad, M.A., 2003: Spatial variation in the power of mountain streams in the Sangre de Cristo Mountains, New Mexico. *Geomorphology*, **55**, 75-96.

Fookes, P.G., and E.M. Lee, 2005: Introduction to Engineering Geomorphology. In: P. G. Fookes, E. M. Lee and G. Milligan (Ed.), Geomorphology for Engineers. Whittles Publishing, Scotland, UK, 1-28.

Foulds, S.A., H.M. Griffiths, M.G. Macklin, and P.A. Brewer, 2014: Geomorphological records of extreme floods and their relationship to decadal-scale climate change. *Geomorphology*, **216**, 193-207.

Fryirs, K., 2013: (Dis)Connectivity in catchment sediment cascades: a fresh look at the sediment delivery problem. *Earth Surf. Process. Land,* **38**, 30–46.

Gaume E., and M. Borga, 2008: Post-flood field investigations in upland catchments after major flash floods: proposal of a methodology and illustrations. *Journal of Flood Risk Management* **1** (4): 175–189.

Gaume, E., 2006: Post flash-flood investigations, methodological note. FLOODsite report T23-06-02. Available from http://www.floodsite.net/html/publications2.asp?documentType=1.

Gaume, E., V., and Co-authors, 2009: A collation of data on European flash floods. *J. Hydrol*., **367**, 70–78.

Germann, U., G. Galli, M. Boscacci, and M. Bolliger, 2006: Radar precipitation measurement in a mountainous region, *Q. J. R. Meteo. Soc*., **132**, 1669-1692.

Giannoni, F., J.A. Smith, Y. Zhang and G. Roth, 2003: Hydrologic modelling of extreme floods using radar rainfall estimates. *Adv. Water Resources*, **26**, 195–200.

Giorgi, F., E.S. Im, E. Coppola, N.S. Diffenbaugh, X.J. Gao, L. Mariotti, and Y. Shi, 2011: Higher Hydroclimatic Intensity with Global Warming. *Journal of Climate*, 24, 5309-5324.

Gires, A., I. Tchiguirinskaia, D. Schertzer, A. Schellart, A. Berne, and S. Lovejoy, 2014: Influence of small scale rainfall variability on standard comparison tools between radar and rain gauge data. *Atmospheric research*, **138**, 125-138.

Gleason, C.J., 2015: Hydraulic geometry of natural rivers: A review and future directions. *Progress in Physical Geography*, 1–24.

Godt, J.W., and J.A. Coe, 2007: Alpine debris flows triggered by a 28 July 1999 thunderstorm in the central Front Range, Colorado. *Geomorphology,* 84, 80–97.

Grant, G.E., J.E. O'Connor, and M.G. Wolman, 2013: A river runs through It Conceptual models in fluvial geomorphology. In: Shroder, J. (Editor in Chief), Wohl, E. (Ed.), Treatise on Geomorphology. Academic Press, San Diego, CA, vol. 9, Fluvial Geomorphology, pp. 6–21.

Gregoretti, C. and G. Dalla Fontana, 2008: The triggering of debris flow due to channel-bed failure in some alpine headwater basins of the Dolomites: analyses of critical runoff. *Hydrol. Process*., **22**, 2248–2263.

Grimaldi, S., A. Petroselli, and N. Romano, 2013: Green-Ampt Curve-Number mixed procedure as an empirical tool for rainfall-runoff modelling in small and ungauged basins. *Hydrol. Process*, **27** (8), 253-1264.

Groisman, P.Y., R.W. Knight, D.R. Easterling, T.R. Karl, G.C. Hegerl, and V.N. Razuvaev, 2005: Trends in intense precipitation in the climate record. *Journal of Climate,* **18** (9), 1326–1350.

Groisman, P.Y., R.W. Knight, T.R. Karl, D.R. Easterling, B. Sun, and J. Lawrimore, 2004: Contemporary changes of the hydrological cycle over the contiguous United States: trends. *J. Hydrometeor*. **5** (1), 64–85.

Hack, J.J., and J.C. Goodlett, 1960: Geomorphology and forest ecology of a mountain region in the Central Appalachians, *US Geological Survey Professional Paper*, **347**, 66 pp.

Harvey, A.M., 2001: Coupling between hillslopes and channels in upland fluvial systems: implications for landscape sensitivity, illustrated from the Howgill Fells, northwest England. *Catena* **42**, 225–250.

Hauer, C., and H. Habersack, 2009: Morphodynamics of a 1000-year flood in the Kamp River, Austria, and impacts on floodplain morphology. *Earth Surf. Process. Land,* **34**, 654–682.

Helbing, D., 2013: Globally networked risks and how to respond. *Nature*, **497** (7447), 51–59.
Henderson, F.M., 1966: Open Channel Flow. MacMillan: New York.
Herschy, R.W., and R.W. Fairbridge, 1998: Encyclopedia of Hydrol. and Water Resources. Kluwer, Dordrecht, The Netherlands.
Herschy, R.W., 2002: The world's maximum observed floods. *Flow Measurement and Instrumentation,* **13** (5–6), 231–235.
Hicks, N.S., J.A. Smith, A.J. Miller, and P.A. Nelson. 2005: Catastrophic flooding from an orographic thunderstorm in the central Appalachians. *Water Resour. Res.,* **41**: W12 428.
Hooke, J.M., 1979: Analysis of the processes of river bank erosion. *J. Hydrol*., **42**, 39–62.
Hooke, J.M., 2003: Coarse sediment connectivity in river channel systems: a conceptual framework and methodology. *Geomorphology,* **56**, 79–94.
Hooke, J.M., 2015: Variations in flood magnitude–effect relations and the implications for flood risk assessment and river management. *Geomorphology,* **263**, 19–38.
Huggett, R.J., 2007: Fundamentals of Geomorphology. Routledge Fundamentals of Physical Geography (2nd edition). Taylor and Francis Group. London and New York.
Hungr, O., G.C. Morgan, and R. Kellerhals, 1984: Quantitative analysis of debris torrent hazards for design of remedial measures. *Can. Geotech. J*., **21**, 663-677.
Huntington, T. G., 2006: Evidence for intensification of the global water cycle: review and synthesis. *J. Hydrol.* **319** (1–4), 83–95.
Iida, T., 1999: A stochastic hydro-geomorphological model for shallow landsliding due to rainstorm. *Catena*, **34**, 293–313.
Iida, T., 2004: Theoretical research on the relationship between return period of rainfall and shallow landslides. *Hydrol. Process,* **18**, 739-756.
Ikeda, S., G. Parker, and Y, Kimura, 1988: Stable width and depth of straight gravel rivers with heterogeneous bed materials. *Water Resour. Res.* **24**: 713–722.
Iverson, R.M., 2000: Landslide triggering by rain infiltration. *Water Resour. Res.,* **36**, 1897–1910.
Jain V, N. Preston, K. Fryirs, and G. Brierley, 2006: Comparative assessment of three approaches for deriving stream power plots along long profiles in the upper Hunter River catchment, New South Wales, Australia. *Geomorphology,* **74**: 297–317.
Jarrett, R. D., 1994: Historic flood evaluation and research needs in mountainous areas. In Hydraulic Engineering, Cotroneo GV, Rumer RR (eds). Proceedings of the symposium sponsored by the American Society of Civil Engineers, Buffalo, New York, August 1–5, 1994: American Society of Civil Engineers: New York; 875–879.
Julian, J.P., and R. Torres, 2006: Hydraulic erosion of cohesive riverbanks. *Geomorphology*, **76**, 193–206.
Kale, V.S., 2008: A half-a-century record of annual energy expenditure and geomorphic effectiveness of the monsoon-fed Narmada River, central India. *Catena* **75**, 154–163.
Kaless, G., L. Mao, and M.A. Lenzi, 2014: Regime theories in gravel-bed rivers: models, controlling variables, and applications in disturbed Italian rivers. *Hydrol. Process*. **28**, 2348–2360.
Kirby, W.H., 1987: Linear error analysis of slope-area discharge determinations. In: W.H. Kirby, S.Q. Hua and L.R. Beard (Editors), Analysis of Extraordinary Flood Events. *J. Hydrol*., **96**, 125-138.
Kirchner, J.W., R.C. Finkel, C.S. Riebe, D.E. Granger, J.L. Clayton, J.G. King, and W.F. Megahan, 2001: Mountain erosion over 10 yr, 10 k.y., and 10 m.y. time scales. *Geology*, **29** (7), 591-594.
Knighton, AD., 1984: Fluvial Forms and Processes, 1st edn. Arnold:London.
Knighton, A.D., 1999: Downstream variation in stream power. *Geomorphology,* **29**, 293-306.
Komac, B., K. Natek, and M. Zorn, 2008: Geografski vidiki poplav v Sloveniji. *Geografija Slovenije,* **20**, 76–79. (in Slovenian).
Krajewski, W.F., and J.A. Smith, 2002: Radar hydrology: rainfall estimation. *Advances in Water Resources* **25**(8-12), 1387-1394.

Krapesch, G., C. Hauer, and H. Habersack, 2011: Scale orientated analysis of river width changes due to extreme flood hazards. *Nat. Hazards Earth Syst. Sci*., **11**, 2137-2147.

Lane, S.N., V. Tayefi, S.C. Reid, D. Yu, and R.J. Hardy, 2007: Interactions between sediment delivery, channel change, climate change and flood risk in a temperate upland environment. *Earth Surf. Process. Land,* **32**, 429-446.

Lanni, C., M. Borga, R. Rigon, and P. Tarolli, 2012: Modelling shallow landslide susceptibility by means of a subsurface flow path connectivity index and estimates of soil depth spatial distribution. *Hydrology and Earth System Sciences*, **16**, 3959-3971.

Larsen, I.J., J.L. Pederson, C. John, and J.C. Schmidt, 2006: Geologic versus wildfire controls on hillslope processes and debris flow initiation in the Green River canyons of Dinosaur National Monument. *Geomorphology*, **81**, 114–127.

Lawler, D.M., 1992: Process dominance in bank erosion systems. In Carling, P.A. & Petts, G.E. (Eds), Lowland Floodplain Rivers: Geomorphological Perspectives, John Wiley, Chichester, 117-143.

Lawler, D.M., 1993: The measurement of river bank erosion and lateral channel change — a review. *Earth Surf. Process. Land.,* **18**, 777–821.

Lawler D.M., J.R. Grove, J.S. Couperthwaite, and G.J.L. Leeks, 1999: Downstream change in river bank erosion rates in the Swale–Ouse system, Northern England*. Hydrol. Process*, **13**, 977–992.

Le Boursicaud, R., L. Pénard, A. Hauet, F. Thollet, and J. Le Coz, 2016: Gauging extreme floods on YouTube: Application of LSPIV to home movies for the post-event determination of stream discharges. *Hydrol. Process*, **30** (1), 90-105.

Lecce, S.A., 1997: Nonlinear downstream changes in stream power on Wisconsin's Blue River. *Annals of the Association of American Geographers*, **87**(3), 471-486.

Lee, E.M., 2005: Rivers. In: P. G. Fookes, E. M. Lee and G. Milligan (Ed.), Geomorphology for Engineers. Whittles Publishing, Scotland, UK, 263-285.

Leopold, L.B., and T. Maddock, 1953: The hydraulic geometry of stream channels and some physiographic implications. *U.S. Geological Survey Professional Paper* **252**, 56 p.

Leopold, L.B., M.G. Wolman and J.P. Miller, 1960: Fluvial Processes in Geomorphology. Textbook of Fluvial Geomorphology. Dover Publications, Inc., New York.

Lucía A., F. Comiti, M. Borga, M. Cavalli, and L. Marchi, 2015: Dynamics of large wood during a flash flood in two mountain catchments. *Natural Hazards and Earth System Sciences Discussion*, **3**, 1643-1680.

Lumbroso, D., and E. Gaume, 2012: Reducing the uncertainty in indirect estimates of extreme flash flood discharges. *J. Hydrol*., **414–415**, 16–30.

Magilligan, F.J., 1992: Thresholds and the spatial variability of flood power during extreme floods. *Geomorphology,* **5**, 373–390.

Magilligan, F.J., E.M. Buraas, and C.E. Renshaw, 2015: The efficacy of stream power and flow duration on geomorphic responses to catastrophic flooding. *Geomorphology*, **228**, 175-188.

Marchi, L., M. Borga, E. Preciso, and E. Gaume, 2010: Characterisation of selected extreme flash floods in Europe and implications for flood risk management. *J. Hydrol*., **394**, 118–133.

Marchi, L., M. Borga, E. Preciso, M. Sangati, E. Gaume, V. Bain, G. Delrieu, L. Bonnifait, and N. Pogan`eik, 2009a: Comprehensive post-event survey of a flash flood in Western Slovenia: observation strategy and lessons learned. *Hydrol. Process*, **23**, 3761– 3770.

Marchi, L., M. Cavalli, M. Sangati and M. Borga, 2009b: Hydrometeorological controls and erosive response of an extreme alpine debris flow. *Hydrol. Process*, **23**(19), 2714–2727.

Marchi, L., M. Cavalli, W. Amponsah, M. Borga and S. Crema, 2016: Upper limits of flash flood stream power in Europe. *Geomorphology*, **272**, 68-77.

Marra, F., E.I. Nikolopoulos, J.D. Creutin, and M. Borga, 2014: Radar rainfall estimation for the identification of debris-flow occurrence thresholds. *J. Hydrol*., **519**, 1607-1619.

Martens B., P. Cabus, I. De Jongh, and N.E.C. Verhoest, 2013: Merging weather radar observations with ground-based measurements of rainfall using an adaptive multiquadric surface fitting algorithm. *J. Hydrol*., **500**, 84-96.

Martin, C., 2010: Les inondations du 15 Juin 2010 dans le centre Var: Reflexion sur un episode exceptionnel. Etudes de Geographie Physique, *Physio-Geo*, **37**, 41–76 (in French).

Meshkova, L.V., P.A. Carling, and T. Buffin-Bélanger, 2012: Nomenclature, Complexity, Semi-alluvial Channels and Sediment-flux-driven Bedrock Erosion, Gravel-bed Rivers Processes, Tools, Environments. Michael Church, Pascale M. Biron &André G. Roy pp. 424-432.

McEwen, L.J., 1994: Channel planform adjustment and stream power variations on the middle River Coe, Western Grampian Highlands, Scotland, *Catena*, **21**, 357-374.

Miller, A.J., 1990: Flood hydrology and geomorphic effectiveness in the central Appalachians. *Earth Surf. Proc. Land*, **15**, 119-134.

Millar, R.G., 2005: Theoretical regime equations for mobile gravel-bed rivers with stable banks. *Geomorphology,* **64**: 207–220.

Milley, P.C.D., R.T. Wetherald, K.A. Dunne, and T.L. Delworth, 2002: Increasing risk of great floods in a changing climate. *Nature*, **415**: 514-517.

Modrick, T.M., and K. P. Georgakakos, 2014: Regional bankfull geometry relationships for southern California mountain streams and hydrologic applications. *Geomorphology,* **221**, 242-260.

Molnar, P., 2013: Network-scale energy distribution. In: Shroder, J. (Editor in chief), Wohl, E. (Ed.), Treatise on Geomorphology. Academic Press, San Diego, CA, vol. 9, Fluvial Geomorphology, pp. 43–49.

Mondini, A.C., A. Viero, M. Cavalli, L. Marchi, G. Herrera, and F. Guzzetti, 2014: Comparison of event landslide inventories: the Pogliaschina catchment test case, Italy. *Nat. Hazards Earth Syst. Sci*., **14**, 1749-1759.

Montgomery, D.R., and J.M. Buffington, 1997: Channel-Reach Morphology in Mountain Drainage Basins. *Bulletin of the Geological Society of America,* **109**, 596-611.

Montgomery, D.R., and W.E. Dietrich, 1994: A physically based model for the topographic control on shallow landsliding. *Water Resour. Res.*, **30**, 1153–1171.

Nanson, G.C., and J.C. Croke, 1992: A genetic classification of floodplains. *Geomorphology* **4**, 459–486.

Nardi, L., and M. Rinaldi, 2015: Spatio-temporal patterns of channel changes in response to a major flood event: the case of the Magra River (central – northern Italy). *Earth Surf Proc Land*, **40**, 326-339.

Nash, I.E., and I.V. Sutcliffe, 1970: River flow forecasting through conceptual models, part I. *J. Hydrol*., **10**, 282–290.

Newson, M., 1980: The geomorphological effectiveness of floods – a contribution simulated by two recent events in mid-Wales. *Earth Surface Processes*, **5**, 1-6.

Nicótina, L.E., E. Alessi Celegon, A. Rinaldo, and M. Marani, 2008: On the impact of rainfall patterns on the hydrologic response. *Water Resour. Res*., **44**, W12401.

Niedda M., W. Amponsah, L. Marchi, D. Zoccatelli, F. Marra, S. Crema, M. Pirastru, R. Marrosu, and M. Borga, 2015: The cyclone Cleopatra of November 18, 2013 in Sardinia, event management, measurement and modelling. *Quaderni di Idronomia Montana*, **32/1**, 47-58 (in Italian, abstract in English).

Norbiato, D., M. Borga, S.D. Esposti, E. Gaume, and S. Anquetin, 2008: Flash flood warning based on rainfall thresholds and soil moisture conditions: An assessment for gauged and ungauged basins. *J. Hydrol*., **362**, 274–290.

O'Connor, J.E., and J.E. Costa, 2004: Spatial distribution of the largest rainfall-runoff floods from basins between 2.6 and 26,000 km^2 in the United States and Puerto Rico. *Water Resources Research*, **40** (1), W01107.

Ogden, F.L., and B. Saghafian, 1997: Green and Ampt infiltration with redistribution. *J.Irrigation and Drainage Engineering-Asce,* **123**(5): 386-393.

Ortega, J.A., and G.G. Heydt, 2009: Geomorphological and sedimentological analysis of flash-flood deposits: the case of the 1997 Rivillas flood Spain. *Geomorphology*, **112**, 1–14.

Pack, R.T., D.G. Tarboton, and C.N. Goodwin, 1998: The SINMAP Approach to Terrain Stability Mapping, 8th Congress of the International Association of Engineering Geology, Vancouver, British Columbia, Canada.

Park, C.C., 1977: World-wide variations in hydraulic geometry exponents of stream channels: An analysis and some observations. *J. Hydrol*., **33**, 133-146.

Parker, G, P.R. Wilcock, C. Paola, W. Dietrich, and J. Pitlick, 2007: Physical basis for Quasi universal relations describing bankfull hydraulic geometry of single-thread gravel bed rivers. *J. Geophysical Research* 112, F04005, doi:10.1029/2006JF000549.

Parker, C., C.R. Thorne, and N.J. Clifford, 2014: Development of ST:REAM: a reach-based stream power balance approach for predicting alluvial river channel adjustment. *Earth Surf. Process. Land,* **40**, 403–413.

Parajka, J., et al., 2013: Prediction of runoff hydrographs in ungauged basins. Chapter 10: In Runoff Prediction in Ungauged Basins: Synthesis across Processes, Places and Scales, ed. G. Blöschl, M. Sivapalan, T. Wagener, A. Viglione and H. G. Savenije. Published by Cambridge University Press.

Payrastre, O., E. Gaume, P. Javelle, B. Janet, P. Fourmigué, Ph. Lefort, A. Martin, B. Boudevillain, P. Brunet, G. Delrieu, L. Marchi, Y. Aubert, E. Dautrey, L. Durand, M. Lang, L. Boissier, J. Douvinet, C. Martin and I. Ruin, 2012: Hydrological analysis of the catastrophic flash flood of 15th June 2010 in the area of Draguignan (Var, France)-TT02D HYMEX. SHF Congress: "River and sea extreme events", Paris, 1-2 February (in French, abstract in English).

Peel, M.C., B.L. Finlayson, and T.A. McMahon, 2007: Updated world map of the Koppen–Geiger climate classification. *Hydrol. Earth Syst. Sci.,* **11** (5), 1633–1644.

Pellarin, T., G. Delrieu, and G.M. Saulner, 2002: Hydrologic visibility of weather radar systems operating in mountainous regions: case study for the Ardeche catchment (France). *J. Hydrometeor*., **3**, 539-555.

Penna, D., H.J. Tromp-van Meerveld, A. Gobbi, M. Borga, and G. Dalla Fontana, 2011: The influence of soil moisture on the threshold runoff generation processes in an alpine headwater catchment. *Hydrol. Earth Syst. Sci.*, **15**, 689 – 702.

Phillips, J.D., 2002: Geomorphic impacts of flash flooding in a forested headwater basin. *J. Hydrol*., **269**, 236-250.

Picco, L., L. Mao, M. Cavalli, E. Buzzi, R. Rainato, and M.A. Lenzi, 2013: Evaluating short-term morphological changes in a gravel-bed braided river using terrestrial laser scanner. *Geomorphology*, **201**, 323-334.

Ponce, V.M., and E.R.H. Hawkins, 1996: Runoff curve number: Has it reached maturity? *J. Hydrol. Eng*., **1**, 11–19.

Prochaska, A.B., P.M. Sant, J.D. Higgins, and S.H. Cannon, 2008: Debris-flow runout predictions based on the average channel slope (ACS). *Eng. Geol*., **98**, 29–40.

Reinfelds, I., T. Cohen, P. Batten, and G. Brierley, 2004: Assessment of downstream trends in channel gradient, total and specific stream power: a GIS approach. *Geomorphology*, **60**, 403-416.

Rhoads, B.L., 1987: Stream power terminology. *Professional Geographer*, **39** (2), 189-195.

Richards, K.S., 1973: Hydraulic geometry and channel roughness-a nonlinear system. *American Journal of Science.* **273**, 877-896.

Richards, K.S., 1976: Complex width-discharge relations in natural river sections. *Geological Society of America Bulletin*, **87**, 199-206.

Righini, M., N. Surian, E.E. Wohl, F. Comiti, W. Amponsah, L. Marchi and M. Borga, 2017: Geomorphic response to an extreme flood in two Mediterranean rivers (northeastern Sardinia, Italy): the role of geomorphic and hydraulic controlling factors. *Geomorphology,* (under revision).

Rinaldi, M., and S.E. Darby, 2007: Modelling river-bank-erosion processes and mass failure mechanisms: progress towards fully coupled simulations. In: Habersack, H., Piégay, H., Rinaldi, M. (Eds.), Developments in Earth Surface Processes. 11. Elsevier, The Netherlands, pp. 213–239.

Rinaldi, M., N. Surian, F. Comiti, and M. Bussettini, 2013: A method for the assessment and analysis of the hydromorphological condition of Italian streams: the Morphological Quality Index (MQI). *Geomorphology*, **180-181**, 96–108.

Rinaldi M., N. Surian, F. Comiti, and M. Bussettini, 2015: A methodological framework for hydromorphological assessment, analysis and monitoring (IDRAIM) aimed at promoting integrated river management. *Geomorphology*, **251**, 122-136.

Rinaldi, M., W. Amponsah, M. Benvenuti, M. Borga, F. Comiti, A.L. Vela, L. Marchi, L. Nardi, M. Righini, and N. Surian, 2016: An integrated approach for investigating geomorphic response to an extreme flood event: the case of the Magra River, Italy. *Earth Surf Proc Land*, **41**, 835–846.

Rodriguez-Iturbe, I., and A. Rinaldo, 1997: Fractal River Basins. Cambridge University Press, 547 pp.

Rosgen, D.L., 1994: A Classification of Natural Rivers. *Catena,* **22**, 169-99.

Rouzeau, M., X. Martin, and J.-C. Pauc, 2010: Retour d'experiencedes inondations survenues dans le departement du Var les 15 et 16 Juin 2010. Inspection Generale de l'Administration Rep.10-070-02, 94 pp (in French).

Ruin, I., and Coauthors, 2014: Social and hydrological responses to extreme precipitations: An interdisciplinary strategy for postflood investigation. *Weather, Climate, and Society*, **6**, 135-153.

Ruiz-Villanueva, V., M. Borga, D. Zoccatelli, L. Marchi, E. Gaume, and U. Ehret, 2012: Extreme flood response to short-duration convective rainfall in South-West Germany. *Hydrol. Earth Syst. Sci*., **16**, 1543–1559.

Rusjan, S, M. Kobold, and M. Mikoš, 2009: Characteristics of the extreme rainfall event and consequent flash floods in W Slovenia in September 2007. *Natural Hazards and Earth System Sciences,* **9** (3): 947–956.

Schumm, S.A., 1977: The Fluvial System. Wiley-Interscience, New York, 338.

Schwanghart, W., and N.J. Kuhn, 2010: TopoToolbox: a set of Matlab functions for topographic analysis. *Environmental Modelling & Software*, **25**, 770-781.

Sidle, R.C., and Y. Onda, 2004: Hydrogeomorphology: overview of an emerging science*. Hydrol. Process.*, **18**, 597–602

Simoni, S., F. Zanotti, G. Bertoldi, and R. Rigon, 2008: Modelling the probability of occurrence of shallow landslides and channelized debris flows using GEOtop-FS. *Hydrol. Process*., **22**, 532–545.

Singh, V.P., 2003: On the theories of hydraulic geometry. *International Journal of Sediment Research*, **18** (3), 196-218.

Sivapalan, M., G. Blöschl, R. Merz, and D. Gutknecht, 2005: Linking flood frequency to long-term water balance: Incorporating effects of seasonality. *Water Resour. Res*., **41** (6), W06012.

Smith, M.W., J.L. Carrivick, J. Hooke, and M.J. Kirkby, 2014: Reconstructing flash flood magnitudes using 'Structure-from-Motion': A rapid assessment tool, *J. Hydrol*., **519**, 1914-1927, ISSN 0022-1694.

Springer, F.M., C.R. Ullrich, and D.J. Hagerty, 1985: Streambank stability. *J. Geotech. Eng*. **111**, 624–640.

Surian, N., M. Righini, A. Lucìa, L. Nardi, W. Amponsah, M. Benvenuti, M. Borga, M. Cavalli, F. Comiti, L. Marchi, M. Rinaldi, and A. Viero, 2016: Channel response to extreme floods: insights on controlling factors from six mountain rivers in northern Apennines, Italy. *Geomorphology*, **272**, 78-91.

Tallaksen, L.M., 1995: A review of baseflow recession analysis. *J. Hydrol.,* **165** (1–4), 349–370.

Tao, J., and A.P. Barros, 2014: Coupled prediction of flood response and debris flow initiation during warm-and cold-season events in the Southern Appalachians, USA. *Hydrol. Earth Syst. Sci.*, **18** (1), 367-388.

Thompson, C., and J. Croke, 2013: Geomorphic effects, flood power, and channel competence of a catastrophic flood in confined and unconfined reaches of the upper Lockyer valley, southeast Queensland, Australia. *Geomorphology*, **197**, 156-169.

Thorne, C.R., 1982: Processes and mechanisms of river bank erosion. In: Hey, R.D., Bathurst, J.C., Thorne, C.R. (Eds.), Gravel-bed Rivers. JohnWiley and Sons, Chichester, pp. 227–271.

Trenberth, K.E., P.D. Jones, P. Ambenje, R. Bojariu, D. Easterling, A. Klein Tank, D. Parker, F. Rahimzadeh, J.A. Renwick, M. Rusticucci, B. Soden, and P. Zhai, 2007: Observations: Surface and Atmospheric Climate Change. In: Climate Change 2007: The Physical Science Basis. Contribution of Working Group I

to the Fourth Assessment Report of the Intergovernmental Panel on Climate Change [Solomon, S., D. Qin, M. Manning, Z. Chen, M. Marquis, K.B. Averyt, M. Tignor and H.L. Miller (eds.)]. Cambridge University Press, Cambridge, United Kingdom and New York, NY, USA.

Vocal Ferencevic, M., and P. Ashmore, 2012: Creating and evaluating digital elevation model-based stream-power map as a Stream Power Assessment Tool. *River Res. Applic.*, **28**, 1394- 1416.

Wainwright, J., A.J. Parsons, J.R. Cooper, P. Gao, J.A. Gillies, L. Mao, J.D. Orford, and P.G. Knight, 2015: The concept of transport capacity in geomorphology. *Reviews of Geophysics*, **53** (4), pp. 1155-1202.

Wheaton, J.M., J. Brasington, S.E. Darby, and D.A. Sear, 2010: Accounting for uncertainty in DEMs from repeat topographic surveys: Improved sediment budgets. *Earth Surf. Proc*, **35** (2), pp. 136-156.

Whipple K.X., G.S. Hancock, and R.S. Anderson, 2000: River incision into bedrock: mechanics and relative efficacy of plucking, abrasion and cavitation. *Geological Society of America Bulletin*, **112**, 490–503.

Williams, G.P., 1983: Paleohydrological methods and some examples from Swedish fluvial environments, I – Cobble and boulder deposits. *Geograf. Annaler*, **65A**, 227-243.

Wohl, E., and A. Wilcox, 2005: Channel geometry of mountain streams in New Zealand. *J. Hydrol*., **300**, 252–266.

Wohl, E.E., D. Cenderelli, and M. Mejia-Navorro, 2001: Channel change from extreme floods in Canyon rivers. In Schumm's volume: Applying Geomorphology to Environmental Management. D.J. Anthony, M.D. Harvey, J.B. Laronne, and M.P. Mosley, eds., Water Resources Publications LLC, Highlands Ranch, CO, pp. 149-174.

Wohl, E., F.L. Ogden, and J. Goode, 2009: Episodic wood loading in a mountainous neotropical watershed. *Geomorphology*, **111** (3-4), 149-159.

Wohl, E., S. Rathburn, S. Chignell, K. Garrett, D.A. Laurel, B. Livers, A. Patton, R. Records, M. Richards, D.M. Schook, N.A. Sutfin, and P. Wegener, 2016: Mapping longitudinal stream connectivity in the North St. Vrain Creek watershed of Colorado, *Geomorphology*, Article in Press, DOI: 10.1016/j.geomorph.2016.05.004

Wolman, M.G., and J.P. Miller, 1960: Magnitude and frequency of forces in geomorphic processes. *J. Geology*, **68**, 54-74.

Wolman, M.G., and R. Gerson, 1978: Relative scales of time and effectiveness of climate in watershed geomorphology. *Earth Surf. Proc*., **3**, 189-208.

Zanon, F., M. Borga, D. Zoccatelli, L. Marchi, E. Gaume, L. Bonnifait, and G. Delrieu, 2010: Hydrological analysis of a flash flood across a climatic and geologic gradient: the September18, 2007 event in Western Slovenia. *J. Hydrol*., **394**, 182–197.

APPENDIX

A1: SELECTED PICTURES DURING POST-FLOOD FIELD SURVEYS OF THE STUDIED FLASH FLOODS

Total station at the Lierza basin

IPEC team for the Cedrino-Posada flood

Field survey in the Magra River

Field survey in the Cedrino River

Field survey in the Vizze River

Field survey in the Lierza River

A2: Dataset of the 119 Surveyed Cross Sections for the Seven Studied Floods

Event	*Code*	*A* [km^2]	Q_p [m^3/s]	*S* [m/m]	A_c [m^2]	*w* [m]	*P* [m]	*R* [m]	*d* [m]	*V* [m/s]	*Fr* [–]	*n* [–]	*Ω* [W/m]	*ω* [W/m^2]
Selška Sora	SS01	2.25	9.0	0.011	6.5	7.0	18.2	0.36	0.93	1.33	0.46	0.040	971	139
	SS02	2.60	7.5	0.011	4.8	6.3	9.9	0.48	0.75	1.62	0.58	0.040	809	128
	SS03	1.93	7	0.020	4.3	4.8	9.7	0.45	0.91	1.24	0.54	0.067	1373	286
	SS04	8.98	40	0.030	11.3	8.0	21.3	0.53	1.41	3.39	0.96	0.033	11772	1472
	SS05	24.72	105	0.020	43.8	38.8	25.0	1.75	1.13	2.13	0.72	0.083	18578	479
	SS06	9.22	100	0.040	23.3	18.0	19.6	1.19	1.29	4.48	1.21	0.050	41375	2299
	SS07	3.87	40	0.060	10.1	13.6	14.2	0.71	0.74	3.90	1.48	0.050	15491	1139
	SS08	40.72	140	0.013	53.4	43.9	44.7	1.19	1.22	3.54	0.76	0.050	16641	379
	SS09	44.84	170	0.014	41.8	24.1	25.9	1.61	1.73	4.02	0.99	0.040	22979	953
	SS10	46.75	200	0.010	69.4	60.0	61.2	1.13	1.16	4.54	0.86	0.040	18227	304
	SS11	9.77	55	0.030	23.3	19.2	20.0	1.25	1.22	3.02	0.68	0.067	15937	830
	SS12	21.42	155	0.020	53.0	28.0	29.6	1.79	1.89	3.16	0.68	0.067	46703	1668
	SS13	4.19	8	0.035	2.9	2.9	4.5	0.65	1.01	2.80	0.86	0.050	4669	1610
	SS14	31.86	100	0.015	39.4	19.7	21.1	1.86	2.00	3.39	0.57	0.067	14974	760
	SS15	80.42	320	0.010	125.5	94.7	96.0	1.31	1.32	4.08	0.71	0.050	29670	313
	SS16	7.46	16	0.050	5.8	5.8	7.8	0.74	1.00	2.75	0.88	0.067	7848	1353
	SS17	95.53	380	0.012	109.0	73.8	78.2	1.39	1.48	4.20	0.92	0.040	35233	477
	SS18	5.68	9	0.020	3.3	2.4	2.6	1.26	1.38	2.48	0.74	0.067	2120	883
	SS19	25.82	43	0.019	14.1	8.2	10.1	1.40	1.72	3.16	0.74	0.050	8015	977
Starzel	SZ01	9.3	9	0.040	3.2	3.1	5.0	0.6	1.0	2.97	0.90	0.050	931	300
	SZ02	53.7	150	0.007	64.7	40.2	41.6	1.6	1.6	3.30	0.58	0.050	14757	367
	SZ03	119.5	125	0.005	49.8	25.5	27.5	1.8	2.0	2.63	0.57	0.040	5623	221
	SZ04	47.5	120	0.007	32.2	13.8	16.5	2.0	2.3	3.53	0.78	0.037	3106	225
	SZ05	87.0	115	0.010	50.7	28.7	29.6	1.7	1.8	2.62	0.54	0.067	55642	1939
	SZ06	1.0	3.7	0.020	2.4	5.7	5.9	0.4	0.4	1.54	0.74	0.050	697	122
	SZ07	1.1	6.4	0.010	4.6	5.9	6.7	0.7	0.8	1.45	0.50	0.050	548	93

Appendix A2 continues

Event	*Code*	*A* [km^2]	Q_p [m^3/s]	*S* [m/m]	A_c [m^2]	*w* [m]	*P* [m]	*R* [m]	*d* [m]	*V* [m/s]	*Fr* [–]	*n* [–]	*Ω* [W/m]	*ω* [W/m^2]
Starzel	SZ08	24.8	20	0.022	6.6	5.8	7.1	0.9	1.1	2.83	0.91	0.050	4291	740
	SZ09	29.9	45	0.024	15.3	14.7	15.5	1.0	1.0	3.83	0.92	0.040	6698	456
	SZ10	30.6	65	0.010	19.0	10.4	11.4	1.7	1.8	3.52	0.81	0.040	6682	642
	SZ11	30.7	80	0.020	24.0	15	18.2	1.3	1.6	3.40	0.84	0.050	15696	1046
	SZ12	36.7	80	0.020	35.0	10	17.0	2.1	3.5	2.29	0.39	0.100	15696	1570
	SZ13	2.2	8	0.025	2.7	1.8	1.8	1.5	1.5	3.11	0.77	0.067	1962	1090
	SZ14	2.1	25	0.025	10.0	7	3.0	3.3	1.4	2.47	0.67	0.143	6131	876
	SZ15	1.8	3	0.020	1.2	1.2	1.4	0.9	1.0	3.19	0.80	0.040	589	491
	SZ16	17.6	20	0.025	6.0	8.5	9.9	0.6	0.7	2.82	1.28	0.040	4905	577
	SZ17	1.9	11	0.030	4.3	5.7	6.3	0.7	0.8	3.35	0.93	0.040	3237	568
Argens	AR01	217	750	0.006	233.6	43.2	47.4	4.93	5.41	3.14	0.43	0.071	47456	1099
	AR02	1646	1200	0.003	377.4	71.3	76.6	4.93	5.41	3.54	0.33	0.077	35316	495
	AR03	1981	2100	0.003	600.8	112.9	121.9	4.93	5.41	3.51	0.34	0.067	61803	547
	AR04	3	10	0.020	5.3	5.4	6.4	0.83	0.99	1.90	0.60	0.067	1962	363
	AR05	6	10	0.020	5.6	5.8	6.8	0.82	0.96	1.90	0.58	0.067	1962	338
	AR06	19	70	0.010	98.6	18.6	20.0	4.93	5.41	3.27	0.69	0.050	556	30
	AR07	35	210	0.010	261.1	51.0	53.0	4.93	5.41	2.98	0.56	0.067	14400	282
	AR08	12	70	0.010	24.0	12.6	13.8	1.75	1.91	2.90	0.67	0.050	6867	545
	AR09	148	350	0.030	88.8	28.4	31.6	2.81	3.13	4.14	0.75	0.083	109323	3847
	AR10	148	350	0.030	84.4	26.7	29.2	2.89	3.16	4.22	0.76	0.083	103005	3861
	AR11	75	200	0.024	56.8	12.0	21.8	2.61	4.75	3.52	0.52	0.083	79598	6661
	AR12	196	400	0.008	114.1	68.1	71.0	1.61	1.68	3.59	0.91	0.033	34570	508
	AR13	3.5	15	0.050	5.3	3.5	6.5	0.81	1.50	3.50	0.74	0.067	14715	4204
	AR14	35	140	0.010	50.0	30.4	31.8	1.57	1.64	3.24	0.69	0.056	20725	681
	AR15	65	370	0.014	84.2	23.7	26.9	3.13	3.56	5.00	0.80	0.056	58474	2472

Appendix A2 continues

Event	*Code*	*A* [km^2]	Q_p [m^3/s]	*S* [m/m]	A_c [m^2]	*w* [m]	*P* [m]	*R* [m]	*d* [m]	*V* [m/s]	*Fr* [–]	*n* [–]	*Ω* [W/m]	*ω* [W/m^2]
Argens	AR16	87	480	0.008	137.0	34.9	40.6	3.37	3.92	4.26	0.63	0.056	24957	714
	AR17	87	460	0.008	139.4	47.6	50.8	2.74	2.93	3.97	0.63	0.056	24278	510
	AR18	62	220	0.020	65.9	17.4	22.9	2.87	3.78	3.64	0.55	0.067	42581	2442
	AR19	54	160	0.036	29.9	14.5	16.6	1.80	2.06	6.00	1.20	0.056	54277	3735
	AR20	4.5	45	0.075	9.9	6.9	9.6	1.04	1.44	4.78	1.27	0.059	31674	4604
	AR21	4.2	22	0.016	11.8	10.8	13.0	0.90	1.09	1.89	0.58	0.063	3354	309
	AR22	19	75	0.013	24.6	9.3	14.8	1.67	2.64	2.89	0.57	0.056	2384	255
	AR23	169	200	0.010	62.7	24.5	27.0	2.32	2.56	3.15	0.63	0.056	18443	752
	AR24	183	250	0.010	94.7	45.2	47.1	2.01	2.10	3.50	0.60	0.067	16260	360
Magra	MA01	7.5	55	0.020	32.0	32.0	34.0	0.94	1.00	1.63	0.65	0.083	10791	337
	MA02	4.6	50	0.029	16.6	12.5	13.7	1.21	1.32	3.00	0.79	0.067	14043	1123
	MA03	30.2	436	0.024	85.5	62.1	90.9	0.94	1.38	3.17	0.74	0.067	97562	1571
	MA04	25.8	90	0.010	31.7	17.1	18.8	1.68	1.85	2.83	0.66	0.050	6984	408
	MA05	13.6	50	0.020	21.3	17.4	18.1	1.18	1.22	2.37	0.68	0.067	11654	672
	MA06	19.9	245	0.020	80.1	44.6	46.0	1.74	1.80	3.07	0.73	0.067	73714	1654
	MA07	3.4	30	0.020	9.9	7.6	8.9	1.11	1.30	3.00	0.85	0.050	7069	933
	MA08	38.6	395	0.019	102.4	38.3	40.3	2.54	2.68	3.85	0.75	0.067	25032	654
	MA09	43.0	340	0.021	87.0	33.9	36.8	2.37	2.57	3.86	0.77	0.067	70844	2091
	MA10	11.8	210	0.040	61.4	35.0	35.9	1.71	1.75	3.40	0.83	0.083	84011	2400
	MA11	23.4	270	0.027	31.2	31.6	33.1	0.94	0.99	3.88	0.81	0.071	73687	2332
	MA12	27.4	90	0.040	24.2	16.8	18.3	1.32	1.44	3.61	0.96	0.067	56488	3368
	MA13	19.6	36	0.025	16.5	17.8	18.4	0.90	0.93	2.21	0.73	0.067	9115	514
	MA14	8.8	22	0.035	8.6	9.0	9.8	0.88	0.95	2.58	0.85	0.067	6572	728
	MA15	10.9	55	0.020	17.4	9.9	12.6	1.39	1.76	3.17	0.76	0.056	12323	1250
	MA16	5.5	115	0.030	32.8	20.0	21.3	1.54	1.64	3.46	0.86	0.067	36428	1821

Appendix A2 continues

Event	*Code*	*A* [km^2]	Q_p [m^3/s]	*S* [m/m]	A_c [m^2]	*w* [m]	*P* [m]	*R* [m]	*d* [m]	*V* [m/s]	*Fr* [–]	*n* [–]	*Ω* [W/m]	*ω* [W/m^2]
Magra	MA17	6.8	29	0.010	12.6	9.7	10.2	1.23	1.30	2.30	0.64	0.050	3269	337
	MA18	21.5	365	0.017	121.5	82.7	83.5	1.45	1.47	3.00	0.95	0.050	61480	743
	MA19	47.4	150	0.023	39.2	24.0	24.8	1.58	1.63	3.40	0.96	0.056	36581	1522
	MA20	12.0	110	0.060	30.9	15.2	17.1	1.81	2.03	3.64	0.82	0.100	61660	4054
	MA21	21.5	75	0.019	43.7	22.5	35.1	1.24	1.94	2.39	0.67	0.067	14818	659
	MA22	8.2	115	0.010	35.3	12.8	16.9	2.09	2.76	3.27	0.63	0.050	11090	867
	MA23	4.5	55	0.020	16.0	8.0	12.0	1.33	2.00	3.43	0.77	0.050	10791	1349
	MA24	33.9	70	0.005	33.4	23.6	24.7	1.35	1.41	2.16	0.58	0.040	2568	109
	MA25	39.6	95	0.035	33.4	20.6	24.7	1.35	1.62	3.70	0.87	0.067	32516	1580
	MA26	77.4	295	0.015	75.1	31.1	37.2	2.02	2.41	3.90	0.80	0.050	47200	1517
	MA27	1.7	37	0.034	12.6	10.0	11.2	1.12	1.26	2.98	0.85	0.067	17771	1784
	MA28	0.5	11	0.150	5.1	3.1	5.9	0.86	1.63	2.10	0.52	0.167	16187	5205
	MA29	5.7	160	0.025	48.9	20.2	24.1	2.03	2.42	3.48	0.75	0.067	46319	2295
	MA30	7.32	200	0.012	67.0	35.5	37.6	1.78	1.89	2.76	0.61	0.061	23878	673
	MA31	3.79	65	0.012	30.4	27.3	28.2	1.08	1.11	1.64	0.50	0.067	8462	310
	MA32	22.35	510	0.020	179.1	113.3	115.3	1.55	1.58	2.84	0.72	0.067	56035	495
	MA33	51.3	280	0.018	81.5	48.2	50.2	1.62	1.69	2.93	0.72	0.067	54936	1140
Vizze	VZ01	72.9	78.4	0.014	24.4	14.0	15.3	1.59	1.74	3.22	0.77	0.050	9306	665
	VZ02	45.2	69.9	0.015	21.8	13.0	14.6	1.50	1.67	3.21	0.79	0.050	4800	369
Cedrino-Posada	CP01	206.2	2100	0.020	356.0	74.8	77.1	4.62	4.76	5.88	0.86	0.067	412020	5510
	CP02	46.8	463	0.005	142.0	37.7	40.5	3.50	3.77	3.26	0.54	0.050	24890	660
	CP03	8.3	200	0.018	54.3	33.1	33.7	1.61	1.64	3.69	0.92	0.050	31039	939
	CP04	124.1	1015	0.018	167.6	38.8	42.2	3.97	4.32	6.05	0.93	0.056	22802	588
	CP05	97	1340	0.012	246.2	59.5	62.6	3.93	4.14	5.46	0.86	0.050	107135	1799
	CP06	118.6	1390	0.013	211.7	39.1	44.0	4.81	5.41	6.55	0.90	0.050	57680	1474

Appendix A2 continues

Event	*Code*	*A* [km^2]	Q_p [m^3/s]	*S* [m/m]	A_c [m^2]	*w* [m]	*P* [m]	*R* [m]	*d* [m]	*V* [m/s]	*Fr* [–]	*n* [–]	*Ω* [W/m]	*ω* [W/m^2]
Cedrino-Posada	CP07	549.7	3400	0.003	612.8	131.3	132.8	4.61	4.67	5.57	0.82	0.029	28017	213
	CP08	542.6	3900	0.005	825.5	130.5	134.6	6.13	6.32	4.74	0.60	0.050	14538	111
	CP09	542.3	3900	0.010	766.3	118.0	123.2	6.22	6.49	6.76	0.85	0.050	406311	3442
	CP10	294.5	3500	0.006	696.9	95.6	101.3	6.88	7.29	5.04	0.60	0.056	206010	2154
	CP11	230.5	3000	0.006	473.2	103.4	105.1	4.50	4.58	6.33	0.94	0.033	176580	1707
	CP12	3.9	100	0.030	30.7	21.1	22.1	1.39	1.45	3.24	0.86	0.067	47696	2259
	CP13	287.8	2100	0.010	437.2	162.2	164.2	2.66	2.70	4.80	0.93	0.040	949912	5856
	CP14	34.4	590	0.010	149.7	73.9	75.2	1.99	2.03	3.96	0.89	0.040	56316	762
	CP15	20.5	410	0.020	92.8	46.2	47.9	1.94	2.01	4.40	0.99	0.050	108436	2345
	CP16	9.7	160	0.030	35.5	18.7	20.9	1.70	1.90	4.44	1.03	0.056	59849	3206
	CP17	21.5	390	0.019	79.5	32.2	34.0	2.34	2.47	4.86	0.99	0.050	49584	1539
Lierza	LZ01	7.29	130	0.010	39.2	17.1	19.0	2.06	2.29	3.24	0.68	0.050	14309	837
	LZ02	4.19	74	0.040	20.5	14.1	15.5	1.32	1.45	3.61	0.96	0.067	15346	1089
	LZ03	1.45	40	0.025	11.4	9.3	10.4	1.10	1.23	3.37	0.97	0.050	2496	269
	LZ04	2.75	54	0.029	15.4	10.3	12.7	1.21	1.50	3.48	0.91	0.056	6087	594
	LZ05	1.47	24	0.030	12.0	11.7	12.5	0.96	1.02	2.02	0.64	0.083	5580	477
	LZ06	12.22	149	0.015	36.1	14.0	16.5	2.19	2.59	4.13	0.82	0.050	5408	387
	LZ07	3.48	53	0.025	18.6	13.1	14.3	1.30	1.42	2.83	0.76	0.067	12769	974

A3: Dataset of the 59 Simulated Cross Sections with Geomorphic Reconnaissance for the Four Recent Floods in Italy

Event	*Code*	*A* [km^2]	*Observations*			*Simulations*								
			XS type (OGE)	Q_p [m^3/s]	$\pm Q_p$ [m^3/s]	Q_p [m^3/s]	*P* [mm]	*RC* [–]	Ω [W/m]	ω [W/m^2]	$\mathcal{E}_e$ [MJ/m^2]	T_{th} [$s*10^3$]	$\mathcal{E}_{th}$ [MJ/m^2]	$\mathcal{E}_r$ [–]
Magra	MA01	7.5	AT (N)	55	48–62	23	163	0.13	4495	140	17	0.0	0.0	0.000
	MA02	4.6	S-A (M)	50	32–69	63	267	0.54	17617	1409	435	18.0	91	0.209
	MA03	30.2	AL (M)	436	274–598	486	385	0.64	108848	1753	847	25.2	252	0.297
	MA04	25.8	S-A (N)	90	78–102	96	207	0.21	7484	438	99	3.6	0.7	0.007
	MA05	13.6	AL (S-M)	50	38–62	28	161	0.08	6464	373	66	1.8	0.1	0.002
	MA06	19.9	AL (M)	245	154–336	486	404	0.60	146245	3281	1152	25.2	368	0.319
	MA07	3.4	AT (N)	30	26–34	43	253	0.43	10158	1340	408	18.0	75	0.183
	MA08	38.6	AL (M)	395	249–542	414	336	0.60	26214	685	397	27.0	53	0.132
	MA09	43.0	S-A (S-M)	340	261–419	243	274	0.51	50613	1494	1279	41.4	583	0.456
	MA10	11.8	S-A (M)	210	132–288	305	465	0.67	122124	3489	1407	28.8	542	0.385
	MA11	23.4	S-A (M)	270	170–370	184	250	0.54	50213	1589	794	25.2	247	0.311
	MA12	27.4	AL (S-M)	90	69–111	79	247	0.47	49687	2963	1342	32.4	815	0.607
	MA13	19.6	AL (S-M)	36	28–44	41	188	0.10	10387	585	200	10.8	10.3	0.052
	MA14	8.8	AL (S-M)	22	17–27	27	238	0.16	7930	878	332	12.6	35	0.104
	MA15	10.9	S-A (S-M)	55	42–68	34	157	0.13	7534	764	103	5.4	4.3	0.042
	MA16	5.5	S-A (M)	115	72–158	124	372	0.61	39129	1956	640	19.8	128	0.200
	MA17	6.8	AL (S-M)	29	22–36	29	209	0.18	3253	335	48	1.8	0.1	0.001
	MA18	21.5	AL (M)	365	230–500	256	242	0.56	43108	521	171	5.4	2.2	0.013
	MA19	47.4	S-A (S-M)	150	115–185	162	222	0.26	39411	1640	546	19.8	154	0.281
	MA20	12.0	AL (S-M)	110	85–136	97	250	0.42	54393	3576	1862	36.0	938	0.504
	MA21	21.5	AL (S-M)	75	58–92	77	234	0.21	15207	676	212	12.6	19	0.090
	MA22	8.2	AT (N)	115	100–131	103	320	0.48	9901	774	336	16.2	38	0.112
	MA23	4.5	AT (N)	55	48–62	17	220	0.47	3320	415	72	5.4	1.6	0.023

Appendix A3 continues

Event	Code	A [km^2]	Observations			Simulations								
			XS type (OGE)	Q_p [m^3/s]	$\pm Q_p$ [m^3/s]	Q_p [m^3/s]	P [mm]	RC [–]	Ω [W/m]	ω [W/m^2]	$\mathcal{E}_e$ [MJ/m^2]	T_{th} [s*10^3]	$\mathcal{E}_{th}$ [MJ/m^2]	$\mathcal{E}_r$ [–]
	MA24	33.9	AT (N)	70	61–80	47	131	0.12	1738	74	8.4	0.0	0.0	0.000
	MA25	39.6	S-A (N)	95	82–108	130	216	0.24	44452	2160	674	25.2	278	0.412
	MA26	77.4	AT (N)	295	255–335	272	224	0.10	43589	1401	415	19.8	121	0.291
	MA27	1.7	S-A (S-M)	37	28–46	56	445	0.66	26716	2682	577	21.6	207	0.358
	MA28	0.5	BR (N)	11	9–13	11	429	0.44	16828	5411	1520	23.4	706	0.465
	MA29	5.7	S-A (S-M)	160	123–197	148	407	0.58	42809	2121	426	23.4	174	0.408
	MA30	7.32	S-A (M)	200	126–274	188	413	0.53	22395	631	134	7.2	5.7	0.042
	MA31	3.79	AL (S-M)	65	50–80	65	305	0.54	8410	308	64	1.8	0.0	0.000
	MA32	22.35	AL (M)	510	321–699	401	390	0.63	44082	389	139	3.6	0.3	0.002
	MA33	51.3	AL (M)	280	176–384	180	222	0.23	35316	733	221	12.6	22	0.098
Vizze	VZ01	72.9	S-A (N)	78.4	68–89	72	38	0.10	8564	612	174	4.6	7.9	0.045
	VZ02	45.2	AL (S-M)	69.9	54–86	64	42	0.22	4372	336	89	2.7	0.2	0.002
Cedrino-Posada	CP01	206.2	BR (N)	2100	1817–2384	1615	181	0.71	316830	4237	908	36	578	0.636
	CP02	46.8	S-A (N)	463	401–526	426	194	0.75	22905	607	117	10.8	8.2	0.070
	CP03	8.3	S-A (S-M)	200	154–246	102	180	0.76	15826	479	60	3.6	0.1	0.002
	CP04	124.1	S-A (S-M)	1015	780–1251	828	339	0.28	18600	480	76	7.2	2.6	0.034
	CP05	97	AL (M)	1340	843–1837	1075	334	0.49	85933	1443	240	18	54	0.225
	CP06	118.6	BR (N)	1390	1202–1578	1268	310	0.48	52625	1345	41	0.0	0.0	0.000
	CP07	549.7	AL (M)	3400	2139–4661	3593	210	0.70	29606	225	61	0.0	0.0	0.000
	CP08	542.6	BR (N)	3900	3374–4427	3644	212	0.72	13582	104	28	0.0	0.0	0.000
	CP09	542.3	S-A (S-M)	3900	2995–4805	3669	212	0.72	382242	3238	1035	39.6	663	0.640
	CP10	294.5	S-A (S-M)	3500	2688–4312	2062	237	0.68	121392	1270	414	39.6	187	0.450
	CP11	230.5	S-A (S-M)	3000	2304–3696	2238	273	0.72	131706	1274	338	36	139	0.412
	CP12	3.9	S-A (S-M)	100	77–123	56	295	0.50	26843	1272	196	18	48	0.245

Appendix A3 continues

Event	*Code*	*A* $[km^2]$	*Observations*			*Simulations*								
			XS type (OGE)	Q_p $[m^3/s]$	$\pm Q_p$ $[m^3/s]$	Q_p $[m^3/s]$	*P* [mm]	*RC* [–]	Ω [W/m]	ω $[W/m^2]$	$\mathcal{E}_e$ $[MJ/m^2]$	T_{th} $[s*10^3]$	$\mathcal{E}_{th}$ $[MJ/m^2]$	$\mathcal{E}_r$ [–]
Cedrino-Posada	CP13	287.8	AL (S-M)	2100	1613–2587	1625	268	0.42	735108	4532	1106	39.6	873	0.789
	CP14	34.4	AL (M)	590	371–809	562	388	0.62	53651	726	125	21.6	27	0.214
	CP15	20.5	S-A (S-M)	410	315–505	310	467	0.34	81950	1772	313	25.2	117	0.374
	CP16	9.7	AL (M)	160	100–219	75	217	0.58	28059	1503	248	32.4	127	0.512
	CP17	21.5	S-A (S-M)	390	300–480	229	261	0.68	29055	902	151	21.6	36	0.236
Lierza	LZ01	7.29	S-A (N)	130	112–148	130	92	0.13	14350	839	60	5.4	16	0.263
	LZ02	4.19	S-A (S-M)	74	56–91	93	108	0.14	19294	1369	88	6.0	38	0.426
	LZ03	1.45	S-A (S-M)	40	31–49	42	96	0.12	2641	285	12.2	0.0	0.0	0.000
	LZ04	2.75	AT (N)	54	47–61	45	73	0.12	5078	495	30	2.4	0.9	0.031
	LZ05	1.47	AL (S-M)	24	18–30	49	121	0.14	11497	982	50	4.8	11	0.209
	LZ06	12.22	AT (N)	149	129–169	151	69	0.12	5489	393	32	3.0	0.8	0.026
	LZ07	3.48	S-A (S-M)	53	40–65	71	100	0.13	17335	1322	96	6.0	35	0.358

A4: DATASET OF THE 159 CHANNEL REACHES FOR THE EIGHT STUDIED RIVERS

River	*Code*	L [m]	A [km^2]	Q_p [m^3/s]	S [m/m]	w_{before} [m]	w_{after} [m]	w_r [–]	ω [W/m^2]	$\mathcal{E}_e$ [MJ/m^2]	$\mathcal{E}_{th}$ [MJ/m^2]	$\mathcal{E}_r$ [–]
Pogliaschina	1	100	2.7	66	0.074	7.5	14.8	2.0	6423	1186	756	0.64
	2	481	2.9	71	0.067	7.6	14.8	1.9	6064	1129	713	0.63
	3	862	4.1	104	0.054	7.3	14.8	2.0	7492	1373	893	0.65
	4	1162	4.9	122	0.046	7.4	14.8	2.0	7531	1448	896	0.62
	5	1538	5.4	133	0.058	4.5	14.8	3.3	16926	3002	1996	0.66
	6	1914	5.7	140	0.046	3.8	12.6	3.4	16775	2962	1967	0.66
	7	2291	6.1	153	0.026	3.8	17.1	4.5	10254	2026	1224	0.60
	8	2667	6.3	163	0.046	3.8	22.5	5.9	19255	3602	2429	0.67
	9	3063	6.7	177	0.005	3.7	22.5	6.1	2272	415	138	0.33
	10	3459	7.0	189	0.029	4.3	30.2	7.1	12624	2253	1378	0.61
	11	3855	7.4	203	0.003	3.3	14.6	4.4	2064	355	94	0.26
	12	4266	7.7	215	0.021	3.1	13.7	4.4	14106	2493	1639	0.66
	13	4678	7.9	222	0.034	3.0	26.4	8.7	24387	4322	2796	0.65
Gravegnola	1	100	9.8	271	0.031	4.6	17.9	3.9	17855	4580	3109	0.68
	2	454	10.8	290	0.034	5.3	20.9	3.9	18355	4907	3346	0.68
	3	809	11.0	292	0.043	6.2	32.3	5.2	20089	5562	4175	0.75
	4	1163	12.0	305	0.031	7.0	19.7	2.8	13276	4108	2891	0.70
	5	1518	12.3	306	0.026	9.7	12.4	1.3	8176	2571	1717	0.67
	6	1872	29.5	481	0.034	14.9	75.4	5.1	10836	4116	2753	0.67
	7	2373	30.2	483	0.025	13.1	65.0	5.0	9135	3684	2341	0.64
	8	2873	31.7	501	0.022	10.8	59.3	5.5	10011	4032	2581	0.64
	9	3374	32.1	511	0.022	10.4	60.7	5.8	10532	4189	2689	0.64
	10	3812	32.4	514	0.017	20.5	57.1	2.8	4233	1721	835	0.49
	11	4250	32.6	516	0.016	22.3	69.3	3.1	3686	1484	705	0.47
	12	4688	32.8	520	0.021	24.3	76.3	3.1	4447	1771	864	0.49
	13	5168	33.6	520	0.024	18.9	96.4	5.1	6469	2488	1419	0.57

Appendix A4 continues

River	*Code*	*L* [m]	*A* [km^2]	Q_p [m^3/s]	*S* [m/m]	w_{before} [m]	w_{after} [m]	w_r [–]	ω [W/m^2]	$\mathcal{E}_e$ [MJ/m^2]	$\mathcal{E}_{th}$ [MJ/m^2]	$\mathcal{E}_r$ [–]
Gravegnola	14	5647	33.8	522	0.010	76.7	190.9	2.5	651	259	25	0.10
Mangiola	1	100	5.6	143	0.058	6.6	29.6	4.5	12326	4180	2406	0.58
	2	481	5.8	148	0.026	13.9	50.3	3.6	2734	938	229	0.24
	3	863	9.5	259	0.031	9.9	23.4	2.4	7868	2682	1112	0.41
	4	1174	12.8	319	0.028	15.0	56.9	3.8	5851	2021	798	0.40
	5	1544	13.6	331	0.036	8.4	35.2	4.2	14083	4846	3647	0.75
	6	1819	13.9	332	0.043	12.3	36.1	2.9	11315	4039	2303	0.57
	7	2094	14.0	332	0.008	7.0	23.7	3.4	3825	1349	425	0.32
	8	2435	14.3	333	0.053	7.6	32.7	4.3	23018	8034	6784	0.84
	9	2783	15.2	340	0.028	7.5	21.6	2.9	12576	4692	3756	0.80
	10	3173	16.1	342	0.046	6.8	26.4	3.9	22635	9037	8498	0.94
	11	3471	16.6	354	0.086	6.2	58.5	9.4	48063	19242	17503	0.91
	12	3728	16.8	363	0.074	6.0	49.3	8.2	44043	18492	16841	0.91
	13	3984	17.0	370	0.061	6.1	39.7	6.5	36501	15257	13797	0.90
	14	4321	17.7	376	0.039	7.2	72.1	10.0	20104	8489	6526	0.77
	15	4658	18.0	381	0.053	6.4	29.7	4.6	30657	13117	11784	0.90
	16	4984	18.6	385	0.044	5.7	22.7	3.9	28896	12682	11374	0.90
	17	5309	18.9	386	0.062	5.3	20.4	3.9	44709	19791	18060	0.91
	18	5709	21.1	397	0.005	6.4	46.5	7.2	2847	1275	399	0.31
	19	5965	21.2	397	0.051	8.3	50.1	6.0	23634	11280	10058	0.89
	20	6220	22.2	398	0.041	13.3	77.0	5.8	12128	6023	4503	0.75
	21	6617	23.1	402	0.022	21.4	75.5	3.5	4108	2054	876	0.43
	22	6999	23.7	403	0.024	15.7	82.9	5.3	6002	2983	1514	0.51
	23	7352	23.9	403	0.022	18.3	91.1	5.0	4659	2318	1071	0.46
	24	7704	24.5	403	0.026	41.1	110.9	2.7	2546	1323	467	0.35

Appendix A4 continues

River	*Code*	*L* [m]	*A* [km^2]	Q_p [m^3/s]	*S* [m/m]	w_{before} [m]	w_{after} [m]	w_r [–]	ω [W/m^2]	$\mathcal{E}_e$ [MJ/m^2]	$\mathcal{E}_{th}$ [MJ/m^2]	$\mathcal{E}_r$ [–]
Mangiola	25	8203	25.7	404	0.025	29.1	90.3	3.1	3462	1824	793	0.43
	26	8572	25.9	404	0.026	21.0	56.2	2.7	4848	2576	1269	0.49
	27	8941	26.1	405	0.018	31.3	64.3	2.1	2304	1253	408	0.33
Osca	1	100	4.0	101	0.034	3.0	23.9	8.0	11123	3321	1704	0.51
	2	396	4.8	117	0.053	3.0	32.2	10.7	20048	5932	4586	0.77
	4	1212	5.5	124	0.050	3.0	19.2	6.4	20412	6170	4775	0.77
	5	1648	8.5	181	0.030	3.0	29.4	9.8	17925	5300	3908	0.74
	6	1978	10.5	205	0.030	3.0	31.7	10.6	20287	5997	4476	0.75
	7	2308	11.5	209	0.025	3.0	31.1	10.4	17263	5150	3648	0.71
	8	2703	11.7	211	0.042	3.0	22.7	7.6	28777	8552	6784	0.79
	9	3098	12.4	211	0.053	3.0	30.8	10.3	36696	10859	8741	0.80
	10	3856	14.4	231	0.028	3.0	18.6	6.2	20816	7128	5386	0.76
	11	4219	14.8	239	0.028	3.0	17.7	5.9	21561	7194	5841	0.81
	12	4582	15.1	244	0.055	4.3	16.9	3.9	30494	10184	8753	0.86
	13	4945	15.2	247	0.006	6.5	18.1	2.8	2368	772	163	0.21
	14	5102	17.3	262	0.028	6.5	24.1	3.7	11299	3685	1694	0.46
	15	5455	18.8	268	0.030	5.4	20.4	3.8	14389	4755	3046	0.64
	16	5790	19.6	274	0.023	4.9	19.4	4.0	12927	4193	2538	0.61
	17	6215	20.2	275	0.025	4.6	27.4	6.0	14754	4844	2873	0.59
	18	6639	20.6	275	0.035	9.5	42.7	4.5	10101	3345	1469	0.44
	19	7064	21.0	277	0.018	10.4	28.3	2.7	4739	1622	559	0.34
	20	7488	21.2	278	0.020	21.7	44.8	2.1	2551	869	188	0.22
	21	7785	21.5	278	0.014	37.5	65.4	1.7	1032	359	32	0.09
	22	8082	21.6	279	0.013	38.1	53.0	1.4	913	331	29	0.09

Appendix A4 continues

River	*Code*	*L* [m]	*A* [km^2]	Q_p [m^3/s]	*S* [m/m]	w_{before} [m]	w_{after} [m]	w_r [–]	ω [W/m^2]	$\mathcal{E}_e$ [MJ/m^2]	$\mathcal{E}_{th}$ [MJ/m^2]	$\mathcal{E}_r$ [–]
Geriola	1	100	0.7	16	0.206	5.6	14.0	2.5	5721	1591	585	0.37
	2	605	2.7	54	0.133	6.6	21.0	3.2	10723	3118	1635	0.52
	3	1133	3.3	63	0.104	6.5	21.5	3.3	9826	2853	1251	0.44
	4	1518	3.6	67	0.078	8.6	19.0	2.2	5967	1807	691	0.38
	5	1904	3.9	70	0.084	8.7	34.1	3.9	6611	1903	738	0.39
	6	2379	5.0	86	0.073	8.9	40.0	4.5	6934	1981	774	0.39
	7	2855	5.7	95	0.074	7.4	36.4	4.9	9209	2634	1142	0.43
	8	3486	6.4	102	0.062	8.0	48.7	6.1	7802	2197	873	0.40
	9	3948	7.6	117	0.042	12.1	53.4	4.4	3988	1163	348	0.30
	10	4494	8.0	119	0.041	9.7	47.6	4.9	4860	1407	477	0.34
	11	5041	8.2	120	0.030	18.8	55.3	2.9	1899	582	81	0.14
	12	5525	8.4	124	0.040	18.3	47.1	2.6	2677	906	234	0.26
Posada	1	100	44.2	620	0.033	17.6	37.7	2.1	11396	2427	1224	0.50
	2	951	112.7	1214	0.035	14.6	47.3	3.2	28539	6244	3660	0.59
	3	1802	113.5	1264	0.020	13.7	50.1	3.7	18096	3857	2015	0.52
	4	2653	114.4	1296	0.022	15.2	55.1	3.6	18395	3888	2033	0.52
	5	3504	114.9	1303	0.018	15.9	41.2	2.6	14469	3077	1583	0.51
	6	4341	116.2	1315	0.016	16.2	50.2	3.1	12744	2680	1366	0.51
	7	5163	117.4	1327	0.017	14.1	49.2	3.5	15690	3225	1667	0.52
	8	5985	118.4	1338	0.011	17.8	47.5	2.7	8114	1634	789	0.48
	9	6821	166.0	1406	0.006	15.1	48	3.2	5481	1472	632	0.43
	10	7672	166.4	1418	0.010	13.8	62.6	4.5	10081	2570	1305	0.51
	11	8523	167.8	1423	0.001	29.3	92.2	3.1	476	120	4	0.03
	12	9374	168.5	1454	0.012	14.8	70.9	4.8	11562	2678	1365	0.51
	13	10273	180.7	1475	0.006	17.6	108.3	6.2	4932	1163	484	0.42

Appendix A4 continues

River	Code	L [m]	A [km^2]	Q_p [m^3/s]	S [m/m]	w_{before} [m]	w_{after} [m]	w_r [–]	ω [W/m^2]	$\mathcal{E}_e$ [MJ/m^2]	$\mathcal{E}_{th}$ [MJ/m^2]	$\mathcal{E}_r$ [–]
Posada	14	11266	181.5	1509	0.008	15.1	64.5	4.3	7844	1802	794	0.44
	15	12305	200.8	1544	0.009	15.3	53.6	3.5	8909	2191	1094	0.50
	16	13256	205.1	1590	0.011	13.2	45	3.4	13001	3747	1947	0.52
	17	14119	207.0	1661	0.004	15.7	72.1	4.6	4152	1160	480	0.41
	18	14982	208.6	1672	0.012	15.8	68.1	4.3	12456	3520	1824	0.52
	19	15846	210.9	1691	0.009	18.1	52.2	2.9	8248	2358	1182	0.50
	20	16709	211.2	1700	0.004	13.3	54.1	4.1	5014	1419	605	0.43
	21	17573	237.4	1972	0.005	28.2	59.5	2.1	3431	1002	435	0.43
	22	18457	542.1	3636	0.006	15.1	83.7	5.5	14174	5006	3162	0.63
	23	19382	542.7	3648	0.006	18.8	98.2	5.2	11421	3949	2253	0.57
	24	20456	546.8	3661	0.001	19.9	111.1	5.6	1805	608	201	0.33
	25	21507	553.4	3680	0.006	24	132.9	5.5	9025	2956	1654	0.56
	26	22462	554.1	3692	0.002	38.2	114.5	3.0	1896	632	207	0.33
	27	23448	559.2	3711	0.008	82.3	101.2	1.2	3539	1316	708	0.54
	28	24409	560.7	3724	0.001	141	156.5	1.1	259	98	0	0.00
Mannu di Bitti	1	100	204.3	1809	0.002	20	52.1	2.6	1775	646	193	0.30
	2	1222	205.2	1858	0.009	19.2	49	2.6	8546	2741	1662	0.61
	3	2217	217.5	1937	0.007	14.2	50.4	3.5	9367	2797	1698	0.61
	4	3208	223.7	1944	0.007	9.3	43.4	4.7	14357	4335	2723	0.63
	5	4323	224.0	1967	0.008	14.7	47.8	3.3	10503	3257	2004	0.62
	6	5438	227.4	1979	0.006	19.8	45.2	2.3	5884	2363	1410	0.60
	7	6553	228.6	1983	0.004	18.9	48.7	2.6	4116	1623	845	0.52
	8	7587	229.5	1988	0.010	15.7	63.4	4.0	12423	4708	2968	0.63
	9	8541	230.5	1993	0.010	22.1	97.7	4.4	8847	3293	2030	0.62
	10	9488	284.0	2072	0.017	12.2	76.1	6.2	28320	10391	6743	0.65

Appendix A4 continues

River	*Code*	*L* [m]	*A* [km^2]	Q_p [m^3/s]	*S* [m/m]	w_{before} [m]	w_{after} [m]	w_r [–]	ω [W/m^2]	$\mathcal{E}_e$ [MJ/m^2]	$\mathcal{E}_{th}$ [MJ/m^2]	$\mathcal{E}_r$ [–]
Mannu di Bitti	11	10357	292.2	2088	0.010	12.5	69.5	5.6	16385	6057	3862	0.64
	12	11264	292.6	2093	0.001	21.5	49.7	2.3	955	364	66	0.18
	13	12177	293.6	2121	0.004	26.8	54.3	2.0	3105	1174	570	0.49
	14	13167	294.7	2121	0.008	27.1	48.2	1.8	6143	2344	1387	0.59
	15	14159	299.1	2149	0.006	15	28.5	1.9	8434	3177	2101	0.66
	16	14975	299.7	2187	0.003	15.5	59	3.8	4153	1288	642	0.50
	17	15921	300.8	2193	0.003	30.6	74.3	2.4	2109	698	261	0.37
	18	16999	301.9	2200	0.006	17.9	59.1	3.3	7234	2293	1244	0.54
	19	18077	302.4	2215	0.002	17.6	40.9	2.3	2470	822	361	0.44
	20	19155	302.9	2221	0.001	16.9	47.2	2.8	1289	410	101	0.25
Lierza	1	100	1.45	40.3	0.100	–	4.4	–	8978	550	411	0.75
	2	130	1.46	40.6	0.066	–	5.7	–	4614	282	154	0.55
	3	155	1.47	41.0	0.045	–	4.1	–	4411	269	146	0.54
	4	171	1.47	41.0	0.070	–	9.1	–	3097	189	80	0.42
	5	206	1.48	41.2	0.110	–	8.2	–	5416	330	185	0.56
	6	260	3.03	64.9	0.045	–	4.1	–	6989	555	415	0.75
	7	292	3.04	65.2	0.054	–	9.6	–	3596	285	170	0.60
	8	326	3.06	65.6	0.052	–	5	–	6693	530	395	0.74
	9	439	3.27	72.0	0.120	–	6	–	14120	1095	1037	0.95
	10	575	3.31	72.3	0.049	–	6.4	–	5428	423	267	0.63
	11	664	3.41	74.9	0.070	–	8.2	–	6275	487	335	0.69
	12	680	3.44	75.5	0.046	–	5.1	–	6683	520	386	0.74
	13	755	3.47	75.8	0.037	–	8.2	–	3355	262	153	0.59
	14	833	3.49	76.0	0.085	–	8.7	–	7281	570	427	0.75
	15	883	4.18	91.7	0.200	–	8.2	–	21942	1687	1628	0.97

Appendix A4 continues

River	*Code*	*L* *[m]*	*A* *[km²]*	Q_p *[m³/s]*	*S* *[m/m]*	w_{before} *[m]*	w_{after} *[m]*	w_r *[–]*	ω *[W/m²]*	$\mathcal{E}_e$ *[MJ/m²]*	$\mathcal{E}_{th}$ *[MJ/m²]*	$\mathcal{E}_r$ *[–]*
Lierza	16	952	4.19	91.7	0.095	–	6.9	–	12385	954	895	0.94
	17	997	4.23	92.4	0.050	–	9.4	–	4820	372	231	0.62
	18	1159	4.28	92.6	0.020	–	6.9	–	2633	205	105	0.51
	19	1257	4.29	91.9	0.180	–	11.8	–	13758	1080	1022	0.95
	20	1370	7.23	127.6	0.130	–	4.9	–	33208	2713	2655	0.98
	21	1560	7.42	130.9	0.140	–	9.5	–	18922	1528	1470	0.96
	22	1616	7.44	131.3	0.220	–	9.8	–	28918	2330	2272	0.97
	23	1669	7.45	131.6	0.050	–	10.5	–	6149	495	365	0.74